Development of a liver tissue organoid

Laura Edwards

Submitted in accordance with the requirements for the degree of Doctor of Philosophy

The University of Leeds

Institute of Medical and Biological Engineering

School of Mechanical Engineering

Faculty of Engineering

Jan 2025

The candidate confirms that the work submitted is her own and that appropriate credit has been given where reference has been made to the work of others.

Acknowledgements

This moment in my life has been long and arduous for all involved. I would firstly like to thank my many Supervisors including Steve Griffin, Jen Edwards, Claire Brockett, Eileen Ingham, Joanne Tipper and Stacy-Paul Wilshaw who have helped provide support, patience and advice throughout the tumultuous journey that was my PhD. Special thanks also goes to Victoria Masters - I could not have completed without your kind words and listening ears. Even though many were there for only a short time, every single person has helped guide me throughout, to create this book, and me as a person. I have learned so, so much over these many, many years.

I would like to give thanks to the amazing support of my mum Pam and my brother Mark, who have been there throughout my life, but particularly so during my PhD. You have been a forever passenger in the rollercoaster that is my life and you still sit alongside me now, which is a true testimony to your perseverance - I am forever appreciative of all you done in both words and actions. I believe that my mum has, albeit unwittingly, created a monster of determination and focus for which there is no stopping. Thank you to both of you.

The foundation upon which this achievement could not have been completed also includes my closest friends. Many a coffee (and alcoholic beverage) has been drunk debating life the universe and everything, the support my emotional health and wellbeing needed during my liver clouded mind. I am so glad for your help to push my mental and emotional boundaries over the past decade – may we continue to push each other's boundaries further over the next decade too.

.

Pure and simple, I'd like to dedicate this thesis to me, and to all the other people out there that dare to dream. Although life can tragically suck in the worst possible way, know that if we persevere and keep on swimming – our dreams can come true. You got this!

Abstract

Despite the ability of liver to regenerate from one third its size, little is known about the cellular mechanisms that underpin such an almost limitless potential for regeneration. *In vitro* culture of cells is often plagued with reductions in cell viability and function, providing limited understanding of regenerative capability outside of *in vivo* environments. Even *in vivo*, once sufficient tissue is lost, native regenerative response limits further regeneration capability. Studies using decellularised liver grafts have potential for understanding the mechanisms behind wound healing and repair as well as providing long term evaluation of drug toxicity after seeding due to the native like biological, biochemical and architectural characteristics.

This study aimed to develop a decellularised porcine liver scaffold with native ~~histioarchitecture~~histoarchitecture and biochemical composition, based on the Leeds method, that can support and develop current knowledge of cell seeding methods. Combination of hypo-and hyper-tonic buffers, low concentration SDS (0.1%) and nucleases resulted in effective decellularisation of tissue and maintenance of ECM ~~histioarchitecture~~histoarchitecture. One cycle of SDS (0.1%) showed sufficient cellular and nuclear removal from native porcine liver tissue, creating a biocompatible scaffold that retained overall histoarchitecture.

Subsequent investigation of seeding methods identified key areas for development including volume of cell suspension for better cell coverage, analysis of seeding time to increase cell attachment, modification of cell density to alter cell attachment and use of dynamic and static culture conditions to maximise cell penetration. HepaRG and Huh7 cells supported cell attachment for up to 28 days culture, and proliferation for up to 14 and 28 days respectively. Furthermore, functional HepaRG were identified even after 28 day culture. Results indicate the potential benefits of HepaRG and/or Huh7 seeded discs in developing understanding of cell repair, regeneration and wound healing, as well as the dysregulation of matrix remodelling after injury.

Table of Contents

List of Figures

List of Tables

Abbreviations

µg	Microgram
µL	Microlitre
µm	Micrometre
2D	Two dimensional
3D	Three dimensional
AB	Alcian blue
AFP	Alpha fetoprotein
ANOVA	Analysis of variance
ATP	Adenosine triphosphate
BAL	Bioartificial liver
BCA	Bicinchoninic acid assay
BCRP	Breast cancer resistance protein
BD	Bile duct
BHK	Haby hamster kidney
BMm	Basement membrane like membrane
bp	Base pair
BrdU	Bromodeoxyuridine
BSEP	Bile salt exporter protein
°C	Degrees celsius
Ca_{2+}	Calcium
CD	Cluster of differentiation
CK	Cytokeratin
cm	Centimetre
conc	Concentration

CO_2	Carbon dioxide
CPS	Counts per second
CPS	Carbomyl phosphate synthetase
CV	Central vein
CYP	Cytochrome P450 family
D	Diastase
DAB	Diamino benzidine
DAMP	Damage associated molecular patterns
DAPI	4'6-diamidino-2-phenylinole
DMB	1,9-dimethylene blue
DMEM	Dulbecco's minimal essential medium
DMSO	Dimethyl sulfoxide
DNA	Deoxyribonucleic acid
dsDNA	Double stranded DNA
dUTP	Deoxyuridine triphosphate
ECL	Enhanced chemi-luminescence
ECM	Extracellular matrix
EDTA	Ethylenediaminetetraacetic acid
EGF	Epidermal growth factor
EGTA	Ethylene glycol-bis(beta-aminoethyl ether)-N,N,N',N'-tetraacetic acid
ELAD	Extracorporeal liver assist device
ELISA	Enzyme linked immunosorbent assay
EpCAM	Epithelial cell adhesion molecule
FAK	Focal adhesion kinase

FBS	Foetal bovine (calf) serum
FXR	Farnesoid X receptor
g	Gram
GAG	Glycosaminoglycan
GAPDH	Glyceraldehyde 3-phosphate dehydrogenase
GelMA	Methacrylate gelatin
GFP	Green fluorescent protein
H&E	Haematoxylin and eosin
HA	Hepatic artery
hADSC	Human adult derived stem cells
HCl	Hydrochloric acid
Hfh	Human foetal hepatocytes
Hfsc	Human foetal stem cell
HGF	Hepatocyte growth factor
HNF	Hepatocyte nuclear factor
Hpsc	Hepatic stem cell
hr	Hour/s
HRP	Horse radish peroxidase
HSC	Hepatic stellate cells
Ig	Immunoglobulin
ISO	International Organisation for Standardisation
kPa	Kilo pascal
L	Litre
LAD	Liver assist device
LAH	Lactalbumin enzymatic hydrolysate

LATS	Large activated tumour suppressor (kinase)
LEM	Liver extracellular matrix
LLL	Left lateral lobe
LML	Left medial lobe
LN	Laminin
LoC	Liver-on-Chip
LSEC	Liver sinusoidal epithelial cell
LXR	Liver X receptor
M	Molar
mbar	Millibar
mg	Milligram/s
Mg_{2+}	Magnesium
min	Minutes/s
mm	Millimetre
MMP	Matrix metalloproteases
mRNA	Messenger ribonucleic acid
MRP	Multi-drug resistant protein
MSC	Mesenchymal stem cell
MSD	Minimum significant difference
MST	Mammalian STE20-like protein kinase
MT	Massons trichrome
Na_2EDTA	Ethylene diaminetetraacetic acid disodium salt
NaOH	Sodium hydroxide
NBF	Neutral buffered formalin
NCAM	Neural cell adhesion molecule

ng	Nanogram
NH_2OH	Hydroxylamine
NHSBT	National Health Service Blood and Transport
nm	Nanometre/s
NTCP	Sodium taurocholate cotransporting polypeptide
Oatp	Organic anion transporter
OCT	Optimal cryotomy temperature
OCT4	Octamer-binding transcription factor 4, or POU5F1
P	Parenchyma
PAA	Peracetic acid
PAS	Periodic acid schiff
PBS	phosphate buffered saline
PCNA	Proliferating Cell Nuclear Antigen
PCR	Polymerase chain reaction
PEG	Polyethylene glycol
pHH	Primary human hepatocyte
PLGA	Poly lactic-co-glycolic acid
POU5F1	POU Class 5 homeobox, or Oct4
PS	Poly-L-lysine coated polystyrene plates
PT	Portal triad
PV	Portal vein
PVDF	Polyvinylidene fluoride
PXR	Pregnane X receptor
qRT-PCR	Quantitative reverse transcriptase polymerase chain reaction
r^2	Coefficient of determination

RLL	Right lateral lobe
RML	Right medial lobe
RNA	Ribonucleic acid
RPH	Revolutions per hour
RPM	Revolutions per minute
s	Second/s
SB	Septal band
SDS	Sodium dodecyl sulphate
soln	Solution
SRY	Sex determining region Y protein
TAE	Tris Acetate EDTA
TAOK	TAO kinases
TAZ	Transcriptional coactivator with PDZ-binding motif
TBS	Tris buffered saline
TBS-T	Tris buffered saline Tween 20
tDNA	Total DNA
TE	Tris EDTA buffer
TEAD	Transcriptional enhanced associate domain
TEL	Tissue engineered liver
TGF	transforming growth factor
TIMP	Tissue inhibitor of matrix metalloproteinases
tRNA	Transfer RNA
TUNEL	Terminal deoxynucleotidyl transferase dUTP nick end labeling
TX-100	Triton X-100
UV	Ultraviolet

V	Volt
v	Volume
Vs.	Versus
w	Weight
W	Watt
Wnt	Wingless-related integration site
YAP	Yes associated protein
α	Alpha
β	Beta
γ	Gamma

~~1.~~1 General Introduction

1.1 The liver; structure and function

The liver is the largest organ in the human body and increases in size up until 15 years of age (Young et al., 2014, Hall et al., 1990) . The liver is responsible for many functions within the body including food metabolism, storage of energy sources and secretion of bile. Experimental models of liver injury (partial hepatectomy or chemical injury) have demonstrated both extracellular and intracellular signalling pathways used to regenerate the liver to 100 % of its normal weight (Summarised in (Michalopoulos, 2014)). The liver contains approximately one million structural units, called hepatic lobules (Figure 1) that are identified by the placement of portal triads and central veins ~~(Figure 1)~~ (Young et al., 2014, Kiernan, 1833). At full maturity, the lobule is predominantly composed of adult

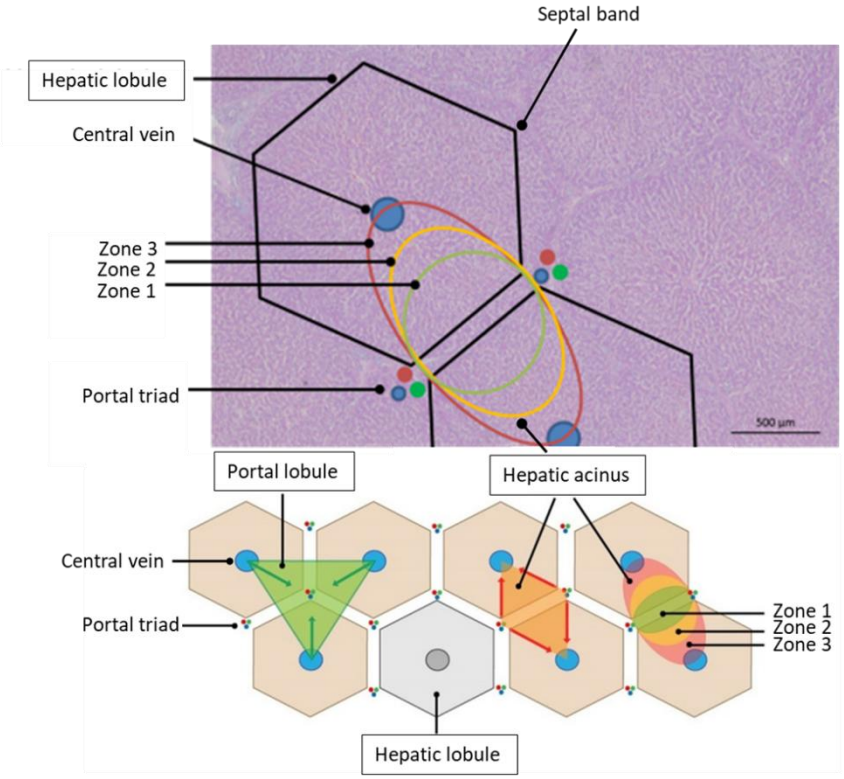

Figure ~~1~~1. Outline of liver structure and related terms. Hepatic lobules are the structural units encased by collagenous septal bands. Positioning of the hepatic lobules and acini are defined by the position of central veins and portal triads. The acinus unit aids in the understanding of metabolic zones that vary across the parenchyma; with zone 1 lying closest to the septal bands and zone 3 lying closest to the central vein. Adapted from (Kulakov).

hepatocytes that are organised into one or two-cell thick plates or cords (Figure 1). Other cell types are present including; stellate cells that secrete extracellular matrix (ECM),

Kupffer cells that remove pathogens, and epithelial cells that line the sinusoids (LSECs), as summarised in Figure 2.

The cords branch and interconnect to form a 3D, sponge-like structure that radiate from the central vein towards the lobule edges (Figure 1). Adjacent hepatocytes are bound by tight junctions forming the apical or canalicular membrane that determines the diameter of the bile canaliculi (1 μm) and separate the apical and basolateral membranes. This unique structure increases surface area for nutrient exchange through exposure to the sinusoids (capillaries) at multiple surfaces (Figure 2).

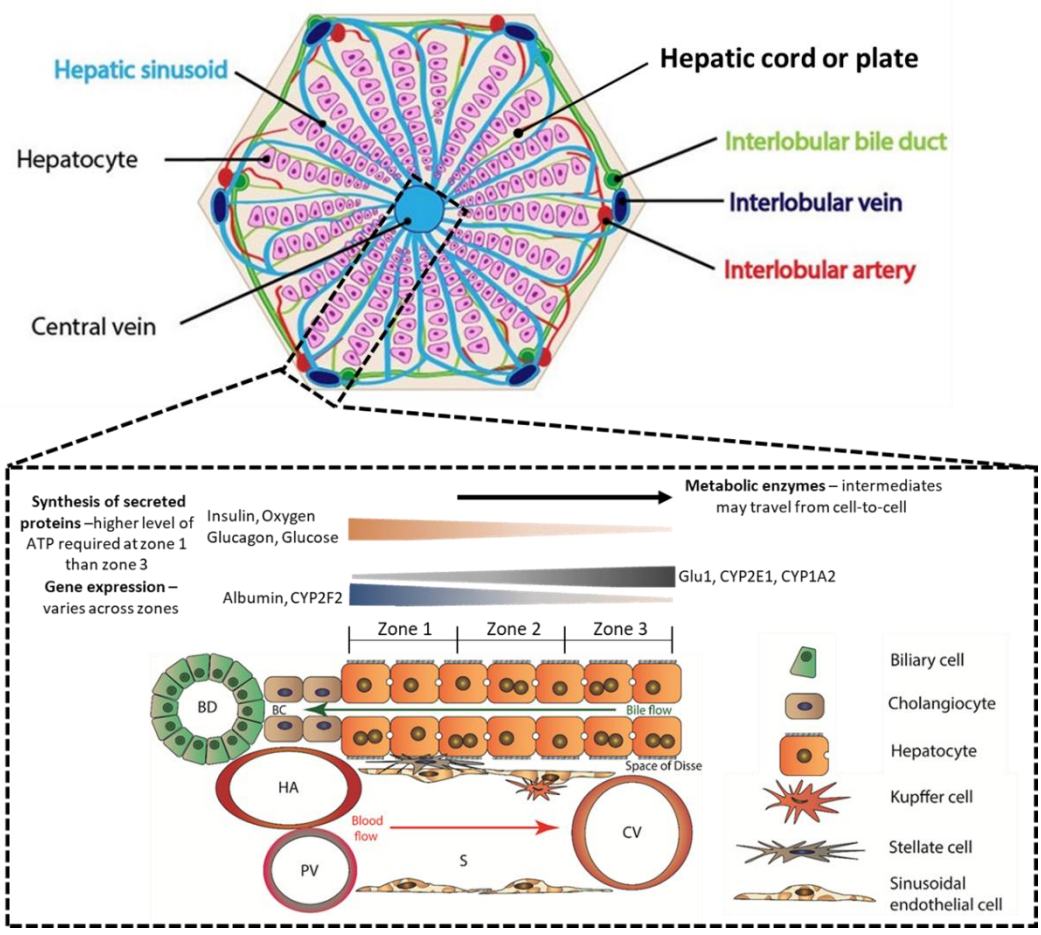

Figure ~~2~~2. Outline of the hepatic lobule and position of the portal triad, central vein, different cell types and sinusoids in relation to each other. Blood flows towards the central vein and bile flows towards the bile ducts, with variance of protein location and expression indicating zonation along the cords (Kulakov). BD = bile duct, HA = hepatic artery, PV = portal vein, CV = central vein, S = sinusoids, BC = bile canaliculi, CYP = cytochrome P450 enzymes involved in metabolisms of various drugs and/or toxins. Adapted from (Kang et al., 2012, Halpern et al., 2017).

The structural integrity of the liver is maintained by a delicate network of ECM in the form of a fine meshwork of reticular fibres that support both hepatocytes and endothelial sinusoidal cells (Young et al., 2014) The reticular fibres are present within the

parenchyma and are primarily composed of collagen III, containing the same protein subunits to those found in septal bands, although arranged differently. Reticular fibres are branched and interwoven to provide strength, flexibility, and stabilise cell position (Martini, 2006). Septal bands surround the parenchyma and are continuous with the Glisson's capsule at the liver periphery, encasing the portal triad, which are located within the lobule apex's (Figure 1) (Young et al., 2014). The unique sinusoidal structures link the portal triad with the central vein, providing extremely low shear stress to maintain reticular fibres and allow efficient nutrient exchange (Figure 2~~Figure 2)~~)(Young et al., 2014). Between the sinusoids and the hepatocytes are the spaces of Disse, within which hepatocyte microvilli are extended to further increase surface area and enhance nutrient exchange (Young et al., 2014) (See Figure 2 ~~Figure 2~~). The unique structure of the liver retains cell polarity and domains, allowing the capability of the liver cells to provide numerous immune, synthetic, metabolic and excretory functions that are vital in maintaining organ and blood homeostasis (~~Table 1~~Table 1).

Table ~~1.~~1. Summary of the numerous roles provided by the liver including in metabolism, storage, and secretion.

Fat metabolism	Oxidises triglycerides to produce energy
	Synthesises plasma lipoproteins, cholesterol and phospholipids
Carbohydrate metabolism	Converts carbohydrates and proteins into fatty acids and triglycerides
	Regulates blood glucose concentration by glycogenolysis and gluconeogenesis
Protein metabolism	Synthesises plasma proteins including albumin and clotting factors
	Detoxifies metabolic waste products (deamination of amino acids and produces urea)
Storage	Glycogen that provides energy for cell processes
	Vitamins for growth and development
	Iron for haem synthesis
Intermediary metabolism	Detoxification of various drugs and toxins (i.e. alcohol)
Secretion	Synthesis and secretion of bile (which is involved in many above processes)

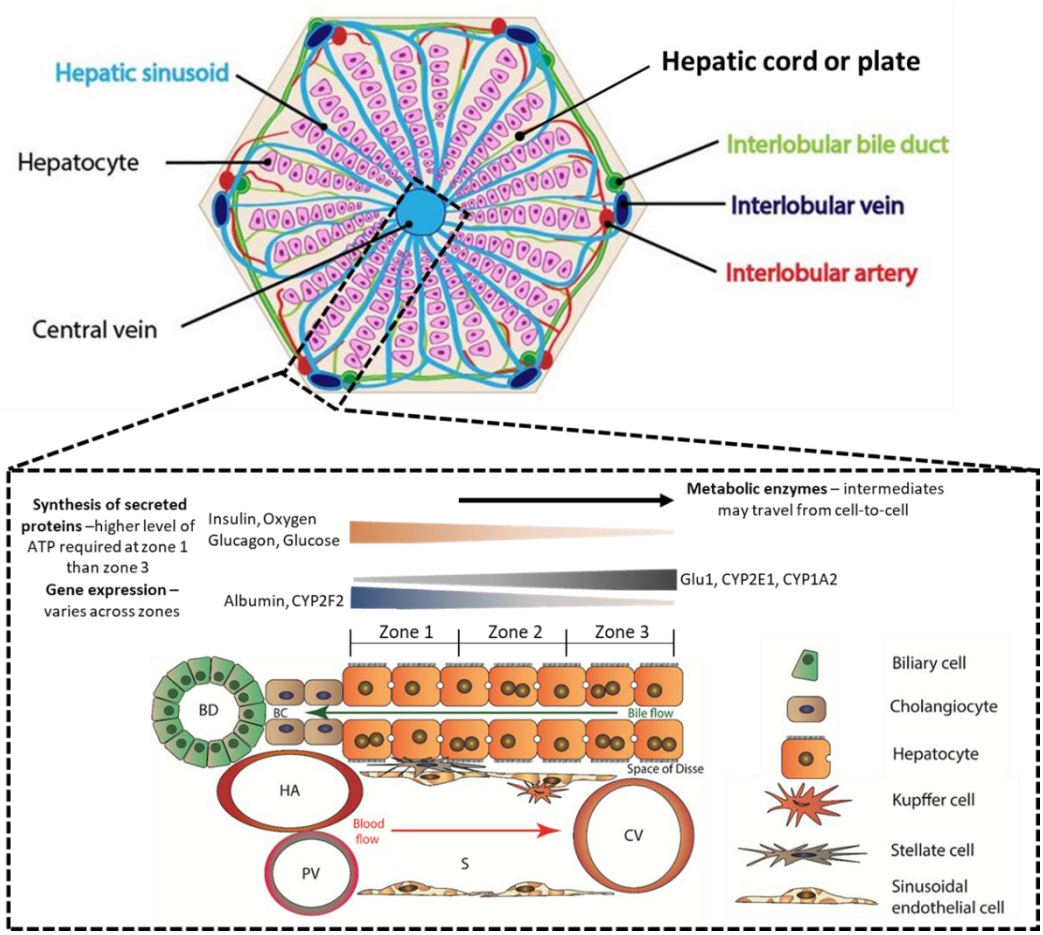

Although the structure of the lobules makes identification easier, the distribution of liver

Fat metabolism	Oxidises triglycerides to produce energy
	Synthesises plasma lipoproteins, cholesterol and phospholipids
Carbohydrate metabolism	Converts carbohydrates and proteins into fatty acids and triglycerides
	Regulates blood glucose concentration by glycogenolysis and gluconeogenesis
Protein metabolism	Synthesises plasma proteins including albumin and clotting factors
	~~Detoxifies metabolic waste products (deamination of amino acids and produces urea)~~
Storage	Glycogen that provides energy for cell processes
	Vitamins for growth and development
	Iron for haem synthesis
Intermediary metabolism	Detoxification of various drugs and toxins (i.e. alcohol)
Secretion	Synthesis and secretion of bile (which is involved in many above processes)

metabolism, oxygenation and variation in ECM composition is best understood if the portal triads are considered to be at the centre of symmetry (Figure 1~~Figure 1~~)(Young et al., 2014). First defined by Rappaport *et al.* in 1954 (Rappaport et al., 1954), the hepatic acinus is a unit of liver parenchyma centred on the portal tracts that lie between two or more terminal hepatic venules (Figure 1). The acinus is similar in size to the lobule (1mm) and is defined by the number of hepatocytes that are supplied by one portal triad.

Fat metabolism	Oxidises triglycerides to produce energy
	Synthesises plasma lipoproteins, cholesterol and phospholipids
Carbohydrate metabolism	Converts carbohydrates and proteins into fatty acids and triglycerides
	Regulates blood glucose concentration by glycogenolysis and gluconeogenesis
Protein metabolism	Synthesises plasma proteins including albumin and clotting factors
	Detoxifies metabolic waste products (deamination of amino acids and produces urea)
Storage	Glycogen that provides energy for cell processes
	Vitamins for growth and development
	Iron for haem synthesis
Intermediary metabolism	Detoxification of various drugs and toxins (i.e. alcohol)
Secretion	Synthesis and secretion of bile (which is involved in many above processes)

~~H~~Hepatocytes that are located within zone 1 (periportal) are closest to the portal triads and involved in the synthesis of glycogen and proteins (Figure 1~~Figure 1~~). Hepatocytes in zone 3 lie nearest the central venule (perivenous) and contain esterases and conjugating enzymes. Hepatocytes that lie between these two zones are in zone 2 (Young et al., 2014). Gradients of oxygen, metabolites and hormones exist along the sinusoids. Hepatocytes in zone 1, where oxygen concentration along the sinusoids is greatest, contain the highest number and largest size of mitochondria (Schmucker et al., 1978). As a result, processes that require the highest levels of ATP, such as gluconeogenesis or urea synthesis occur where glycolytic capacity is greatest, at Zones 1 and 2 (Braeuning et al., 2006). Hepatocytes within zone 1 have higher levels of oxygen saturation, peroxisomes, glucose-6-phosphatase (G6P) and urea activity, bile acid uptake and glycogen synthesis than that seen in other areas (Gebhardt, 1992, MacSween, 1994). During increased demand however, hepatocytes in zones 2 and 3 increase bile acid uptake (Malarkey et al., 2005). Glutamine synthetase is only expressed in hepatocytes from zone 3, whereas enzymes like glucokinase, carboxylesterase or CYP2E1 are present in all zones, but at higher levels in Zone 3 (Malarkey et al., 2005). Further towards zone 3, oxygen pressure decreases by 50 % (Jungermann and Kietzmann, 2000), and glycolytic capability is reduced.

The use of single molecule and single cell fluorescence in situ hybridisation has since isolated, and validated, a graded variation of hepatocyte gene expression across the lobule in mice. As a result, global expression profiles of approximately 3500 genes across the liver lobule have been mapped with high resolution and show gradients of expression along the liver lobule (Halpern et al., 2017). The following trends have subsequently been concluded:-

~~1.4.1.~~• Graded expression patterns exist across lobule layers.

~~1.4.2.~~• Energy demanding tasks, such as synthesis of secreted proteins, are more likely to occur where higher ATP yield can occur, ie at zone 1 (Figure 2~~Figure 2~~).

~~1.4.3.~~• Specific hepatocyte tasks occur at the mid lobule layers ie at zone 2.

~~1.4.4.~~• Enzymes of the metabolic pathways are predominantly expressed in sequential layers ie at zones 2 and 3, indicating that metabolic intermediates may transfer from one layer to the next rather than activities occurring entirely in one zone (Figure 2~~Figure 2~~).

~~1.4.5.~~• Enzyme and transporter properties expressed along the liver lobule are matched to ligand concentrations.

Table~~-~~ 2~~2~~. Hepatoblast behaviour after culture on plates coated with various ECM components. Results indicate that components within the environment can influence cell survival, maintenance and phenotype. N/S = no stated. Adapted from (McClelland et al., 2008).

The complex structure of the liver provides a unique orientation upon which functional capability is defined. Recreation of this would be extremely difficult.

1.2 Matrix components optimise cell activity

Specific ECM components vary between mature and immature tissues, with foetal and neonatal liver containing mostly laminin, collagens III and IV, hyaluronans and poorly sulphated proteoglycans, whereas mature liver, contains primarily fibronectin, and c~~C~~ollagens I and II, highly-sulphated proteoglycans and an absence of laminin, collagen IV and hyaluronan (Martinez-Hernandez and Amenta, 1995, Zern and Reid, 1994, Gebhardt, 1992, Fraser et al., 1997). Culture on ECM component coated plates has revealed that matrix components may also be involved in determining cell phenotype, viability and morphology (Table 2~~Table 2~~). Culture of hepatoblasts on collagen coated plates results in the formation of cell monolayers that survive for longer than ten days in culture. Rapid proliferation is noted in human foetal liver cells cultured on collagen ~~3~~III or collagen IV~~4~~ coated plates, which aligns with ECM components present on foetal and neonatal liver tissue. Hepatoblasts cultured on collagen III or IV, also expressed EpCAM and NCAM but not AFP, indicating a selection for development into hepatic stem cell monolayers (HPSCs).

Plate coating	Attachment		Activity	Survival
Fibronectin	Y	N/S	Rapid differentiation	Rapid cell death
Collagen I	Y	Monolayer	None	>10 days
Collagen III	Y	Monolayer	Rapid proliferation	>10 days
Collagen IV	Y	Monolayer	Rapid proliferation, particularly within HpSCs	>10 days
Laminin	Y	Spheroid	Spheroid	>10 days

Rapid proliferation was seen on laminin coated plates after 12 days culture, although cells differed from other ECM components through the formation of spheroids, not monolayers. Cells cultured on Collagen I or fibronectin did not maintain proliferation, instead losing expression of the hepatic progenitor CK19. Both collagen I and fibronectin are associated with the matrix of mature liver tissue, where hepatocytes do not actively proliferate and are terminally differentiated ~~(Table 2)~~(McClelland et al., 2008).

Variation in matrix stiffness has also been proposed to alter cell behaviour. Hepatocyte culture in progressively cross-linked collagen and Matrigel™ hydrogels has shown an increased progression through the cell cycle and hepatic de-differentiation with increasing gel rigidity, as well as altering the 3D formation of hepatocytes and their response to growth factors and fibronectin (Semler et al., 2005, Semler et al., 2000, Hansen et al., 2006). Furthermore, increasing hydrogel stiffness resulted in increased matrix synthesis and alterations to the regulation of gene expression in the TGF-β signalling pathways (tissue development, homeostasis and repair). Seeding of three fibronectin functionalised polyacrylamide hydrogels of various shear moduli (rigid = 9.21 ±0.08, firm = 5.63 ±0.07 and compliant = 1.93 ±0.05 kPa respectively) ~~Polymerisation of fibronectin functionalised polyacrylamide hydrogels, crosslinked using differing ratio of bisacrylamide monomers (0.028-1.8 % w/v) to acrylamide backbone monomers (20% w/v) to form three gel types (rigid, firm and compliant) with different shear moduli (9.21 ±0.08, 5.63~~ has shown differing results. ~~±0.07 and 1.93 ±0.05 kPa respectively).~~ Rigid gels were associated with increased cell spreading and cyclin D1 expression, a protein associated with progression through the cell cycle, and decreased expression of albumin and p450 mRNA ~~expression~~, whereas compliant gels were associated with the opposite. It was also found that increased fibronectin densities exacerbated the relative responses further in all gel rigidities. The association between increased proliferation and culture on surfaces with high stiffness has also been shown in hepatic stellate cells (HSCs), where HSCs cultured on increasingly fibrotic decellularised rat livers showed increased rates of proliferation, contrary to hepatoblast culture in monolayer (Chen et al., 2023). Expression of integrin β1 and increased nuclear expression of YAP (Yes associated protein), a protein involved in the control of tissue growth and size, were higher in scaffolds with high stiffness (Chen et al., 2023) and further indicate the role stiffness has to play in cell activity.

1.3 How does the liver respond to injury?

One of the most unique properties of the liver is the ability to regenerate following substantial loss of liver mass (70 %), first applied to rodents in 1931 (Higgins, 1931). Following partial hepatectomy in both rodents and humans (three of the five liver lobes), regeneration occurs within two-three weeks and four-six weeks respectively (Michalopoulos, 2007). As a result, great interest in understanding more about the liver, in particular its potential for replication exists.

1.3.1 Acute injury

After an acute injury, a large proportion of hepatocytes proliferate to replace lost cell mass and architecture (Campana et al., 2021), with rapid restoration of liver mass achievable within days in rats, or weeks in humans (Stöcker and Heine, 1971, Stocker et al., 1973). Following removal of up to 2/3 liver mass, hepatocytes within the remaining lobes proliferate, starting in periportal regions where blood flow and oxygen concentration are greatest, and also in biliary epithelial cell regions. Although a small percentage of hepatocytes ~~proliferate~~ divide a second time, the majority of proliferated cells apoptose to reduce risk of overexpansion. Mitogens such as epidermal growth factor (EGF) or hepatocyte growth factor (HGF) are thought to increase rates of hepatocyte proliferation. Although the mechanisms of how biliary epithelial cells contribute to liver cell replacement have not been as extensively reported, expression of YAP is thought to be involved due to its variable expression during homeostasis and the reprogramming of hepatocytes into biliary epithelial cells after injury (Pepe-Mooney et al., 2019) (Campana et al., 2021).

1.3.2 Chronic injury

Chronic liver injury, however, is associated with increased hepatocytes expression of p21 and p16, and p53 expression indicating cell senescence and death (Michalopoulos, 2007, Michalopoulos and DeFrances, 1997, Lu et al., 2015), and associated with the formation of fibrotic and cirrhotic lesions (Zhang et al., 2012). Proliferation and differentiation of biliary epithelial cells, although at low rates, has shown capability to repopulate a large proportion of the lost parenchyma (Lu et al., 2015). Lu (2015) further investigated liver repopulation through identification of a specific subset of hepatic progenitor cells that are activated upon both chronic liver injury, and during hepatocyte senescence. Hepatic progenitor cells were shown to express cell adhesion proteins and glycoproteins EpCAM,

CD24 and CD133, and loss of protein expression associated with immature / immune related proteins CD45, CD31 and Ter119. Chronic liver injury is also associated with the increased population of cells expressing SRY-related high mobility group box-9 (SOX-9), resulting from the increased expression of YAP. Differentiation of bipotential biliary epithelial cells into hepatocytes or biliary epithelial cells occurs through increased Wnt or Notch signalling respectively. Upon continuation of liver damage, chronic fibrosis and cirrhosis can present. Misalignment of ECM remodelling results in the upregulation of tissue inhibitors of matrix degrading metalloproteases (TIMPs), and excessive matrix deposition. Increased deposition of Type I and III collagens by hepatic stellate cells within the spaces of Disse result in the loss of hepatocyte microvilli and therefore reduction in hepatocyte function, resulting in hepatocyte regeneration, septal angiogenesis and ECM crosslinking (Campana et al., 2021, Iredale, 1997)).

1.4 How can liver function be restored?

1.4.1 Organ transplantation

The only definitive treatment for liver failure is transplantation and there are limited numbers of livers suitable for transplantation (Schramm et al., 2010). The increasing number of inadequate organs due to an increase in excessively damaged livers, fatty liver disease and alcoholism reduce this further (Halon et al., 2006, Guidotti and Chisari, 2006). Livers from donors designated as "increased risk" (infected with hepatitis B, hepatitis C or Human Immunodeficiency Virus) are promising, due to strong evidence supporting a low risk of transmission to recipients (1 in 300 to 1 in 1000), with those agreeing to liver transplantation from high risk donors having a 2.3x greater rate of transplantation and 44% decrease in death rates whilst on the donor waiting list, and median waiting times reduced from 14 months, to 11 months (University of California, San Francisco between August 2013 and November 2019) (Kelly et al., 2022). As of~~In~~ March 2024~~3~~, the NHSBT reported 741~~818~~ patients were on the UK liver transplant list (NHSBT, 2024) with 9,183~~210~~ liver transplants performed over the previous ten years (2014-2024, not including Dublin)(NHSBT, 2024). ~~Those on the active transplant list in 2023 (n=697) have risen from 549 in 2014.~~ Furthermore, up to 65 % ~~38 %~~ of those on the list were still waiting for a transplant over six months post registration (Edinburgh) (NHSBT, 2024). Of those who received a transplant, overall long term patient survival drops from 95.2~~1~~ % after one year to 824.9~~1~~ % after five years~~, and reduced further for those with cancer, primary sclerosing cholangitis, autoimmune and cryptogenic, metabolic or other liver~~

~~diseases~~ (NHSBT, 2024)~~{NHSBT, 2014 #475}~~. Due to extensive organ donor shortages, hepatocyte transplantation has become a potential short-term alternative to liver failure.

1.4.2 Hepatocyte transplantation

Hepatocyte transplantation using primary hepatocytes from blood group compatible donors aids in the supplementation of liver function. The first human clinical success was achieved in 1998 on a child with Crigler-Najjar disease, a condition that affects bilirubin metabolism (Fox et al., 1998). Hepatocyte transplantation is minimally invasive and can be provided to those too ill to survive transplantation. Its effectiveness is, however, limited by poor cellular attachment (often less than 30 %), demand for large quantities (2.5-7.5 $x10^9$ cells) and lack of demonstrated long-term function (Palakkan et al., 2013, Fukumitsu et al., 2011, Vacanti and Kulig, 2014). Furthermore, people can be perfused with up to only 5 % of liver mass per session, which is inadequate to treat a large amount of tissue necrosis. The application of hepatocyte transplantation is therefore currently limited to treatment of acute diseases, reduction of decompensation factors, or small tissue resections only.

1.4.3 Bioartificial liver assist devices (BALs)

Failing livers can also be supported through synthetic or bioartificial liver assist devices (BALs) . Synthetic devices filter the blood and remove toxins. Initially, devices removed water soluble toxins, such as ammonia or mercaptans through simple adsorbers such as activated charcoal or through continuous haemodialysis (Ash, 1994). The removal of lipid soluble toxins such as bilirubin, bile acids and fatty acids was limited due to the binding to blood borne proteins such as albumin. Although subsequent LADs have shown similar reductions in toxin levels and patient symptoms, there is no substantial evidence of improved patient survival (Tan, 2004, Jalan et al., 2003, Koivusalo et al., 2005, Zhou et al., 2004). Combining cell bioreactors with additional filters and dialysers led to the creation of bioartificial liver devices (BALs) that address the lack of synthesising and regulatory pathways seen in LAD predecessors (Matsumura et al., 1987).

One of the major drawbacks of BALs is the identification of an appropriate cell source. The ideal cell source would display an unlimited supply, controlled proliferation, human liver-specific metabolism and low immunological response (Weber et al., 2010). The additional use of cells results in the secretion of matrix proteins that clog device membranes and reduce device efficacy (MacDonald et al., 2001). As a result, continuous replacement of cell membranes makes the use of BALs expensive. Better understanding of hepatocyte secretion and environmental remodelling would lead to reduction in the secretion and

deposition of matrix proteins, and extension of device capability thereby reducing maintenance costs. Hepatocytes are, therefore, cultured in the lab for a variety of reasons and in the treatment of a variety of pathologies, even though understanding of their various functions and regenerative capability is still ill-defined.

There is an increasing body of evidence to suggest that 3D culture enhances and/or extends cell function, polarisation and enzyme activity (Godoy et al., 2013, Glicklis et al., 2000, Semino et al., 2003). Studies indicate human hepatocyte interactions with 3D porcine ECM improve cell attachment, survival, growth and long-term hepatocyte viability (Lang et al., 2011). The complex interactions between liver cell types and their environment are thought to be essential in regulating and maintaining native hepatic function, therefore, accurate *in-vitro* culturing systems should aim to replicate as many of these as possible (Godoy et al., 2013). The complexity and composition of native liver ECM cannot currently be replicated using other methods of scaffold preparation, such as the addition of growth factors or through micropatterning techniques. Loss of cell function associated with de-differentiation of cells cultured in monolayer is well known, and particularly applicable to hepatocytes which are responsible for the greatest volume of liver function. Native hepatocyte morphology shows hepatocytes as polygonal, with multi-polarised surfaces that have at least two basolateral surfaces and two apical surfaces (Braiterman and Hubbard, 2009) that are critical to the maintenance of liver function. Maintenance of both hepatocyte morphology and function is, therefore, critical for drug testing, expansion of cell number for cell therapies or support through liver failure using bioartificial liver devices (Godoy et al., 2013).

1.5 What are the challenges experienced during hepatocyte culture?

1.5.1 Hepatocyte isolation

Primary hepatocytes can be isolated from liver resections, foetal livers and xenogeneic donors, although those derived from non-transplantable human livers are the most common source for cell therapy. A comparison of hepatocytes isolated from various liver tissue conditions found that hepatocyte isolation was achievable from both normal and diseased livers, but cell quantity, morphology and function (urea and albumin synthesis) were extremely variable (Bhogal et al., 2011). When compared with other hepatocytes,

those isolated from donors classe~~s~~d as normal, normal resected and biliary cirrhosis showed significantly higher albumin synthesis, and those obtained from donors with alcoholic liver disease yielded significantly lower. Significantly increased urea secretion was noted in those donors classe~~d~~d~~s~~ as normal and biliary cirrhosis, and those with alcoholic liver disease showed significantly lower cell yields (Bhogal et al., 2011). Better cell yields were seen in hepatocytes completely processed within 3 hr of donation and in those obtained from hepatic resections resulting from benign disease and cut-down specimens (Bhogal et al., 2011). It should be noted, however, that higher yields and cell functions were obtained from livers of donors diagnosed with primary biliary cirrhosis, which may have been attributed to patient use of a cytoprotective therapeutic agent, instead of disease characteristics (Bhogal et al., 2011). Immediately after isolation, human hepatocytes typically display similar cell structures and functions to *in-vivo* hepatocytes (Bhogal et al., 2011). After isolation, cells can be cultured in various formats such as in suspension, in monolayer on tissue culture plastic, in sandwich culture or in spheroids, as represented in Figure 3. Variance in hepatocyte functionality and/or viability in these formats are discussed below.

1.5.2 Culture

Although many different types of culture exist, the outcomes required for each method aid in determining which method, and/or cell type, would be most applicable. Examples of these are provided in Table 3.

Table ~~3~~1. Summary of outcomes required from culture of hepatocytes.

	Current limitations	Areas for development	Desired outcomes
Drug testing	Reduced liver function compared with native liver and loss of cell function over time.	Comparable rates of liver function required.	Maintenance of hepatocyte function comparable to native liver cell function beyond 8 weeks.
Cell therapy	Insufficient cell numbers produced. Suboptimal cell attachment.	Greater understanding of how cells attach to liver and ways to promote cell proliferation.	Increase rates of hepatocyte attachment and/or methods to increase hepatocyte proliferation rates.
Bioartificial liver devices	Excessive secretion of matrix proteins clogging device membranes.	Better understanding of cell interaction with matrices and processes of matrix secretion.	Creation of membranes containing functional hepatocytes that do not secrete matrix proteins that clog membranes and/or are maintained long term.
Understanding cell replication and organ size	Cancer formation results in uncontrolled cell proliferation. Incomplete understanding of how organ size is defined and maintained	Better understanding of processes and factors that can affect cell cycle regulation.	Understanding of cell cycle regulation and ways that progression through the cycle can be altered.
Understanding fibrosis formation and development into cirhhosis	Drugs/ viruses can alter the secretion of matrix proteins resulting in excessive matrix deposition and loss of cell/organ function	Better understanding of how pathological mechanisms can affect formation of fibrotic and cirrhotic lesions.	Creation of liver models of pathological disorders / conditions to study formation and reduction of fibrotic and cirrhotic lesions.

1.5.2.1 Culture in 2D orientations

Even though hepatocytes can be cultured in suspension (Figure 3a.)), cells rapidly lose cell function and viability within four hours, thought to result from the loss of polarity that occurs through cell isolation (Elaut et al., 2006, Godoy et al., 2013). In comparison, culture of hepatocytes on tissue culture plastic (Figure 3b.)) has shown extended function and viability compared to culture in suspension. Hepatocyte-like gene expression from hepatocytes cultured on 2D plates is better maintained than those cultured in suspension. Extraction of total RNA (Qiagen Oligotex mRNA kit) and subsequent mRNA microarray analysis identified increased expression of twenty-nine genes in hepatocytes cultured on collagen coated plates compared with those cultured in suspension, with many of the genes involved in cell structure, metabolism and cell cycle regulation, such as actin α4, CK18, Apolipoprotein E and Adenine nucleotide translocator-2 increased. The extension of cell function is not maintained, however. When cultured in conventional 2D conditions, hepatocytes aggregate and form bile canalicular structures. Early phenotypic alterations are seen even though cells survive for only a few days (Waring et al., 2003). Bile acid homeostasis and circulation of bile acids is affected within 24 hr, with similar reductions in other transport proteins including Oatp1a1, Oatp1a4, MRP2 on basolateral membranes and BSEP in the apical membranes (Rippin et al., 2001). Furthermore, loss of functional transporter proteins was also associated with an increase in proliferating markers such as MRP1 in hepatocytes (Roelofsen et al., 1997), indicating a change from epithelial to mesenchymal cell states. Similar results have also been noticed in other species. Rat hepatocytes, for example, lose expression of the sodium taurocholate co-transporting

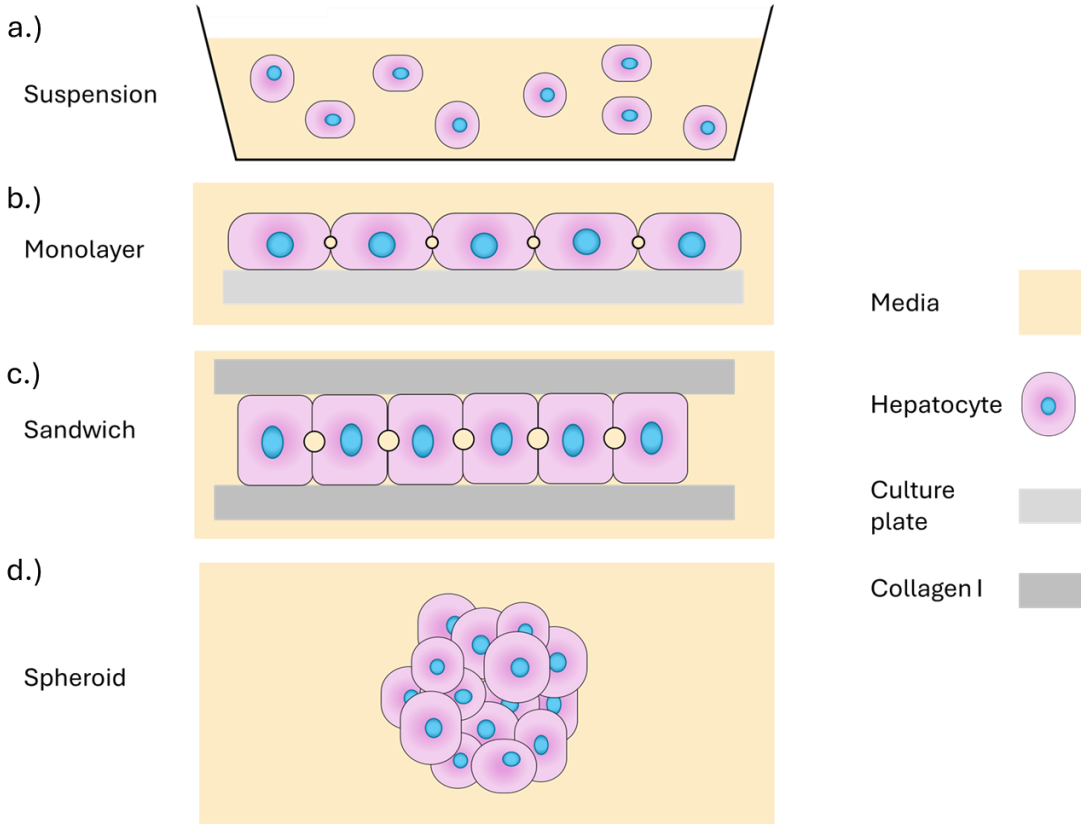

Figure 3. Representation of different hepatocyte culture methods.. a.) = culture in suspension, b.) = monolayer culture, c.) = sandwich culture, d.) = spheroid culture

-polypeptide NTCP mRNA (<27 % mRNA expression and 48 % protein expression) after 24 hr culture, with subsequent taurocholate uptake reduced to 5 % after 72 hr culture, even when cultured on collagen-coated plates (Rippin et al., 2001). In comparison with native liver, however, cells cultured *in-vitro* displayed lower expression of various cell adhesion, cell cycle regulation and cell metabolism genes compared with liver tissue, including fibronectin 1, CYP 3A4 and α1-antichymotrypsin (Waring et al., 2003). Retention of hepatocyte function on tissue culture plastic can be monitored through production of albumin and urea as well as cytochrome P450 activity for a short period, however, is followed by a rapid decline in cell function within one week (Godoy et al., 2013). Hepatocyte function can be extended in various ways; for example through the addition of chromatin remodelling agents such as DMSO (dimethylsulfoxide) or trichostatin A, through the use of highly specialised media such as Lanford's medium, or through the use of Matrigel™ or sandwich configurations (Isom et al., 1985, Henkens et al., 2007, Ferrini et al., 1997, Dunn et al., 1989, Guguen-Guillouzo et al., 1983, Clement et al., 1984). Long term, however, hepatocyte polarity and morphology are altered, with hepatocyte function,

phenotype and lifespan reduced when compared with native conditions (Wells, 2008, Soltys et al., 2010, Gomez-Lechon et al., 1998).

Sandwich culture

Sandwich culture involves overlaying hepatocytes previously cultured on a layer of collagen I, with a second layer of collagen I (Figure 3c.). Originally designed to more closely emulate 3D like conditions by providing a second layer for hepatocytes to attach (Dunn et al., 1989), results showed maintenance of polygonal hepatocyte morphology for seven weeks, as opposed to three days seen when cultured in 2D. Furthermore, albumin secretion was maintained up to six weeks, five weeks longer than that seen in 2D culture. Culture of rat hepatocytes on three different culture models (collagen coated, sandwich culture and liver decellularised ECM) resulted in the identification of two main markers of differentiation; hepatocyte morphology and function (Lin et al., 2004). Those cultured on collagen coated plates showed a rapid decline in function over time, becoming almost absent within five days culture and were associated with flat cell morphologies and long protruding lamellopodia. The use of one collagen layer alone was insufficient to retain hepatocyte function, whereas the addition of a second layer in a sandwich orientation was enough to extend cell function to many weeks (Lin et al., 2004). Since its first use, hepatocyte sandwich culture has been associated with better formation of hepatocyte morphology including bile canaliculi, restoration of cell:cell contacts, more defined cell polarisation, enhanced function, in particular CYP activity, and increased longevity. Even though there are many advantages, loss of cell function is still seen over time (Kern et al., 1997, LeCluyse et al., 1994, De Bruyn et al., 2013). First reported in 1989 (Dunn et al.), extension of rat hepatocyte viability was achieved through sandwiching rat hepatocytes between two layers of collagen I. After 24 hr, hepatocyte cords with typical polygonal morphology were seen, and maintained for seven weeks. Albumin secretion was higher than hepatocytes cultured on one layer of collagen I. Albumin levels in hepatocytes cultured on collagen I coated plates reduced after one week, although could be restored for a few days after the addition of a second layer. Although the addition of collagen I to culture plates and 3D gels similarly raised albumin tRNA levels, the lack of appropriate morphology using culture plates was thought to hinder albumin secretion (Dunn et al., 1989). Culturing hepatocytes in collagen-sandwich culture (Type I) results in the maintenance, or even increase, in protein expression of canalicular transporters including: bile salt exporter pump (BSEP), and the ATP-binding cassette transporter proteins MRP2

and BCRP over five days, when compared to native liver levels (Schaefer et al., 2012). Significant extension and/or increase in the secretion of liver proteins (albumin, transferrin, bile salts, urea and fibrinogen) were seen over six weeks culture in sandwich configurations compared with coated plates (Dunn et al., 1991). Identification of stress fibres, using phalloidin staining, showed increased cell stress with hepatocytes cultured on collagen I coated plates after 24 hr, whereas stress fibres were not seen in sandwich culture. Rearrangement of actin filaments, proteins involved in cytoskeletal organisation and connection to the ECM, has also been seen in sandwich culture (Dunn et al., 1991).

Matrigel™ / supplementation of sandwich culture with matrigel™

Substitution of rat tail collagen with EHS sarcoma derived gel (Matrigel™) has increased hepatocyte function beyond that seen with sandwich culture (Moghe et al., 1997). Although a marked difference in rat hepatocyte function was noted between single layered and sandwich culture collagen Type I, similar functions were seen with both single (2.75 x10^8 rat hepatocytes on a 0.5 mL layer of Matrigel™ diluted in DMEM and incubated at 37 °C for 30 min to allow gelation) and sandwich culture (as single layer, with an additional 1 mL layer of Matrigel™ overlayed on the hepatocyte surface 18 hr post-seeding before replacement of media) using Matrigel™ (Dunn et al., 1991, Moghe et al., 1996). Hepatocyte aggregates form in collagen sandwich culture, with flattened morphologies that decrease in surface area with increasing cell seeding densities. Hepatocytes cultured on single layered Matrigel™ comparatively were rounded at low cell densities, with higher seeding densities associated with larger, multicellular aggregates. Furthermore, cell function (albumin secretion) was higher in Matrigel™ cultured cells particularly at lower densities, compared with cells cultured in collagen-sandwich culture (Moghe et al., 1997).

1.5.2.2 Culture in 3D orientations

Various culture methods can result in the formation of cell aggregates including static overlay techniques, spinner flasks or rocking in suspension cultures (Landry et al., 1985, Sakai et al., 1996). Cell aggregate formation is associated with reductions in cell death, thought to result from increased expression of cell adhesion, structural, metabolistic and cell cycle genes (Waring et al., 2003). Over the past four years, increased investments have been made towards organoids, spheroids, liver on chip (LoC) and 3D bioprinting, although further research is required to provide a reproducible, repeatable system capable of high throughput for these to be used as they are (Mehta et al., 2024).

Spheroids

Culturing cells in spheroids can offer several advantages over 2D culture methods including the study of cell-cell interactions, which are more prevalent, extended maintenance of cell function and viability, and the applicability for use in through put workflows. As a result, spheroids are more likely to be suitable for toxicity testing and disease modelling. Spheroids can be created through static overlay techniques, involving culturing cells on non-adherent tissue culture flasks to induce self-assembly. Isolated rat liver cells cultured in this way show spontaneous re-aggregation into spheroids of up to 175 µm in size, that are shown to self-organise into lobular type structures. Furthermore, hepatocytes were shown to secrete and organise ECM components collagen, laminin, and fibronectin (Landry et al., 1985). Initially cells loosely attached, with tight bonds forming within 24 hr indicating formation of cell-to-cell junctions that are morphologically similar to cells seen in foetal tissue. Furthermore, a single-cell layer surrounding the spheroids were indicated histologically to be of mesothelial origin, expressing the same cytoskeletal markers as the Glisson's capsule. The use of hepatocytes spheroids may potentially increase cell scale-up to clinically relevant levels for use in bioartificial devices (Nyberg et al., 2005).

Spheroids have also been created using hydrogels containing matrix components such as ECM-based Matrigel™ or collagen-based Extracel™, with both showing increased cell function and enzyme activity (Moghe et al., 1997, Prestwich et al., 2007). In addition, it was indicated that cell function in Matrigel™ based spheroids may be dependent on matrix derived cues that negate other cues, such as albumin received from cell-cell contacts. A simple morphometric approach was taken to the evaluation of hepatocyte function within this study due to the varying levels of cell-cell and cell-matrix contacts, which is not ideal (Moghe et al., 1997). Further cell-based analysis is therefore warranted. Although advantages of hydrogel use are seen, methods of cell recovery have not currently been identified nor standardised (Godoy et al., 2013, Gómez-Lechón et al., 2014, Soldatow et al., 2013, Dash et al., 2009, Schmelzer et al., 2010, Mueller et al., 2011, Legendre et al., 2013). Cell-cell contact was important in the maintenance of cell function in collagen-sandwich culture, whereas this was not the case for Matrigel™ cultured hepatocytes. In addition, the product is associated with significant batch variations (Dunn et al., 1991). To reduce batch variability, the use of polyethylene glycol (PEG) hydrogels have been developed, with cells cultured under such conditions showing consistent urea synthesis and CYP3A4 activity. Furthermore, hepatocyte function can be increased further with supplementation of poly(lactic-co-glycolic) acid (PLGA), which increased hydrogel

permeability whilst maintaining patternability (Lee et al., 2010). Supplementation with heparin (10% wt.%) has also shown significant improvements in albumin secretion and urea synthesis when compared to hydrogel alone (Kim et al., 2010). Whether this is attributed to better gel porosity or alterations of the matrix stiffness closer to that seen in the native liver (~1500 Pa for native liver vs 2300 Pa in hydrogel) has not been established (Kim et al., 2010). The non-animal based alginate sponge Algimatrix™ reportedly provides a 3D structure that minimally interacts with the hepatocytes, thereby allowing aggregates to form inside the voids. As a result, spheroid cellular aggregates are limited in size to the void within which it occupies, reducing the formation of necrotic centres (Prestwich et al., 2007). Studies suggest that primary rat hepatocytes synthesise a higher level of albumin using Algimatrix™ in comparison with collagen coated 2D surfaces, thereby indicating better cell function (Glicklis et al., 2000). Further comparison of Algimatrix™ and Matrigel™ may aid evaluation of cell-cell and cell-matrix contacts on cell differentiation. Hydrogels infused with liver tissue extracts and growth factors, have indicated successful support of hepatocyte function (albumin secretion and urea synthesis) and proliferation over four weeks (Skardal et al., 2012). Furthermore, the addition of ECM into an injectable hydrogel may provide an additional method for cellular implantation in failing livers, providing a mechanism that could potentially release hepatocytes slowly over time. The additional inclusion of matrix proteins to culture conditions has shown increased cell function (albumin secretion). The high cost in development of high throughput applications and lack of sufficiently comparable data still, presently, limit the use of hydrogels.

Synthetic scaffolds and Microfluidics

Microfluidic devices have the potential to link in the effects of "entire systems" though combination of liver-like systems, with kidney- like systems and similar organ systems, thereby creating an entire body approach to drug testing. The small culture vessels can precisely alter media flow and drug concentration whilst also allowing microscopic evaluation of cell morphology. The potential for these devices in understanding how chemicals can affect the entire body has unlimited potential, although there is much work still to be done in their creation and combination. Along with other synthetic scaffolds such as those made through fibre bonding, phase separation, particulate leaching, melt molding, gas foaming and/or freeze drying, these culture conditions, however, lack necessary hepatocyte attachment motifs and have significantly altered mechanical properties when compared with native tissue. Work detailed in this investigation, therefore, focuses on understanding how to recreate normal hepatocyte function using

natural matrices that contain underlying ECM structures, rather than the enhancement of synthetic structures. Microfluidic devices are not, therefore, covered in this review.

1.6 Use of natural scaffolds

Natural scaffolds can provide a 3D structural environment that is truly representative of the native tissue, or at the very least, are able to provide biological components such as attachment motifs and/or extracellular signalling mechanisms that are not provided using other culture methods. The complex interaction between liver cells and the environment are thought to be essential in regulating and maintaining native hepatic function, therefore, accurate *in-vitro* culturing systems should aim to replicate as many of these as possible (Godoy et al., 2013). Use of natural scaffolds could, therefore, lead to extension and/or maintenance of cell function and viability, aiding in effective long term drug testing and better understanding of cellular replication and organ size, as well as a better understanding of the signalling pathways involved in regulation of matrix protein secretion and pathological disease states. As a result, focus is placed on the use of decellularised liver matrices that already contain the complexity and components of native liver, and potentially leading to developments in a greater range of outputs.
Decellularisation is an attractive technique that involves the creation of a biocompatible ECM scaffold that retains the original tissues structural and architectural microenvironment as well as components required for cell-cell and cell-matrix interactions, biological and biochemical cytokines and growth factors. It should also be noted, that once cells have been removed, the remaining components of the extracellular matrix are similar even though the cells' interaction with the matrix may differ (Statzer and Ewald, 2020, Kular et al., 2014). Optimal decellularisation and sterilisation protocols would remove all cellular and nuclear material whilst retaining the biological activity, ultra-structural components and mechanical integrity of the native matrix (Crapo et al., 2011). The most effective methods employed and/or reagent concentrations used, can vary widely and is affected by tissue density, cellularity and fat content (Gilbert et al., 2006). Commonly used methods use a variety of solutions and concentrations, such as hypotonic and/or hypertonic solutions, Triton X-100 or sodium dodecyl sulphate (SDS) that often employ both physical and chemical treatments (Crapo et al., 2011, Gilbert et al., 2006). To date, research into decellularised matrix development has primarily been aimed towards implantation, for example a decellularised porcine dermal implant used in hernia repair (Permacol™) (Covidien, 2015, Giordano et al., 2015), or a decellularised human skin implant used in breast reconstruction, for example Alloderm® (Lifecell, 2015), with the

number of clinical products increasing dramatically since introduction. Although results have shown positive, or at the very least comparable results to current methods of treatment, more questions than answers have often been highlighted. In complex cases where large and complex abdominal wall repair is required due to previous infection or complications such as seroma formation, fistulas and mesh tearing, the use of decellularised porcine dermal implants have shown comparable morbidity and recurrence rates as those seen in non-complex abdominal wall repair (Giordano et al., 2015). Although pre-pectoral and submuscular breast reconstruction using decellularised dermal matrices were thought not to increase subsequent post-surgery complication rates (Cuomo, 2020), subsequent research has identified potential differences in safety profiles between decellularised matrices which should be factored in when decellularised matrices are used (Diffley et al., 2025).

Biological ECM scaffolds are now being applied in regenerative medicine strategies for both tissue and organ replacement (Crapo et al., 2011). The retained matrices are highly conserved, and therefore well tolerated in both allogeneic and xenogeneic recipients although the structural organisation and biomechanical properties from which the matrix originates varies widely. Optimal decellularisation and sterilisation protocols would remove all cellular and nuclear material whilst retaining the biological activity, ultra-structural components and mechanical integrity of the native matrix (Crapo et al., 2011). The most effective methods employed and/or reagent concentrations used, can vary widely and is affected by the tissues' density, cellularity and fat content (Gilbert et al., 2006). Commonly used methods use a variety of solutions and concentrations, such as hypotonic and/or hypertonic solutions, Triton X-100 or SDS that often employ both physical and chemical treatments, which can damage or disrupt the matrix (Crapo et al., 2011, Gilbert et al., 2006). During decellularisation, cells are initially lysed or pierced, resulting in cell contents distributed amongst the surrounding tissues. This often occurs using physical methods such as freeze thawing that result in the formation of intracellular ice crystals or through the use of hyper and hypotonic solutions that lyse cells through osmotic shock. The use of chelating agents or enzymatic agents, such as ethylenediaminetetraacetic acid (EDTA) and trypsin, may be added to bind divalent metallic ions and cleave peptide bonds, thereby disrupting cellular adhesion to the surrounding matrices and maximising cell exposure. Detergents are often employed to disrupt membrane stability, thereby aiding in cell destruction. Ionic detergents such as SDS achieve this through the solubilisation of cellular and nuclear membranes, whereas ionic detergents, such as Triton X-100 disrupt lipid-lipid and lipid-protein interactions.

The choice, concentration and duration of detergent exposure is a balance determined through the effective removal of cellular and nuclear membranes, and minimisation of ECM damage (Gilbert et al., 2006). Subsequently, cellular and nuclear contents require removal from the tissue, often occurring through the application of mechanical agitation, repeated replacement of solutions and/or enzymatic digestion. The use of mechanical agitation also benefits the distribution of reagents to the cells within a 3D structure. Exposure of cytoplasmic contents to the matrix leads to matrix degradation, although damage can be minimised with the use of protease inhibitors. DNA and RNA levels may be reduced using enzymatic digestion, for example using glycoproteins that catalyse the cleavage of phosphodiester bonds within the DNA or RNA backbone, resulting in smaller nucleotide strands (DNAses and RNAses) (Gilbert et al., 2006). Finally, all chemicals and/or enzymes need to be removed from the decellularised tissue as not to invoke a negative immunological or toxic response upon implantation. Although the work detailed within this thesis is focused on developing methods of re-seeding decellularised liver discs *in-vitro*, indication of the sufficient removal of chemical and/or enzymatic components are not required. The potential scope of decellularised liver discs outside of this thesis may, however, involve transplantation. Therefore, ensuring sufficient removal of chemicals and/or enzymes during protocol development (Chapter 3) has been included as a requirement. This is achieved using osmotically neutral or buffered solutions such as phosphate buffered saline (PBS).

1.6.1 Application of SDS and/or Triton X-100 in porcine liver

Use of either SDS (0.1 %) and/or Triton X-100 (1 %) have been shown to successfully remove sufficient cellular and nuclear components from porcine liver (Mattei et al., 2014). SDS removed sufficient nuclear and cellular detail within three days, although extension of exposure times resulted in significant lobular degradation. In addition, the use of SDS (0.1 %) showed greater retention of fibronectin, laminin and collagen type IV compared with Triton x100 (1 %)(Mattei et al., 2014). Increasing gradients of Triton X-100 (1 %, 2 % and 3 %) has been perfused through the hepatic artery of the porcine liver, followed by 30 min perfusion with 0.1 % SDS to aid in Triton X-100 removal. Although hepatic architecture was maintained, the hexagonal lobular structures could not be identified on images provided. No reports of immunohistochemical staining of native ECM components, DNA quantification or bp length assessment were reported before implantation or seeding and therefore, its success in porcine tissue cannot be effectively reported. It appeared that tissue damage was too great to identify clear structures, although cells were still able to attach to the decellularised porcine liver (Mirmalek-Sani et al., 2013). The use of low

concentrations of SDS have been applied to liver before; through perfusion of increasing gradients SDS, and also through immersion and agitation of liver slices in 0.1 % SDS, with varying levels of success. Increasing gradients (0.25 -0.5 %) of SDS were perfused in the right lobe of porcine liver tissue, and washed with water to remove SDS before crosslinking the tissue with formalin (10 %)(Barakat et al., 2012). H&E staining showed the retention of liver architecture, including central vein and portal triads, with native vasculature intact, determined through vascular corrosion and fluoroscopic examination. Collagen I was seen around the portal triad, collagen Type IV and fibronectin was also seen within the decellularised lobules, albeit less intensely stained than native tissue. The basement membrane stained positive for laminin. Unfortunately, a small number of residual nuclei were reported, indicating that decellularisation was not complete (Barakat et al., 2012). Freeze-thawed (min. 12 hr) decellularised porcine liver was subsequently perfused with increasing gradients SDS (0.01-1 %), followed by a short rinse with Triton X-100 to remove remaining SDS, before being immersed using peracetic acid (0.1 %)(Yagi et al., 2013). Although total DNA content of the decellularised tissue had decreased by 98.8 ±0.8 % (0.04-0.2 $\mu g.mg^{-1}$ dry weight) compared to native tissue (12.12 $\mu g.mg^{-1}$), three of the four lobes tested retained more than the 50 $ng.mg^{-1}$ dsDNA guided for successful decellularisation (Crapo et al., 2011). This may have been achieved, although as the author chose to quantify total DNA, as opposed to dsDNA, the evidence cannot support such conclusions (Yagi et al., 2013, Crapo et al., 2011). Assessment of base pair length was also difficult to assess due to low fluorescence levels seen in native tissue bands, which would result in any lower DNA concentrations difficult to identify. Porcine liver slices have been decellularised using 0.1% SDS alongside mechanical agitation, with successful removal of nuclear (DAPI) and cytoplasmic (H&E) staining and retention of lobular structure. DNA quantification (double stranded, dry weight) of decellularised matrices indicated successful removal (42.5 ±3.21 $ng.mg^{-1}$), with the use of peracetic acid significantly reducing dsDNA content further. In addition, staining was not seen in wells containing decellularised tissue DNA samples after agarose gel electrophoresis, indicating that DNA content was less than 200 base pairs in length (Hussein et al., 2013a). The concentration of DNA loaded into the well was, however, not defined indicating that a low concentration may also have been the cause for a lack of positive staining within the agarose gel. Although the efficacy of perfusing 0.1 % SDS into porcine liver remains questionable, its application through immersion and agitation provides hope. Low concentration SDS does have applicability in the decellularisation of porcine liver tissue although, successful proof in removal of sufficient amounts of dsDNA is limited to liver

slices up to 0.3 cm in thickness. Its use in DNA removal through perfusion of lobes or entire livers has not been evidently reported, and its use in thicker liver tissues has not been applied.

1.7 How does the addition of decellularised matrices affect cells?

Decellularised liver matrices may also be used to supplement synthetic materials with biological components. Lyophilisation of decellularised liver matrices creates powders, or particulates, that can be embedded within synthetic polymers, combining the uniformity and reproducibility of both the mechanical and material properties of synthetic components in addition to providing matrix bioactivity, leading to enhanced cell growth and/or function (Figure 4) (Lee et al., 2014).

Figure 4. Outline of the process to use decellularised matrices as a coating or additive to culture conditions to alter cell function and/or protein expression in 2D and 3D formats. TX-100 = Triton X-100, NH_2OH = hydroxylamine LEM = liver extracellular matrix, HCl = hydrochloric acid. Image taken from (Lee et al., 2014).

Hepatocyte adhesion, viability and function (albumin secretion and urea synthesis) was notably greater in liver matrix coated plates compared with collagen I coated plates, and Matrigel™ coated substrates (Lee et al., 2014). Live dead staining of primary rat hepatocytes cultured on decellularised liver matrix-coated plates (0.2mg.mL^{-1}) enhanced rat hepatocyte viability at day seven compared with rat hepatocytes cultured on standard culture plates, or those coated in collagen I only. Furthermore, cell adherence as well as albumin secretion and urea synthesis were also enhanced when cells were cultured on matrix coated plates (Lee et al., 2014). Although albumin secretion peaked at day three in all groups, urea synthesis reduced throughout the seven-day culture period in all groups indicating that function may not currently be retained beyond seven days. Increase in primary rat hepatocyte adherence and viability were also shown when higher concentrations of liver matrices were used (2mg.mL^{-1} vs 0.2mg.mL^{-1}) (Lee et al., 2014). In addition, specific use of decellularised liver matrices, as opposed to decellularised

matrices from other tissues, resulted in greater primary rat hepatocyte adherence (Lee et al., 2014). Supplementation with decellularised matrices therefore indicates an increase in hepatocyte adherence, viability and function, and when additionally combined with 3D arrangements and/or higher concentrations, hepatocyte viability and function can be increased/extended even further. Hydrogels infused with liver tissue extracts and growth factors have indicated successful support of hepatocyte function (albumin secretion and urea synthesis) and proliferation over four weeks (Skardal et al., 2012). Furthermore, the addition of ECM into an injectable hydrogel may provide an additional method for cellular implantation in failing livers, and through time-based gel degradation, may provide a longer-term mechanism that could potentially release hepatocytes slowly over time. Subsequent perfusion of decellularised rat liver scaffolds with hepatocyte cell suspensions for five days have indicated the retention of *in-vitro* levels of liver specific functions including albumin secretion, urea synthesis, and cytochrome P450 expression when compared with static sandwich culture (Uygun et al., 2010). LDH release, a sign of membrane damage, was low across all timepoints with similar levels seen in sandwich culture and approximately 20 % cells apoptotic on day two (TUNEL staining). Although urea secretion was seen to be higher in hepatocytes present in recellularised grafts than those cultured in sandwich, albumin levels were comparable between the two, both of which were lower than that seen in native adult rat liver. Successful transplantation of these recellularised grafts into rats for eight hr showed hepatocyte survival and function (albumin and urea) alongside minimal ischaemic damage (TUNEL staining). The retention of native tissue architecture allows for better blood and oxygen transport throughout the tissue, and minimal hepatocyte damage. Functional levels, however, reported no universal advantage over hepatocytes cultured in sandwich orientations. It must be noted, that this study was completed within five days, providing only short-term information on cell activity and function. Further monitoring of functional levels over longer time periods are required (Uygun et al., 2010). Implantation of a recellularised scaffold containing sufficient volume of liver cells (10 % total liver cell number) into hepatectomised (90 %) rats extended mean lifespan from 16 to 72 hr with viable, functional hepatocytes seen in the transplanted tissue engineered liver (TEL) 72 hr post operation (Bao et al., 2011). Although mean lifespan was extended, this did not occur indefinitely. Ammonia levels continued to rise, albeit slower, in those rats transplanted with tissue engineered liver compared with control rats, with TEL implanted rats displaying small-for-size syndrome and portal hypertension, complicated by gastrointestinal congestion and ascites that were more severe in the TEL implanted group, as opposed to the normal liver grafted group.

Transplantation of TEL grafts therefore are a short-term option only. Whether this is a result of the implantation of cell spheroids, as opposed to isolated cells, or whether this resulted from the addition of thrombin to the decellularised tissue is not clear. Nevertheless, the potential short-term applicability of these graft types shows promise.

The positive response to the addition of decellularised liver matrices does not only apply to primary hepatocytes, but also to hepatic human adult derived stem cells (hADSCs). hADSCs cultured on decellularised liver matrix coated plates were shown to partly differentiate within 21 days, with increased marker expression of hepatic lineage genes including HGF, α1- antitrypsin and albumin detected using qRT-PCR (Lee et al., 2014). The use of decellularised tissue may, therefore, provide environmental conditions that enhance cell adherence, viability and function in mature cells and aid cell differentiation in immature cell types. Hepatocyte attachment and cellular adaptation occurs through the induction of specific intracellular signalling pathways that cannot be replicated easily. In addition, the ECM provides an important structural framework for cellular attachment and migration, and alters cellular differentiation, and directs repair and development (Reid et al., 1992, Martinez-Hernandez and Amenta, 1993, Schuppan et al., 2001). As a result, the use of native liver matrices, where the environmental conditions are already close to those found in-vivo, is advantageous.

1.8 Recellularisation of decellularised matrices

Three methods to recellularise decellularised liver tissue have been compared; direct injection within multiple lobes, continual perfusion using native vasculature and multi-step perfusion using native vasculature of hepatocytes (10-50 $x10^6$ cells.mL^{-1})(Soto-Gutierrez et al., 2011). Rates of proliferation (% Ki-67 positive nuclei) ammonia metabolism (% removal $x10^6$ cells) and CYP1A2 activity (pmol.min.$x10^6$ cells) were varied. Multistep perfusion provided a greater cell attachment rate (86.0 ±5.0 %) than that seen with continuous perfusion (69.0 ±9.0 %) or injection (12.6 ±9.0 %) (Soto-Gutierrez et al., 2011). Engraftment rates were similar between those perfused at different flow rates (1 $mL.min^{-1}$ vs 2$mL.min^{-1}$ (Ren et al., 2013, Soto-Gutierrez et al., 2011), indicating that small changes in flow rate do not play a large factor in hepatocyte engraftment. Initially, cells attached to larger vessels and subsequently moved to surrounding structures / vessels (Ren et al., 2013, Uygun et al., 2011), with some evidence of proliferation seen, albeit low amounts (3.0 ±0.6 %) (Soto-Gutierrez et al., 2011). After seven days culture, albumin expression was highest in those tissue reseeded using multi-step infusion, followed by continual perfusion and direct injection, however, no differentiation was reported

regarding cell numbers. The difference in albumin expression could, therefore, be a reflection of cell number, or cell activity (Soto-Gutierrez et al., 2011). The application of flow is not, therefore, the only indicator of cell activity. Static seeding of decellularised heart valve leaflets with porcine fibroblasts showed differing morphologies based on seeding density. Lowest seeding densities (low = 1 x10^3 – 1 x10^4 cells.cm^2) were associated with spread morphologies and sparse cell distribution, whereas higher densities (medium = 5 x10^4 cells.cm^2) provided confluent monolayers. Cell densities higher than this (high = 1 x10^6 cells.cm^2) formed multiple, dense cell layers on the peripheral surfaces, with large amounts of unattached cells and cellular debris seen (Wilcox et al., 2005). Medium cell densities migrated around the disc surface to form a monolayer within two weeks culture and migrated towards more central tissue areas within four weeks (Wilcox et al., 2005).

1.9 What are the relative merits of the various cell types when re-seeding decellularised matrices?

Multiple cell types can be seeded on to decellularised matrices however certain characteristics are required; they should attach to, proliferate on / in and become functional / differentiate after seeding has occurred. The best cells would be hardy enough to withstand seeding, proliferate quickly to rapidly populate an area and become functionally reflective of native conditions once the tissue is repopulated. Finding a cell that has all these properties, and at the right times to facilitate repopulation, is not simple.

1.9.1 Primary hepatocytes

Within the literature, three main species have been investigated for use in liver decellularisation and re-seeding; human, murine and porcine hepatocytes. Cell types can be broadly classified into three types; fully differentiated hepatocytes of either the same or different species as the original tissue from which the scaffold was generated, mesenchymal stem cells (MSCs), immature cells or those of a progenitor phenotype and fully differentiated cell lines.

1.9.1.1 Human

Although primary human hepatocyte culture is widely used as a tool to study drug transport, metabolism and/or toxicity there are limits in cell efficacy and longevity. High donor variability in hepatocyte function, short functional culture periods, and limited maintenance of cell function associated with the loss of differentiation, is evident (Guguen-

Guillouzo and Guillouzo, 2010). Human hepatocytes are routinely cultured as a monolayer on collagen-coated 2D surfaces, with conditioned medium. Cells cultured this way have been shown to retain cell function through production of albumin and urea as well as cytochrome P450 activity, however rapid decline of cell function occurs within one week in culture (Godoy et al., 2013). Cell function and polarity can be maintained further through the addition of a second layer of collagen in a sandwich culture (Dunn et al., 1989, Dunn et al., 1991), inducing the formation of lateral and apical membranes (Taguchi et al., 1996). Static culture of human hepatocytes on decellularised porcine liver discs, however, have shown significant increases in hepatocyte function (albumin secretion detected via ELISA) and number from seven days up to 21 days in culture, greater than hepatocytes cultured on polystyrene culture plates and/or on collagen sandwich plates (Lang et al., 2011). Interestingly, however, hepatocytes formed layers on top of the matrices and did not penetrate within the tissue, with no significant movement seen even though over 90 % hepatocytes were viable (Live/dead stain) (Lang et al., 2011). Hepatocytes from other species have also been investigated due to wider availability, with decellularised tissue from the same, and other, species as the cells of interest representing allogeneic and xenogeneic comparators respectively. Although primary human hepatocytes are preferred, the lack of appropriate cell numbers, reduced cell function post hepatocyte isolation, alongside low engraftment rates and significant batch variability, make the effective use of primary human cells in 3D culture limited at present.

1.9.1.2 Murine

Increased adhesion, viability and function have been shown after seeding of rat hepatocytes on rat ECM coated plates (allogeneic), irrespective of 3D arrangement (Lee et al., 2014) (Table 4). Hepatocyte adhesion was significantly increased with rat ECM (0.2 $mg.mL^{-1}$) or collagen I coated plates (0.2 $mg.mL^{-1}$) when compared with poly-L-lysine coated polystyrene plates (PS coated). Cell adhesion and viability was, however, greater with rat ECM coated plates after one day, with functional activity (albumin and urea secretion) increasing further at seven days. Furthermore, seeding of rat hepatocytes on hydrogels supplemented with decellularised rat liver showed greater adhesion at day one and comparable viability at day three, when compared with seeding on Matrigel™, a basement membrane matrix obtained from mouse sarcoma cells. This suggests that liver specific ECM contains select adhesion proteins that are not seen in other ECM based gels, and that hepatocyte viability and function can also be enhanced with the use of liver specific ECM tissue components when culturing in 2D (Lee et al., 2014). Results therefore

Table ~~4~~2. Available literature summarising current methods used to seed rat hepatocytes on decellularised liver tissues. N/A = not ~~a~~applicable/reported. Initial functionality = seven days or less. Longer term = longer than seven days. SDS = sodium dodecyl sulphate, TX-100 = Triton X-100, ECM = extracellular matrix

Author	Decellularisation		Cell delivery		Rat hepatocytes	Engraftment Rates	Cell viability	Functionality		Other
	Species tissue	Physical parameters	Method	Route				Initial (up to 7 days)	Longer term (7 days plus)	
Ren 2013	Murine (Rat)	Organ	Multi-step perfusion	Portal vein, 1mL.min^{-1}	Rat hepatocytes	89.7 ±5.1% for SDS and 90.6 ±5.7% for TX-100	N/A	**Up to 4 days**: Hepatocytes attached to larger vessels and surrounding parenchyma. Function was higher in hepatocytes cultured on ECM vs control	No long term studies performed	
Lee 2014	Murine (Rat)	Organ	Plate coated with ECM powder	Coating on culture plate	Rat hepatocytes	N/A	Significantly greater than controls	Heptocytes adhesion, viability and function significantly hgher with liver specific ECM coating	No long term studies performed	Increase in adhesion, viability and function were all concentration dependant
			3D hydrogel	Encapsulated		N/A	Significantly greater than controls	Significantly higher viability and function in ECM supplemented gels vs collagen I hydrogel	No long term studies performed	
Uygun 2011	Murine (Rat)	Organ	Multi-step perfusion	Portal vein	Rat hepatocytes	95.6 ±3.4%	<20% apoptotic at day 2	**4-48 hr**: Most cells remain in and around vessels and distrbute through the matrix. **5 days**: Higher albumin and urea secretion compared to sandwich culture, comparable drug metabolising enzyme levels	**10 day:** comparable albumin and urea secretion, alongside bile synthesis when compared to static sandwich culture	
Lin 2004	Porcine	5mm thick sheet	Culture on ECM sheet	Sheets 5mm	Rat hepatocytes	N/A	N/A	Hepatocytes showed less surface area attachment on ECM sheet compared to those cultured on plates / sandwich culture.	Scaffold remained viable for 35 days with significant remodelling seen. Albumin secretion highest in sandwich culture, then on ECM with single layer collagen lowest.	Significant variation in function seen between liver ECM.
Soto-Gutierrez 2011	Murine (Rat)	Organ	Injection	Injected into lobes	Rat hepatocytes	12.6 ±9.0%	N/A	Hepatocytes attached around vessels, followed by surrouding vessels. Similar expression to native liver	**7 days**: Albumin secretion = 6.0 ±0.2 µg.mL^{-1}.	
			Continuous perfusion	Portal vein, 2mL.min^{-1}		69.0 ±0.5%	N/A	Hepatocytes attached around vessels, followed by surrouding vessels. Lower albumin expression compared to native liver	**7 days**: Albumin secretion = 8.7 ±0.3 µg.mL^{-1}.	
			Multi-step infusion	Portal vein, 2mL.min^{-1}		86.0 ±5.0%	N/A	Hepatocytes attached around vessels, followed by surrouding vessels. Similar expression to native liver. 3.0 ±0.6% hepatocytes proliferating	**7 days**: Albumin secretion = 16.5 ±1.8 µg.mL^{-1}. Much greater CYP activity seen with this method also, compared to other methods tested.	

indicate that allogeneic cell / matrix combinations can enhance cell function in both 2D and 3D applications. Obtaining an entire decellularised rat organ can be easily achieved due to the small organ size, with literature showing multi-step perfusion to be the most common method for subsequent seeding (Soto-Gutierrez et al., 2011, Uygun et al., 2011, Ren et al., 2013), although continuous perfusion and injection-based methods have also been applied (Soto-Gutierrez et al., 2011). Although seeding of rat hepatocytes on 5 mm thick decellularised porcine ECM sheets initially showed decreased hepatocyte function, with similar decreases in cell function seen in comparative methods (sandwich culture and collage I coated plates), function was, however, maintained for between 12 to 25 days in culture (~7µg.day), after which, function significantly increased for the remaining culture period (35 days total)(Lin et al., 2004). Results indicated that the use of a collagen layer alone was insufficient to retain hepatocyte function, whereas the xenogeneic decellularised liver was able to extend cell function long term. It should also be noted, however, that significant variability of seeding efficiency was seen between repeated experiments (n=8), possibly resulting from the variation in location of seeding, tissue topography, function of isolated primary cells or animal to animal variability. The cause of which is not known. The use of liver specific ECM shows good cell adhesion and cell viability with the potential to enhance cell function over longer times, even where matrices differ in original species compared to the hepatocyte species cultured. Only one study seeded hepatocytes on porcine tissue decellularised using Triton X-100, and over time frames longer than other studies using decellularised rat liver.

1.9.1.3 Porcine

Seeding of primary porcine hepatocytes on decellularised porcine liver tissue using a multistep perfusion-based method resulted in a 74 ±13 % engraftment rate. Higher levels of albumin expression, and both albumin and urea secretion were seen within four days when compared with hepatocytes seeded on a single layer of collagen, however, increased function was not maintained up to seven days in culture. Furthermore, at day seven almost half of cells (47.8 ±5.4 %) were apoptotic. Although this data suggests an initial positive cellular response upon seeding on decellularised porcine liver, long term functional retention was not seen (Table 5). Although functional levels of rat (Section 0) and porcine (Section 0) hepatocytes on decellularised porcine liver are initially greater

Table ~~3~~ 53. Available literature summarising current methods used to seed human and porcine hepatocytes on decellularised liver tissues. N/A = not applicable/reported, ECM = extracellular matrix

Author	Decellularisation		Cell delivery		Human hepatocytes	Engraftment Rates	Cell viability	Functionality		Other
	Species tissue	Physical parameters	Method	Route				Initial	Longer term	
Skardal 2012	Porcine	ECM supplemented hydrogel / media	Culture on ECM coated surfaces or ECM supplmented media	ECM sheets 3mm / ECM supplemented media	Human hepatocytes	N/A	N/A	N/A	Of all the hydrogel variations tested, only the heparin conjugated, hyaluronic acid gel containing ECM and growth factors successfully supported hepatocyte proliferation and function over 4 weeks	Can create intercnnected hepatocyute multicellular structures that are stable and remain viable. ECM supplemented gels outperformed ECM supplemented media.
Lang 2011	Porcine	3mm slices cut in to 10-15mm diameter discs	Culture on ECM discs	Pippetted onto centre, static culture	Human hepatocytes	N/A	>90% cells viable at day 21	Number of cells did not change for 2 weeks	Significantly greater cell numbers seen at day 21 compared to comparators. Cells present on, not in, tissue. Significantly higher albumin levels secreted, and stable over 3 weeks compared with collagen gels / polystyrene plates	
Yagi 2013	Porcine	Organ	Multi-step perfusion	Portal vein, 4 $mL.min^{-1}$	Isolated porcine hepatocytes	74 ±13%	6.6 ±2.7% at day 1, 21 ±8.6 % at day 4, 47.8 ±5.4% at day 7	Hepatocytes present in parenchyma and producing albumin at days 4-7	Albumin staining decreased after day 7, although higher than collagen cultured comparator	Sandwich culture showed greater albumin and urea secretion

than that seen with other culture techniques, these are shown not to be maintained long-term (Yagi et al., 2013, Lin et al., 2004). With human hepatocytes, however, both cell number and function are greater when cultured on porcine liver tissue as opposed to collagen sandwich or polystyrene culture plates. Whether this difference is attributed to cell species, and/or seeding and culture method is yet to be determined. Hepatocyte growth into interconnected, multi-cellular structures has been shown to successfully support hepatocyte viability, proliferation and consistent cell function (urea and albumin secretion) over four weeks (Skardal et al., 2012). Results indicate that the inclusion of matrix proteins such as collagen or heparin-modified hyaluronic acid form interconnected hepatocyte structures, with inclusion of ECM derived extracts or gels resulting in the enhanced maintenance of cell number and longevity. Although the use of hyaluronic acid alone did not support the formation of interconnected structures, its conjugation with heparin within ECM supplemented hydrogels resulted in the formation of large interconnected structures that remained stable over four weeks (Skardal et al., 2012). Larger concentrations of multiple growth factors including EGF & HGF were also seen in decellularised liver extracts (17.74 vs 0.93 $pg.mL^{-1}$ and 17.45 vs 0.00 $pg.mL^{-1}$ respectively), when compared with liver tissue extracts. From these results it can be concluded that liver ECM contains additional factors, over collagen alone, that can stabilise structures resulting in enhanced hepatocyte longevity (Skardal et al., 2012). The culture of human hepatocytes on decellularised porcine liver has also shown a retention of >90 % viability after 21 days culture (Lang et al., 2011). Although cells did not increase in cell number for the first two weeks of culture, increases were seen after 21 days even though limited cell permeation was seen. Albumin secretion (per $x10^4$ cells) also remained stable for two weeks and significantly increased at day 21 (Lang et al., 2011). Through evaluation of multiple hepatocyte species, it is thought that cell activity and/or function may increase if cell viability is maintained beyond three weeks culture.

1.9.2 Cell lines

Unlike primary human hepatocytes, the use of cell lines provides an almost unlimited supply of cells and repeatability of results. Furthermore, hepatoblastoma derived cell lines, such as HepG2 have overcome the limited functionality and reduced number of isolated cells associated with the use of primary human hepatocytes. The tumour derived cell line C3A, derived from HepG2, is currently used within the ELAD bioartificial liver, however, there are concerns over the effectiveness of this cell line, with reduced enzyme

activity, amino acid metabolism and urea cycle activity seen, possibly resulting from reduced expression of the urea cycle genes. Furthermore, concern over viral zoonotic transmission, for example porcine endogenous retro virus (PERV) or SARS-Cov-2 has limited the use of cell lines to extracorporeal devices only, even though no evidence of transmission has been reported (Zhang et al., 2006, Maggi et al., 2020). As a result, attempts to immortalise non-tumour derived foetal hepatocytes have been made with some success. HepCL cells have been used to treat acute liver failure, with results indicating similar function when compared with primary human foetal hepatocytes (Chen et al., 2010). The use of cell lines in a multi-co-axial hollow-fibre BAL device has also shown limited duration due to the deposition of ECM and other cell components which pollute and clog the device, leading to nutrient blockage, cell death, and subsequent device failure (MacDonald et al., 2001). Although this may be attributed to the use of cell lines in particular, the applicability could also be attributed to many other causes including type of media flow and/or speed, pore size, membrane material, as well as cell type.

Seeding of HepG2 cells, a tumour derived cell line derived from the liver of a 15 year old Caucasian male, has occurred on both decellularised porcine (Mirmalek-Sani et al., 2013, Lang et al., 2011) and rat livers (Zhang et al., 2009). With the use of porcine sheets of different depth, HepG2 have shown minimum tissue penetration in tissue of lower depth (1mm) and multilayer penetration on depths of 3mm (Mirmalek-Sani et al., 2013, Lang et al., 2011), although comparison of static and dynamic culture conditions were shown to affect the amount of cell penetration (Lang et al., 2011). When decellularised liver matrices were implanted into the subcutaneous adipose tissue of rats, no fibrous encapsulation of scaffolds were observed and host cells populated the matrices throughout the 28 day culture period. The decellularised tissue appeared not to be, or release, cytotoxic components over 28 days culture. The insertion of decellularised scaffolds within a living model, in the presence of flow conditions was associated with increased cell movement (Mirmalek-Sani et al., 2013). When HepG2 were cultured on rat ECM coated plates, increased HepG2 adhesion and number were seen within four days and HepG2 function at 14 days culture (Zhang et al., 2009). Although HepG2 are often used instead of primary hepatocytes due to the low cost and ease of culture, key enzymes involved in drug metabolism are expressed in low amounts, or are absent, making this cell type unusable in drug toxicity or metabolism studies (Guo et al., 2011). Other cell lines, however, may be more applicable. Results indicate that the seeding of cell lines may be a viable alternative to primary hepatocytes due to increased cell numbers and functions

seen with the use of dynamic culture conditions, with only 14 days until changes in function are seen compared to 21 days with hepatocytes of various species.

1.9.3 Foetal / immature cell types

Although hepatocyte cell lines and primary hepatocytes have been shown to adhere to, proliferate and become functional on decellularised liver tissue, the ECM has also been shown to aid in cell maturation. Use of these cell types may help provide a better understanding of organ development and regeneration. Two studies using rabbit or mouse MSCs have shown adhesion and proliferation within two days when immersed and agitated, and increased liver specific cell function within seven days when perfused through mouse MSC seeded decellularised mouse livers (Jiang et al., 2014), and within 21 days when rabbit MSC seeded decellularised porcine liver tissue was immersed and agitated (Mansilla et al., 2007) (Table 6.). Both species of MSC differentiated into cells that express liver specific cell markers. Seeding of other immature cell types has been investigated, with human foetal stellate cells (Hfscs) and human foetal hepatocytes (Hfh) perfused in to decellularised porcine liver through both portal and hepatic veins at 1.5 $mL.min^{-1}$. Engraftment efficiencies of both cell types indicated >90 % engraftment , with cells present in portal and hepatic veins by day three, and around large vessels and surrounding tissues at day 13. Around 40 % cells were proliferating (Ki-67 positively labelled), the majority of which were located at proximal sections and in Hfh. Those cells in more distal areas showed greater levels (30 %) nuclear damage when compared to more proximal areas, as determined by TUNEL staining (Barakat et al., 2012). Maturation of Hfh was shown throughout the culture period. Approximately 70 % Hfh stained positive for albumin and were located alongside areas of increased glycogen deposition and CYP3A4 staining. In addition, decreased staining for the foetal hepatoblast marker AFP was also seen. Cell morphology was similar between seven and-13 days, with no morphological evidence of bile duct formation seen. Cells were rounded with a high nuclear:cytoplasmic ratio, positively staining with the liver specific intermediate filament protein CK18. Results indicated that hepatocytes were able to proliferate and differentiate within the decellularised tissue, however, increased distance from the media source was associated with increased apoptosis. Seeded Hfh were also shown to be functional after seeding showing increased cell function over time, however, reductions in albumin staining indicated that cell viability could not be maintained for 13 days (Barakat et al., 2012). Seeding of human stem cells on decellularised rat liver also showed quicker cell

Table 64. Available literature summarising current methods used to seed immature cell types and hepatocyte cell lines on decellularised liver tissues. N/A = not applicable/reported, ECM = extracellular matrix. HfH = human foetal hepatocytes, HSC = hepatocyte stem cells.

Author	Decellularisation		Cell delivery		Immature cell	Engraftment Rates	Cell viability	Functionality		Other
	Species tissue	Physical parameters	Method	Route				Initial	Longer term	
Jiang 2014	Murine (Mouse)	Organ	Multi-step perfusion	Portal vein, 1mL.min^{-1} 60 mins	Mouse MSC	N/A	N/A	Signficantly higher cell function after7 days compared to culture dish	Signficantly higher cell function after 4 weeks compared to culture dish	Differentiated into cells expressing hepatocyte markers
Mansilla 2007	Porcine - immature	Lobe	Immersion and agitation	1cm^3 cubes	Rabbit MSCs	N/A	N/A	Adhesion and proliferation after 2 days	Differentiation of cells that expressed liver specific markers at day 21, not present in fibrin comparator	Differentiated into cells expressing hepatocyte markers to day 21
Barakat 2012	Porcine	Organ	Continuous perfusion	Portal vein and hepatic artery	HfH, HSC	>95%	<30% apoptotic at 13 days, particularly in distal sections	Increase in albumin secretion over 3 days	Increased metabolism and decrease in media oxygen concentration. Increased albumin secretion not maintained up to 13 days	40% (HfH) and 20% (HSC) cells proliferating after 13 days, particularly in proximal areas
Wang 2011	Murine (Rat)	Organ	Perfusion	Portal vein	Human hepatocyte stem cells	"essentially 100% of viable cells"	N/A	Stem cells divided "once or twice" and transitioned into cell cycle arrest, and into 3D cord-like morphologies typical of mature parenchymal cells, including cell specific genes for hepatocytes or cholangiocytes.	Cultures remained morphologically stable and functional for eight weeks	Quicker attachment to matrices compared with collagen type I
Mirmalek-Sani 2013	Porcine	Organ	Static seeding and culture	1mm sheets, 15mm diameter	HepG2	N/A	No apoptotic markers seen at day 7 or 21 (TUNEL)	Cells seen attached to matrix surface, and minimal penetration seen.	Dense cell layers seen at 21 days culture. Images show cell presence in outer parenchymal tissue	
Lang 2011	Porcine	3mm slices cut in to 10-15mm diameter discs	Culture on ECM discs, with agitation	Pippetted onto centre	HepG2	N/A	N/A	Unifrom multi layer constructs formed	Culture up to day 12 similar to that at earlier time points	Dynamic culture conditions resultsed in greater cell penetration into discs
Zhang 2009	Murine (Rat)	Organ	Plate coated with ECM powder	Coating on culture plate	HepG2	N/A	N/A	ECM markedly enhances cell adhesion, with no tissue specificity	After day 4, cell types proliferated best on ECM derived of its own origin and showed cell specific morphology and marker expression for up to 14 days	DAPI staining showed presence of whole nuclei

attachment when compared with collagen I based cultural methods, with cells dividing "once or twice" before cell cycle arrest was seen, with 3D cord like orientations typical of the native liver were seen, very similar to that seen with acute liver injury. Seeded structures lost immature cell markers (EpCAM and CXCR4) and increased expression for markers of mature liver cells, such as urea and cytochrome P450. In addition, seeded cells remained stable and functional for eight weeks, versus two weeks seen with HpSCs cultured on collagen I (Wang et al., 2014). HepG2 cells were also seeded to assess viability, growth and proliferation on porcine liver decellularised using six different methods (water, PBS and salt-based solutions, with and without peracetic acid) (Wang et al., 2014). Twelve days culture resulted in the formation of multiple cell layers on the decellularised matrix, with cell penetration only seen on water washed liver ECM structures. Although cell proliferation was initially reduced on matrices decellularised using water, proliferation rates significantly increased over time when compared with other decellularisation methods, indicating that the method of decellularisation can affect proliferation rates. Furthermore, it was also reported that the addition of peracetic acid often resulted in lack of cell growth (Lang et al., 2011). The removal of peracetic acid wash steps, however, results in increased risk of contamination and should not be considered unless necessary. Interaction between hepatocytes and neighbouring cells, such as LSECs, reportedly alters hepatocyte growth, migration and/or differentiation, stabilising adult hepatocyte phenotype. These alterations are thought to result from cell signalling and interactions between cells. Studies of the role of cell types during repair and regeneration in both foetal (HHyP) and adult liver hepatobiliary precursors has been studied using single cell RNA sequencing, and highlights the important role of YAP, part of the Hippo signalling pathway, with upregulation of YAP resulting in the induction and maintenance of cell proliferation during liver injury (Saviano et al., 2020). During chronic damage, hepatocyte damage results in the production of cytokines and chemokines from inflammatory cells, and signals for hepatic stellate cells to form myofibroblasts, resulting in increased deposition of ECM and formation of fibrotic lesions, which are one of the defining histological features of liver damage (Saviano et al., 2020). LSECs secrete proteins involved in cell:cell interaction, regulate organ function and homeostasis and cell regeneration. Interactions of HSC and LSECs with non-parenchymal cells

were found to be wide ranging. LSECS for example were found to upregulate genes responsible for lipid metabolism, antigen presentation and release of chemokines, as well as decreased expression of other genes involved in vascular development and homeostasis (Saviano et al., 2020). Interactions between monocytes and LSECs are also critical in determining the differentiation of monocytes into macrophages and provide a means for monocyte entry into the liver lobules. Other cell interactions defined from RNA sequencing are summarised by Saviano et al (2020).

The use of cell lines provides an almost unlimited supply of cells and repeatability of results. Furthermore, tumour derived cell lines, such as HepG2, have overcome the limited functionality and reduced number of isolated cells associated with the use of primary human hepatocytes. The human cell line C3A is currently used within the ELAD bioartificial liver, however, there are concerns over the effectiveness of this cell line, with reduced enzyme activity, amino acid metabolism and urea cycle activity seen, possibly as a result of reduced expression of the urea cycle genes. Furthermore, concern over disease transmission has limited the use of cell lines to extracorporeal devices only, even though no evidence of transmission has been reported (Zhang et al., 2006, Ellis et al., 1996, Millis et al., 2002). As a result, attempts to immortalise non-tumour derived foetal hepatocytes have been made with some success. HepCL cells have been used to treat acute liver failure, with results indicating similar function when compared with primary human foetal hepatocytes (Chen et al., 2010).

1.9.4 Cell co-culture

Although hepatocytes provide the majority of cell function, there are still a lot unknown regarding the interplay between cell types within the liver which has yet to be understood. Co-culture has also shown improvements in expression of both phase I and II enzymes and remains higher after drug induction. Cell:cell contacts are improved alongside cell polarity and formation of bile canaliculi, which extended cell viability. Once again, however, high variability between vell viability and differentiation is observed (Guguen-Guillouzo et al., 1983, Inamori et al., 2009). Co-culture of the rat epithelial cells (type not stated) with human

hepatocytes resulted in high albumin secretion, hepatocyte survival for over two months and secretion of new matrix components, particularly collagen type 3 (Clement et al., 1984). An additional study using foetal hepatocytes also showed increased albumin secretion, and matrix components were deposited between the two cell types and included collagen III, and

also fibronectin (Guguen-Guillouzo et al., 1983). The time at which endothelial cells were added altered the level of albumin secreted, with four hr seeding showing greatest values, and co-culture seeding showing both enhanced and extended levels of albumin secretion. Amount secreted however, was shown to decrease between nine and 11 days after making their efficacy short lived (Guguen-Guillouzo et al., 1983). Even though co-culture of liver specific cells seems highly preferable, the specific needs of each cell type must still be met to ensure cell function and survival, making this process highly complex to undertake. Furthermore, the lack of high throughput methods and substantial variability between labs do not match the requirements of the pharmaceutical industry to make co-culture-based methods viable and more work is required. The advantages of co-culture could aid in the maintenance of cell function long term, and/or the regeneration capacity of the liver as seen in-vivo, however, presently developments with single cell culture are required first.

~~Culture in 2D~~

~~{Elaut, 2006 #1178}{Godoy, 2013 #89}{Gissen, 2015 #1180} When cultured in conventional 2D conditions, hepatocytes aggregate and form bile canalicular structures. Early phenotypic alterations are seen even though cells survive for only a few days, even on collagen IV coated plates {Waring, 2003 #693}(See Figure 3), which has been noticed in other species also. Rat hepatocytes, for example, lose expression of the sodium taurocholate co-transporting polypeptide NTCP mRNA (<27 % mRNA expression and 48 % protein expression) after 24 hr culture, with subsequent taurocholate uptake reduced to 5 % after 72 hr culture, even when cultured on collagen-coated plates {Rippin, 2001 #963}. Results indicate that bile acid homeostasis and circulation of bile acids is affected within 24 hr. Similar reductions in other transport proteins including Oatp1a1, Oatp1a4, MRP2 on basolateral membranes and BSEP in the apical membranes have also been seen {Rippin, 2001 #963}. Loss of these functional transporter proteins is also associated with an increase in proliferating markers such as MRP1 in hepatocytes {Roelofsen, 1997 #957}. Hepatocyte-like gene expression from hepatocytes cultured on 2D plates is, however,~~

~~better maintained than those cultured in suspension. Extraction of total RNA (Qiagen Oligotex mRNA kit) and subsequent mRNA microarray analysis identified increased expression of twenty-nine genes in hepatocytes cultured on collagen coated plates compared with those cultured in suspension, with many of the genes involved in cell structure, metabolism and cell cycle regulation, such as actin α4, CK18, Apolipoprotein E and Adenine nucleotide translocator-2. Furthermore, cells cultured *in-vitro* displayed lower expression of various cell adhesion, cell cycle regulation and cell metabolism genes compared with liver tissue, including fibronectin 1, CYP 3A4 and α1-antichymotrypsin {Waring, 2003 #693}.~~

~~Monolayers of hepatocytes cultured on collagen-coated 2D surfaces often use cell conditioned medium that contain cell secreted proteins. Retention of hepatocyte function can be monitored through production of albumin and urea as well as cytochrome P450 activity for a short period, however, is followed by a rapid decline in cell function within one week {Godoy, 2013 #89}. Even though retention of hepatocyte function is retained for longer when cultured on collagen coated plates, as opposed to in suspension, hepatocyte polarity and morphology are altered with function, phenotype and lifespan reduced when compared with native conditions {Wells, 2008 #203;Soltys, 2010 #192;Gomez-Lechon, 1998 #94}.Hepatocyte function can be extended in various ways; for example through the addition of chromatin remodelling agents such as DMSO (dimethylsulfoxide) or trichostatin A, through the use of highly specialised media such as Lanford's medium, or through the use of Matrigel™ or sandwich configurations {Isom, 1985 #634;Henkens, 2007 #635;Ferrini, 1997 #637;Dunn, 1989 #22;Guguen-Guillouzo, 1983 #639;Clement, 1984 #640}. Cell density has also been shown to modify cell behaviour through the Hippo~~

signalling pathway, which centres around a kinase signalling cascade. Cell density regulates the phosphorylation, and therefore location, of the YAP/TAZ bound protein complex.{Pocaterra, 2020 #1177} {Zhao, 2007 #1145}Multiple cell types (3T3, MCF10A) have shown increased nuclear expression of YAP when seeded at low density, with high densities associated with cytoplasmic YAP {Zhao, 2007 #1145}. Phosphorylation of LATS results in the transference of the YAP/TAZ complex out of the nucleus and into the cytoplasm, where it is either retained or degraded. When non-phosphorylated, the interaction of TEAD and the YAP/TAZ complex leads to increased transcription of genes that enhance cell growth and inhibit apoptosis {Koontz, 2013 #1162}. Efficiency of tissue repopulation and distribution is affected by cell attachment, with better cell distribution and adhesion occurring within initial time of seeding. Computer modelling of human

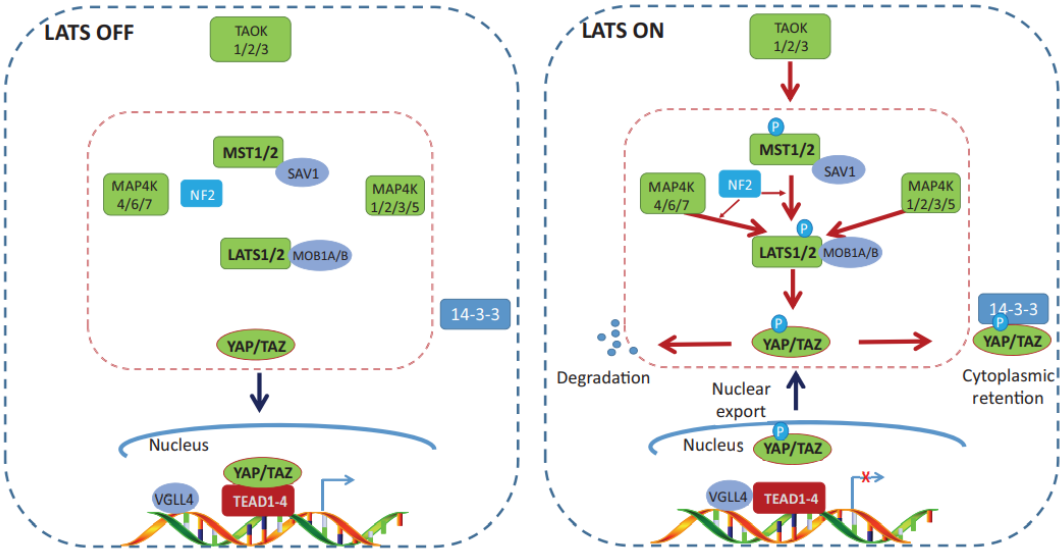

Figure 1. Outline of the kinase cascade central to the Hippo signalling pathway. When the pathway is not active, the unphosphorylated YAP/TAZ complex binds to TEAD-4 and results in gene transcription (a.)). Activation of the Hippo signalling pathway results in MST1/2 phosphorylation, leading to phosphorylation of LATS1/2, facilitated by scaffold proteins, which lead to YAP/TAZ phosphorylation and leads to movement out of the nucleus into the cytoplasm, and resulting in YAP/TAZ inactivation or destruction. LATS –large activated tumour suppressor, TEAD – transcriptional

articular chondrocytes perfused at 100 cycles.sec^{-1} (oscillating) indicated that cell attachment was highest within the first 30 minutes of

efficiency peaking at 60 % {Olivares, 2012 #979}. The seeding efficiency was shown to be similar at two hr as it was at 16 hr, with limited movement towards deeper areas of the matrix seen {Olivares, 2012 #979}. Use of the biliary canals for perfusion of parenchymal cells, rather than the portal vein, has resulted in a three-fold increased cell attachment efficiency within the parenchyma. Portal vein perfusion was also associated with a large proportion of cells retained in the lumen {Ogiso, 2016 #1092}. Three methods to

recellularise decellularised liver tissue have been compared; direct injection within multiple lobes, continual perfusion using native vasculature and multi-step perfusion using native vasculature of hepatocytes (10-50 x10^6 cells.mL^{-1}){Soto-Gutierrez, 2011 #66}. Rates of proliferation (% Ki-67 positive nuclei) ammonia metabolism (% removal x10^6 cells) and CYP1A2 activity (pmol.min.x10^6 cells) were varied; with multi-step perfusion associated with the greatest amount, and continuous perfusion the lowest. Albumin production (pg.mL^{-1}.5x10^6 cells) was also greatest with multi-step perfusion, whereas direct injection was associated with the least. The application of flow is not, therefore, the only indicator of cell activity. Static seeding of decellularised heart valve leaflets with porcine fibroblasts showed differing morphologies based on seeding density. Lowest seeding densities (low = 1 x10^3 – 1 x10^4 cells.cm^2) were associated with spread morphologies and sparse cell distribution, whereas higher densities (medium = 5 x10^4 cells.cm^2) provided confluent monolayers. Cell densities higher than this (high = 1 x10^6 cells.cm^2) formed multiple, dense cell layers on the peripheral surfaces, with large amounts of unattached cells and cellular debris seen {Wilcox, 2005 #1093}. Medium cell densities migrated around the disc surface to form a monolayer within two weeks culture, and migrated towards more central tissue areas within four weeks {Wilcox, 2005 #1093}.

1. Sandwich culture

{Dunn, 1989 #22}Culture of rat hepatocytes on three different culture models (collagen coated, sandwich culture and liver decellularised ECM) resulted in the identification of two main markers of differentiation; hepatocyte morphology and function {Lin, 2004 #43}. Those cultured on collagen coated plates showed a rapid decline in function over time, becoming almost absent within five days culture and were associated with flat cell morphologies and long protruding lamellopodia. The use of one collagen layer alone was insufficient to retain hepatocyte function, whereas the addition of a second layer in a sandwich orientation was enough to extend cell function to many weeks {Lin, 2004 #43}. Since its first use, hepatocyte sandwich culture has been associated with better formation of hepatocyte morphology including bile canaliculi, restoration of cell:cell contacts, more defined cell polarisation, enhanced function, in particular CYP activity, and increased longevity. Even though there are many advantages, loss of cell function is still seen over time {Kern, 1997 #110}{LeCluyse, 1994 #111}{De Bruyn, 2013 #1096}. First reported in 1989 {Dunn, #22}, extension of rat hepatocyte viability was achieved through sandwiching rat hepatocytes between two layers of collagen I. After 24 hr, hepatocyte cords with typical polygonal morphology were seen, and maintained for seven weeks. Albumin secretion was higher than hepatocytes cultured on one layer of collagen I.

Albumin levels in hepatocytes cultured on collagen I coated plates reduced after one week, although could be restored for a few days after the addition of a second layer. Although the addition of collagen I to culture plates and 3D gels similarly raised albumin tRNA levels, the lack of appropriate morphology using culture plates was thought to hinder albumin secretion {Dunn, 1989 #22}. Culturing hepatocytes in collagen-sandwich culture (Type I) results in the maintenance, or even increase, in protein expression of canalicular transporters including: bile salt exporter pump (BSEP), and the ATP-binding cassette transporter proteins MRP2 and BCRP over five days, when compared to native liver levels {Schaefer, 2012 #978}. Significant extension and/or increase in the secretion of liver proteins (albumin, transferrin, bile salts, urea and fibrinogen) were seen over six weeks culture in sandwich configurations compared with coated plates {Dunn, 1991 #95}. Identification of stress fibres, using phalloidin staining, showed increased cell stress with hepatocytes cultured on collagen I coated plates after 24 hr, whereas stress fibres were not seen in sandwich culture. Rearrangement of actin filaments, proteins involved in cytoskeletal organisation and connection to the ECM, has also been seen in sandwich culture {Dunn, 1991 #95}.

Matrigel™ has increased hepatocyte function beyond that seen with sandwich culture {Moghe, 1997 #538}. Although a marked difference in cell function was noted between single layered and sandwich culture Collagen Type I, similar functions were seen with single and sandwich culture using Matrigel™ {Dunn, 1991 #95}{Moghe, 1996 #956}. Hepatocyte aggregates form in collagen sandwich culture, with flattened morphologies that decrease in surface area with increasing cell seeding densities. Hepatocytes cultured on single layered Matrigel™ were comparatively rounded at low cell densities, with higher seeding densities associated with larger, multicellular aggregates. Furthermore, cell function (albumin secretion) was higher in Matrigel™ cultured cells particularly at lower densities, compared with cells cultured in collagen-sandwich culture {Moghe, 1997 #538}. Cell-cell contact was important in the maintenance of cell function in collagen-sandwich culture, whereas this was not the case for Matrigel™ cultured hepatocytes. In addition, the product is associated with significant batch variations {Dunn, 1991 #95}. To reduce batch variability, the use of polyethylene glycol (PEG) hydrogels have been developed, with cells cultured under such conditions showing consistent urea synthesis and CYP3A4 activity. Furthermore, hepatocyte function is increased further with supplementation of poly(lactic-co-glycolic) acid (PLGA), which increased hydrogel permeability whilst maintaining patternability {Lee, 2010 #975}. Supplementation with heparin (10% wt.%) has also shown significant improvements in albumin secretion and urea synthesis when

compared to hydrogel alone {Kim, 2010 #972}. Whether this is attributed to better gel porosity or alterations of the matrix stiffness closer to that seen in the native liver (~1500 Pa for native liver vs 2300 Pa in hydrogel) has not been established {Kim, 2010 #972}. The high cost in development of high throughput applications and lack of sufficiently comparable data still, however, limit their use.

Cell aggregation

Various culture methods can result in the formation of cell aggregates including static overlay techniques, spinner flasks or rocking in suspension cultures {Landry, 1985 #465;Sakai, 1996 #466}). Cell aggregate formation is associated with reductions in cell death, thought to result from increased expression of cell adhesion, structural, metabolistic and cell cycle genes {Waring, 2003 #693}. Over the past four years, increased investments have been made towards organoids, spheroids, liver on chip (LoC) and 3D bioprinting, although further research is required to provide a reproducible, repeatable system capable of high throughput for these to be used as they are {Mehta, 2024 #1099}.

Spheroids

Static overlay techniques involve culturing cells on non-adherent tissue culture flasks to induce self-assembly. Isolated rat liver cells cultured in this way show spontaneous re-aggregation into spheroids of up to 175 µm in size, that are shown to self-organise into lobular type structures. Furthermore, hepatocytes were shown to secrete and organise ECM components collagen, laminin, and fibronectin {Landry, 1985 #465}. Initially cells loosely attached, with tight bonds forming within 24 hr indicating formation of cell-to-cell junctions that are morphologically similar to cells seen in foetal tissue. Furthermore, a single-cell layer surrounding the spheroids were indicated histologically to be of mesothelial origin, expressing the same cytoskeletal markers as the Glisson's capsule. The use of hepatocytes spheroids may potentially increase cell scale-up to clinically relevant levels for use in bioartificial devices {Nyberg, 2005 #467}.

Spheroids have also been created using hydrogels such as ECM-based Matrigel™ or collagen-based Extracel™, with both showing increased cell function and enzyme activity {Moghe, 1997 #538;Prestwich, 2007 #539}. Studies using isolated rat hepatocytes cultured in Matrigel™ indicate that lowering seeding density results in an increase in cell-cell contacts and more stable structures. In addition, it was indicated that cell function in Matrigel™ based spheroids may be dependent on matrix derived cues that negate other cues, such as albumin received from cell-cell contacts. A simple morphometric approach

was taken to the evaluation of hepatocyte function within this study due to the varying levels of cell-cell and cell-matrix contacts, which is not ideal {Moghe, 1997 #538}. Further cell-based analysis is therefore warranted. Although advantages of hydrogel use are seen, methods of cell recovery have not been identified nor standardised {Godoy, 2013 #89}{Gómez-Lechón, 2014 #1100}{Soldatow, 2013 #1101}{Dash, 2009 #1102}{Schmelzer, 2010 #1103}{Mueller, 2011 #1105}{Legendre, 2013 #1106}. The non-animal based alginate sponge Algimatrix™ reportedly provides a 3D structure that minimally interacts with the hepatocytes, thereby allowing aggregates to form inside the voids. As a result, spheroid cellular aggregates are limited in size to the void within which it occupies, reducing the formation of necrotic centres {Prestwich, 2007 #539}. Studies suggest that primary rat hepatocytes synthesise a higher level of albumin using Algimatrix™ in comparison with collagen coated 2D surfaces, thereby indicating better cell function {Glicklis, 2000 #96}. Further comparison of Algimatrix™ and Matrigel™ may aid evaluation of cell-cell and cell-matrix contacts on cell differentiation.

Hydrogels infused with liver tissue extracts and growth factors, have indicated successful support of hepatocyte function (albumin secretion and urea synthesis) and proliferation over four weeks {Skardal, 2012 #65}. Furthermore, the addition of ECM into an injectable hydrogel may provide an additional method for cellular implantation in failing livers, providing a mechanism that could potentially release hepatocytes slowly over time. The additional inclusion of matrix proteins to culture conditions has been increase cell function (albumin secretion).

Synthetic scaffolds and Microfluidics

Microfluidic devices are small culture vessels that can precisely alter media flow and drug concentration whilst also allowing microscopic evaluation of cell morphology. Along with other synthetic scaffolds such as those made through fibre bonding, phase separation, particulate leaching, melt molding, gas foaming and/or freeze drying, these culture conditions lack necessary hepatocyte attachment motifs and have significantly altered mechanical properties when compared with native tissue. Work detailed in this investigation, therefore, focuses on understanding how to recreate normal hepatocyte function using natural matrices that contain underlying ECM structures, rather than the enhancement of synthetic structures. Microfluidic devices are not, therefore, covered in this review.

Inclusion of proteins native to liver ECM

Decellularised liver matrices have been used to supplement synthetic materials with biological components {Lee, 2014 #616}. Lyophilisation of decellularised native liver matrices creates powders, or particulates, that can be embedded within synthetic polymers, combining the uniformity and reproducibility of both the mechanical aspects of synthetic components with the material properties of native tissues, and leading to enhanced cell growth and/or function {Lee, 2014 #616}.

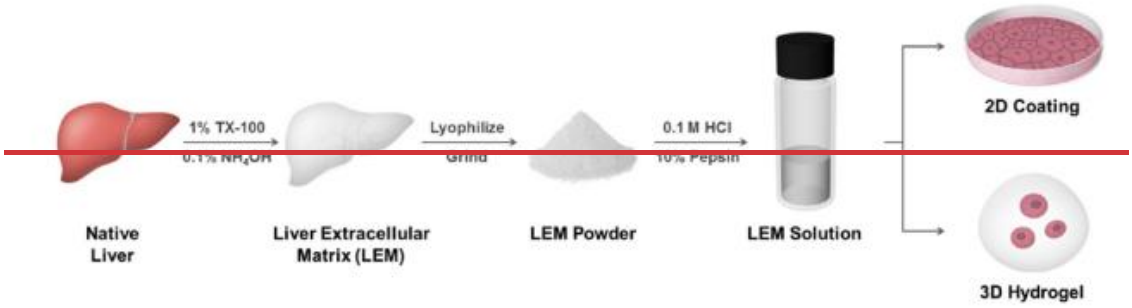

Figure 2. Outline of the process to use decellularised matrices as a coating or additive to culture conditions to alter cell function and/or protein expression in 2D and 3D formats. TX-100 – Triton X-100, NH_4OH – hydroxylamine, LEM – liver extracellular matrix, HCl –

Live dead staining of primary rat hepatocytes cultured on decellularised liver matrix-coated plates (0.2mg.mL^{-1}) enhanced rat hepatocyte viability at day seven compared with rat hepatocytes cultured on standard culture plates, or those coated in collagen I only. Furthermore, cell adherence as well as albumin secretion and urea synthesis were also enhanced when cells were cultured on matrix coated plates {Lee, 2014 #616}. Although albumin secretion peaked at day three in all groups, urea synthesis reduced throughout the seven-day culture period in all groups indicating that function may not currently be retained beyond seven days. Increase in primary rat hepatocyte adherence and viability were also shown when higher concentrations of liver matrices were used (2mg.mL^{-1} vs 0.2mg.mL^{-1}) {Lee, 2014 #616}. In addition, specific use of decellularised liver matrices, as opposed to decellularised matrices from other tissues, resulted in greater primary rat hepatocyte adherence {Lee, 2014 #616}. Supplementation with decellularised matrices therefore indicates an increase in hepatocyte adherence, viability and function, and when additionally combined with 3D arrangements and/or higher concentrations, hepatocyte viability and function can be increased/extended even further. The positive response to the addition of decellularised liver matrices does not only apply to primary hepatocytes, but also to hepatic human adult derived stem cells (hADSCs) . hADSCs cultured on decellularised liver matrix coated plates, hADSCs were shown to partly differentiate

within 21 days, with increased marker expression of hepatic lineage genes including HGF, α1- antitrypsin and albumin detected using qRT-PCR {Lee, 2014 #616}. The use of decellularised tissue may, therefore, provide environmental conditions that enhance cell adherence, viability and function in mature cells and aid cell differentiation in immature cell types. Hepatocyte attachment and cellular adaptation occurs through the induction of specific intracellular signalling pathways that cannot be replicated easily. In addition, the ECM provides an important structural framework for cellular attachment and migration, and alters cellular differentiation, and directs repair and development {Reid, 1992 #476;Martinez-Hernandez, 1993 #45;Schuppan, 2001 #324}. As a result, the use of native liver matrices, where the environmental conditions are already close to those found in-vivo, is advantageous.

Matrix stiffness

The effect of matrix stiffness on cell differentiation and progression through the cell cycle has been demonstrated through culturing hepatocytes on progressively cross-linked collagen and Matrigel™ hydrogels. Results show that increased gel rigidity leads to an increase in cell cycle progression and de-differentiation, and alter the 3D formation of hepatocytes, as well as cell response to growth factors and fibronectin {Semler, 2005 #968;Hansen, 2006 #128;Covidien, 2015 #694}. Increasing the hydrogel stiffness increases matrix synthesis and alters the TGF-β signalling pathways. Fibrotic livers are characterised by excessive deposition of extracellular matrix components, such as collagen I, known to enhance cell differentiation, around the portal tracts, fibrous septae and blood vessels. Furthermore, Collagen I secreting cells also strongly express collagen IV, which enhances cell proliferation, and vimentin, a mesenchymal cell intermediate filament (IF) protein that is thought to provide cell integrity and resilience. Vimentin was also seen within epithelial cells of proliferating bile ducts but were not noted within hepatocytes, indicating a potential differentiative role in wound healing {Young, 2014 #146;McClelland, 2008 #325}. Culturing hepatocytes with more than one surface has been shown to lead to better hepatocyte morphology and function, with the use of additional matrix components leading to even greater function. The use of a 3D scaffold containing all the native matrix components should, therefore, provide optimal conditions for functional hepatocyte levels to be reflect those seen within native liver tissue.

What are the methods used, and advantages of, using matrix scaffolds?

The complex interactions between liver cell types and their environment are thought to be essential in regulating and maintaining native hepatic function, therefore, accurate *in-vitro* culturing systems should aim to replicate as many of these as possible {Godoy, 2013 #89}. As a result, focus is placed on the use of decellularised liver matrices that already contain the complexity and components of native liver. Decellularisation is an attractive technique that involves the creation of a biocompatible ECM scaffold that retains the original tissues structural and architectural microenvironment as well as components required for cell-cell and cell-matrix interactions, biological and biochemical cytokines and growth factors. Optimal decellularisation and sterilisation protocols would remove all cellular and nuclear material whilst retaining the biological activity, ultra-structural components and mechanical integrity of the native matrix {Crapo, 2011 #172}. The most effective methods employed and/or reagent concentrations used, can vary widely and is affected by tissue density, cellularity and fat content {Gilbert, 2006 #653}. Commonly used methods use a variety of solutions and concentrations, such as hypotonic and/or hypertonic solutions, Triton X-100 or sodium dodecyl sulphate (SDS) that often employ both physical and chemical treatments {Crapo, 2011 #172;Gilbert, 2006 #653}. To date, research into decellularised matrix development has primarily been aimed towards implantation, for example a decellularised porcine dermal implant used in hernia repair (Permacol™) {Covidien, 2015 #694}{Giordano, 2015 #1188}, or a decellularised human skin implant used in breast reconstruction (Alloderm®) {Lifecell, 2015 #695}, with the number of clinical products increasing dramatically since introduction. {Giordano, 2015 #1188}{Cuomo, 2020 #1191}{Diffley, 2025 #1189}Biological ECM scaffolds are now being applied in regenerative medicine strategies for both tissue and organ replacement {Crapo, 2011 #172}. The retained matrices are highly conserved, and therefore well tolerated in both allogeneic and xenogeneic recipients although the structural organisation and biomechanical properties from which the matrix originates varies widely. Optimal decellularisation and sterilisation protocols would remove all cellular and nuclear material whilst retaining the biological activity, ultra-structural components and mechanical integrity of the native matrix {Crapo, 2011 #172}. The most effective methods employed and/or reagent concentrations used, can vary widely and is affected by the tissues' density, cellularity and fat content {Gilbert, 2006 #653}. Commonly used methods use a variety of solutions and concentrations, such as hypotonic and/or hypertonic

solutions, Triton X-100 or SDS that often employ both physical and chemical treatments, which can damage or disrupt the matrix {Crapo, 2011 #172;Gilbert, 2006 #653}.

During decellularisation, cells are initially lysed or pierced, resulting in cell contents distributed amongst the surrounding tissues. This often occurs using physical methods such as freeze thawing that result in the formation of intracellular ice crystals, or using hyper and hypotonic solutions that lyse cells through osmotic shock. The use of chelating agents or enzymatic agents, such as ethylenediaminetetraacetic acid (EDTA) and trypsin, may be added to bind divalent metallic ions and cleave peptide bonds, thereby disrupting cellular adhesion to the surrounding matrices and maximising cell exposure. Detergents are often employed to disrupt membrane stability, thereby aiding in cell destruction. Ionic detergents such as SDS achieve this through the solubilisation of cellular and nuclear membranes, whereas ionic detergents, such as Triton X-100 disrupt lipid-lipid and lipid-protein interactions. The choice, concentration and duration of detergent exposure is a balance determined through the effective removal of cellular and nuclear membranes, and minimisation of ECM damage {Gilbert, 2006 #653}. Subsequently, cellular and nuclear contents require removal from the tissue, often occurring through the application of mechanical agitation, repeated replacement of solutions and/or enzymatic digestion. The use of mechanical agitation also benefits the distribution of reagents to the cells within a 3D structure. Exposure of cytoplasmic contents to the matrix leads to matrix degradation, although damage can be minimised with the use of protease inhibitors. DNA and RNA levels may be reduced using enzymatic digestion (DNAses and RNAses) {Gilbert, 2006 #653}. Finally, all chemicals and/or enzymes need to be removed from the decellularised tissue as not to invoke a negative immunological or toxic response upon implantation. This is achieved using osmotically neutral or buffered solutions such as phosphate buffered saline (PBS).

Application of SDS and/or Triton X-100 in porcine liver

Use of either SDS (0.1 %) and/or Triton X-100 (1 %) have been shown to successfully remove sufficient cellular and nuclear components from porcine liver {Mattei, 2014 #618}. SDS removed sufficient nuclear and cellular detail within three days, although extension of exposure times resulted in significant lobular degradation. In addition, the use of SDS (0.1 %) showed greater retention of fibronectin, laminin and collagen type 4 compared with Triton x100 (1 %){Mattei, 2014 #618}. Increasing gradients of Triton X-100 (1 %, 2 % and 3 %) has been perfused through the hepatic artery of the porcine liver, followed by 30 min perfusion with 0.1 % SDS to aid in Triton X-100 removal. Although hepatic

~~architecture was maintained, the hexagonal lobular structures could not be identified on images provided. No immunohistochemical staining of native ECM components, DNA quantification or bp length assessment was not reported before implantation or seeding and therefore, its success in porcine tissue cannot be reported. It appeared that tissue damage was too great to identify clear structures, although cells were still able to attach to the decellularised porcine liver {Mirmalek-Sani, 2013 #48}. The use of low concentrations of SDS have been applied to liver before; through perfusion of increasing gradients SDS, and also through immersion and agitation of liver slices in 0.1 % SDS, with varying levels of success. Increasing gradients (0.25 -0.5 %) of SDS were perfused in the right lobe of porcine liver tissue, and washed with water to remove SDS before crosslinking the tissue with formalin (10 %){Barakat, 2012 #7}. H&E staining showed the retention of liver architecture, including central vein and portal triads, with native vasculature intact, determined through vascular corrosion and fluoroscopic examination. Collagen I was seen around the portal triad, Collagen Type IV and fibronectin was also seen within the decellularised lobules, albeit less intensely stained than native tissue. The basement membrane stained positive for laminin. Unfortunately, a small number of residual nuclei were reported, indicating that decellularisation was not complete {Barakat, 2012 #7}. Freeze-thawed (min. 12 hr) decellularised porcine liver was subsequently perfused with increasing gradients SDS (0.01-1 %), followed by a short rinse with Triton X-100 to remove remaining SDS, before being sterilised using peracetic acid (0.1 %){Yagi, 2013 #626}. Although total DNA content of the decellularised tissue had decreased by 98.8 ±0.8 % (0.04-0.2 μg.mg^{-1} dry weight) compared to native tissue (12.12 μg.mg^{-1}), three of the four lobes tested retained more than the 50 ng.mg^{-1} dsDNA guided for successful decellularisation {Crapo, 2011 #172}. This may have been achieved, although as the author chose to quantify total DNA, as opposed to dsDNA, the evidence cannot support such conclusions {Yagi, 2013 #626;Crapo, 2011 #172}. Assessment of base pair length was also difficult to assess due to low fluorescence levels seen in native tissue bands, which would result in any lower DNA concentrations difficult to identify. Porcine liver slices have been decellularised using 0.1% SDS alongside mechanical agitation, with successful removal of nuclear (DAPI) and cytoplasmic (H&E) staining and retention of lobular structure. DNA quantification (double stranded, dry weight) of decellularised matrices indicated successful removal (42.5 ±3.21 ng.mg^{-1}), with the use of peracetic acid significantly reducing dsDNA content further. In addition, staining was not seen in wells containing decellularised tissue DNA samples after agarose gel electrophoresis, indicating that DNA content was less than 200 base pairs in length {Hussein, 2013 #31}. The~~

concentration of DNA loaded into the well was, however, not defined indicating that a low concentration may also have been the cause for a lack of positive staining within the agarose gel. Although the efficacy of perfusing 0.1 % SDS into porcine liver remains questionable, its application through immersion and agitation provides hope. Low concentration SDS does have applicability in the decellularisation of porcine liver tissue although, successful proof in removal of sufficient amounts of dsDNA is limited to liver slices up to 0.3 cm in thickness. Its use in DNA removal through perfusion of lobes or entire livers has not been evidently reported, and its use in thicker liver tissues has not been applied.

How does the addition of decellularised matrices affect cells?

Decellularised liver matrices may also be used to supplement synthetic materials with biological components. Lyophilisation of decellularised liver matrices creates powders, or particulates, that can be embedded within synthetic polymers, combining the uniformity and reproducibility of both the mechanical and material properties of synthetic components in addition to providing matrix bioactivity, leading to enhanced cell growth and/or function {Lee, 2014 #616}. Hepatocyte adhesion, viability and function (albumin secretion and urea synthesis) was notably greater in liver matrix coated plates compared with collagen I coated plates, and Matrigel™ coated substrates {Lee, 2014 #616}. Hydrogels infused with liver tissue extracts and growth factors have indicated successful support of hepatocyte function (albumin secretion and urea synthesis) and proliferation over four weeks {Skardal, 2012 #65}. Furthermore, the addition of ECM into an injectable hydrogel may provide an additional method for cellular implantation in failing livers, and through time-based gel degradation, may provide a longer-term mechanism that could potentially release hepatocytes slowly over time. Subsequent perfusion of decellularised rat liver scaffolds with hepatocyte cell suspensions for five days have indicated the retention of *in-vitro* levels of liver specific functions including albumin secretion, urea synthesis, and cytochrome P450 expression when compared with static sandwich culture {Uygun, 2010 #72}. LDH release, a sign of membrane damage, was low across all timepoints and similar to levels seen in sandwich culture, with 20 % cells apoptotic on day two (TUNEL staining). Although urea secretion was seen to be higher in hepatocytes present in recellularised grafts than those cultured in sandwich, albumin levels were comparable between the two, both of which were lower than that seen in native adult rat liver. Successful transplantation of these recellularised grafts into rats for eight hr showed hepatocyte survival and function (albumin and urea) alongside minimal ischaemic damage

(TUNEL staining). The retention of native tissue architecture allows for better blood and oxygen transport throughout the tissue, and minimal hepatocyte damage. Functional levels, however, reported no universal advantage over hepatocytes cultured in sandwich orientations. It must be noted, that this study was completed within five days, providing only short-term information on cell activity and function. Further monitoring of functional levels over longer time periods are required (Uygun, 2010 #72).

Implantation of a recellularised scaffold containing sufficient volume of liver cells (10 % total liver cell number) into hepatectomised (90 %) rats extended mean lifespan from 16 to 72 hr with viable, functional hepatocytes seen in the transplanted tissue engineered liver (TEL) 72 hr post operation (Bao, 2011 #3). Although mean lifespan was extended, this did not occur indefinitely. Ammonia levels continued to rise, albeit slower, in those rats transplanted with tissue engineered liver compared with control rats, with TEL implanted rats displaying small-for-size syndrome and portal hypertension, complicated by gastrointestinal congestion and ascites that were more severe in the implanted group, as opposed to the normal liver grafted group. Transplantation of TEL grafts therefore was a short term option only. Whether this is a result of the implantation of cell spheroids, as opposed to isolated cells, or whether this resulted from the addition of thrombin to the decellularised tissue is not clear. Nevertheless, the potential short-term applicability of these graft types shows promise.

What are the relative merits of the various cell types when re-seeding decellularised matrices?

Multiple cell types can be seeded on to decellularised matrices however certain characteristics are required; they should attach to, proliferate on / in and become functional / differentiate after seeding has occurred. The best cells would be hardy enough to withstand seeding, proliferate quickly to rapidly populate an area and become functionally reflective of native conditions once the tissue is repopulated. Finding a cell that has all these properties, and at the right times to facilitate repopulation, is not simple.

Primary hepatocytes

Although primary hepatocyte culture is widely used as a tool to study drug transport, metabolism and/or toxicity there are limits in cell efficacy and longevity. High donor variability in hepatocyte function, short functional culture periods, and limited maintenance of cell function associated with the loss of differentiation, is evident (Guguen-

Guillouzo, 2010 #769}. Hepatocytes are routinely cultured as a monolayer on collagen-coated 2D surfaces, with conditioned medium. Cells cultured this way have been shown to retain cell function through production of albumin and urea as well as cytochrome P450 activity, however rapid decline of cell function occurs within one week in culture {Godoy, 2013 #89}. Cell function and polarity can be maintained further through the addition of a second layer of collagen in a sandwich culture, inducing the formation of lateral and apical membranes {Taguchi, 1996 #458}. Although primary hepatocytes are preferred, the lack of appropriate cell numbers, and reduced cell function, alongside low engraftment rates and batch variability, make the effective use of primary cells limited at present. {Statzer, 2020 #1181}{Kular, 2014 #1182}

Species

Within the literature, three main species have been investigated for use in liver decellularisation and re-seeding; humans, murine and porcine. Cell types can be broadly classified into three types; fully differentiated hepatocytes of either the same or different species, mesenchymal stem cells (MSCs), immature cells or those of a progenitor phenotype and fully differentiated cell lines.

Hepatocytes: Murine

Increased adhesion, viability and function resulted after seeding of rat hepatocytes on rat ECM coated plates, irrespective of 3D arrangement {Lee, 2014 #616}. Hepatocyte adhesion was significantly increased with rat ECM (0.2 $mg.mL^{-1}$) or collagen I coated plates (0.2 $mg.mL^{-1}$) when compared with poly-L-lysine coated polystyrene plates (PS coated). Cell adhesion and viability was, however, greater with ECM coated plates after one day, and after seven days, functional activity (albumin and urea secretion) was also greater. Furthermore, seeding of hepatocytes on decellularised liver hydrogels showed greater adhesion at day one and comparable viability at day three, when compared with seeding on Matrigel™. This suggests that liver specific ECM contains select adhesion proteins that are not seen in other ECM based gels, and that hepatocyte viability and function can also be enhanced with the use of ECM tissue components {Lee, 2014 #616}. Entire decellularised rat organs as opposed to single lobes, can be easily achieved due to their small size. Literature shows multi-step perfusion to be the most common seeding method {Soto-Gutierrez, 2011 #66;Uygun, 2011 #71;Ren, 2013 #56}, although continuous perfusion and injection-based methods have also been applied {Soto-Gutierrez, 2011 #66}. Multistep perfusion provides a greater cell attachment rate (86.0 ±5.0 %) than that seen

with continuous perfusion (69.0 ±9.0 %) or injection (12.6 ±9.0 %) {Soto-Gutierrez, 2011 #66}. Engraftment rates are similar between those perfused at different flow rates (1 mL.min^{-1} vs 2mL.min^{-1} {Ren, 2013 #56;Soto-Gutierrez, 2011 #66}, indicating that small changes in flow rate do not play a large factor in hepatocyte engraftment. Initially, cells attach to larger vessels and subsequently move to surrounding structures / vessels {Ren, 2013 #56;Uygun, 2011 #71}, with some evidence of proliferation seen, albeit low amounts (3.0 ±0.6 %) {Soto-Gutierrez, 2011 #66}). After seven days culture, albumin expression was highest in those tissue reseeded using multi-step infusion, followed by continual perfusion and direct injection, however, no differentiation was reported regarding cell numbers. The difference in albumin expression could, therefore, be a reflection of cell number, or cell activity {Soto-Gutierrez, 2011 #66}. At day ten, comparable albumin expression was seen between reseeded discs and static sandwich culture, indicating that the use of decellularised liver tissue is at least comparable to current methods. Seeding of rat hepatocytes on 5 mm thick decellularised porcine ECM sheets have initially showed decreased hepatocyte function, with similar decreases in cell function seen in comparative methods (sandwich culture and collage I coated plates). Hepatocyte function was, however, maintained for between 12 to 25 days in culture (~7µg.day), after which

Table 1. Available literature summarising current methods used to seed rat hepatocytes on decellularised liver tissues. N/A = not applicable/reported. Initial functionality = seven days or less. Longer term = longer than seven days. SDS = sodium dodecyl sulphate. TX-100 = Triton X-100. ECM =

Author	Decellularisation		Cell delivery		Rat hepatocytes	Engraftment Rates	Cell viability	Functionality		Other
	Species tissue	Physical parameters	Method	Route				Initial (up to 7 days)	Longer term (7 days plus)	
Ren 2013	Murine (Rat)	Organ	Multi-step perfusion	Portal vein, 1mL.min^{-1}	Rat hepatocytes	89.7 ±5.1% for SDS and 90.6 ±5.7% for TX-100	N/A	**Up to 4 days**: Hepatocytes attached to larger vessels and surrounding parenchyma. Function was higher in hepatocytes cultured on ECM vs control	No long term studies performed	
Lee 2014	Murine (Rat)	Organ	Plate coated with ECM powder	Coating on culture plate	Rat hepatocytes	N/A	Significantly greater than controls	Heptocytes adhesion, viability and function significantly hgher with liver specific ECM coating	No long term studies performed	Increase in adhesion, viability and function were all concentration dependant
			3D hydrogel	Encapsulated		N/A	Significantly greater than controls	Significantly higher viability and function in ECM supplemented gels vs collagen I hydrogel	No long term studies performed	
Uygun 2011	Murine (Rat)	Organ	Multi-step perfusion	Portal vein	Rat hepatocytes	95.6 ±3.4%	<20% apoptotic at day 2	**4-48 hr**: Most cells remain in and around vessels and distrbute through the matrix. **5 days**: Higher albumin and urea secretion compared to sandwich culture, comparable drug-metabolising enzyme levels	**10 day:** comparable albumin and urea secretion, alongside bile synthesis when compared to static sandwich culture	
Lin 2004	Porcine	mm thick sheet	Culture on ECM sheet	Sheets 5mm	Rat hepatocytes	N/A	N/A	Hepatocytes showed less surface area attachment on ECM sheet compared to those cultured on plates / sandwich culture.	Scaffold remained viable for 35 days with significant remodelling seen. Albumin secretion highest in sandwich culture, then on ECM with single layer collagen lowest.	Significant variation in function seen between liver ECM.
Soto-Gutierrez 2011	Murine (Rat)	Organ	Injection	Injected into lobes	Rat hepatocytes	12.6 ±9.0%	N/A	Hepatocytes attached around vessels, followed by surrouding vessels. Similar expression to native liver	**7 days**: Albumin secretion = 6.0 ±0.2 µg.mL^{-1}.	
			Continuous perfusion	Portal vein, 2mL.min^{-1}		69.0 ±0.5%	N/A	Hepatocytes attached around vessels, followed by surrouding vessels. Lower albumin expression compared to native liver	**7 days**: Albumin secretion = 8.7 ±0.3 µg.mL^{-1}.	
			Multi-step infusion	Portal vein, 2mL.min^{-1}		86.0 ±5.0%	N/A	Hepatocytes attached around vessels, followed by surrouding vessels. Similar expression to native liver. 3.0 ±0.6% hepatocytes proliferating	**7 days**: Albumin secretion = 16.5 ±1.8 µg.mL^{-1}. Much greater CYP activity seen with this method also, compared to other methods tested.	

function significantly increased for the remaining culture period (35 days total){Lin, 2004 #43}. Results indicated that the use of a collagen layer alone was insufficient to retain hepatocyte function, whereas the decellularised liver was able to extend cell function long term. It should also be noted, however, that significant variability of seeding efficiency was seen between repeated experiments (n=8), possibly resulting from the variation in location of seeding, tissue topography, function of isolated primary cells or animal to animal variability. The cause of which is not known. The use of liver specific ECM shows good cell adhesion and cell viability with the potential to enhance cell function over longer times. Only one study seeded hepatocytes on porcine tissue decellularised using Triton X-100, and over time frames longer than other studies using decellularised rat liver.

Hepatocytes: Human

Static culture of human hepatocytes on decellularised porcine liver discs has shown significant increases in hepatocyte function (albumin secretion detected via ELISA) from seven days up to 21 days in culture, greater than hepatocytes cultured on polystyrene culture plates and/or on collagen sandwich plates. Significantly greater numbers of hepatocytes were also seen after 21 days culture {Lang, 2011 #40}. Interestingly, however, hepatocytes formed layers on top of the matrices and did not penetrate it, with no significant movement even though over 90 % were viable (Live/dead stain) {Lang, 2011 #40}. Increased function in both human and rat hepatocytes have therefore been seen after three weeks when seeding on decellularised porcine liver, therefore, indicating that cell function may not be species dependant.

Hepatocytes: Porcine

Seeding of primary porcine hepatocytes on decellularised porcine liver tissue using a multistep perfusion-based method resulted in a 74 ±13 % engraftment rate. Higher levels of albumin expression, and both albumin and urea secretion were seen within four days when compared with hepatocytes seeded on a single layer of collagen, however, increased function was not maintained up to seven days in culture. Furthermore, at day seven almost half of cells (47.8 ±5.4 %) were apoptotic. Although this data suggests an initial positive cellular response upon seeding on decellularised porcine liver, long term functional retention was not seen. Although functional levels of rat (Section 1.8.2.1) and porcine (Section 1.8.2.3) hepatocytes on decellularised porcine liver are initially greater than that seen with other culture techniques, these are not maintained long-term {Yagi, 2013 #626;Lin, 2004 #1041}. With human hepatocytes, however, both cell number and

~~function are greater when cultured on porcine liver tissue as opposed to collagen sandwich or polystyrene culture plates. Whether this difference is attributed to cell species, and/or seeding and culture method is yet to be determined. Hepatocyte growth into interconnected, multi-cellular structures has been shown to successfully support hepatocyte viability, proliferation and consistent cell function (urea and albumin secretion) over four weeks {Skardal, 2012 #65}. Results indicate that the inclusion of matrix proteins such as collagen or heparin-modified hyaluronic acid form interconnected hepatocyte structures, with inclusion of ECM derived extracts or gels resulting in the enhanced maintenance of cell number and longevity. Although the use of hyaluronic acid alone did not support the formation of interconnected structures, its conjugation with heparin within ECM supplemented hydrogels resulted in the formation of large interconnected structures that remained stable over four weeks {Skardal, 2012 #65}. Larger concentrations of multiple growth factors including EGF & HGF were also seen in decellularised liver extracts (17.74 vs 0.93 pg.mL^{-1} and 17.45 vs 0.00 pg.mL^{-1} respectively), when compared with liver tissue extracts. From these results it can be concluded that liver ECM contains additional factors, over collagen alone, that can stabilise structures resulting in enhanced hepatocyte longevity {Skardal, 2012 #65}. The culture of human hepatocytes~~

Table 2. Available literature summarising current methods used to seed human and porcine hepatocytes on decellularised liver tissues. N/A = not applicable/reported. ECM = extracellular matrix

Author	Decellularisation		Cell delivery		Human hepatocytes	Engraftment Rates	Cell viability	Functionality		Other
	Species tissue	Physical parameters	Method	Route				Initial	Longer term	
Skardal 2012	Porcine	ECM supplemented hydrogel / media	Culture on ECM coated surfaces or ECM supplmented media	ECM sheets 3mm / ECM supplemented media	Human hepatocytes	N/A	N/A	N/A	Of all the hydrogel variations tested, only the heparin conjugated, hyaluronic acid gel containing ECM and growth factors successfully supported hepatocyte proliferation and function over 4 weeks	Can create intercnnected hepatocyute multicellular structures that are stable and remain viable. ECM supplemented gels outperformed ECM supplemented media.
									Significantly greater cell numbers seen at day 21 compared to comparators. Cells present on, not in, tissue. Significantly higher albumin levels secreted, and stable over 3 weeks compared with collagen gels / polystyrene plates	
Lang 2011	Porcine	3mm slices cut in to 10-15mm diameter discs	Culture on ECM discs	Pippetted onto centre, static culture	Human hepatocytes	N/A	>90% cells viable at day 21	Number of cells did not change for 2 weeks		
Yagi 2013	Porcine	Organ	Multi-step perfusion	Portal vein, 4 $mL.min^{-1}$	Isolated porcine hepatocytes	74 ±13%	6.6 ±2.7% at day 1, 21 ±8.6 % at day 4, 47.8 ±5.4% at day 7	Hepatocytes present in parenchyma and producing albumin at days 4-7	Albumin staining decreased after day 7, although higher than collagen cultured comparator	Sandwich culture showed greater albumin and urea secretion

on decellularised porcine liver has also shown a retention of >90 % viability after 21 days culture {Lang, 2011 #40}. Although cells did not increase in cell number for the first two weeks of culture, increases were seen after 21 days even though limited cell permeation was seen. Albumin secretion (per x10^4 cells) also remained stable for two weeks and significantly increased at day 21 {Lang, 2011 #40}. Through evaluation of multiple hepatocyte species, it is thought that cell activity and/or function may increase if cell viability is maintained beyond three weeks culture.

Cell lines

The use of cell lines provides an almost unlimited supply of cells and repeatability of results. Furthermore, hepatoblastoma derived cell lines, such as HepG2 have overcome the limited functionality and reduced number of isolated cells associated with the use of primary human hepatocytes. The tumour derived cell line C3A, derived from HepG2, is currently used within the ELAD bioartificial liver, however, there are concerns over the effectiveness of this cell line, with reduced enzyme activity, amino acid metabolism and urea cycle activity seen, possibly resulting from reduced expression of the urea cycle genes. Furthermore, concern over viral zoonotic transmission, for example porcine endogenous retro virus (PERV) or SARS-Cov-2 has limited the use of cell lines to extracorporeal devices only, even though no evidence of transmission has been reported {Zhang, 2006 #444}{Maggi, 2020 #1166}. As a result, attempts to immortalise non-tumour derived foetal hepatocytes have been made with some success. HepCL cells have been used to treat acute liver failure, with results indicating similar function when compared with primary human foetal hepatocytes {Chen, 2010 #447}. The use of cell lines in a multi-co-axial hollow-fibre BAL device has also shown limited duration due to the deposition of ECM and other cell components which pollute and clog the device, leading to nutrient blockage, cell death, and subsequent device failure {MacDonald, 2001 #243}. Although this may be attributed to the use of cell lines in particular, the applicability could also be attributed to many other causes including type of media flow and/or speed, pore size, membrane material, as well as cell type.

Seeding of HepG2 cells, a tumour derived cell line liver of a 15 year old Caucasian male, has occurred on both decellularised porcine {Mirmalek-Sani, 2013 #48;Lang, 2011 #40} and rat livers {Zhang, 2009 #80}. With the use of porcine sheets of different depth, HepG2 have shown minimum tissue penetration in tissue of lower depth (1mm) and multilayer penetration on depths of 3mm {Mirmalek-Sani, 2013 #48}{Lang, 2011 #40}, although comparison of static and dynamic culture conditions were shown to affect the amount of

cell penetration {Lang, 2011 #40}. When decellularised liver matrices were implanted into the subcutaneous adipose tissue of rats, no fibrous encapsulation of scaffolds were observed and host cells populated the matrices throughout the 28 day culture period. The decellularised tissue appeared not to be, or release, cytotoxic components over 28 days culture. The insertion of decellularised scaffolds within a living model, in the presence of flow conditions was associated with increased cell movement {Mirmalek-Sani, 2013 #48}. When HepG2 were cultured on rat ECM coated plates, increased HepG2 adhesion and number were seen within four days and HepG2 function at 14 days culture {Zhang, 2009 #80}. Although HepG2 are often used instead of primary hepatocytes due to the low cost and ease of culture, key enzymes involved in drug metabolism are expressed in low amounts, or are absent, making this cell type unusable in drug toxicity or metabolism studies {Guo, 2011 #976}. Other cell lines, however, may be more applicable. Results indicate that the seeding of cell lines may be a viable alternative to primary hepatocytes as the increases in cell number and function can be seen with the use of dynamic culture conditions, with only 14 days until changes in function are seen, compared to 21 days with hepatocytes of various species.

Foetal / immature cell types

Although hepatocyte cell lines and primary hepatocytes have been shown to adhere to, proliferate and become functional on decellularised liver tissue, the ECM has also been shown to aid in cell maturation. Two studies using rabbit or mouse MSCs have shown adhesion and proliferation within two days when immersed and agitated, and increased liver specific cell function within seven days when perfused through mouse MSC seeded decellularised mouse livers {Jiang, 2014 #35}, and within 21 days when rabbit MSC seeded decellularised porcine liver tissue was immersed and agitated {Mansilla, 2007 #44}. Both species of MSC differentiated into cells that express liver specific cell markers. Seeding of other immature cell types has been investigated, with human foetal stellate cells (Hfscs) and human foetal hepatocytes (Hfh) perfused in to decellularised porcine liver through both portal and hepatic veins at 1.5 mL.min^{-1}. Engraftment efficiencies of both cell types indicated >90 % engraftment , with cells present in portal and hepatic veins by day three, and around large vessels and surrounding tissues at day 13. Around 40 % cells were proliferating (Ki-67 positively labelled), the majority of which were located at proximal sections and in Hfh. Those cells in more distal areas showed greater levels (30 %) nuclear

damage when compared to more proximal areas, as determined by TUNEL staining {Barakat, 2012 #7}. Maturation of Hfh was shown throughout the culture period. Approximately 70 % Hfh stained positive for albumin and were located alongside areas of increased glycogen deposition and CYP3A4 staining. In addition, decreased staining for the foetal hepatoblast marker AFP was also seen. Cell morphology was similar between seven and 13 days, with no morphological evidence of bile duct formation seen. Cells were rounded with a high nuclear:cytoplasmic ratio, positively staining with the liver specific intermediate filament protein CK18. Results indicated that hepatocytes were able to proliferate and differentiate within the decellularised tissue, however, increased distance from the media source was associated with increased apoptosis. Seeded Hfh

Table 3. Available literature summarising current methods used to seed immature cell types and hepatocyte cell lines on decellularised liver tissues. N/A = not applicable/reported, ECM = extracellular matrix. HfH = human foetal hepatocytes, HSC = hepatocyte stem cells

Author	Decellularisation		Cell delivery		Immature cell	Engraftment Rates	Cell viability	Functionality		Other
	Species tissue	Physical parameters	Method	Route				Initial	Longer term	
Jiang 2014	Murine (Mouse)	Organ	Multi-step perfusion	Portal vein, 1mL.min^{-1} 60 mins	Mouse MSC	N/A	N/A	Signficantly higher cell function after7 days compared to culture dish	Signficantly higher cell function after 4 weeks compared to culture dish	Differentiated into cells expressing hepatocyte markers
Mansilla 2007	Porcine - immature	Lobe	Immersion and agitation	1cm^3 cubes	Rabbit MSCs	N/A	N/A	Adhesion and proliferation after 2 days	Differentiation of cells that expressed liver specific markers at day 21, not present in fibrin comparator	Differentiated into cells expressing hepatocyte markers to day 21
Barakat 2012	Porcine	Organ	Continuous perfusion	Portal vein and hepatic artery	HfH, HSC	>95%	<30% apoptotic at 13 days, particularly in distal sections	Increase in albumin secretion over 3 days	Increased metabolism and decrease in media oxygen concentration. Increased albumin secretion not maintained up to 13 days	40% (HfH) and 20% (HSC) cells proliferating after 13 days, particularly in proximal areas
Wang 2011	Murine (Rat)	Organ	Perfusion	Portal vein	Human hepatocyte stem cells	"essentially 100% of viable cells"	N/A	Stem cells divided "once or twice" and transitioned into cell cycle arrest, and into 3D cord-like morphologies typical of mature parenchymal cells, including cell specific genes for hepatocytes or cholangiocytes.	Cultures remained morphologically stable and functional for eight weeks	Quicker attachment to matrices compared with collagen type I
Mirmalek-Sani 2013	Porcine	Organ	Static seeding and culture	1mm sheets, 15mm diameter	HepG2	N/A	No apoptotic markers seen at day 7 or 21 (TUNEL)	Cells seen attached to matrix surface, and minimal penetration seen.	Dense cell layers seen at 21 days culture. Images show cell presence in outer parenchymal tissue	
Lang 2011	Porcine	3mm slices cut in to 10-15mm diameter discs	Culture on ECM discs, with agitation	Pippetted onto centre	HepG2	N/A	N/A	Unifrom multi layer constructs formed	Culture up to day 12 similar to that at earlier time points	Dynamic culture conditions resultsed in greater cell penetration into discs
Zhang 2009	Murine (Rat)	Organ	Plate coated with ECM powder	Coating on culture plate	HepG2	N/A	N/A	ECM markedly enhances cell adhesion, with no tissue specificity	After day 4, cell types proliferated best on ECM derived of its own origin and showed cell specific morphology and marker expression for up to 14 days	DAPI staining showed presence of whole nuclei

were also shown to be functional after seeding showing increased cell function over time, however, reductions in albumin staining indicated that cell viability could not be maintained for 13 days {Barakat, 2012 #7}. Seeding of human stem cells on decellularised rat liver also showed quicker cell attachment when compared with collagen I based cultural methods, with cells dividing "once or twice" before cell cycle arrest was seen, with 3D cord like orientations typical of the native liver were seen. Seeded structures lost immature cell markers (EpCAM and CXCR4) and increased expression for markers of mature liver cells, such as urea and cytochrome P450. In addition, seeded cells remained stable and functional for eight weeks, versus two weeks seen with HpSCs cultured on collagen I {Wang, 2014 #225}. HepG2 cells were also seeded to assess viability, growth and proliferation on porcine liver decellularised using six different methods (water, PBS and salt-based solutions, with and without peracetic acid) {Wang, 2014 #225}. Twelve days culture resulted in the formation of multiple cell layers on the decellularised matrix, with cell penetration only seen on water washed liver ECM structures. Although cell proliferation was initially reduced on matrices decellularised using water, proliferation rates significantly increased over time when compared with other decellularisation methods, indicating that the method of decellularisation can affect proliferation rates. Furthermore, it was also reported that the addition of peracetic acid often resulted in lack of cell growth {Lang, 2011 #40}. The removal of peracetic acid wash steps, however, results in increased risk of contamination and should not be considered unless necessary. Interaction between hepatocytes and neighbouring cells, such as LSECs, reportedly alters hepatocyte growth, migration and/or differentiation, stabilising adult hepatocyte phenotype. These alterations are thought to result from cell signalling and interactions between cells. Studies of the role of cell types during repair and regeneration in both foetal (HHyP) and adult liver hepatobiliary precursors has been studied using single cell RNA sequencing, and highlights the important role of YAP, part of the Hippo signalling pathway, with upregulation of YAP resulting in the induction and maintenance of cell proliferation during liver injury {Saviano, 2020 #1167}. During chronic damage, hepatocyte damage results in the production of cytokines and chemokines from inflammatory cells, and signals for hepatic stellate cells to form myofibroblasts, resulting in increased deposition of ECM and formation of fibrotic lesions, which are one of the defining histological features of liver damage {Saviano, 2020 #1167}. LSECs secrete proteins involved in cell:cell interaction, regulate organ function and homeostasis and cell regeneration. Interactions of HSC and LSECs with non-parenchymal cells were found to be wide ranging. LSECS for example were found to upregulate genes responsible for lipid metabolism, antigen presentation and release of chemokines, as well as decreased expression of other genes involved in vascular development and homeostasis {Saviano, 2020 #1167}.

Interactions between monocytes and LSECs are also critical in determining the differentiation of monocytes into macrophages and provide a means for monocyte entry into the liver lobules. Other cell interactions defined from RNA sequencing are summarised by Saviano et al {, 2020 #1167}.

The use of cell lines provides an almost unlimited supply of cells and repeatability of results. Furthermore, tumour derived cell lines, such as HepG2, have overcome the limited functionality and reduced number of isolated cells associated with the use of primary human hepatocytes. The human cell line C3A is currently used within the ELAD bioartificial liver, however, there are concerns over the effectiveness of this cell line, with reduced enzyme activity, amino acid metabolism and urea cycle activity seen, possibly as a result of reduced expression of the urea cycle genes. Furthermore, concern over disease transmission has limited the use of cell lines to extracorporeal devices only, even though no evidence of transmission has been reported {Zhang, 2006 #444;Ellis, 1996 #189;Millis, 2002 #280}. As a result, attempts to immortalise non-tumour derived foetal hepatocytes have been made with some success. HepCL cells have been used to treat acute liver failure, with results indicating similar function when compared with primary human foetal hepatocytes {Chen, 2010 #447}.

1. Co-culture

Co-culture has also shown improvements in expression of both phase I and II enzymes and remains higher after drug induction. Cell:cell contacts are improved alongside cell polarity and formation of bile canaliculi, which extended cell viability. Once again, however, high variability between vell viability and differentiation is observed {Guguen-Guillouzo, 1983 #639;Inamori, 2009 #113}. Co-culture of the rat epithelial cells (type not stated) with human hepatocytes resulted in high albumin secretion, hepatocyte survival for over two months and secretion of new matrix components, particularly collagen type 3 {Clement, 1984 #640}. An additional study using foetal hepatocytes also showed increased albumin secretion, and matrix components were deposited between the two cell types and included collagen III, and also fibronectin {Guguen-Guillouzo, 1983 #639}. The time at which endothelial cells were added altered the level of albumin secreted, with four hr seeding showing greatest values, and co-culture seeding showing both enhanced and extended levels of albumin secretion. Amount secreted however, was shown to decrease between nine and 11 days after making their efficacy short lived {Guguen-Guillouzo, 1983 #639}. Even though co-culture of liver specific cells seems highly preferable, the specific needs of each cell type must still be met to ensure cell function and

~~survival, making this process highly complex to undertake. Furthermore, the lack of high throughput methods and substantial variability between labs do not match the requirements of the pharmaceutical industry to make co-culture-based methods viable and more work is required. The advantages of co-culture could aid in the maintenance of cell function long term, and/or the regeneration capacity of the liver as seen in-vivo, however, presently developments with single cell culture are required first.~~

1.10 Project aims and objectives

1.10.1 Aims

The aims of this project are to develop methodologies to ascertain whether porcine liver derived scaffolds and supplemented porcine liver derived scaffold platforms, can extend hepatocyte differentiation.

1.10.2 ~~These will be achieved through completion of the following objectives~~Objectives

1. To develop a biocompatible decellularised porcine liver scaffold, validated through assessment of DNA content, ~~histioarchitecture~~histoarchitecture and cytotoxicity
2. To biologically compare decellularised liver scaffold with native liver tissue to assess retention of ~~histioarchitecture~~histoarchitecture and specific matrix proteins through histological and biochemical methods
3. To determine markers of cellular proliferation and differentiation through 2D culture of hepatocyte cell lines
4. To develop methods to incorporate decellularised porcine liver scaffolds into 2D or 3D platforms
5. To assess the effect of decellularised liver scaffolds and supplemented platforms on the culture of hepatocyte cell lines

~~2.~~2 Materials and Methods

2.1 Materials

2.1.1 Materials used

The details and sources of general materials used throughout the study are listed in Table 7.~~Table 6.~~

Table ~~7~~10. General materials used and the relevant suppliers and reference codes. N/S = not stated

~~Table 6. General materials used and the relevant suppliers and reference codes. N/S = not stated~~

Materials	Supplier	Reference
Acetic acid (glacial)	Fisher Scientific	A/0430/PB08
Acetone	Fisher Scientific	A/0400/PB08
Adhesive tape	3M	Steri-strip
Alcian Blue 8 GX	Atom Scientific	RRSP4-F
Alcian Blue	Gurr	N/S
Ammonia solution (25 %)	Sigma	30501
Antigen unmasking solution	Vector Laboratories	H3300
Aprotonin (10000 KIU.mL^{-1})	Mayfair house Leeds Teaching Hospital Pharmacy	AP012
ATP-Lite-M® assay	Perkin Elmer, Albany street, Boston.	6016941
BCA Protein Assay Kit (Pierce™)	Thermo Scientific	23227
Benzonase (purity >99%, 25 U.µL^{-1})	Merck Millipore	70664
Bouin's fixative	Atom Scientific	RRFF5010
Bovine serum albumin	Sigma-Aldrich	85041C

Materials	Supplier	Reference
Calcium acetate (anhydrous/dried)	Thermo Fischer Scientific Ltd	C/0920/50
Calcium chloride	BDH	ALFA 12316.A1
Calf thymus DNA Type XV, Activated, lyophilized powder	Sigma-Aldrich	D4522
Corning Tissue culture flask with vented lid, 150 / 175 cm^2	Sigma Aldrich	430825
Cyanoacrylate contact adhesive	Sigma-Aldrich	Z105902-1EA
DAPI stain (4',6-diamidino-2-phenylindole dihydrochloride)	Sigma-Aldrich	D9564
Dimethyl sulphoxide (DMSO)	Sigma	D26650
Diastase (alpha-amylase)	Sigma-Aldrich	A3176
Diaminoethane tetra-acetic acid disodium salt (EDTA)	Fisher	E/P140/65
DNeasy blood and tissue kit	Qiagen	69506
DPX mountant	Thermo Fischer Scientific Ltd	M81330/C
Dulbecco's PBS tablets	Oxoid	BR0014
Dulbecco's minimal essential media (DMEM)	Sigma	D6546
Eosin Y	Merck Millipore	1.09844.1000
Ethanol (100 %)	Fisher Scientific, Loughborough, UK.	E/650DF/17
Ethyl cyanoacrylate	3M	SGAD 876

Materials	Supplier	Reference
Ferric ammonium sulphate (ammonium iron (III) sulphate)	Sigma	F3629
Fluorescent mounting medium	DAKO	S3023
Foetal calf serum	Sigma	EU-000
Formaldehyde (37-40 %)	Gentamedical, Tockwith, UK.	F40050
Formalin, neutral buffered (10%)	Atom Scientific	RRFF4000-G
Gel Doc	BioRad	12012147
Gel tank	BioRad	1640302
GeneRuler 100 bp DNA ladder	Thermo Fisher Scientific Ltd	SM0243
Gentamycin sulphate	Biochrom	A271-23
L-glutamine (200 mM)	Sigma	G7513
Glasgow's minimal essential medium	Sigma	G5154
Gold (III) chloride	Sigma	379948
Haematoxylin, Gills (III)	Sigma	GH5316
Histoclear III	National Diagnostics	HS-204
Hoechst nuclear stain	Molecular Probes	33342
Hydrochloric acid (37 %)	Fisher Scientific	H/1200/PB17
Hydrogen Peroxide	Sigma-Aldrich	H1009
ImmEdge Hydrophobic barrier pen	Vector Laboratories	H-4000
Magnesium chloride	Thermo Fischer Scientific Ltd	22321-1000

Materials	Supplier	Reference
Masson's Trichrome (Light green) kit	Atom Scientific	RRSK21
Mayer's haematoxylin	Atom Scientific	RRSP60
Methylated spirits	VWR International West Chester, UK.	23684.36
Nuclear Fast Red	Sigma	229113
Nuclease free water	Severn Biotech Ltd, Worcestershire, UK.	20-9000-01
Neutral buffered formalin (10 %)	Atom Scientific	RRFF4000-G
OCT embedding media	Raymond A Lamb	LAMB/OCT
Optical Instrument Cleaner	RS components	692-918
Oxalic acid	BDH	1017440
Paraffin wax (Shandon Histoplast)	Thermo Fischer Scientific Ltd	6774060
Penicillin (5,000 $U.mL^{-1}$)-streptomycin (5 $mg.mL^{-1}$) solution	Sigma	P4458
Peracetic acid 32 wt. % in dilute acetic acid	Sigma-Aldrich	26,933-6
Periodic acid solution (aqueous), 0.1%	Sigma	395132
Phosphate buffered saline with Ca2+ and Mg2+	Sigma Aldrich	D8662
Phosphate buffered saline without Ca2+ and Mg2+	Sigma Aldrich	D8537
Phosphotungstic acid (10% w/v)	Sigma-Aldrich	HT 152
Polymyxin B sulphate salt	CalBiochem	5291

Materials	Supplier	Reference
Potassium permanganate	BDH	102174M
ProLong™ Gold antifade mountant solution with DNA stains DAPI	Invitrogen	P36935
Proteinase K	DAKO	S3020
Quant-iT™ Picogreen ds DNA assay	Invitrogen Life Sciences, Paisley, UK.	P7589
Purelab Option distilled water still	ELGA LabWater, High Wycombe, UK.	N/S
Schiff's reagent	Sigma-Aldrich	3952016
Scott's tap water substitute	Atom Scientific	RRSP190
Sodium acetate	Fisher Scientific, Loughborough, UK	S/2120/70
Sodium azide (1 % solution)	G Biosciences	786-299
Sodium chloride	Thermo Fischer Scientific Ltd	S42429-5000
Sodium citrate	Sigma, Surrey, UK.	N/S
Sodium dodecyl sulphate, 10 %	Invitrogen Life Sciences, Paisley, UK.	24730-020
Sodium hydroxide	Fisher Scientific	S/400/60
Sodium thiosulphate pentahydrate	VWR	27905.293
Steri-strips	3M	R1540
Superfrost Plus microcope slides	Scientific Laboratory Supplies Ltd.	MIC3022
Trigene	Scientific Laboratory Supplies Ltd.	CLE1230

Materials	Supplier	Reference
TRIZMA base	Sigma-Aldrich Ltd, Poole, UK.	T1503
Trypan Blue (0.4 %)	Sigma, Surrey, UK.	T8154
Trypsin, 0.5 % with EDTA (10x)	Sigma, Surrey, UK.	T3924
Tryptone Phosphate Broth	Sigma, Surrey, UK.	T8782
Tween 20	Sigma-Aldrich	P1379
Ultrapure™ agarose gel	Invitrogen	16500500
Ultra-vision One detection system	Thermo Fischer Scientific Ltd	TL-125-HLJ
Ultra-vision One Large Volume Detection system, DAB plus substrate	Thermo Fischer Scientific Ltd	TLA-125-HDX
Vancomycin hydrochloride hydrate	Sigma-Aldrich	861987-1G
Virkon	Scientific Laboratory Supplies Ltd.	CLE1554
Xylene	Genta Medical	LS8A950/G
Zinc acetate	Sigma Aldrich	383317
Zinc chloride	Fluka	96470

2.1.2 Equipment used

The details and sources of the general equipment used throughout the study are listed in- Table 8~~Table 7~~.

~~Table of~~ *Table 8. List of equipment used and the relevant suppliers and reference codes. N/S = not stated* ~~7. List equipment used and the relevant suppliers and reference codes. N/S = not stated~~

Equipment used	Supplier	Reference
5% (v/v) CO_2 in air	BOC Ltd., West Sussex, UK.	N/S
Autoclave, bench top (12L)	Prestige Medical	Classic
Automatic pipettes	Gilson	Various
Balance-4 figure	Jencons PLC, Bedforshire, UK	AND GR-200
Balance-4 figure	Jencons PLC, Bedforshire, UK	AND GX-2000
Bijoux tubes (5 mL)	Scientific Laboratory Supplies Ltd (SLS), Nottingham, UK.	SLS7522
Roller Bottle apparatus	Integra Biosciences	CellRoll
Centrifuge	SANYO Biomedical Europe BV,	Harrier 15/80
Centrifuge-Micro	MSE	Microcentaur I
Class II safety cabinet (Heraeus 85)	Heraus Whiteley, Hants, UK.	CL2 N/S
CO_2 Incubator	SANYO Biomedical Europe BV, Amsterdam, Holland	MCO-20A1C
Counting Chamber Improved Neubauer	Scientific Laboratory Supplies Ltd (SLS), Nottingham, UK.	HIRS8100103
Coverslips (22x64 mm)	Scientific Laboratory Supplies Ltd (SLS), Nottingham, UK.	No. 1
Coverslips (19mm)	Thermo Fisher Scientific	46
Cryotome	Leica	CM1850

Equipment used	Supplier	Reference
Digital camera	Zeiss	AXIOCAM MRc5
Dissection kit	Thackeray Instruments	Various
DPX mountant	ABC Pure	RRSP29-B
Filter unit (250 mL, 0.2 µm)	Nalgene	126-0020
Freezer -25 °C	Jencons PLC, Bedforshire, UK	Electrolux 3000
Freezer -70 °C	SANYO Biomedical Europe BV	MDF-U53v
Freeze dryer	Thermosavant	ModulyoD-230
Heated forcepsFume hood	Bios EuropeWhiteley, Hants, UK.	Speciceps System IIN/S
Histocassettes (plastic)Heated forceps	VWR InternationalBios Europe	720-0887Speciceps System II
Histology mouldsHistocassettes (plastic)	Raymond A LambVWR International	E10.8/416172 0-0887
Histology water bathHistology moulds	Barnstead ElectrothermalRaymond A Lamb	MH8515E10.8 /4161
HotplateHistology water bath	Raymond A LambBarnstead Electrothermal	E18/1MH8515
HotplateHotplate	Scientific Laboratory Supplies Ltd (SLS), Nottingham, UK.Raymond A Lamb	Slide drying benchE18/1

Equipment used	Supplier	Reference
Hot wax ovenHotplate	Scientific Laboratory Supplies Ltd (SLS), Nottingham, UK.Scientific Laboratory Supplies Ltd (SLS), Nottingham, UK.	GPWAX-50-HYDSlide drying bench
Magnetic stirrerHot wax oven	Stuart ScientificScientific Laboratory Supplies Ltd (SLS), Nottingham, UK.	CB161GPWAX-50-HYD
Microscope-Inverted Magnetic stirrer	Olympus Optical Co (UK) Ltd, Southall, UK.Stuart Scientific	IX71CB161
Microscope-Inverted Microscope-Inverted	NikonOlympus Optical Co (UK) Ltd, Southall, UK.	Eclipse T5100IX71
Microscope-Upright Microscope-Inverted	ZeissNikon	Imager M2 AXIOEclipse T5100
Microscope image captureMicroscope-Upright	NikonZeiss	Digital Sight Ds-Fi1Imager M2 AXIO
MicrotomeMicroscope image capture	Leica MicrosystemsNikon	RM 2125 RTFDigital Sight Ds-Fi1
Orbital shakerMicrotome	Grant Instruments LtdLeica Microsystems	PSU-10iRM 2125 RTF
Pasteur pipettesOrbital shaker	Sigma-AldrichGrant Instruments Ltd	747760PSU-10i
pH meter Pasteur pippettes	Jenway Ltd, Dumow, UK.Sigma-Aldrich	3510747760

Equipment used	Supplier	Reference
Pipette boypH meter	Star LabsJenway Ltd, Dumow, UK.	Ergo One Fast3510
Plate readerPipette boy	HIDEXStar Labs	ChameleonErgo One Fast
Precision SlicerPlate reader	Andrew JamesHIDEX	AS-19Chameleon
Safety Cabinet, Class IIPrecision Slicer	Heraeus H518Andrew James	KendroAS-19
Specimen pot (100 mL, 250 mL)Safety Cabinet, Class II	Scientific Laboratory Supplies Ltd (SLS), Nottingham, UK.Heraeus H518	VariousKendro
SpectrophotometerSpecimen pot (100 mL, 250 mL)	Labtech internationalScientific Laboratory Supplies Ltd (SLS), Nottingham, UK.	Nanodrop ND-1000Various
Superfrost plus slidesSpectrophotometer	ThermoscientificLabtech international	J1800AMNZNanodrop ND-1000
ThermomixerSuperfrost plus slides	EppendorfThermoscientific	5355J1800AMNZ
Tissue Culture Flask (75 and 175 cm^2)Thermomixer	Fisher Scientific, Loughborough, UK.Eppendorf	Various5355
Tissue Culture Plates (6, 96)Tissue Culture Flask (75 and 175 cm^2)	Thermo Fisher Scientific LtdFisher Scientific, Loughborough, UK.	Nunc, variousVarious

Equipment used	Supplier	Reference
Tissue dissection equipmentTissue Culture Plates (6, 96)	Thermo Fisher Scientific LtdThermo Fisher Scientific Ltd	VariousNunc, various
Tissue punch biopsy (8 mm)Tissue dissection equipment	World Precision InstrumentsThermo Fisher Scientific Ltd	504535Various
Tissue punch biopsy (10 mm)Tissue punch biopsy (8 mm)	Acuderm Inc USAWorld Precision Instruments	P1025504535
Tissue punch biopsy (12 mm)Tissue punch biopsy (10 mm)	Acuderm Inc USAAcuderm Inc USA	P3525P1025
Tissue processorTissue punch biopsy (12 mm)	Leica TP1020Acuderm Inc USA	Leica Microsystems P3525
Universal/centrifuge tube (30 mL)Tissue processor	Scientific Laboratory Supplies Ltd (SLS), Nottingham, UK.Leica TP1020	CON9000Leica Microsystems
Vortexer Universal/centrifuge tube (30 mL)	Jencons PLC, Bedforshire, UKScientific Laboratory Supplies Ltd (SLS), Nottingham, UK.	GrantCON9000
Water bathVortexer	Fisher Scientific, Loughborough, UK.Jencons PLC, Bedforshire, UK	N/SGrant
Wax dispenserWater bath	Raymond A LambFisher Scientific, Loughborough, UK.	E66N/S

Equipment used	Supplier	Reference
Wax ovenWax dispenser	SLSRaymond A Lamb	GPwax/30/ssE 66
Wax oven	SLS	GPwax/30/ss

2.2 Methods

2.2.1 General solutions

2.2.1.1 Phosphate buffered saline

Ten phosphate buffered saline tablets were immersed in one litre distilled water and mixed using a magnetic stirrer and bar. pH was subsequently adjusted to pH7.2-7.4 if required using 6 M hydrochloric acid or 6 M sodium hydroxide dropwise (see Section 2.2.4). Solutions were autoclaved and stored for up to one month.

2.2.1.2 Sodium hydroxide solution (NaOH), 6M

NaOH pellets (120 g) were added to 500 mL distilled water and agitated until dissolved, before storage at room temperature for up to six months.

2.2.1.3 Ethanol (70 %; v/v)

Distilled water (200mL) was added to 100 % (v/v) ethanol (700 mL) to make 1 L of 70 % (v/v) ethanol.

2.2.1.4 Virkon solution (1 %; w/v)

Virkon powder (50 g) was added to 5 L distilled water to make Virkon solution (1 %; w/v).

2.2.1.5 DAPI dye solution (1 mg.mL^{-1})

10 mg DAPI was reconstituted in 10 mL nuclease-free water and stored at -25°C for up to six months wrapped in foil.

2.2.1.6 DAPI working dye solution (0.1 µg.mL^{-1})

DAPI dye solution (2.5 µL) was added to 25 mL dye buffer and inverted to mix.

The pH was adjusted to 7.4 using 6 M hydrochloric acid or 6 M sodium hydroxide added drop wise and the solution was used immediately (See Section 2.2.4).

2.2.1.7 Zinc fixative

A solution containing 0.5 % (w/v) calcium acetate, 0.5 % (w/v) zinc acetate, and 0.05 % (w/v) zinc chloride was dissolved into 0.1 M Tris solution. The pH was subsequently adjusted to pH 7.4 (See Section 2.2.4) and ~~sterilised by autoclaving~~autoclaved (See Section 2.2.3.2) before stored at 25 °C until required.

2.2.1.8 Scott's tap water working solution

A working dilution of Scott's tap water was made using a commercially available stock solution. Concentrated solution (10x; 25 mL) with added to 225 mL distilled water and stored at 25 °C until required.

2.2.2 Glassware

All glassware (beakers / bottles ranging between 10 mL to 2000 mL) were cleaned through immersion overnight in Virkon detergent solution (1 % v/v) (Neutracon®, Decon laboratories Ltd.). Glassware was subsequently rinsed in tap water and distilled water to remove residual detergent, and dried and ~~sterilised~~ autoclaved as described in Section 0.

2.2.3 Sterilisation

2.2.3.1 Dry heat sterilisation

Items for~~to be sterilised~~ dry heat sterilisation ~~by dry heat~~ were placed in an oven and held at a temperature of 180 ˚C for four hr.

2.2.3.2 Moist heat sterilisation

Objects and solutions unsuitable for dry heat sterilisation were ~~sterilised by autoclaving~~autoclaved at 121˚C, 15 pounds.inch^2 (psi) for 20 min.

2.2.4 Measurement of pH

The pH of a solution was measured using a Jenway 3510 pH meter. The pH meter was initially calibrated using solutions of pH 4, pH 7 and pH 10 and pH measured using a temperature probe to account for measurement alterations as a result of temperature. For pH adjustment of solutions, 1 M hydrochloric acid or 1 M sodium hydroxide was added drop-wise whilst stirring using a magnetic stirrer and bar.

2.2.5 Microscopy

2.2.5.1 Bright field microscopy

B~~Normal Koehler or b~~right field microscopy was performed using an Axio Imager M2 (Zeiss) microscope, in conjunction with an AxioCam MRc5 digital camera (Zeiss); the

microscope and camera were controlled using Zen Pro software (Zeiss). All images were captured digitally.

2.2.5.2 Phase contrast microscopy

Phase contrast microscopy was performed using a BX51 Inverted Microscope (Olympus), images were captured using an XC-50 Camera (Olympus) and Cell B Software (Olympus). All images were captured digitally.

2.2.5.3 Fluorescent microscopy

Fluorescent microscopy was carried out using an Axio Imager M2 (Zeiss) microscope, in conjunction with an AxioCam MRc5 digital camera (Zeiss). GFP (λ_{ex}: λ_{em} 470:525 nm) and DAPI (λ_{ex}: λ_{em} 365:445nm) filters were used in combination with a fluorescent illuminator (HXP 120V). The microscope and camera were controlled using Zen Pro software (Zeiss).

2.2.5.4 Confocal microscopy of decellularised porcine liver discs

Seeded discs were placed cell seeded side down on a microscope slide, with one to two drops PBS added periodically to prevent evaporation from the disc surface. Exposure times for each primary antibody was determined using non-stained seeded discs, with time remaining constant for each subsequent treatment conditions. Images were taken using an LSM880 inverted confocal microscope, with Z stack images of 100 µm depth from five locations per disc, with three seeded and stained discs per condition. Multiple images taken along the same Z line were stacked into one image using Zen Pro software (Zeiss).

2.2.6 Tissue procurement, dissection and storage

Porcine livers were obtained from a local abattoir (J Penny, Rawdon, Leeds, United Kingdom) and delivered to the laboratory within 12 hr of slaughter. Livers were taken from large white Yorkshire pigs between 24 and 26 weeks of age, all animals were slaughtered as part of the normal food chain. Livers were orientated to locate the left, right, medial, lateral, and caudate lobes. Appropriate lobes (Right medial and lateral, and left medial and lateral) were separated and labelled accordingly (Figure 5). Cores of liver (5-7 mm depth) were taken using a sterile punch biopsy tool of various diameters (8mm, 10mm, 12mm) and washed three times using phosphate buffered

saline (PBS) solution at room temperature with gentle agitation. Samples were stored at -70 °C on PBS moistened filter paper until needed (min. 24 hr).

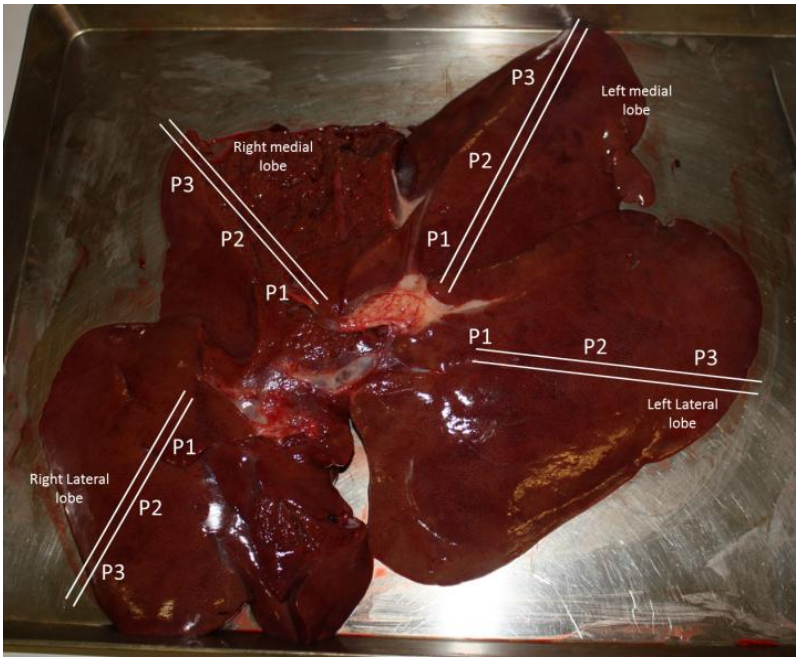

Figure 5. Image of porcine liver prior to dissection; ~~d~~digital labels added identify each lobe and positions within each lobe. RLL = right lateral lobe, RML = right medial lobe, LML = left medial lobe, LLL = left lateral lobe. P1 = position one, P2 = position two, P3 = position three.

2.2.7 General histological techniques

2.2.7.1 Tissue fixation

Formalin fixative

Tissue samples were placed into individual pencil labelled histology cassettes and immersed in 10 % (v/v) neutral buffered formalin (NBF; pH 7.5) for seven days (one hr if the sample was to be labelled using antibodies) at room temperature.

Zinc based fixative

Tissue samples were placed into individual pencil labelled histology cassettes and immersed in zinc fixative (0.1 M Tris-HCL, 0.5 g calcium acetate, 5 g zinc acetate & 5 g zinc chloride, pH 7.4) for 16 hr at room temperature.

2.2.7.2 Paraffin wax embedding of fixed tissue samples

Fixed tissue samples were dehydrated and impregnated with molten paraffin wax using an automatic tissue processor (Leica TP1020), the program used is detailed in Table 9.

Table 94. Program used to process fixed samples for paraffin wax histology

Station	Reagent	Temperature	Duration (hr)
1	10 % (v/v) Neutral buffered formalin	21 °C	0
2	70 % (v/v) Ethanol	21 °C	2
3	90 % (v/v) Ethanol	21 °C	2
4	100 % (v/v) Ethanol	21 °C	1
5	100 % (v/v) Ethanol	21 °C	1
6	100 % (v/v) Ethanol	21 °C	2
7	100 % (v/v) Xylene	21 °C	2
8	100 % (v/v) Xylene	21 °C	2
9	100 % (v/v) Xylene	21 °C	2
10	Paraffin Wax	50 °C	2
11	Paraffin Wax	50 °C	2
12	Paraffin Wax	50 °C	2

Following completion of the automated tissue processor, histology cassettes were transferred into molten wax and tissue was transferred into metal wax block moulds using heated forceps. Tissues were covered in molten wax and left to cool on ice for a minimum of two hr. Once the wax fully hardened, the moulds were removed and excess wax trimmed. All wax blocks were stored in a cool, dry atmosphere, away from direct sunlight.

2.2.7.3 Cryoembedding of tissue samples

Tissue samples were cryoembedded using OCT. A base layer of OCT media was placed in a plastic mould and frozen at -22 °C. Tissue samples were anatomically arranged, placed onto the frozen OCT embedding media and more OCT media was added until the entire tissue was covered. OCT media was frozen until the media turned white and subsequently stored at -70 °C until needed.

2.2.7.4 Tissue microtomy

Paraffin wax embedded tissues were cooled and subsequently sectioned at a thickness of between 4 and 6 µm using a Leica RM2125 RTF microtome. Using forceps and a brush, sections were floated in a heated water bath (45 °C - 50 °C) to remove folds and transferred onto positively charged slides (Superfrost Plus). If required, numerous levels were cut from the tissue to view various tissue depths from the surface (~~Figure 6~~Figure 6). Slides were placed on

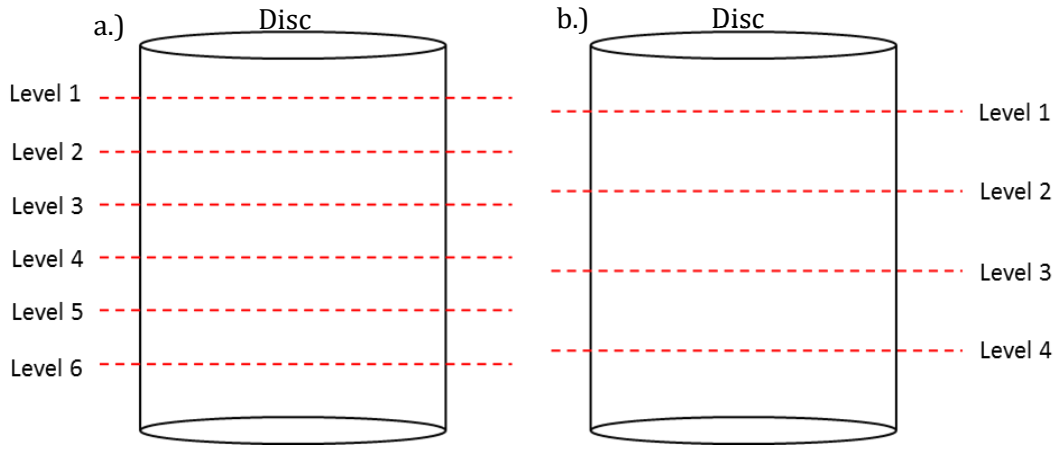

Figure 6. Outline of the regions within a tissue where multiple levels were taken during tissue microtomy. (a.) = six levels; b.) = four levels.

to a hot plate (55 °C -60 °C) for a minimum of one hr, wrapped in tin foil and subsequently placed in a hot air oven (60 °C) overnight ~~to sterilise~~ (See Section 2.2.3.1). Slides were left to cool before use.

2.2.7.5 Tissue cryotomy

OCT embedded samples were attached to a metal chuck and sectioned at between -21 °C and -24 °C, to a thickness of 8 µm using a CM1850 Leica cryostat. Sections were transferred onto positively charged slides (Superfrost Plus) and left to air dry for 30 seconds. Slides were subsequently placed in 70 % (v/v) ethanol for one minute and left to air dry, before staining.

2.2.7.6 Dewaxing and hydration of paraffin wax embedded tissue sections

Slides were immersed in two changes of Histoclear III or Xylene for ten min each. Slides were immersed into three changes of 100 % (v/v) ethanol for three min, two min, and two min consecutively. Slides were immersed in 70 % (v/v) ethanol for two min before gently rinsing in running tap water for three min to rehydrate each tissue section.

2.2.7.7 Tissue dehydration and cover slipping

Slides were immersed in 70 % (v/v) Ethanol for five s, followed by immersion in three changes of 100 % (v/v) Ethanol for one, two and three min respectively. Slides were immersed in Xylene twice, for ten min each before mounted on glass coverslips with DPX mountant and a glass coverslip. Slides were left for a minimum of four hr in a fume cupboard before visualisation.

2.2.8 Histological staining

2.2.8.1 Haematoxylin & eosin staining

Haematoxylin and eosin stains tissue architecture and cell nuclei. Haematoxylin binds to negatively charged deoxyribonucleic acid (DNA), staining nuclei purple and subsequently "blue'd" in Scott's tap water substitute. The retaining ~~histioarchitecture~~histoarchitecture was stained pink through the binding of Eosin to components of the cell cytoplasm and extracellular matrix.

Sections were rehydrated (Section 2.2.7.6) and immersed in Mayer's haematoxylin for one minute before rinsing in running tap water for three min. Sections were immersed in Scott's tap water substitute for three min and rinsed again in running tap water for one minute. Sections were subsequently immersed in eosin for three min before dehydration and mounted on glass coverslips using DPX mountant (Section 2.2.7.7). All slides were viewed under ~~normal Köhler illumination~~brightfield microscopy (Section 2.2.5.1).

Nuclei stain purple, blood stains red/dark pink and cytoplasm and extracellular matrix stain various shades of mid to light pink. Liver histoarchitecture can be identified thorough gross morphological features, with areas of darker pink in a hexagonal orientation signifying the presence of septal bands that surround the hepatic lobules. Within the septal bands, portal triads are identified through the presence of circular spaces with no visible staining present at the centre. Upon higher magnification of the portal triads, bile ducts are identified by closely arranged columnar cells with nuclei present at the lower cytoplasmic cell regions. Cells appear closely aligned and highly organised. Veins and arteries also surround circular areas with an absence of staining at the centre, encased within a thin pink perimeter, with veins being thinner than arteries. Arteries are differentiated by darker pink stained thicker perimeters than those seen with veins. Parenchymal cords run from the septal bands towards a circular area with a lack of staining (central vein). Parenchymal cords run perpendicular to the septal bands, in cords approximately one or two cells thick, separated by long adjacent areas with a lack of

haematoxylin staining. Areas of higher degradation within the septal bands are identified through separation of the collagen within the septal bands producing spaces between the hexagonally arranged septal bands and also thinning of the parenchymal cords resulting in greater diameters of the canaliculi where staining is absent.

2.2.8.2 DAPI labelling

DAPI (4'6-diamidino-2-phenylinole) used to stain double stranded DNA within tissue sections. When DAPI binds with adenine and thymine regions within the minor groove of double stranded DNA, fluorescence emitted can be detected using a fluorescent microscope fitted with a DAPI filter. Sections of tissue were dewaxed and rehydrated through graded alcohols (Section 2.2.7.6) before being immersed in DAPI working dye solution for ten min at room temperature. Slides were rinsed in three consecutive washes of PBS for ten min each before mounted on glass coverslips using aqueous mountant. All slides were viewed under fluorescent illumination using a DAPI and/or GFP filters (Section 2.2.5.3).

Nuclear staining is identified through the presence of circular areas of blue fluorescing areas. Larger fragment clumps / strands of DNA are identified through brighter areas of blue fluorescence. Extracellular matrix fluoresces green, with septal bands lying in a hexagonal orientation, with portal triads identified through a circular absence of fluorescence. Hexagonal cords fluorescence green, lying perpendicular to the hexagonal septal bands and lying adjacent to longer areas with an absence of fluorescence, leading towards a circular absence of fluorescence that signifies the central vein.

2.2.8.3 Masson's Trichrome staining

Hydrated sections were fixed for 24 hr in Bouin's fixative. Sections were stained with Weigert's haematoxylin for 25 min and differentiated with 0.5 % (w/v) acid alcohol for one minute. Slides were immersed within Ponceau Fuchsin for five min, immersed in tap water for one s before immersing in 1 % (w/v) phosphotungstic acid solution for 16 min. Sections were stained with light green, for 15 min and immersed in 1 % (w/v) phosphotungstic acid before placing in 1 % (v/v) acetic acid for five min. After rinsing in tap water for five s, slides were dehydrated by dipping two times through graded alcohols to prevent removal of the light green colour. Sections were subsequently mounted on glass coverslips using DPX mountant. All slides were viewed under ~~normal Köhler illumination~~brightfield microscopy (Section 2.2.5.1).

Nuclei stain brown, with circular brown stained areas identifying nuclei within the cells. Cells were stained fuchsia pink. Septal bands were identified through green stained strands in a hexagonal orientation, with circular non stained areas signifying the presence of the portal

triad. Fuchsia pink stained cells / parenchymal cords lie adjacent to the septal bands in lines that congregate to a green lined circular area absent of staining and signifying the presence of a central vein. Fine strands of green staining lie adjacent to the parenchymal cords when viewed under high magnification (Section 2.2.5.1), representing collagen strands that support hepatocytes of the parenchymal cords.

2.2.8.4 Picrosirius red and millers elastin

Combined staining of tissues with picrosirius red and millers elastin stains were used for the identification of collagen and elastin fibres respectively. Potassium permanganate (5 % w/v) was prepared by mixing 15 g potassium permanganate with 300 mL distilled water. Slides were rehydrated in graded alcohols (Section 2.2.7.6) and immersed in potassium permanganate for 5 min. Oxalic acid (1 % w/v) was prepared by mixing 1 g oxalic acid with 100 mL distilled water. Sections were rinsed in distilled water before immersion in oxalic acid for two min, followed by a one min rinse in distilled water, before re-immersion in oxalic acid for a further four min. Sections were sequentially dehydrated through immersed in 70 % ethanol (v/v, with distilled water) and 95 % ethanol (v/v with distilled water) for one min each, followed by immersion in Millers stain for one hr. Sections were rinsed in 70 % ethanol (v/v) until clear, and rehydrated in 96 % ethanol (v/v) before rinsing in running tap water for two min. Nuclei were stained for 10 min with commercially available Weigerts Haematoxylin (1:1 dilution of solution A and solution B) and rinsed for one min in running tap water and 30 s in distilled water. Sections were subsequently immersed in Sirius red (0.1% w/v, 0.1 g Sirius red and 100 mL saturated picric acid solution) for one hr, rinsed in distilled water and blotted dry. Sections were quickly dehydrated (five s each solution, (Section 2.2.7.7) and viewed using a bright field microscope (Section 2.2.5.1).

Dark pink stained hexagonal areas aid the identification of septal bands that surround the parenchyma. Parenchyma run perpendicular to the septal bands which are lined by darker stained pink strands of matrix that run in cords towards a circular area with an absence of staining, identified as the central vein. Within the septal bands, circular areas with an absence of staining and lined peripherally by darker pink stained matrix that represent the portal triad; namely the bile ducts, hepatic arteries and portal veins.

2.2.8.5 Reticulin staining

Reticulin stain was used to stain fine reticular fibres within the sinusoids of the hepatic parenchyma. Slides were rehydrated in graded alcohols (Section 2.2.7.6) and oxidised with potassium permanganate for five min, before bleaching in oxalic acid for one minute. Sections

were covered with iron alum for 15 min, before immersion in freshly prepared ammoniacal silver solution Ammoniacal Silver solution for two min. Sections were reduced for two min in 10 % (v/v) formalin, before being toned in 0.2 % (w/v) gold chloride for three min. Excess silver solution was removed through immersion in hypo solution for three min. Sections were counterstained with acidified neutral red for two min before dehydration and coverslipping using DPX mountant (Section 2.2.7.7).

Extracellular matrix stains black, lying in strands within a hexagonal orientation, aiding in the identification of septal bands. Lying adjacent to the parenchymal cords, fine reticulin staining black strands that stretch across the cannuliculi. Nuclei are identified as black, peripherally stained circles. Portal triads are identified through circular areas within the septal bands that show an absence of black staining. Cells are identified through identification of circular pale pink staining.

Ammoniacal Silver solution

All solutions should be made using glassware that has been rinsed in tap water three times, followed by rinsing in distilled water once. Ammonia (37 % v/v) was added dropwise to 5 mL 10 % (w/v) aqueous silver nitrate solution until a precipitate was formed. 5 mL 3 % sodium hydroxide (w/v) was added and ammonia (37 % v/v) was added dropwise until the resulting precipitate was almost completely dissolved. Solution was made up to 50 mL using distilled water. In subsequent staining procedures, two steps were changed. Sections were immersed in Iron alum for ten min instead of 15 min, and counterstained with eosin for three min instead of acidified neutral red.

~~Alcian blue staining~~

~~Alcian blue at different pH can be used to identify various types of acidic mucins through the ionisation of reacting groups. Alcian blue dye can be diluted in various acids to create differing pH's (Table 9). Slides were dewaxed and rehydrated through graded alcohols (Section 2.2.7.6) before immersing in 1 % (w/v) alcian blue for 15 min. Slides were rinsed in running tap water for ten s followed by rinsing slides in distilled water for ten s. If required, diastase staining and/or combined PAS staining can take place at this point. Slides were counterstained with 0.1 % (w/v) nuclear fast red for five min, subsequently dehydrated and mounted on cover slips using DPX mountant (Section 2.2.7.7).~~

Table 5. Diluents used in the preparation of alcian blue stains at varying pH's

~~Diluent (100 mL)~~	~~pH~~
~~10 % (v/v) sulphuric acid~~	~~0.2~~
~~0.2 M sulphuric acid~~	~~0.5~~
~~0.1 M hydrochloric acid~~	~~1.0~~
~~3 % (v/v) acetic acid~~	~~2.5~~
~~0.5 % (v/v) acetic acid~~	~~3.2~~

2.2.8.6 Periodic acid Schiff staining

Two tissue sections were stained from each block. Sections were dewaxed and rehydrated through graded alcohols (Section 2.2.7.6), rinsed in distilled water for 30 s and one of the two slides was immersed in diastase solution (0.5 % (w/v) α-amylase) before heating the diastase solution for 20 s in a microwave. Diastase treated slides were subsequently rinsed in running tap water for five min.

All slides (diastase treated and non-diastase treated) were immersed in 0.1 % (v/v) periodic acid solution for five min and rinsed in distilled water, before immersion on Schiff's reagent for 15 min. Slides were rinsed in running tap water for five min before immersion in Weigert's haematoxylin for 90 s. Slides were rinsed in running tap water until the water ran clear, and quickly immersed in 70 % (v/v) ethanol for five s before dehydration in 100 % (v/v) ethanol and xylene. Slides were mounted on glass coverslips using DPX mountant (See Section 2.2.7.7).

~~Combined ABPAS/D~~

~~Combined alcian blue staining with periodic acid Schiff staining involves staining one section with both stains. Two tissue sections were stained from each block. Sections were dewaxed and rehydrated through graded alcohols (Section 2.2.7.6) before immersion in 1 % (w/v) alcian blue for 15 min. Slides were rinsed in running tap water for ten s followed by rinsing slides in distilled water for ten s. One of the two slides was immersed in diastase solution (0.5 % (w/v) α-amylase) before heating the diastase solution for 20 s in a microwave. These slides were subsequently rinsed in running tap water for five min. All slides (diastase treated and non-diastase treated) were immersed in 0.1 % (v/v) periodic acid solution for five min and rinsed in distilled water, before immersion in Schiff's reagent for 15 min. Slides were rinsed in running tap water for five min before immersion in Weigert's haematoxylin for 90 s. Slides were rinsed in running tap water until the water ran clear and quickly immersed in 70 % (v/v) ethanol for five s before dehydration in 100 % ethanol and xylene. Slides were mounted on glass coverslips using using DPX mountant.~~

2.2.9 Labelling of proteins

2.2.9.1 Antibodies

The antibodies used in immunocytochemical studies, including the clone and lot numbers along with the antigen retrieval where needed can be found below (Table 1010 ~~-~~– Table 12~~Table 14~~).

Table~~-~~ 10~~10~~. Primary antibodies used throughout the study

Antibody	Clone	Conc. (µg.mL^{-1})	Retrieval technique	Time (min)	Isotype
Collagen I	MAB3391	10.00	Proteinase K	20	IgG1
	ab34710	2.00	Unmasking solution	MW5	IgG
Collagen III	ab7778	1.00	Proteinase K	20	IgG

Collagen IV	CIV 22	0.25	Proteinase K & Trypsin digestion	20 & 0.5	IgG1
Fibronectin	A0245	4.90	Proteinase K	20	Poly
Laminin	LAM-89	1.00	Proteinase K	20	IgG1

Table- 1111. Isotype control antibodies used throughout the study.

Antibody	Clone	Conc. (µg.mL^{-1})
Rabbit immunoglobulin (poly)	X0936	4.9
Mouse immunoglobulin G1 (IgG1)	X0931	0.25 ,10.00
Rabbit immunoglobulin (IgG)	GTX 35035	1.00, 2.00

Table 1212. Secondary antibodies used throughout the study.

Antibody	Clone	Dilution
Goat anti-mouse	A4416	1 in 5000
Goat anti-rabbit	A6154	1 in 5000

2.2.9.2 Antigen retrieval

All antigen retrieval techniques were used to expose certain epitopes or sites that were masked through fixation, thereby improving the accessibility of the antibodies to target sites within the tissue

2.2.9.3 Proteinase K

Slides were placed in slide rack and sections were circled with ImmEdge hydrophobic pen. Proteinase K solution was dropped onto the tissue section, ensuring all tissue areas were covered. Sections were incubated for 20 min at room temperature.

2.2.9.4 Antigen unmasking solution

A concentrated (100x) citrate-based antigen unmasking solution (Vector Laboratories) was diluted with distilled water (1 mL : 106.67 mL) and placed in either a coplin jar (50 mL) or staining pot (250 mL). Solutions were heated in a water bath to 95 °C for either 20, 30 or 40 min, or in a microwave for five min.

2.2.9.5 Immunohistochemical labelling of tissues

Slides were dewaxed (Section 2.2.7.6) and relevant antigen retrieval performed (Section 2.2.9.2). Sections were immersed in 3 % (v/v) hydrogen peroxide in PBS and washed in Tris buffered saline (TBS) for ten min, Ultra V block was dropped onto the entire section and incubated for ten min at room temperature, before washing twice in TBS for ten min each at room temperature. Primary antibody, isotype control or TBS were placed on each relevant section for one hr at room temperature in a moist environment (or overnight at 37 °C), corresponding to test sections, isotype control sections and negative control sections respectively. Sections were washed twice with TBS-Tween and twice with TBS for ten min each before application of HRP polymer to the entire sections for 30 min at room temperature in the dark. Sections were washed twice with TBS-Tween and twice with TBS for ten min each at room temperature and substrate chromogen was added to entire sections before incubating at room temperature for ten min. Slides were rinsed four times with distilled water for ten s each, counterstained in haematoxylin for ten s and rinsing in tap water until clear. Haematoxylin-stained nuclei were "blue'd" with Scott's tap water for three min. Slides were rinsed in tap water for three min and rehydrated through graded alcohols to Xylene. Sections were mounted on glass coverslips using DPX mountant and glass coverslips (Section 2.2.7.7). Sections were imaged using an upright brightfield microscope and images taken using a digital camera (Section 2.2.5.1).

Locations of the proteins of interest are identified through the presence of brown staining, with nuclei stained blue.

2.2.9.6 Immunofluorescent labelling of tissue sections

All procedures were performed at room temperature unless otherwise stated. Slides were dewaxed (Section 2.2.7.6) and relevant antigen retrieval performed (Section 2.2.9.2). All wash steps were performed using TBS with gentle agitation. Sections were washed in Tris buffered saline (TBS) for ten min and incubated in block solution (goat serum) for one hr. Diluted primary or isotype control antibodies (in antibody diluent) at relevant concentration (or antibody diluent for negative control) were added to test, isotype control and negative control sections respectively and incubated for one hr (Table 13 and Table 14). TBS-T washes were performed with gentle agitation for ten min before incubation in appropriate concentration of secondary antibody (in antibody diluent) for 30 min in a humidified chamber in the dark (See Table 14). Sections were washed for ten min in TBS-T, before counterstaining nuclei for ten min with DAPI working solution in the dark. Sections were washed in the dark for 15 mins and

mounted using fluorescent mounting media, before visualisation under fluorescence illumination using appropriate filters. Images were captured digitally (Section 2.2.5.3).

2.2.9.7 Immunofluorescent labelling of cells cultured in wells

Cells were cultured on 13 or 19 mm diameter coverslips, washed three times (500 µL PBS) and fixed in 4% soln of paraformaldehyde (w/v in PBS) for 10-15 min. All subsequent steps used 500 µL solution unless otherwise stated. Cells were washed three times (PBS). Cells were either stained immediately or stored at 4 °C for up to seven days. Cells were permeabilised in Triton X-100 (0.1-0.2 % in PBS) for five min before washing three times in PBS. Primary antibody (50 µL, pre diluted in 10 % foetal bovine serum (FBS) in PBS to appropriate concentration) was added to seeded coverslips and incubated in a sealed humidified chamber for one hr at room temperature, or overnight at 4 °C. Seeded coverslips were washed three times in PBS, with secondary antibody (50 µL prediluted to 1:500 in 10 % FCS) added for one hr at room temperature in the dark. Cells were washed three times in PBS and mounted on slides using ProLong Gold anti-fade mountant solution with DAPI before visualisation using an Axio Imager M2, with Hoechst (λ_{ex}: λ_{em} 365:445nm) and TexasRed (λ_{ex}: λ_{em} 594:610nm) filters.

Table 136. Primary antibodies used to label cells.

Antibody	Marker	Reference / Clone	Dilution
Ki-67	Cell proliferation marker	SP6	1 in 200
EpCAM	Cell adhesion marker	VU109	1 in 800
Albumin	Functional hepatocyte marker	15C7	1 in 1000

Table -141814. Alexa fluor secondary antibodies used to fluorescently label cells.

Target	Species	Dilution
Anti-mouse 594 nm	Goat	1 in 500
Anti-mouse 594 nm	Donkey	1 in 500
Anti-mouse 488 nm	Goat	1 in 500

Anti-mouse 488 nm	Donkey	1 in 500
Anti-rabbit 594 nm	Goat	1 in 500
Anti-rabbit 594 nm	Donkey	1 in 500
Anti-rabbit 488 nm	Goat	1 in 500
Anti-rabbit 548 nm	Donkey	1 in 500

2.2.9.8 Live / dead staining of cells cultured on discs

Cell viability was assessed using a commercially available Live / dead viability kit. Calcein am is able to transfers across the membrane of viable cells, whereas ethidium homodimer-1 can only penetrate the damaged membranes of dead cells, binding to cell proteins and/or DNA. Upon subsequent excitation, viable cells fluoresce green, whereas non-viable cells fluoresce red. Calcein AM (5 µL) and ethidium homodimer-1 (20 µL) were added to 10 mL dPBS to create a working solution. Seeded discs and/or wells were rinsed with dPBS three times, and sufficient working solution was added to the discs (or wells) to cover the discs or bottom of the cell monolayer (1 mL for discs or 100-200 µL for wells), and subsequently incubated for 30 min at room temperature. Discs were imaged using an inverted confocal microscope (See Section 2.2.5.4), with 530 nm filters for Calcein AM labelled cells (green fluorescence) and 546 nm filters for ethidium homodimer labelled cells (Section 2.2.5.4).

2.2.10 DNA extraction

2.2.10.1 Tissue lyophilisation

Using a scalpel, samples of tissue were macerated and placed in sterile Eppendorf tubes. Samples were weighed in triplicate to a mean wet weight before being freeze dried at -50 °C, 0.15-0.2 mbar. Samples weights were measured every 24 hr until constant.

2.2.10.2 DNA extraction - ~~DNA extraction~~Method

DNA was extracted from freeze dried samples of liver using Qiagen DNeasy Blood and Tissue kit and two methods were used to quantify DNA. Total extracted DNA was quantified spectrophotometrically using a Nanodrop and double stranded DNA was quantified using a Quant-iT Picogreen® dsDNA Assay kit.

Samples of tissue (25 mg) were lyophilised to a constant weight and subsequently macerated. Buffer ATL (360 µL) and 40 µL proteinase K were added to each tube before thorough vortexing for 15 s. Samples re digested overnight at 56 °C with agitation (650 RPM). Once the tissue was dissolved, 400 µL Buffer AL was added, samples were thoroughly vortexed and 400 µL ice cold

ethanol (96-100% v/v) was added before thorough vortexing again for 15 s. 600 µL samples solution were pipetted onto a spin column and subsequently placed inside a 2 mL tube. Tubes were centrifuged at 6000 g for one minute and flow-through was discarded. Remaining solution was pipetted onto the spin column and tubes were centrifuged at 6000g for one minute before flow through was discarded. Buffer AW1 (500 µL) was added to the spin column before centrifugation for one minute at 6000 g. Flow through and tubes were discarded, 500 µL Buffer AW2 was added to each spin column and samples were centrifuged at 16,100 g for six min before discarding the flow-through. Buffer AE (200 µL) was added directly to the membrane and tubes were incubated for one minute at room temperature. Tubes were centrifuged at 6000 g for one minute, to elute the DNA. Yield was maximised by adding an additional 100 µL Buffer AE directly to the membrane, incubating at room temperature for one minute, and centrifuging for one minute at 6000 g. Extracted DNA was stored at either 4 °C for short periods (24 hr) or -20°C for extended periods (>24 hr).

2.2.11 Total and double stranded DNA quantification

2.2.11.1 Spectrophotometry

Total DNA was quantified by measuring absorbance using a Nanodrop spectrophotometer at 260 nm, blanked against Buffer AE. Each sample was vortexed for five s before quantification and measured in triplicate. Samples were blanked before quantification of a subsequent sample. Adjusting the readouts to account for the final volume and amount (mg) of tissue used, provides the amount of DNA in the tissue (recorded as $\mu g.mg^{-1}$). A standard curve of known concentrations (0 to 50 $ng.mL^{-1}$) of calf thymus DNA was also measured to assess the accuracy of the technique.

2.2.11.2 PicoGreen

Double stranded DNA was selectively quantified using a Quant-iT Picogreen® dsDNA Assay kit. A standard curve of lambda DNA was diluted with TE buffer, to concentrations of 1 through 1000 $ng.mL^{-1}$. 100 µL of each solution was added to a black, 96-well plate in triplicate. Test samples were diluted in TE buffer to an appropriate dilution (10 µL, 5 µL or 2 µL in 300 µL) and 100 µL of each test sample was added in triplicate to the 96-well plate. 100 µL Picogreen reagent was added to each well, plates were excited at 485 nm and emission spectra read at 535 nm using a Chameleon platereader. Standard curve results were plotted on a graph using GraphPad prism 6. Test fluorescence values were interpolated from the standard curve and DNA content per mg tissue calculated using lyophilised tissue weights and appropriate dilutions.

2.2.12 Assessment of DNA length using agarose gel electrophoresis

Quantification of base pair length of DNA extracted from either native and/or decellularised porcine liver was achieved through gel electrophoresis. Agarose gels (2 %) were made using heated Ultrapure™ agarose (Invitrogen™) and Tris acetate-EDTA (TAE) buffer. Agarose solution was added to a casting plate with ethidium bromide (0.01% v/v) and a well comb before being allowed to set at room temperature. The gel was submerged in 1x TAE buffer inside a gel tank (BioRad) before addition of 10 µL extracted DNA to individual wells, previously diluted as required in Buffer AE (Qiagen). A 500 bp DNA ladder (Thermo Scientific™) was placed in one well as a reference. Samples were run with a constant voltage of 120V for 20 – 40 min, and DNA was visualised and captured using a UV lightbox and GelDoc™.

2.2.13 Decellularisation

2.2.13.1 Preparation of solutions

Antibiotic solution (0.05 mg.mL^{-1}, vancomycin, 0.5 mg.mL^{-1}, gentamicin, 0.2 mg.mL^{-1}, polymyxin B)

To 100 mL PBS, vancomycin hydrochloride (50 mg), gentamicin sulphate (500 mg) and polymyxin B (200 mg) were added. pH was adjusted to 7.2 – 7.4 as described in Section 0, before being was made up to 1L with PBS. The solution was used within one hr of production.

EDTA solution (200 mM)

EDTA (74.4 g) was added to 1 L distilled water and after thorough mixing, the pH was adjusted to 7.2 – 7.4 as described in Section 2.2.4. The solution was autoclaved as described in Section 2.2.3.2 and stored for up to one month at room temperature.

Hypotonic buffer (10 mM Tris, 2.7 mM EDTA, 10 KIU. mL^{-1} aprotinin)

EDTA (1g) and Trizma base (1.21 g) were added to 900 mL distilled water and after thorough mixing, the pH was adjusted to 8.0 – 8.2 as described in Section 2.2.4 and autoclaved as described in Section 2.2.3.2. The solution was stored for up to one month at room temperature. Immediately before use, 1 mL of aprotinin (10,000 KIU. mL^{-1}) was added using a needle and syringe.

SDS hypotonic buffer (0.1 % (w/v) SDS, 10 mM Tris, 2.7 mM EDTA, 10 KIU. mL^{-1} aprotinin)

To 990 mL autoclaved hypotonic buffer, sodium dodecyl sulphate (SDS) solution (10 mL; 10 %(w/v)) was added. 1 mL of aprotinin (10 KIU.mL^{-1}) was added to the solution using a needle and syringe immediately before use.

PBS EDTA solution (2.7 mM EDTA, 10 KIU. mL^{-1} aprotinin)

EDTA (1g) and ten PBS tablets were dissolved in 1 L distilled water. The pH was adjusted to 7.2 – 7.4 as described in Section 2.2.4, and the solution was autoclaved as described in Section 2.2.3.2. The solution was stored for up to one month at room temperature. 1 mL aprotinin (10 KIU.mL-1) was aseptically added using a needle and syringe immediately before use.

Nuclease solution (50 mM Tris, 1 mM MgCl2.6H2O, 1 U.mL^{-1} Benzonase)

Magnesium chloride (0.203 g) and trizma base (6.1 g) were added to 100 mL distilled water and, after thorough mixing, the pH was adjusted to 7.5 – 7.7 as described in Section 0. The solution was autoclaved as described in Section 0, before storing at room temperature for up to one month. Immediately before use, 4 µL of Benzonase (250 U.µL^{-1}) was added aseptically.

Hypertonic solution (50 mM Tris, 1.5 M NaCl)

Sodium chloride (87.66 g) and Trizma base (6.06 g) were added to 900 mL distilled water and the pH was adjusted to 7.5 – 7.7 as described in in Section 2.2.4. The solution was autoclaved as described in Section 2.2.3.2. The solution was stored for up to one month at room temperature.

PAA solution (0.1 % v/v)

Peracetic acid stock solution (1 mL) was added to 1 L phosphate buffered saline solution and pH was adjusted to pH 7.0 as described in Section 2.2.4. The solution was used immediately.

2.2.13.2 Decellularisation - Method

All solutions were normalised to their working temperature before use. Samples were removed from frozen storage and thawed at 37 °C for between 30-60 min. All following steps were performed within a roller bottle at 37 °C, rolling at 6 RPM on an Integra Cell Roll machine unless otherwise stated. Tissue was incubated in disinfection solution for 30 min at 37 °C. Tissues were incubated at 4° C in of 200 mM EDTA solution for 24 hr: 37 °C in hypotonic buffer for 24 hr: 37 °C in 0.1 % (v/v) SDS hypotonic buffer for 24 hr: at which point tissue was washed three times in PBS at 37 °C for 30 min each. Tissue samples were placed in PBS at 37 °C for 24 hr and washed in PBS EDTA solution at 4 °C for 48-72 hr. Tissue samples were placed in nuclease solution twice at 37°C, for three hr each and immersed in PBS at 37 °C for 24 hr. Tissue samples were washed in PBS at 37 °C for 24 hr and incubated in hypertonic solution at 37 °C for 24 hr before immersion in PBS at 37 °C for 24 hr. Tissue samples were washed in PBS solution at 37

°C for thirty min before ~~sterilisation~~ being immersed with 0.1% (v/v) PAA solution for three h~~2.2.13~~r at 21 °C. The samples were rinsed in PBS at 37 °C for 30 min within a class II safety cabinet. Tissues were aseptically washed up to eleven times with PBS solution to ensure adequate removal of peracetic acid solution.

The above procedure describes a one cycle protocol, however in two cycle and three cycle protocols, extra cycles of SDS and hypotonic buffer immersion~~s~~ were performed before immersion in the nuclease solutions.

2.2.14 Biochemical analysis

2.2.14.1 Acid hydrolysis

Tissue was lyophilised as described in Section 0 and placed in vented glass tubes containing 5 mL HCl (6M). Samples were hydrolysed using a bench top autoclave which was heated to 121 °C for four hours at a pressure of 103 kPa, before being neutralised using NaOH (6M). The final volume of hydrolysed sample was recorded.

2.2.14.2 Quantification of hydroxyproline content

As the amino acid hydroxyproline is present at known frequencies in the amino acid sequence of collagen, its quantification can be used as a marker of collagen content. Originally based on a colourimetric assay (Edwards and O'Brien, 1980), the oxidation of hydroxyproline forms pyrroles that react with p-dimethylaminobenzaldehyde. The resulting red chromophore can be quantified using a spectrophotometer.

Hydroxyproline buffer was made adding 13.3 g citric acid, 32g of sodium acetate-3-hydrate, 9.1 g sodium hydroxide, 3.2 mL glacial acetic acid and 80 mL propan-1-ol, made up to 400 mL with distilled water. After tissue lyophilisation (Section 2.2.10.1) and acid hydrolysis (Section 2.2.14.1), standards of known concentration (0-30 $\mu g.mL^{-1}$) were created through diluting trans-4-hydroxy-L-proline in hydroxyproline buffer. Test samples were diluted 1:20 in hydroxyproline buffer and 50 µL of standards and test samples were added, in triplicate, to a clear flat-bottomed 96-well plate. Chloramine T solution was prepared by mixing 1.41g Chloramine T with 100 mL distilled, with 100 µL added to each plate well. Plates were incubated at room temperature for five min with agitation. Erhlich's reagent was prepared by adding p-dimethylbenzaldehyde, 13 mL perchloric acid (62 % v/v) and 30 mL propan-1-ol and sufficient distilled water to make up to 50 mL solution. Ehrlich's reagent (100 µL) was added to each well and plates were incubated for 45 min (60 °C). Optical density of each well was measured (570 nm) using a microplate spectrophotometer. A standard curve (absorbance vs

concentration) was generated from standard values and used to interpolate unknown test samples. All values were normalised with corresponding diluting volume and dry tissue weight.

2.2.14.3 Quantification of denatured hydroxyproline content

Samples were lyophilised, as outlined in Section 2.2.10.1. Digestion buffer was made by mixing Trizma base (1.21 g), calcium chloride (0.15 g) and 100 mL distilled water using a magnetic stirrer and bar. pH was subsequently adjusted to pH7.8 (if required) using 6 M hydrochloric acid or 6 M sodium hydroxide dropwise. 20 mL digestion buffer was mixed with 100 mg α-chymotrypsin (≥40 units.mg^{-1}) to create a digestion solution (5 mg.mL^{-1} conc). Samples were incubated in digestion solution (5 mL) for 24 hr at 30 °C, and then centrifuged at 600 g for ten min. Supernatant was removed and transferred to vented glass test tubes before being hydrolysed and neutralised as described in Section 2.2.14.1. Denatured hydroxyproline content was subsequently calculated as described in Section 2.2.14.2, without the need for dilution in hydroxyproline buffer.

2.2.14.4 Quantification of sulphated glycosaminoglycan content

Sulphated glycosaminoglycans were quantified using a colourimetric assay originally developed by Farndale and colleagues (1986). Under acidic conditions sulphated GAGs react with the cationic dye 1,9-dimethylene blue (DMB) to produce a colour that can be measured spectrophotometrically and compared to standards of known concentration. Tissue samples were lyophilised (as per Section 2.2.10.1). Papain digest buffer (pH 6.0) was made by mixing 0.788 g L cysteine hydrochloride and 1.8612 g Na_2EDTA with 1L distilled water. Papain (1250 U) was mixed with digest buffer (25 mL) to form a digestion solution, 5 mL of which was added to each sample. Samples were incubated for 36 hr at 60 °C. Sodium di-hydrogen orthophosphate solution (0.1 M, Solution A) was made by mixing 3.45 g sodium di-hydrogen orthophosphate with 250 mL distilled water. Di-sodium hydrogen orthophosphate solution (0.1 M, Solution B) was made by mixing 3.55 g di-sodium hydrogen orthophosphate with 250 mL distilled water. Assay buffer (pH 6.0) was made by mixing 137 mL Solution A with 63 mL Solution B (63 mL). Standards of known concentration (0-200 µg.mL^{-1}) were created by diluting chondroitin sulphate B with assay buffer, before loading 40 µL of standards and test samples in triplicate on a clear, flat-bottomed 96-well plate. DMB dye (pH 3.0) was made by adding 16 mg DMB, 2 mL formic acid, 5 mL ethanol (100 % v/v) with 2g sodium formate and making the solution up to 1 L with distilled water. DMB dye (250 µL) was added to each well, and the plate was incubated with gentle agitation for two min at room temperature, before spectrophotometrically measuring optical density of each well (525 nm). A standard curve of absorbance vs concentration was created using samples of known chondroitin sulphate B

concentration. Chondroitin B standard curve was used to quantify GAG content in test samples, which was subsequently normalised for dilution volume.

2.2.15 Measurement of cell activity using a GlucCell glucose monitoring system

Metabolic activity was determined through measurement of glucose uptake from the surrounding medium. Small volumes of medium (20 µL) were removed at the end of the experiment before disposal and glucose was quantified using a GlucCell glucose monitoring system and testing strips. Glucose concentration at each time point was subtracted from the glucose concentration at day 0 (initial glucose concentration in the culture medium) to determine glucose uptake (positive values) or glucose production (negative values).

2.2.16 Tissue culture maintenance and cell lines~~{Nakabayashi, 1982 #909}{Gripon, 2002 #885}~~

2.2.16.1 Cell details and m~~M~~edia preparation

L929

First derived in 1948, NCTC clone 929 (L929) cells are an adherent fibroblast-like cell line derived from the subcutaneous connective tissue of a 100 day old male C3H/An mouse. This specific cell line is used for toxicity testing (ATCC: CCL-1). To Dulbecco's minimal essential medium (DMEM), 10 % (v/v) Foetal bovine serum (FBS), penicillin (100 $mg.mL^{-1}$)/ streptomycin (100 $U.mL^{-1}$) and 2 mM L-glutamine were added and the solution was inverted twice to mix.

Double strength medium - Foetal bovine serum (20%), L-glutamine (4mM) and penicillin (200$mg.mL^{-1}$)/ streptomycin (200 $U.mL^{-1}$) were aseptically added to 14.8 mL DMEM. Solutions were inverted twice to mix.

BHK

BHK-21 (C-13) cells are an adherent fibroblast cell line originally derived in 1961 from the uninfected kidneys of five unsexed, 1 day old Syrian golden hamsters (ATCC: CCL-10). To Glasgow's minimal essential medium (GMEM), 5% (v/v) foetal bovine serum (FBS), 5% (w/v) tryptose phosphate broth, penicillin (100 $mg.mL^{-1}$)/ streptomycin (100 $U.mL^{-1}$) and 2 mM L-glutamine were added and the solution was inverted twice to mix.

Double strength medium – Foetal bovine serum (10%), L-glutamine (4mM), 4 mL Tris phosphate buffer and penicillin (200$mg.mL^{-1}$)/ streptomycin (200 $U.mL^{-1}$) were aseptically added to 12.8 mL DMEM. Solutions were inverted twice to mix

Huh7

Huh7 cells are an epithelial-like hepatocyte derived immortalised cell line derived from the hepatocellular carcinoma of a 57-year old Japanese Male (Nakabayashi et al., 1982). To 500 mL Dulbecco's minimal essential media, 50 mL 10% foetal bovine serum, 5 mL penicillin / streptomycin and 5 mL non-essential amino acid mixture was added. Differentiation media was made by adding 1.5 - 2 % DMSO (v/v) (dimethylsulphoxide) to the standard media

HepaRG

The HepaRG cell line is a terminally differentiated, immortalised cell line derived from the liver of an adult female patient with hepatocarcinoma and hepatitis C infection (Gripon et al., 2002). HepaRG cells can be induced to differentiate using 2% DMSO and support infection with hepatitis B virus. To 500 mL William's media, 50 mL (10 %) foetal bovine serum (non-heat inactivated), 5 mL penicillin / streptomycin and 5 mL glutaMAX, 0.5 mL human insulin (40 $IE.mL^{-1}$), 600 µL hydrocortisone (4.4 $mg.mL^{-1}$) and 800 µL gentamycin were added. Differentiation media was made by adding 1.8 - 2 % (v/v) DMSO to the standard media.

2.2.17 Long term storage and resuspension of cell lines

Cell lines were stored in medium with 20 %(v/v) DMSO in the vapour phase of liquid nitrogen until they were rapidly thawed in a water bath of 37°C for two min. 10 mL of the appropriate medium was added drop-wise to reduce the chance of osmotic shock to the cells. To remove the toxic DMSO, the suspension was centrifuged at 150 g for ten min. The supernatant was removed and the cell pellet was resuspended in 1 mL of fresh medium, which was diluted 1/10 before being transferred to a sterile 75 mL cell culture flask and incubated at 37°C with 5% (v/v) CO_2 in air.

2.2.18 Cell passaging

Cell culture medium was removed and gently washed twice with 10 mL PBS (without Ca_{2+} or Mg_{2+}). Adherent cells were detached from the tissue culture plastic by adding trypsin/ EDTA solution (2 mL) and incubating the flask for ~~five~~ up to ten min. Flasks were then gently tapped to ensure cell detachment, and appropriate cell culture medium (10 mL) was added to inactivate the trypsin. A cell pellet was generated by centrifugation of the cell suspension at 150 g for ten min. The cell pellet was re-suspended in 1 mL relevant culture medium and cells were counted using a haemocytometer. The cell suspension was then adjusted to the appropriate cell density and transferred to a T175 tissue culture flask with 20 mL fresh culture medium. Cell culture medium was replaced every 48 hr until cells had reached approximately 70 - 80 % confluency.

2.2.19 Culture on tissue culture plastic

2.2.19.1 L929. BHK and Huh7 cell lines on tissue culture plastic

Media was changed every two to three days and cell confluency checked at every media change. To ensure cells remain in a proliferative state, cell were passaged at sub-confluent levels (70 % - 80 %). Cells were rinsed three times with PBS solution and detached using 3-5 mL trypsin at 37 °C, 5 % CO_2 for up to ten min. Trypsin was neutralised by adding double the amount of cell media, and a suitable amount of cell suspension was transferred to a 175 cm^2 flask, which was made up to 20 mL with additional media. Flasks were incubated at 37 °C, 5 % CO_2 until sub-confluent. Only Huh7 were differentiated at low to medium density to maximise free space for subsequent cell division. Huh7 were differentiated with the addition of 1.5 – 2 % (v/v) DMSO to standard media. DMSO supplemented media was changed every 72 hr.

2.2.19.2 HepaRG cell lines on tissue culture plastic

Every three to four days, cells were washed with PBS solution (containing Ca_{2+} and Mg_{2+}) and pre-warmed media (37 °C) was added to a suitable volume for the flask (25 mL in 175 cm^2 flask). Cells were passaged at sub-confluent levels (70 % - 80 %) to maintain a proliferative state. Cells were rinsed with PBS solution and detached using trypsin at 37 °C, 5 % CO_2 for up to ten min. Trypsin was neutralised by adding double the volume of cell media and a suitable amount of cell suspension was transferred to a 175 cm^2 flask, which was made up to 20 mL with additional media. Cell suspensions were diluted no more than 1:5. Flasks were incubated at 37 °C, 5 % CO_2 until sub-confluent. Differentiation media was used after two weeks of culture, or after three media changes, to induce cell differentiation. Cells were cultured for a further two weeks, with media changed every three to four days.

2.2.20 Cell seeding on decellularised porcine liver discs

All transferring procedures occurred aseptically within a ~~fume hood~~Class II safety cabinet at room temperature to minimise the risk of cellular contamination.

2.2.2016.1 Direct pipetting on decellularised porcine liver discs

All seeding procedures occurred aseptically within a Class II safety cabinet ~~fume hood~~ at room temperature to minimise the risk of cellular contamination. HepaRG or Huh7 cells of varying concentrations (outlined in individual chapters) were pipetted directly on the upper most surface of the decellularised porcine liver discs in several stages. Unless otherwise stated, cell suspension was pipetted at 1 x10^6 cells.mL^{-1}. Decellularised discs were immersed in appropriate cell culture media for two hours. Decellularised porcine liver discs were dried on ~~sterilised~~ autoclaved filter paper (Section 2.2.3.1) for a total of ten min, placed in a 24 well plate and 20 µL cell suspension was added to one side of the disc. Discs were covered and left for 15 min to allow absorption of cell suspension. A further 20 µL cell suspension was pipetted and covered for ten min. Covered

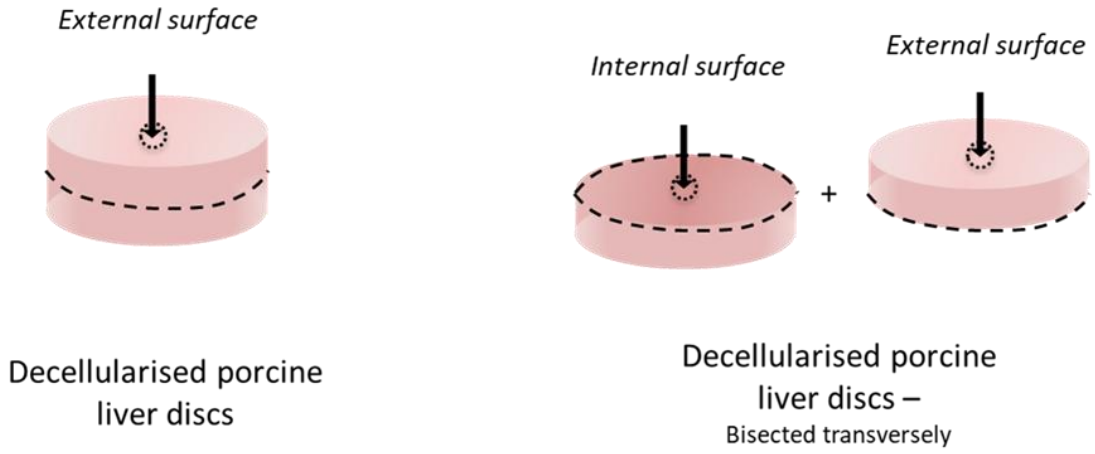

Figure~~8~~ 7. Outline of location of seeding of cells on the external and internal surfaces of decellularised porcine liver scaffolds using a pipette.

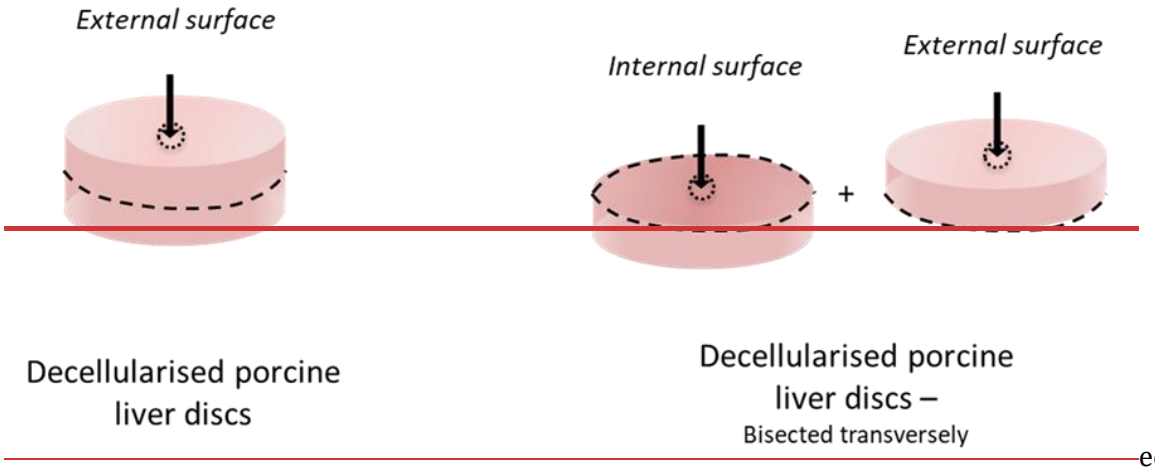

ed in plates were placed in an incubator at 37 °C, 5 % CO_2 to allow cell attachment for varying times, as detailed in individual Chapters (see Figure 7~~Figure 7~~). .

2.2.2016.2 Injection within decellularised porcine liver discs

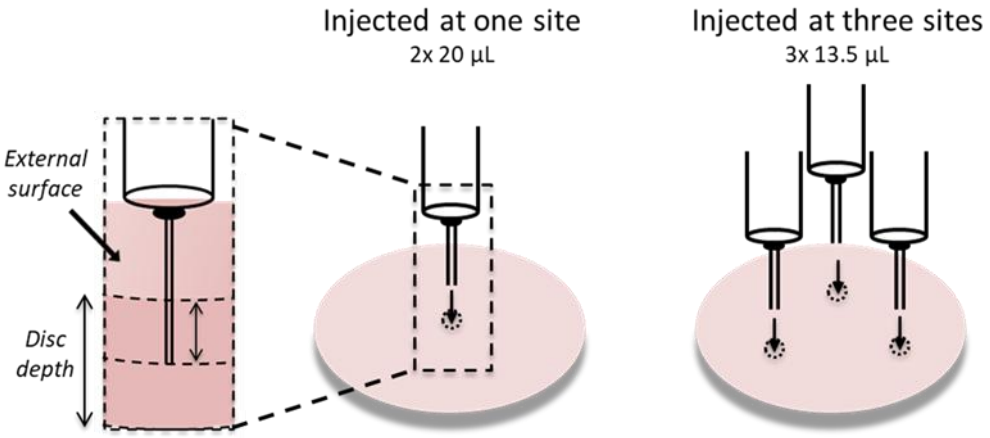

Figure 810. Outline of methods used to inject cells in to decellularised porcine liver matrices.

HepaRG or Huh7 cells were injected in to decellularised porcine liver discs using either a 18G needle or pipette tip (1-50 µL). Needles / pipette tips were inserted approximately half-way through the centre of the decellularised discs as shown in Figure 8Figure 8..

2.2.2016.3 Dynamic seeding of decellularised porcine liver discs in cell suspension

All seeding procedures occurred aseptically within a Class II safety cabinetfume hood at room temperature to minimise the risk of cellular contamination. Decelluarised discs were immersed in appropriate cell culture media for two hours. Decellularised porcine liver discs were aseptically dried on sterilised autoclaved filter paper (Section 2.2.3.1) for a total of ten min before being placed inside a universal containing cell suspension. Unless otherwise stated, 6mL of cell suspension ($4x10^6$ cells.mL^{-1}) was used, with a maximum of three discs per universal. Universals were placed in either an incubator at 37 °C, 5 % CO_2 (v/v) or in an incubator at 37 °C. Cells were rotated at 35 RPM for 24 hr unless otherwise stated.

2.2.21 Cell culture of seeded decellularised porcine liver discs

All transferring procedures occurred aseptically within a Class II safety cabinet ~~fume hood~~ at room temperature to minimise the risk of cellular contamination.

2.2.21.1 Static culture

Seeded decellularised porcine liver discs were placed in a 24 well plate and standard culture media was added (400 µL). ~~Sterilised~~ Autoclaved water (500 µL) was placed in the outer well to prevent media loss. Plates were placed in an incubator at 37 °C, 5 % CO_2 (v/v) for culture. Media was replaced as and when required, as outlined in individual chapters.

2.2.21.2 Dynamic culture using a universal

Seeded decellularised porcine liver discs were placed inside a universal containing 6mL standard culture media unless otherwise stated (Figure 9, a.)), ~~-~~ with a maximum of three discs per universal. Universals were placed in either an incubator at 37 °C, 5 % CO_2 (v/v) or in an incubator at 37 °C. Cells were rotated at 35 RPM unless otherwise stated. Cell suspension was replaced with standard culture media every 24 hr – 48 hr, as required (See Figure 9a.)).

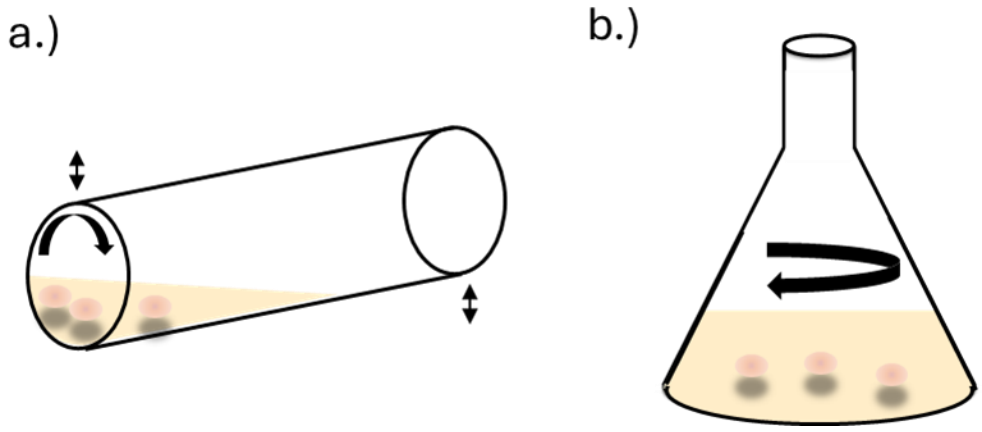

~~Table 15. Dilutions used in the preparation of a bovine serum albumin standard curve10~~ Figure 9~~10~~. Representation of dynamic culture methods .

2.2.21.3 Dynamic culture using a cell spinner

Seeded decellularised porcine liver discs were placed inside a cell spinner containing 75 mL

~~*Figure 8. Outline of methods used to inject cells in to decellularised porcine liver matrices.*~~

~~*10Figure 8. Outline of methods used to inject cells in to decellularised porcine liver matrices.*~~

standard culture media (See Figure 9b.)). Cell spinners were placed in an incubator at 37 °C, 5 %

CO_2 (v/v). Cells were rotated at 35 RPM for up to 14 days, with media changed every three to four days.

2.2.22 Cell counting and determination of cell viability

Cells were counted using Trypan blue to determine cell viability, with 97-98 % viability ideal. Trypan blue was added to cell suspensions in a 1:1 ratio, and cells were counted within the 25 large chambers of a haemocytometer and repeated. The following calculations were performed to determine the number of viable cells within 1 mL^{-1} cell suspension and were dependant on the concentration of Trypan blue applied.

$$\text{Number of viable cells (1:1 ratio)} = \frac{(cell\ count\ 1 + cell\ count\ 2\ \ldots\ldots)}{number\ of\ counts}\ x\ 10^{-4}\ x\ \frac{2}{1}$$

2.2.23 Direct (contact) and indirect (extract) cytotoxicity testing

2.2.23.1 Contact

Two decellularised liver cores were attached to the centre of two wells from a six-well plate using sterile adhesive tape. Cyanoacrylate contact adhesive and sterile adhesive tape were used as positive and negative controls respectively. 2 mL cell suspension was added (500,000 cells per well) and plates were incubated at 37 °C in 5 % (v/v) CO_2 in air for between 48 and 72 hr. Plates were examined microscopically and images taken using a digital camera. Media was aspirated and wells were rinsed with 2 mL PBS (with calcium and magnesium). Cells were fixed with neutral buffered formalin (10% w/v) and stained with Giemsa solution for five min. Plates were rinsed with running water until clear before air drying. Wells were viewed using a microscope with images taken using a digital camera (Section 2.2.5.2).

2.2.23.2 Extract

Exposure to toxic substances causes membranes to degrade, resulting in ATP leakage, therefore quantification of ATP from the surrounding cell media of cells exposed to decellularised conditioned media is a suitable method to assess the potential of tissues to leak toxic substances. Soluble components were extracted and cultured with adherent cell lines (Baby Hamster Kidney and mouse 3T3 fibroblast cells) and ATP (adenosine triphosphate) content was quantitatively measured. One decellularised and one native core were aseptically macerated and immersed in sterile media (1 mL media per 100 mg tissue). Tissues were incubated at 37 °C with agitation at 240 RPM for 72 hr. Supernatant was subsequently centrifuged and tissue pellets discarded. Sterility was checked by aseptically plating media onto nutrient agar, fresh blood agar and Sabouraud's agar and incubating for 48 hr at 37 °C, 37 °C and 30 °C respectively.

Supernatant were stored at -20 °C until sterility was confirmed. Cells were cultured in a 96 well tissue culture plate (25,000 L929 cells per 200 µL DMEM media and 10,000 BHK cells per 200 µL GMEM media) and incubated at 37 °C in 5% (v/v) CO_2 in air until approximately 80-90 % confluency was achieved. Media was removed and replaced with 100 µL double strength media (Section 2.2.16). DMSO (40 % v/v) was used as a positive control and negative controls were composed of cells and standard media only. 100 µL of either test or control extracts were subsequently added to the corresponding wells and plates were incubated for 48 hr at 37 °C in 5% (v/v) CO_2 in air. Plates were incubated at room temperature with agitation, and 50 µL ATPlite assay substrate solution containing the luciferase enzyme was added. Plates were incubated with agitation for five min at room temperature with luminescence determined using a Chameleon plate reader. Luminescence values were produced as counts per s (CPS) and plotted using GraphPad prism 6.

2.2.24 Protein lysate collection

Cultured cells were aseptically washed with PBS solution. 1.5 mL PBS was added to the dish and cells were scraped off the culture dish using a cell scraper. The cell suspension was transferred into 1.5 mL eppendorfs and centrifuged at 12000 g for four min. Supernatant was subsequently removed and cells were re-suspended in 200 µL ECB buffer. Protein lysates were stored at -20 °C until use.

2.2.25 Quantification of protein content using a BCA Protein assay

BSA standard was prepared to generate a standard curve of protein content vs absorbance (See Table 15). Standards and samples (100 µL) were added in triplicate to wells of a 96 well plate. Working reagent was made by mixing BCA Reagent A with BCA Reagent B in a 50:1 ratio, and added to each well (200 µL per well, in triplicate), before incubating at 37 °C for 30 min. Absorbance of each tube was measured spectrophotometrically at 562 nm. Blank values were subtracted from sample and standards (mean of triplicate values used to generate a standard curve.

Table 15. Dilutions used in the preparation of a bovine serum albumin standard curve

Vial	Volume of diluent (µL)	Volume and source of BSA (µL)	Final BSA concentration ($\mu g.mL^{-1}$)
A	0	300	2000
B	125	375	1500
C	325	325	1000

D	175	175 of B	750
E	325	325 of C	500
F	325	325 of E	250
G	325	325 of F	125
H	400	100 of G	25
I	400	0	0

2.2.26 -Western blot

Protein lysates were diluted to obtain a relative amount of cells per lysate (1 x10^6 cells) for comparison of protein content per cell. Equal amounts of SDS loading dye were added to the diluted lysates and lysates were heated to 95 °C for five min.

Polyacrylamide gels were made to an appropriate concentration, and 5 µL DNA ladder was added to the first well, with 20 µL sample loaded into other wells. One gel was made per antibody tested. Only 10 µL samples were loaded onto the gel subsequently incubated with GAPDH due to the large quantities of GAPDH present within the cells. Gels were run in Tris-glycine buffer at 160 V for approximately one hr, until the loading dye was at the bottom of the gel. Gels were immersed in Towbin buffer for up to two min to prevent dehydration and placed on a PVDF membrane between thick blotting paper. Proteins were transferred onto membranes at 15V for one hr. Membranes were incubated with 10 mL blocking solution for ten min (5% skimmed milk in TBS in 0.1 % tween), rinsed with 10 mL TBS-tween (0.1 %) for ten min three times and incubated in 10 mL primary antibody (diluted in blocking solution) overnight at 4 °C (see Table 16). Membranes were rinsed with 10 mL TBS-tween (0.1 %) three times for ten min each and incubated in 10 mL secondary antibody (diluted with blocking solution) before washing membranes with 10 mL TBS-tween (0.1 %) three times for five min. Membranes were incubated in 2 mL ECL working solution for 30 s and briefly dipped in distilled water. Membranes were placed within a plastic sheet and sealed to prevent moisture loss in the dark. X-ray film was placed on top of the membranes and subsequently developed in a xenograph machine for various times.

Table 16. Primary antibodies used for Western blots throughout the study.

Antibody	Marker	Molecular size (kDa)	Reference / Clone	Dilution
Nestin	Stem cell marker	200-220	MAB5326	1 in 1000
Ki-67	Cell proliferation marker	359	ab16667	1 in 5000
CYP3A4	Drug metabolising enzyme present in functional adult hepatocytes	50-57	18227-1-AP	1 in 1000
Albumin	Functional hepatocyte marker	65	ab10241	1 in 2500
GAPDH	Positive control	37	AM4300	1 in 20000

2.2.27 Statistical analyses

2.2.27.1 Basic Statistical terms

$$Sum\ of = \sum$$

$$Individual\ value = x$$

$$Sample\ number = n$$

$$Mean = \frac{\sum x}{n}$$

2.2.27.2 Comparison of means

Students T-test was used for comparison of two means. Data with three or more groups was analysed using one- and two-way analysis of variance (ANOVA). Individual differences between group means were subsequently determined, if required, by calculating the minimum significant differences (MSD) at $p<0.05$, using GraphPad prism 6. In one-way ANOVA, Dunnett's multiple comparison testing was performed to identify the location of the difference in variance compared with a control group. In two-way ANOVA analyses, Tukey's post-hoc test was applied to identify the location of the difference in variance. If the difference in two means was greater than the critical value, then they were considered statistically different.

$$MSD = critical\ value\ x\ SE$$

$$Critical\ value = Q \propto [K, v]\ the\ studentised\ range$$

$$K = No.\ group\ means\ to\ be\ compared$$

$$v = Degrees\ of\ freedom\ from\ MSD\ within$$

$$SE = \sqrt{\frac{\bar{x}\ within\ groups}{n}}$$

$$Tukey's\ post\ hoc\ test = critical\ value \sqrt{\frac{MSE}{n}}$$

$$MSE = \frac{1}{n}\sum_{i=1}^{n}\left(\hat{Y}_i - Y_i\right)^2$$

$$Dunnett's multiple\ comparison\ test = t_{\propto}(k-1, n-k)\sqrt{MSE\left(\frac{1}{n_i}+\frac{1}{n_c}\right)}$$

2.2.27.3 Linear regression analysis

Where interpolation of the results was performed, a linear regression of standard curves was carried out using Graphpad Prism 6.

The coefficient of determination (r^2) was used to statistically measure the accuracy of data through the deviation from the fitted regression line. Values of zero indicate that the linear model used explains none of the variability of the data from around its mean, whereas values of one indicate that the linear model explains the variability of the data around its mean. This was calculated using GraphPad prism 6 as follows:-

$$r^2 = \frac{Explained\ variation}{Total\ variation}$$

~~3.~~3 Application and development of decellularisation methodology for porcine liver

3.1 Introduction

Growing evidence supports that a biological scaffold containing near-native structural, biological, and biochemical components can be created through the removal of cellular and nuclear material from porcine liver. Such scaffolds have been generated through decellularisation via various methods, which have, in turn, been applied to numerous other tissues from different species. Although no rigid definition of a decellularised scaffold currently exists, three guiding principles, based on the removal of sufficient nuclear material, have been proposed to prevent adverse immunological and/or tissue remodelling responses upon subsequent implantation. These include the lack of whole cell nuclei and nuclear material upon tissue sections stained with either haematoxylin and eosin (H&E), or 4',6-diamidino-2-phenylindole (DAPI) and the detection of less than 50 ng double stranded DNA (dsDNA) per mg tissue (dry weight), with fragments of no more than 200 base pairs (bp) in length (Crapo et al., 2011).

3.1.1 Methods used/tested to achieve efficient decellularisation of porcine liver tissue.

The proprietary University of Leeds decellularisation process ~~(Patent reference 7354749)~~(Fisher, 2002) has been shown to reduce a significant amount of DNA and preserve key basement membrane components in a number of different tissues including skin, bone, tendon and blood vessels (Jones et al., 2017, Luo et al., 2014a, Wilshaw et al., 2012, Hogg et al., 2015, Norbertczak et al., 2022, Aldridge et al., 2018)~~(~~. The method in this study uses low concentration SDS (0.1 %; w/v), protease inhibitors, hypo- and hypertonic buffers, and nuclease treatment (Figure 10). However, variations in time and temperature must be applied to address differences between tissues caused by variations in tissue components and densities, as discussed in Section 1.6. and detailed in Section 2.2.13. The Leeds decellularisation process has been successfully applied to entire human liver lobes, resulting in a significant reduction in hepatic DNA content ~~(Hakeem~~ (Hakeem, 2018)~~, Abdul - Unpublished data)~~, whilst retaining vasculature. Given that there are approximately 120 x10^6 cells per gram tissue, and the average weight of the human liver is

1800 g (male) or 1400 g (female), the average number of cells in the liver would therefore be between approximately 1.68 x10^{11} and 2.16 x10^{11} cells in total. Seeding an entire porcine liver lobe would be unfeasible, therefore, the decellularisation of smaller liver pieces was investigated. The specific microarchitectural and biochemical organization of the collagenous liver ECM is crucial to support cell function, allowing effective cell attachment and subsequent polarisation. Various biological components in the parenchyma including collagen IV, laminin and fibronectin provide topographical guidelines to enable cell attachment and migration along the ECM and zonal differentiation within the parenchyma.

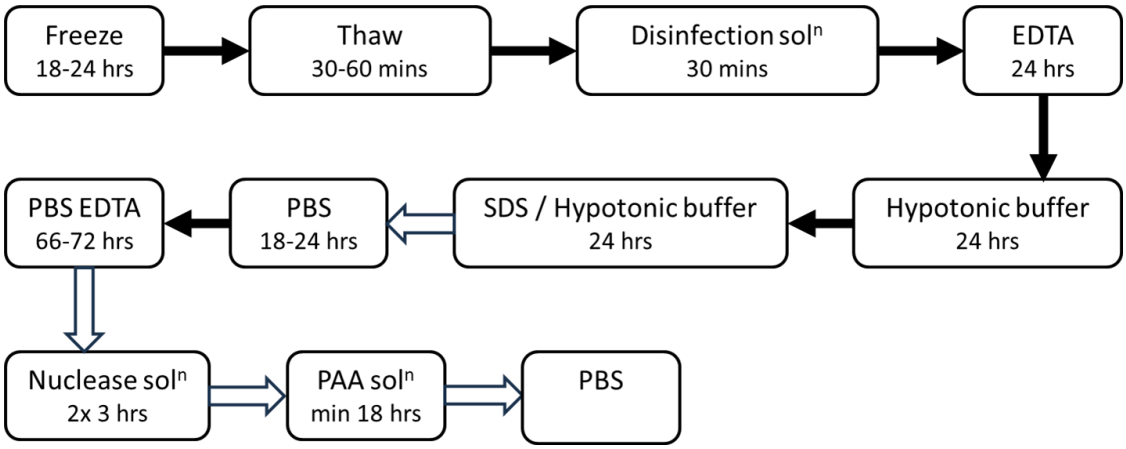

Figure 10. Outline of decellularisation method applied to discs of porcine liver, based on the proprietary method developed at the University of Leeds ~~(Patent reference 7354749)~~(Fisher, 2002). Black arrows indicate one wash, white arrows signify three washes in phosphate buffered saline solution (PBS). EDTA = ethylenediaminetetraacetic acid, SDS = sodium dodecyl sulphate, PAA = peracetic acid. Full details are provided in Section 2.2.13.

The proprietary Leeds method (Fisher, 2002) ~~(Patent reference 7354749)~~ incorporates multiple steps to disrupt and or degrade membranes, and release cell components for subsequent removal by rinsing with phosphate buffered saline (PBS). Freeze thawing of the tissue after dissection disrupts cell membranes through the formation of intracellular ice crystals. Agitation enhances reagent distribution and removal of cellular components. EDTA, a chelating agent, aids the disruption of cell adhesions to the ECM by binding calcium ions (Ca^{2+}) . Degradation of cell membranes, and nuclear laminae occurs by inclusion of SDS and the combined used of hyper- and hypo- tonic solutions that induce cell lysis through osmotic shock. Breakdown of DNA and RNA is catalysed via the addition of nucleases. Peracetic acid (PAA) is used as a ~~terminal~~ sterilisation step, with additional ability to remove residual nucleic material. Use of the protease inhibitor aprotinin, along with the use of buffered solutions (pH 7.2-7.4, pH 7.5-7.7 and pH 8.0-8.2 depending on

solution used see 2.2.13) (Gilbert et al., 2006, Crapo et al., 2011, Wilshaw et al., 2012) minimises tissue degradation resulting from long decellularisation procedures. Variations in the number of SDS cycles were assessed for different tissue diameters to tailor the Leeds decellularisation process to porcine liver.

Although definition of a decellularised product has not been define, guidance based on the removal of sufficient nuclear material to hinder an immunological response upon implantation has been suggested (Crapo et al., 2011), namely:-

1. <50 ng dsDNA per mg of matrix (dry weight).
2. DNA fragment length <200 bp.
3. Absence of whole cell nuclei and nuclear material on H&E stained or 4',6-diamidino-2-phenylindole (DAPI) labelled tissue sections.

Although the above criteria define the successful removal of nuclear, and therefore cellular, content it does not provide assessment for the successful retention of matrix structure and/or protein retention.

3.1.2 Evaluation of structural components in native and decellularised porcine liver

Histological stains used within this chapter are widely used in diagnostic laboratories and have been for decades, providing specific binding of chemicals and reagents to allow for specific identification of matrix structures such as collagen, elastin and/or reticular fibres. Along with more recent advances in immunohistochemical labelling, they provide not only the presence and location of these proteins but can also provide qualitative measure through staining intensity. A hydroxyproline assay based on a method developed by Edwards and O'Brien (1980) was performed to quantify collagen within the discs before and after decellularisation. Occurrence of hydroxyproline within the amino acid sequence of vertebrate collagen is well known (12-14%). Collagen content can, therefore, be determined through a conversion factor of 7.52 (Udenfriend, 1966)(Figure 24). A glycosaminoglycan (GAG) assay was also performed on both decellularised and native porcine liver using an assay based on the methods described by Farndale et al (1986)(Figure 29). Alongside the hydroxyproline and denatured hydroxyproline assays, comparison of GAG content pre and post decellularisation provided a more thorough understanding of overall biochemical composition and degradation. The Massons Trichrome (MT)(Figure 25) and Sirius Red stains (Bancroft and Gamble, 2002)(Figure 26)

were performed to compare collagen location and degradation in both native and decellularised porcine liver. Tissue stained with Sirius red / Millers ~~was co-stained with~~ elastin to identify collagen and elastin localisation and/or degradation. Native and decellularised tissue sections were immunohistochemically labelled with antibodies for collagens I, III and IV and visualised using DAB, to identify and locate specific collagen types (Figure 27). Assessment of both presence and location provides a way to monitor structural damage across the entire tissue. A Gordon and Sweets Reticulin stain (Bancroft and Gamble, 2002) was performed to selectively identify reticular fibres, known to support the matrix during tissue regeneration and, therefore, considered critical during cellular repopulation of decellularised tissues (Figure 28). Laminin and fibronectin were immunohistochemically labelled on sections of native and decellularised porcine liver and visualised using DAB (Figure 30). Cell attachment is associated with the retention of laminin and/or fibronectin, therefore, its retention after decellularisation may be a key factor in successful cellular repopulation.

3.1.3 Evaluation of tissue scaffold cytotoxicity post decellularisation.

Assessment of the decellularised porcine liver scaffolds to identify any residual cytotoxicity resulting from tissue exposure to the chemicals applied, in particular SDS, was assessed using three different cell types through procedures outlined in ISO standard 10993-5:2009. L929 are stated within ISO 1993-5:2009, BHK are another suitable cell line commonly used in the laboratory and HepaRG were used as a representative tissue-specific cell type that will be used during further investigations. Contact cytotoxicity (Figure 22) was performed to assess the potential for toxicity via insoluble factors. Cells were cultured alongside decellularised tissues, with morphology and viability assessed visually alongside positive and negative controls, after staining with Giemsa. BHK typically display a rounded morphology, L929 display an elongated, spindle morphology whereas HepaRG display a proliferative, endothelial morphology. An indirect cytotoxicity assay (Figure 23) was used to assess the potential for toxicity via soluble factors. Scaffold conditioned media was applied to cell monolayers, with cell activity quantified using an ATPLite assay.

~~3.~~ 3.2 Aims and objectives

3.2.1 Aims

~~To develop a decellularisation process to obtain discs of decellularised porcine liver that contains less than 50 ng.mg^{-1} dsDNA (dry weight) of no greater than 200 bp in length, and displaying a lack of whole cell nuclei confirmed through both H&E and DAPI To characterize the biochemical and architectural structures in native and decellularised porcine liver and assess the effects of decellularisation on specific structural (collagen I and III) and functional (laminin, fibronectin, and collagen IV) ECM components that are crucial for cell adhesion, survival, and migration.~~ The aim of this Chapter was to apply and develop the University of Leeds decellularisation procedure to create a porcine liver scaffold that was structurally and biologically similar to native porcine liver and would maintain cell viability after exposure.

3.2.2 Objectives

1. To identify the minimum number of cycles of low concentration SDS (0.1% v/v) required to successfully remove whole cell nuclei from native porcine liver, whilst maintaining gross liver structure including parenchymal cords, portal triad and septal bands.
2. To identify the maximum tissue dimensions required to keep retained DNA levels within the decellularised porcine liver scaffolds below 50 ng.mg^{-1}, and fragment size below 200 bp in length.
3. To compare the loss of key structural (total collagen content, collagen I and III), and biological (GAG content, collagen IV, laminin and fibronectin) proteins after decellularisation has been applied when compared with those seen in native porcine liver.
4. To identify whether the decellularised porcine liver scaffolds would inhibit viability of BHK, L929 and HepaRG cells after direct and indirect exposure.

~~1. To determine the number of cycles of low concentration SDS required to remove whole cell nuclei and retain general tissue architecture.~~

~~2. To determine the maximum tissue diameter to achieve less than 50 ng.mg^{-1} dsDNA of no greater than 200 base pairs in length, and lack of whole cell nuclei confirmed through both H&E and DAPI, for subsequent cell seeding.~~

~~3. To assess the direct and/or indirect toxicity through the inhibition of cell attachment and membrane permeability~~

~~4. To qualitatively compare intensity and location of specific structural components of decellularised porcine liver tissues with native porcine liver tissue, including collagen I, III and IV, laminin and fibronectin.~~

~~5. To quantify and compare retained collagen, denatured collagen, and GAG concentration in native and decellularised porcine liver tissue.~~

3.3 Results

Various decellularisation protocols were applied to native porcine liver tissues (Table 17). Experiment one confirmed the number of cycles SDS hypotonic buffer required to remove whole nuclei and DNA from the tissue with minimal architectural destruction; one, two and three cycles SDS hypotonic buffer were applied. Experiment two determined the tissue depths that will ensure retention of less than 50 ng.mg^{-1} double stranded DNA (dsDNA) in an 8 mm core porcine liver decellularised using one cycle SDS hypotonic buffer. Experiment three established that tissue discs were successfully decellularised up to 12 mm in diameter, using one cycle SDS and tissue depths up to 7 mm. Experiment 4 collated all the results achieved, decellularising porcine liver discs of 10 mm diameter, 5-7mm in depth using one cycle SDS (0.1%). See Section 2.2.13 for the final decellularisation procedure applied thereafter.

Table 17. Outline of developmental variations in decellularisation procedures applied to native porcine liver. Initial work varied number of SDS cycles for 5-7 mm thick tissue discs. After choosing the appropriate cycle number, further studies investigated the effects of varying depth and diameter.

Experiment		Protocol	Number cycles SDS in hypotonic buffer	Tissue depth	Tissue diameter
1	A	1	1	5-7	8
	B	2	2		
	C	3	3		
2	A	1	1	2-4	8
	B			5-7	
	C			9-11	
3	A	1	1	5-7	8
	B				10
	C				12
4	A	1	1	5-7	10
	B				
	C				
	D				

General liver ~~histioarchitecture~~histoarchitecture and absence of whole cell nuclei was achieved using H&E and/or DAPI staining (Sections 2.2.8.1 and 2.2.8.2) of native and decellularised porcine liver, and visualised using ~~Köehler illumination~~brightfield and/or fluorescent microscopy (Section 2.2.5.1 and 2.2.5.3)(Figures 10-14). Overall lobular structure, parenchymal cords and septal bands were compared.

3.3.1 How many cycles of SDS are required to remove whole cell nuclei and maximise retention of structural architecture?

As mentioned previously (Sections 1.6 and 3.1.1), successful decellularisation involves a balance between removal of cell components and minimisation of protein denaturation. Using the Leeds method, protein denaturation is minimised through the use of low concentration (0.1%) SDS, however, exposure can also be reduced through altering the time in SDS solution. Primary investigation therefore focused on reducing time of exposure, and determined through the lack of whole cell nuclei and retention of ~~histioarchitecture~~histoarchitecture after H&E staining.

Analysis of native porcine liver revealed multiple polygonal units (lobules) across a range of sizes, surrounded by thickened bands of collagen (septal bands, Figure 11a.)-c.) SB). Arteries (HA), veins (PV) and bile ducts (BD) of differing sizes and orientations were found at various points within the septal bands (Figure 11b.). Arterial and veinous walls were both one cell thick, with red blood cells often found within the lumen. Within the portal triad, arteries displayed thicker walls, and more pronounced nuclei than veins. Bile ducts were present, comprised of highly organised cuboidal epithelial cells with large, and rounded nuclei (Figure 11b.). Lobules consist of hepatocyte cords (yellow arrow), or islands up to four cells thick. Between these cords are small spaces (sinusoids) that contain small numbers of red blood cells (Figure 11c.), black and red arrows respectively). Hepatocytes contained one or more large, circular nuclei, with a high nuclear to cytoplasmic ratio (Figure 11a.), b.) & c.)). By contrast, following progressive cycles of SDS using the Leeds protocol, whole cell nuclei were removed from native porcine liver when decellularised using one (Figure 11, d.) & e.)), two (Figure 11, f.) & g.)), three cycles (Figure 11, h.) & i.)), of SDS (0.1% w/v). Progressive loss of macro-architecture was observed as cycle number increased, with parenchyma becoming thin and sparse (Figure 11d.), f.) & h.), green arrows), sinusoids increased in width (Figure 11.),g.) & i.) blue lines) and septal bands frayed and separated (Figure 11c.)) red

~~lines). Parenchymal detachment from septal bands (Figure 13b.)), and decreased uptake of eosin dye~~

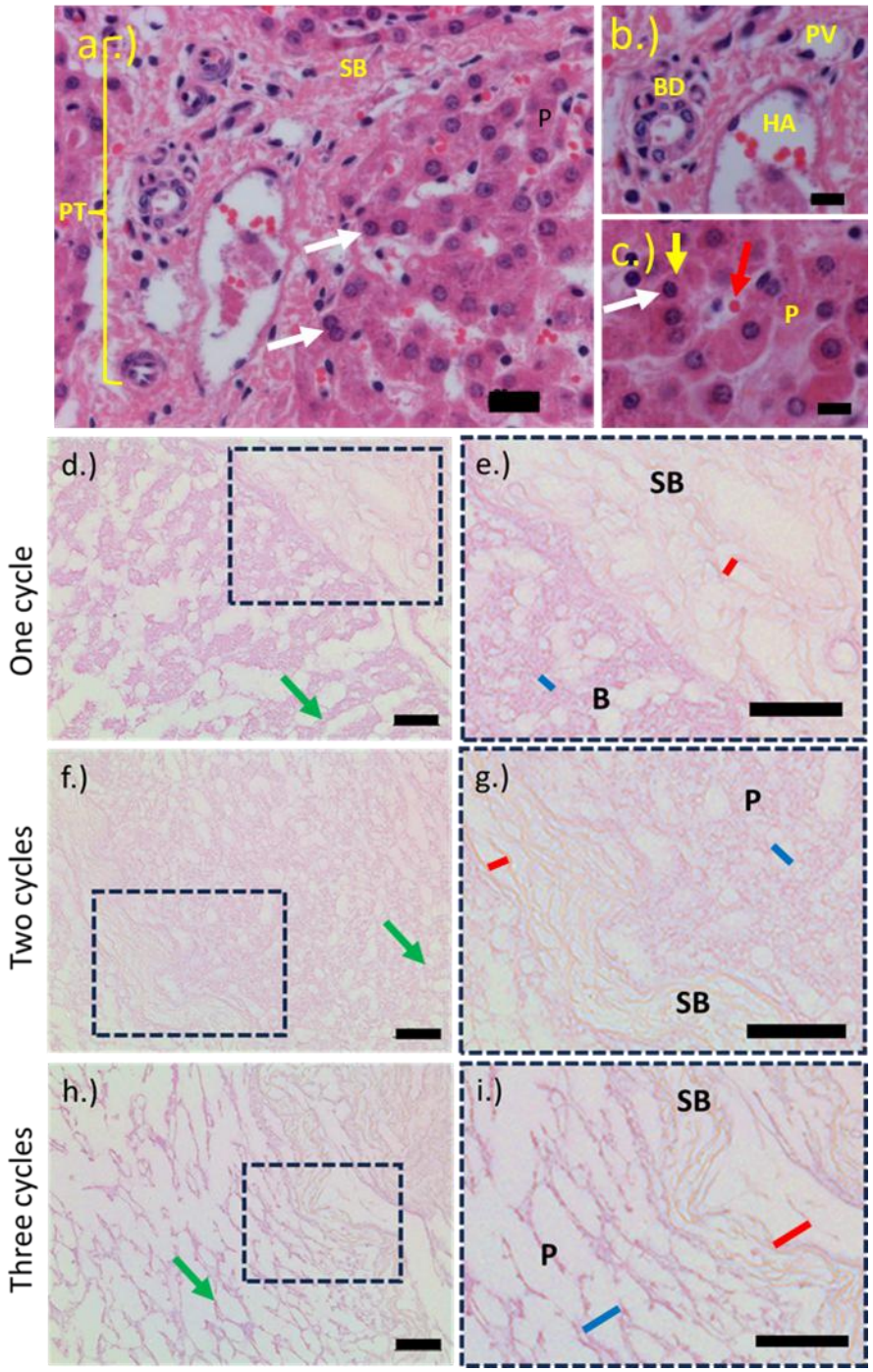

Figure 113. Degradation of tissue histoarchitecture with increasing number of cycles of 0.1% (v/v) sodium deoxycholic acid (SDS). Results indicate successful removal of whole cell nuclei with one cycle SDS, Liver histoarchitecture was best retained with one cycle SDS, with degradation increasing with number of cycles. Native tissue = a.), b.) and c.), decellularised porcine matrices exposed to one (d.) and e.)), two (f.) and g.) and three (h.) and i.)) cycles of SDS. Purple = haematoxylin staining of nuclei, pink = eosin counterstain. P = parenchyma, SB = septal band, PT = portal triad, HA = hepatic artery, PV = portal vein, BD = bile duct. Scale bar corresponds to 20 µm in a.) and 10 µm in b.) and c.) and 50 µm in c.)-h.). White arrows = whole cell nuclei, yellow arrow = cytoplasm, red arrow = red blood cells, green arrows = hepatic cords, red lines -= gaps in septal bands, blue lines = sinusoidal spaces. Dashed squares on d.), f.) and h.) indicate areas examined under higher magnification (e.), g.) and i.) respectively.

lines). Parenchymal detachment from septal bands (Figure 11b.)), and decreased uptake of eosin dye indicated increasing tissue fragility when cycle number was increased (Figure 11d.), f.) & h.)). Greater ECM degradation was found at external tissue surfaces, than that found centrally (figure 12a.)). As a result of the lack of whole cell nuclei, and minimised loss of ECM degradation seen with one cycle SDS, this protocol was used for all remaining experiments.

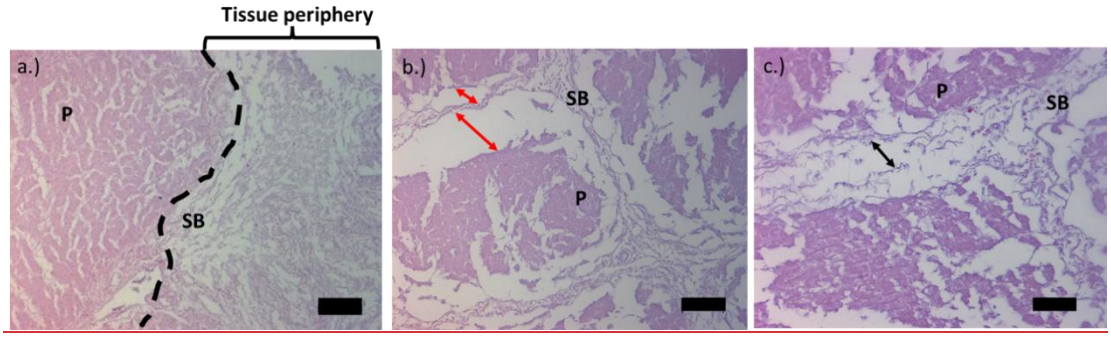

Figure 12. Representative images outlining the level of degradation in decellularised porcine liver grafts. Greater levels were seen at the tissue periphery of H&E-stained sections (a.)). Separation of parenchyma from sinusoidal bands were noted with no particular pattern identified (b.) red arrows). In a

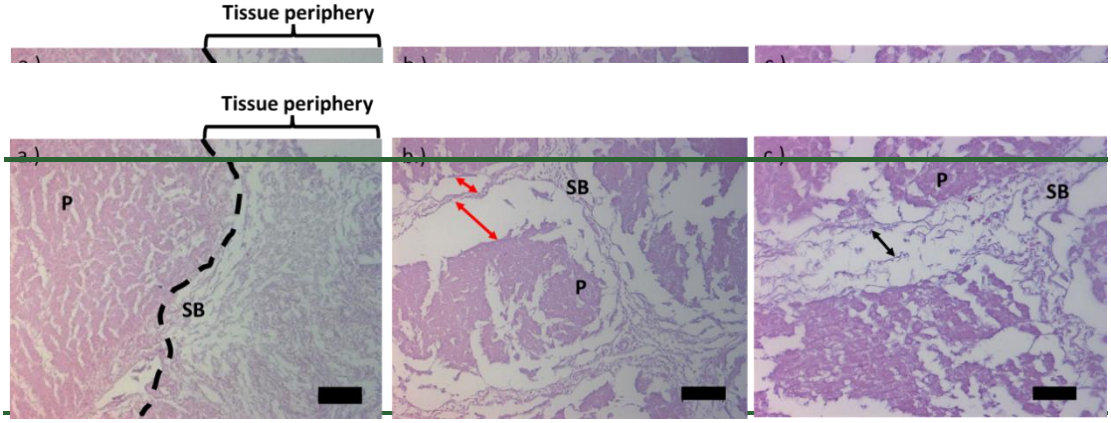

3.3.2 What is a suitable depth of porcine liver tissue to be decellularised?

Although entire human liver lobules have been successfully decellularised previously ~~(Abdul Hakeem, unpublished data)~~ (Hakeem, 2018), for this investigation smaller sections of tissue were decellularised to enable the study of how cells attach, and respond to, the porcine liver matrix. Larger tissue sizes require high cell numbers and limit oxygen diffusion across the tissue, whereas smaller tissues were difficult to handle. Under

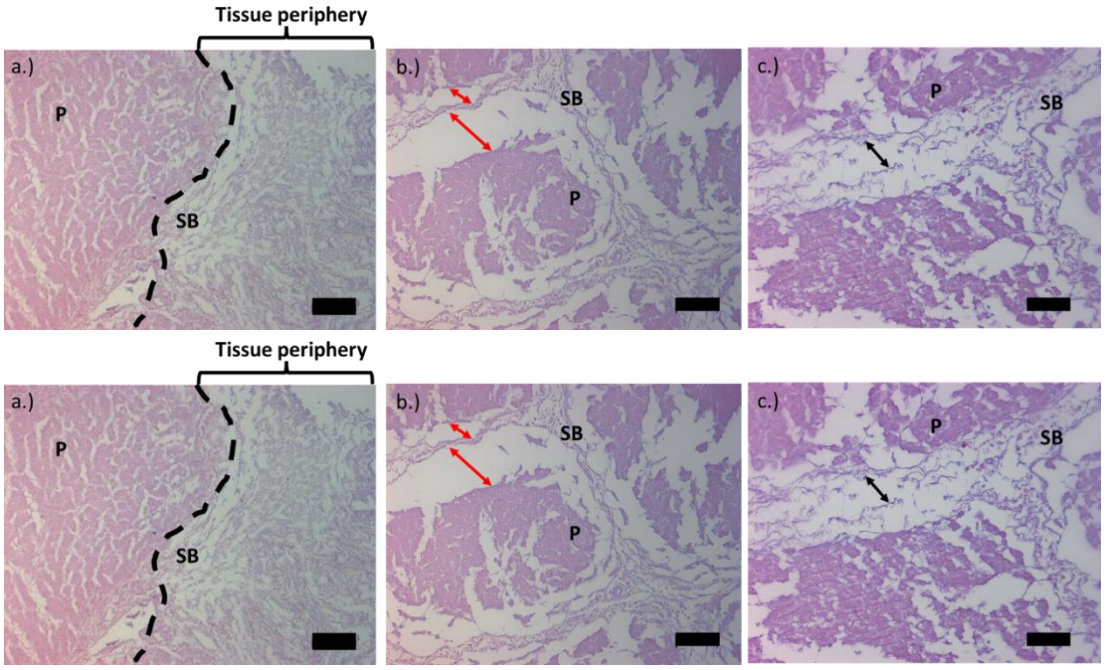

modifications of Fick's law (Place et al., 2017), oxygen diffusion rate is proportionally dependent on barrier, such as medium and/or tissue, thickness and the oxygen concentration gradient. Hepatocyte spheroids that completely lack vasculature are limited in size (200 µm) due to the formation of necrotic cores resulting from severe oxygen depletion (Curcio et al., 2007), with successful function and viability limited further to between 5000 and 12,500 cells (Aleksandrova et al., 2016a, Aleksandrova et al., 2016b). Matrices created through decellularisation retain native vasculature to help facilitate nutrient transfer, therefore, it is postulated that tissues greater than 200 µm can be used. For static studies to take place within a 24 well plate, upper limits no greater than 11 mm depth were used. Using punch biopsies of the same diameter (8mm), tissue slices of various depths

Figure 13. Histoarchitecture and absence of whole cell nuclei in decellularised porcine liver discs of 9-11 mm in depth. No whole cell nuclei staining was seen within any H&E stained sections of decellularised porcine liver discs (a.)-f.)), with successful retention of histoarchitecture seen in all tissue depths. (a.) & b.)), 5-7 mm in depth (c.) & d.)) and 2-4 mm in depth (e.) & f.)). P = parenchyma, SB = septal band, CV = central vein. Purple = nuclei, pink = counterstain. Scale bars = 50 µm (a.), c.) & e.)) and 20 µm (b.), d.) & f.)).

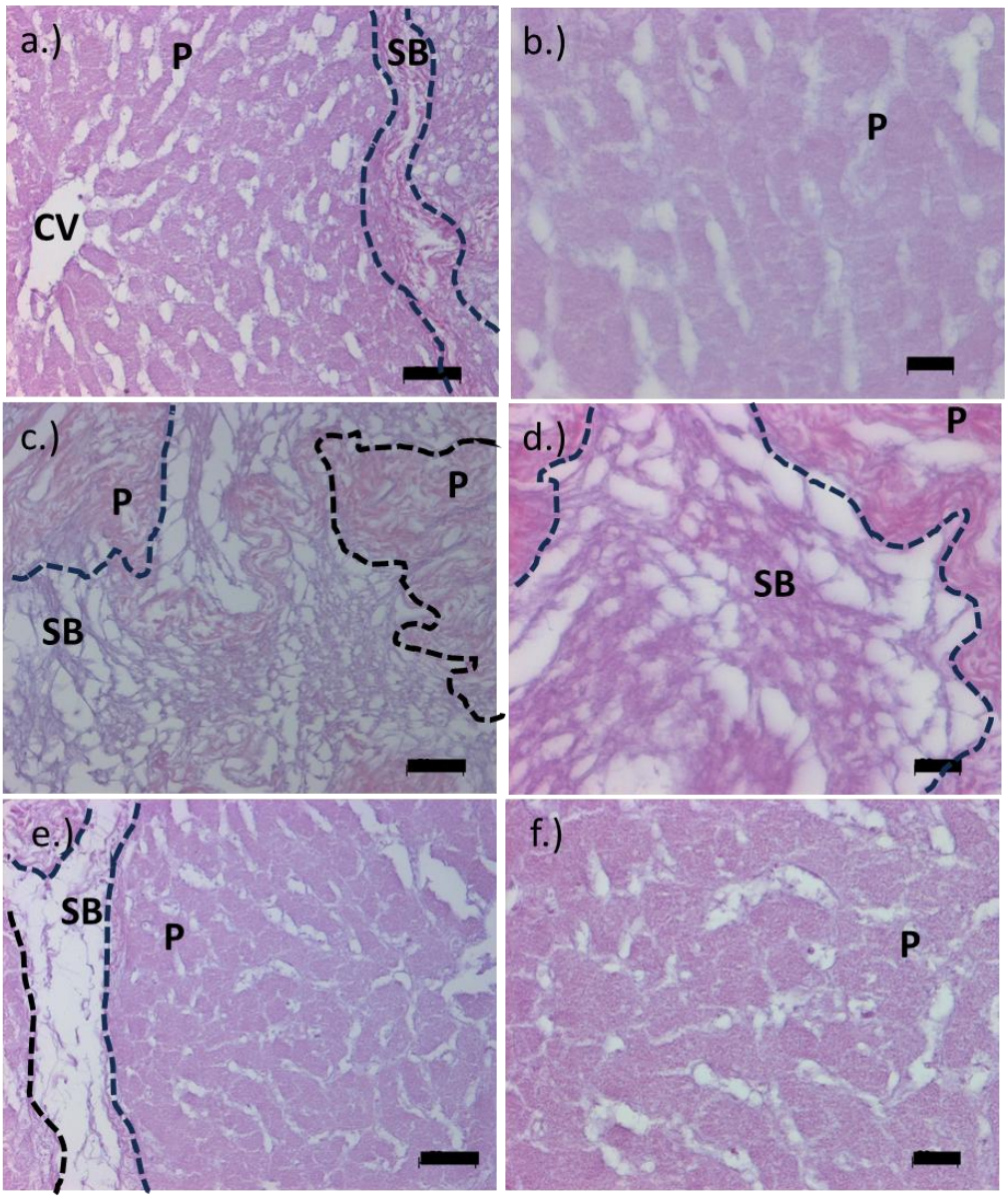

(2-4mm, 5-7mm and 9-11 mm) were cut to the same diameter and decellularised according to the process outlined in Section 2.2.13. Greatest overall tissue~~the formation of necrotic cores resulting from severe oxygen depletion ({Curcio, 2007 #1074}), with successful function and viability limited further to between 5000 and 12,500 cells {Aleksandrova, 2016 #806}{Aleksandrova, 2016 #1072}. Matrices created through decellularisation retain native vasculature to help facilitate nutrient transfer, therefore, it is postulated that tissues greater than 200 µm can be used. For static studies to take place within a 24 well plate, upper limits no greater than 11 mm depth were used. Using punch biopsies of the same diameter (8mm), tissue slices of various depths (2-4mm, 5-7mm and 9-11 mm) were cut to the same diameter and decellularised according to the process outlined in Section 2.2.13. Greatest overall tissue~~ destruction was found with the lowest

tissue depths (2-4mm, Figure 13a.) & b.)); with a loss of overall lobular structure, thinning of hepatic cords, increased sinusoidal spaces, frayed and coiled septal bands found through all areas (Figure 13~~a.) & b.)).~~ a.)& b.)). Better retention of lobular architecture, hepatic cords and septal bands were found in discs 5 mm and above (Figure 13)~~Figure 12c.) f.))~~. Gradual degradation of peripheral tissue lobules was also found throughout experiments in tissue depths of 5 mm and greater (for example see- Figure 13~~Figure 13. Representative images outlining the level of degradation in decellularised porcine liver grafts. Greater levels were seen at the tissue periphery of H&E-stained sections (a.)). Separation of parenchyma from sinusoidal bands were noted with no particular pattern identified (b.) red arrows). In addition, septal bands were seen to thin, and separate, as SDS exposure increased (c.) black arrows. Pink = eosin stained tissue matrix. P = parenchyma, SB = septal bands. Scale bars = 100 µm in a.) & b.), 50 µm in c.).Figure 11~~). No cell nuclei were seen in any depth of tissue decellularised using -one cycle SDS (for

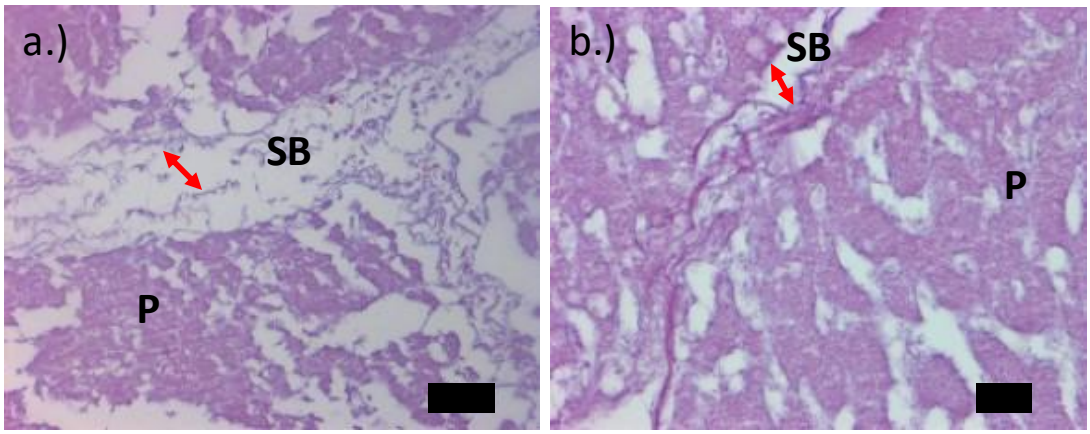

Figure 14. H&E staining of native and decellularised liver from 10 & 12 mm discs. Absence of whole cell nuclei in decellularised porcine liver tissue. Separation within septal bands seen at the tissue periphery's (a.), red arrows). P = parenchyma, SB = septal band. Purple = haematoxylin- -stained nuclei, pink = eosin counterstain. Scale bars = 50 µm in a.) and 20 µm in b.).

example see ~~Figure 14~~Figure 13). Due to the extensive degradation of tissue seen below 5 mm in depth, tissue depths of 5-7mm were~~as~~ adopted for subsequent experiments. Slices of porcine liver (5-7mm depth) were cut using punch biopsy devices to defined diameters to obtain discs of increasing diameter (8mm, 10mm and 12 mm). Preservation of liver histoarchitecture was assessed as previously described (Section 3.3.1) following one cycle of decellularisation treatment, as described in section 2.2.13. Lobular architecture was best retained with tissue of diameters 10mm and above, although detachment of septal bands was still found throughout all tissue diameters (Figure 14, a.)). Detachment of lobules was seen in the

majority of peripheral lobules, and some adjoining medial lobules (Figure 13, a.)-e.) red arrows). ~~As disc diameter size increased, greater amounts of degradation of septal bands was seen, marked by graded~~

~~Slices of porcine liver (5-7mm depth) were cut using punch biopsy devices to defined diameters to obtain discs of increasing diameter (8mm, 10mm and 12 mm). Preservation of liver histioarchitecture was assessed as previously described (Section 3.3.1) following one cycle of decellularisation treatment, as described in section 2.2.13.~~

As disc diameter size increased, greater amounts of degradation of septal bands was seen, marked by graded fraying and degradation of collagen. No nuclei were present in any decellularised porcine liver tissue between 8 mm and 12 mm in diameter. Discs of 10 mm diameter were determined to be carried forward for further investigation.

Figure 4. ~~Histioarchitecture~~Histoarchitecture and absence of whole cell nuclei in decellularised porcine liver discs of 9-11 mm in depth. No whole cell nuclei staining was seen within any H&E stained sections of decellularised porcine liver discs (a.)-f.)), with successful retention of ~~histioarchitecture~~histoarchitecture seen in all tissue depths. (a.) & b.)), 5-7 mm in depth (c.) & d.)) and 2-4 mm in depth (e.) & f.)). P = parenchyma, SB = septal band, CV = central vein. Purple = nuclei, pink = counterstain. Scale bars = 50 µm

~~Lobular architecture was best retained with tissue of diameters 10mm and above, although detachment of septal bands was still found throughout all tissue diameters (**Figure 13**, a.)). Detachment of lobules was seen in the majority of peripheral lobules, and some adjoining medial lobules (**Figure 13**, a.) c.) red arrows). As disc diameter size increased, greater amounts of degradation of septal bands was seen, marked by graded fraying and degradation of collagen. No nuclei were present in any decellularised porcine liver tissue between 8 mm and 12 mm in diameter. Discs of 10 mm diameter was determined to be carried forward for further investigation.~~

3.3.3 Did the disc dimensions meet all the guided criteria for successful decellularisation?

Guidance provided for successful decellularisation includes assessment of base pair length, dsDNA content as well as the lack of whole cell nuclei (Crapo et al., 2011). Further investigation therefore focused on assessment of DNA retention and quality. Presence of nuclear remnants was assessed qualitatively using DAPI staining of decellularised tissue sections (Figure 15), and retained DNA level was quantitatively assessed using either spectrophotometry (tDNA) and/or a Picogreen assay (dsDNA). A first line assessment of total DNA content was made spectrophotometrically to quantify the amount of double stranded DNA, as this method was quicker and cheaper than measuring double stranded DNA only. When quantities of total DNA were found to be over the recommended guided amounts (≤50 ng.mg^{-1}), further analysis was made to quantify double stranded DNA only using a Picogreen assay. The vastly reduced dsDNA content when compared to total DNA

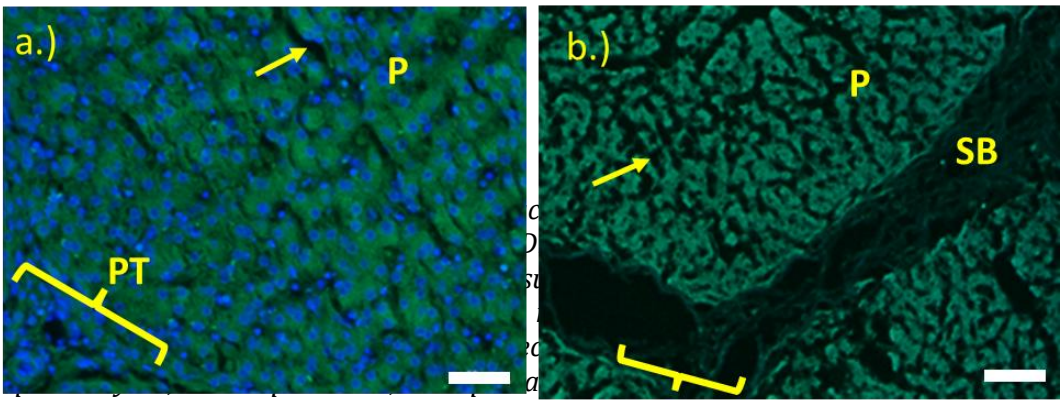

sinusoids. Scale bars = 200 µm in a.) and 50 µm in b.)

content, indicated that quantification of dsDNA only was a more valuable marker than total DNA content. Therefore, all DNA quantification was assessed using a Picogreen assay moving forward. DNA length was

qualitatively assessed using gel electrophoresis. Presence of whole cell nuclei was shown throughout native porcine liver sections (Figure 15~~Figure 14. a.)))~~), with a lack of blue fluorescence seen across multiple sections of decellularised tissue.

DNA was extracted using a Qiagen DNeasy Blood and Tissue kit (Section 2.2.10). Total DNA was quantified using a Nanodrop ND-100 (Section 2.2.11.1) with a standard curve generated using calf thymus DNA to assess the accuracy of the Spectrophotometer (Figure 16a.)~~Figure 15 a.)~~). Double stranded DNA was quantified from the same samples using a Picogreen assay, as described in Section 2.2.11.2, with lambda DNA used to create a standard curve (Figure 16b.)~~Figure 15 b.)~~) in which unknown values of test samples could be interpolated. DNA content (ng.mg^{-1}) was subsequently normalised for dilution volume and dry tissue weight. Any standard line of best fit that lay below $r^2 = 0.96$ was repeated.

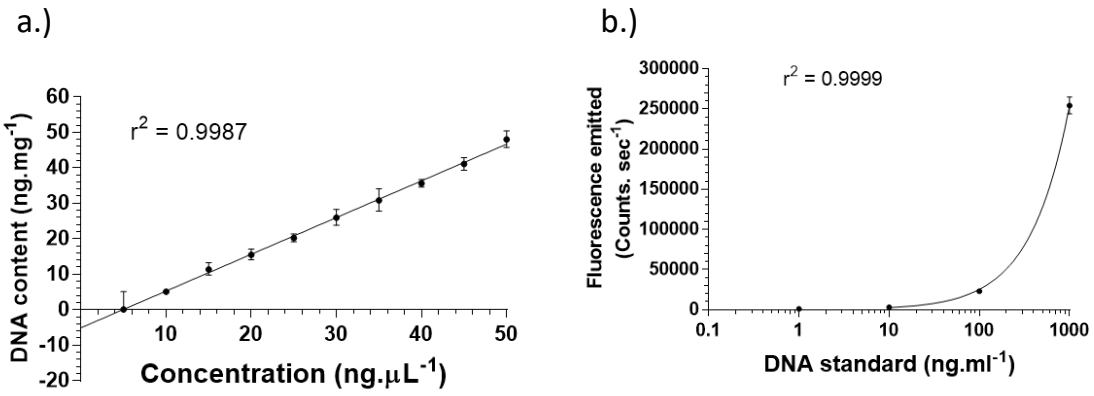

Figure 16. Validation of total and double stranded DNA content measurement. Linear relationship between calf thymus DNA concentration and measured content of calf thymus DNA standards. Results indicated good correlation between ~~expected~~ known and unknown DNA concentration. (a.)). Standard curve of lambda DNA concentration against fluorescence emitted (b.)). Data represented as mean (n=3) ± 95% confidence limits. ~~.~~

Assessment of native tissue variability in DNA content between lobes was compared. Total DNA content of native porcine liver was 6361.85 ng.mg^{-1}, 6059.89 ng.mg^{-1}, 5754.82 ng.mg^{-1} and 6065.38 ng.mg^{-1} for right lateral, right medial, left medial and left lateral lobes respectively (Figure 17~~Figure 16, a.)).~~). No significant difference in tDNA content between lobes was found (2-way ANOVA, $p<0.05$). tDNA content in native porcine liver tissue

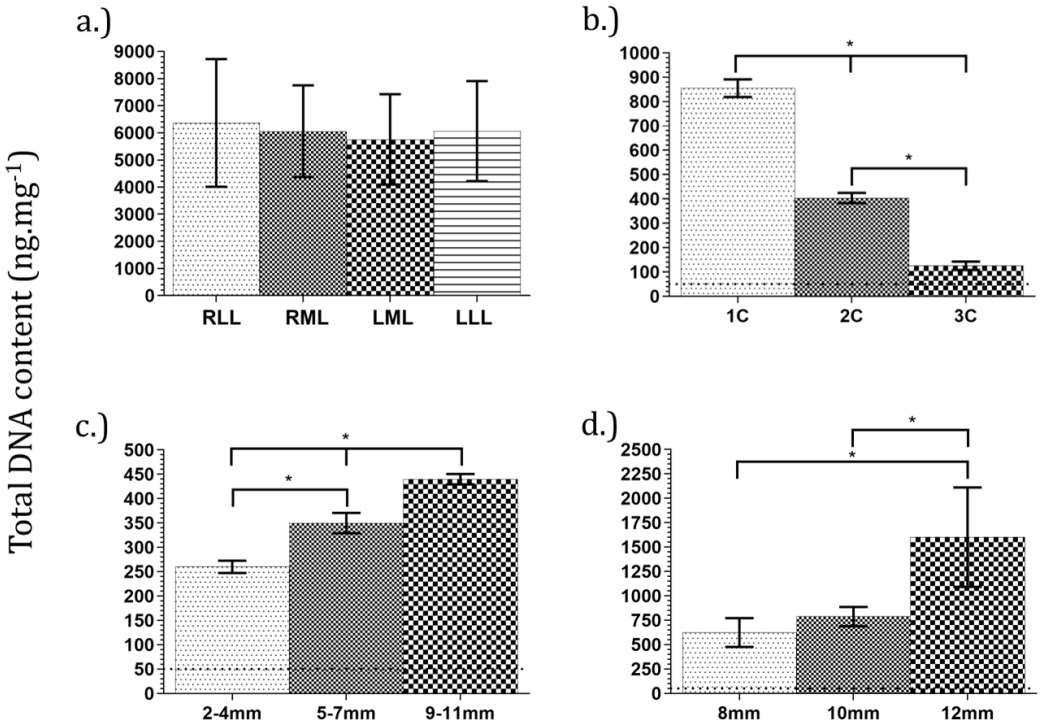

showed no statistically significant difference between lobes (a.), 2-way ANOVA). Variation of tDNA content within each lobe was high. Increasing SDS cycles was shown to decrease tDNA content, however, even with three cycles of SDS, tDNA levels were above 50 ng.mg-1 (dry weight) (Figure 17), increasing both tissue depth and/or increasing tissue diameter resulted in increasing levels of retained tDNA, all dimensions of which were above the level guided in the literature (Crapo et al., 2011).

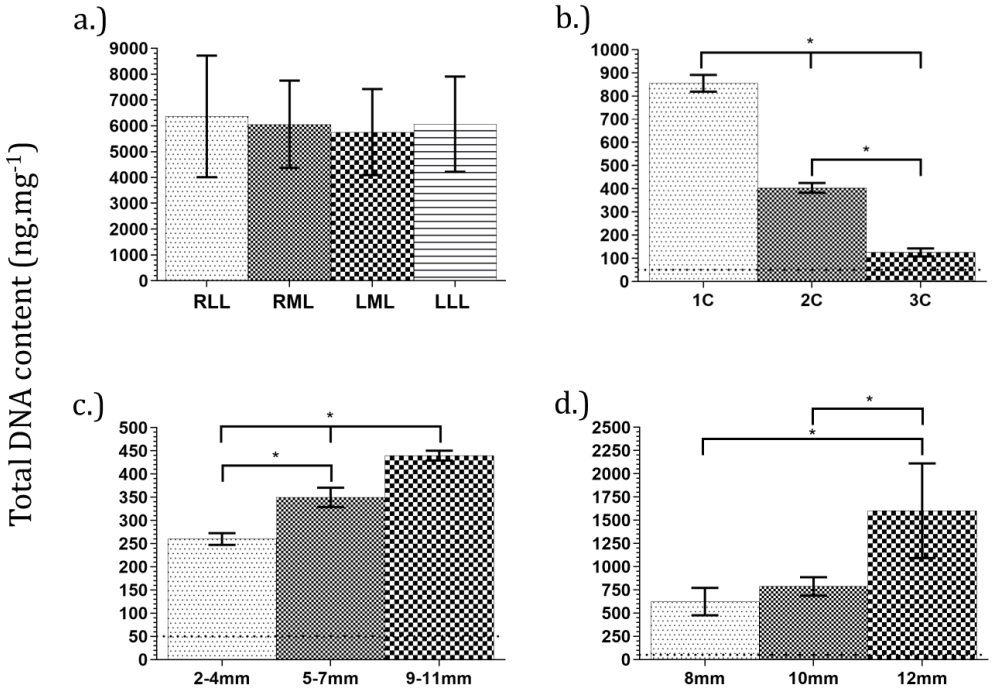

*Figure 17. Quantification and comparison of total DNA (tDNA) content in native and decellularised porcine liver. No statistical difference in tDNA content was seen between lobes (2-way ANOVA, 95% CI) (a.)). Higher than 50 ng.mg^{-1} (dry weight) tDNA was seen in porcine liver decellularised with one, two and three cycles of sodium dodecyl sulphate (b.)),and at tissue dimensions between two and 11 mm in depth (c.)), and 8-12mm in diameter (d.)). Values of tDNA content provided in e.). RLL = right lateral lobe, RML = right medial lobe, LML = left lateral lobe and LLL = left lateral lobe). Dashed line indicates 50 ng.mg^{-1} tDNA. Statistically significance labelled as * and determined via 2-way ANOVA n=3, ± 95% confidence interval.~~n=3, ± 95%~~*

Further analysis focused on quantification of dsDNA only. No significant difference in dsDNA content was seen between native porcine liver lobes (2-way ANOVA), however, there was high variation within lobes. Levels of dsDNA (dry weight) in discs with dimensions between 2-11 mm depth and 8-12 mm diameter were all below 50 ng.mg^{-1} indicating sufficient removal of dsDNA (Figure 18).

To identify the minimum amount of DNA that could be effectively visualized on 2% agarose gels, serial dilutions of a known quantity of tDNA extracted from native porcine liver were run on 2% agarose gels (Section 2.2.12). White bars are seen in wells corresponding to DNA levels between 158.3 ng and 7.9 ng.well^{-1} (wells 1-4), indicating that clear identification of DNA in 2% agarose gels can be obtained from levels at 7.9 ng

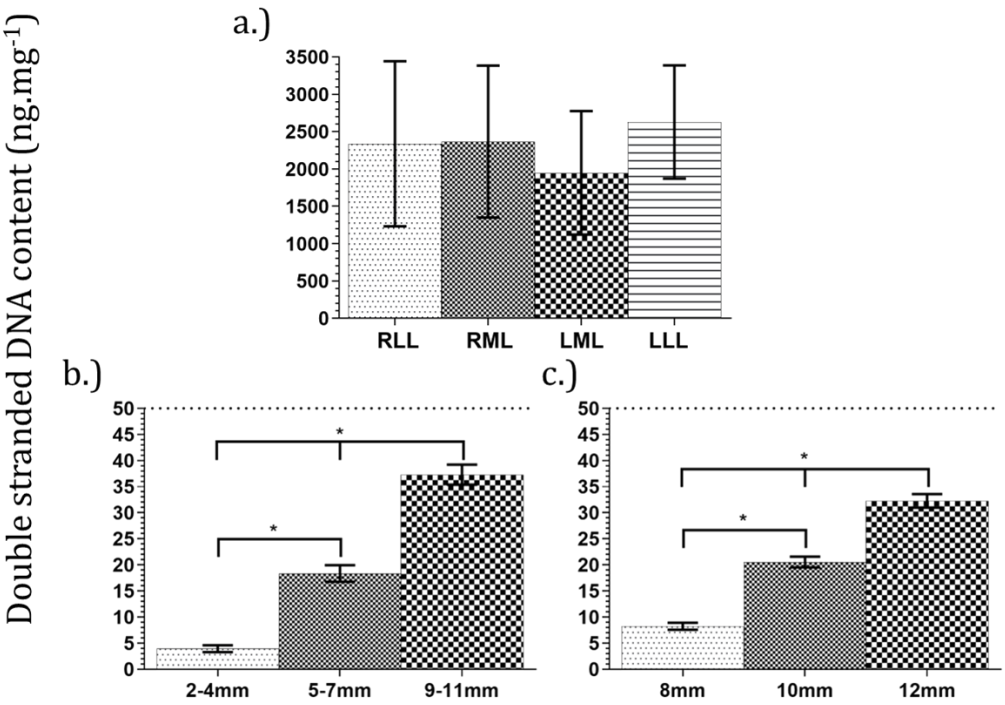

*Figure 18. Concentration of double stranded DNA (dsDNA) from various regions of native and decellularised porcine liver. (a.)) porcine liver, decellularised porcine liver of various depths (2-4mm, 5-7mm, 9-11mm)(b.)), and decellularised porcine liver of various diameters (8mm, 10mm, 12mm)(c.)). RLL = right lateral love, RML = right medial lobe, LML = left medial lobe, LLL = left lateral lobe. Dashed line indicates 50 ng.mg^{-1} dsDNA. Statistically significance labelled as * and determined via 2-way ANOVA n=3, ± 95% confidence interval.*

and above. DNA presence cannot be distinguished below this amount (Figure 19). Presence of bands throughout the length of the gel indicate the presence of multiple bp lengths in native, extracted, DNA with lesser intensities seen at smaller base pair lengths (150 bp or less) and also with lower DNA concentrations.

Comparative assessment of base pair length in extracted DNA from native and decellularised porcine liver discs showed marked differences. Native porcine liver well (Figure 20, well 1) showed the presence of DNA between 150 bp to over 500 bp in length. Wells corresponding to porcine liver decellularised with one, two and three cycles SDS (Figure 6. Base pair lengths of native (1) and decellularised (2-10) porcine liver examined by agarose gel (2%) electrophoresis of extracted DNA. *Investigation into optimal cycle number (2-4); 2 = one cycle sodium dodecyl sulphate (SDS), 3 = two cycles SDS, 4 = three cycles SDS. Investigation of tissue depth (5-7); 5 = 2-4 mm, 6 = 5-7 mm, 7 = 9-11 mm depths. Investigation of tissue diameter in discs (8-10); 8 = 8mm, 9 = 10mm, 10 = 12 mm diameter. 11 = reference bp ladder. Amount of DNA added to agarose gel (2%) is all greater than 8 ng. Yellow bracket parenthesis = possible presence of tDNA. n=3*

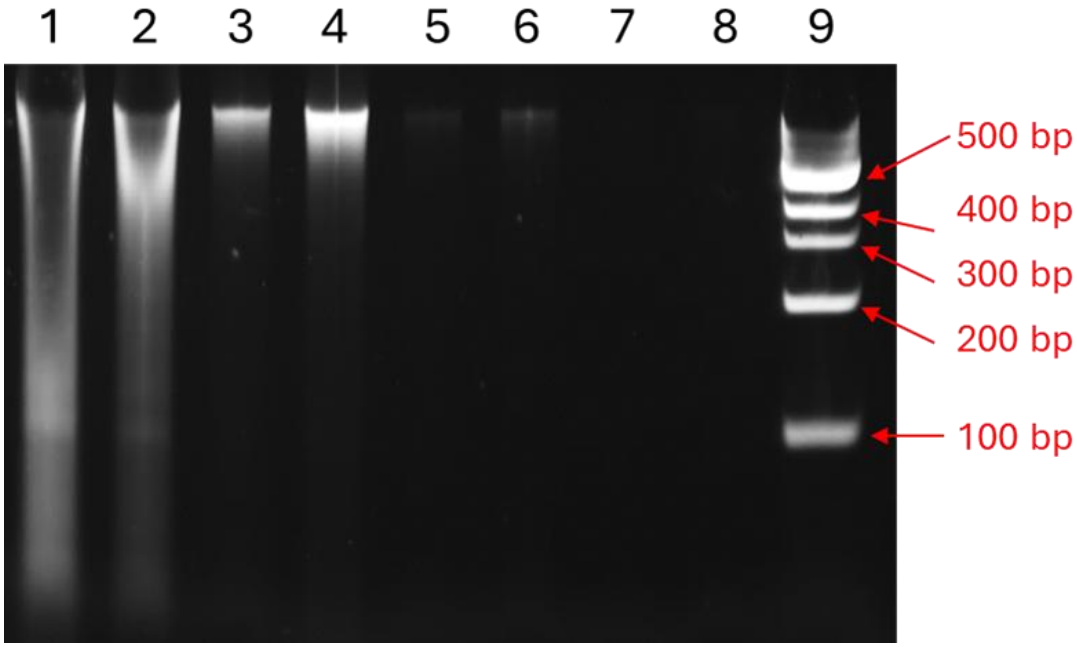

Figure 19. Identification of minimum DNA concentration required to visualise DNA on an agarose gel (2 %). DNA content lower than 7.9 ng per well cannot effectively be visualised. 1 = 158.3 ng, 2 = 79.2 ng, 3 = 15.8 ng, 4 = 7.9 ng, 5 = 1.6 ng, 6 = 0.8 ng, 7 = negative control, 8 = blank and 9= reference base pair ladder.

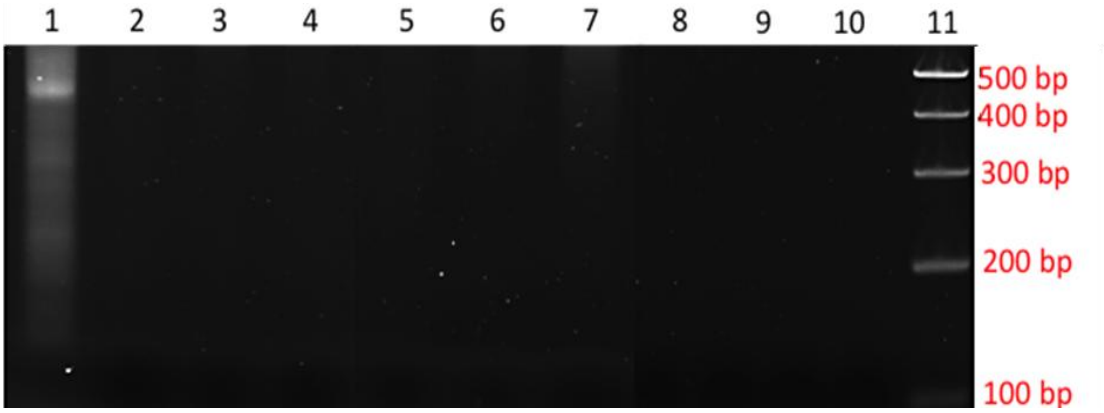

Figure 205. Confirmation of sufficient nuclear removal from optimised decellularisation procedures on porcine liver. a.) = Quantification of extracted double stranded DNA from decellularised (one cycle sodium dodecyl sulphate) and native porcine liver. b.) = Assessment of retained DNA base pair length. 1 = reference base pair ladder, 2-5 = total DNA (tDNA) extracted from decellularised porcine liver, 6-9 = tDNA extracted from native porcine liver. n=3

20, wells 2, 3 and 4 respectively), with tissue dimensions differing in depth (Figure 20, wells 5 = 2-4mm and 6 =5-7mm respectively) and diameter (Figure 20, wells 8=8mm, 9=10mm and 11~~1~~0=12mm respectively) all showing an absence of DNA content. ~~Well 7 (Figure 19, 9-11mm depth), however, displayed a very faint band of DNA equal to lengths~~

~~of between300 and 500 bp in length (Figure 19,, yellow bracket parenthesis). To ensure that retention of DNA is reduced further, extra PBS wash steps were included in the overall decellularisation procedure.~~

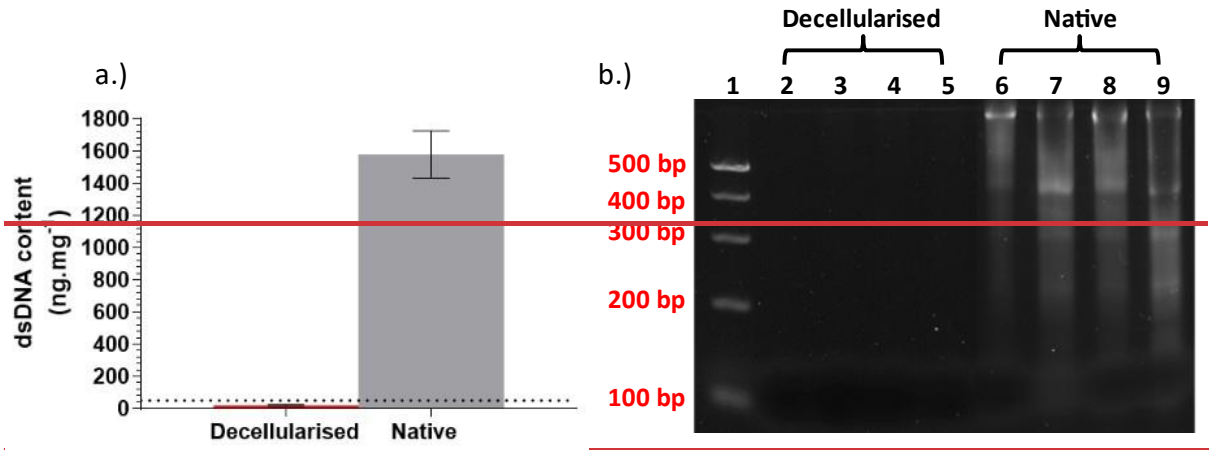

To assess whether the additional washes effectively removed the small amount of DNA remaining, decellularisation was repeated four times. Total DNA was extracted from all samples, and dsDNA was quantified using a Picogreen assay (Section 2.2.11.2). Base pair length was assessed using gel electrophoresis (Section 2.2.12). Total and ds DNA content of decellularised porcine liver were 1580.11 ng.mg^{-1} and 20.30 ng.mg^{-1} respectively

*Figure 7. Concentration of double stranded DNA (dsDNA) from various regions of native and decellularised porcine liver. (a.)) porcine liver, decellularised porcine liver of various depths (2-4mm, 5-7mm, 9-11mm)(b.)), and decellularised porcine liver of various diameters (8mm, 10mm, 12mm)(c.)). RLL = right lateral love, RML = right medial lobe, LML = left medial lobe, LLL = left lateral lobe. Dashed line indicates 50 ng.mg^{-1} dsDNA. Statistically significance labelled as * and determined via 2-way ANOVA n=3, ± 95% confidence interval.*

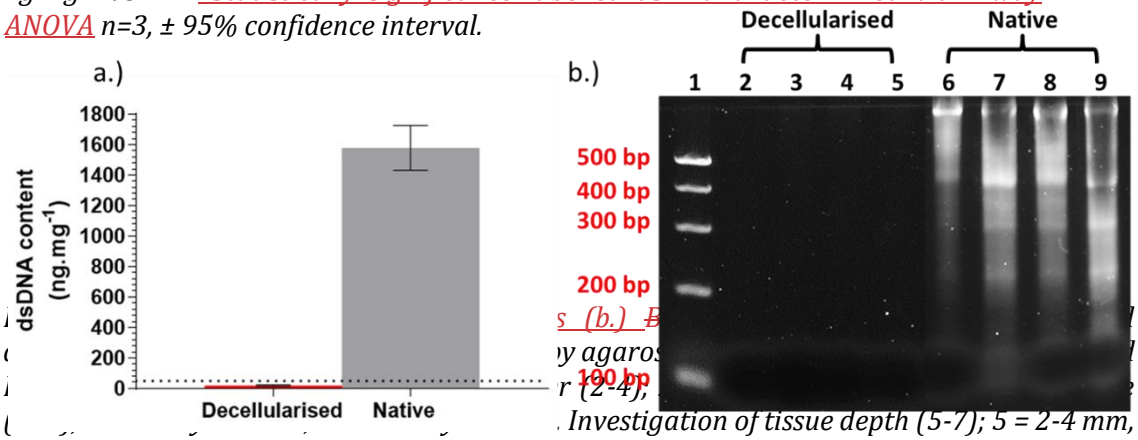

s (b.) B
y agaros
r (2-4), *l by*
*Investigation of tissue depth (5-7); 5 = 2-4 mm, 6 = 5-7 mm, 7 = 9-11 mm depths. Investigation of tissue diameter in discs (8-10); 8 = 8mm, 9 = 10mm, 10 = 12 mm diameter. 11 = reference bp ladder. Amount of DNA added to agarose gel (2%) is all greater than 8 ng. ~~Yellow bracket parenthesis = possible presence of tDNA. n=3~~ Statistically significance labelled as * and determined via 2-way ANOVA n=3, ± 95% confidence*

(Figure 21~~, a.))~~, a.)), and indicated that the decellularisation method with extra wash steps maintained sufficient capability to remove DNA below guided levels . Assessment of base pair length was made ~~DNA below guided levels . Assessment of base pair length was assessed~~ through agarose gel electrophoresis of extracted DNA from all four decellularised livers. Porcine liver samples decellularised with additional wash steps Figure 21, b.) wells 2-5) showed no fluorescing EtBr labelled DNA, of any base pair size, and the corresponding native liver samples (Figure 205. Confirmation of sufficient nuclear removal from optimised decellularisation procedures on porcine liver. a.) = Quantification of extracted double stranded DNA from decellularised (one cycle sodium dodecyl sulphate) and native porcine liver. b.) = Assessment of retained DNA base pair length. 1 = reference base pair ladder, 2-5 = total DNA (tDNA) extracted from decellularised porcine liver, 6-9 = tDNA extracted from native porcine liver. n=3, wells 6-9) showed the presence of multiple sizes of DNA Since the ds DNA content of decellularised tissue lay below 50 ng.mg^{-1}, with DNA strands 200 bp or larger not found, successful creation of the decellularisation procedure was confirmed. Decellularised porcine liver using one cycle SDS, in tissues 5-7 mm depth and 10 mm diameter were therefore subject to further analysis.~~—~~

3.3.4 Does the decellularised tissue hinder cell growth?

~~Biocompatibility~~ Cytotoxicity of porcine liver discs using the developed protocol were assessed using both contact and extract cytotoxicity assays of three distinct cell lines: BHK, L929 and HepaRG

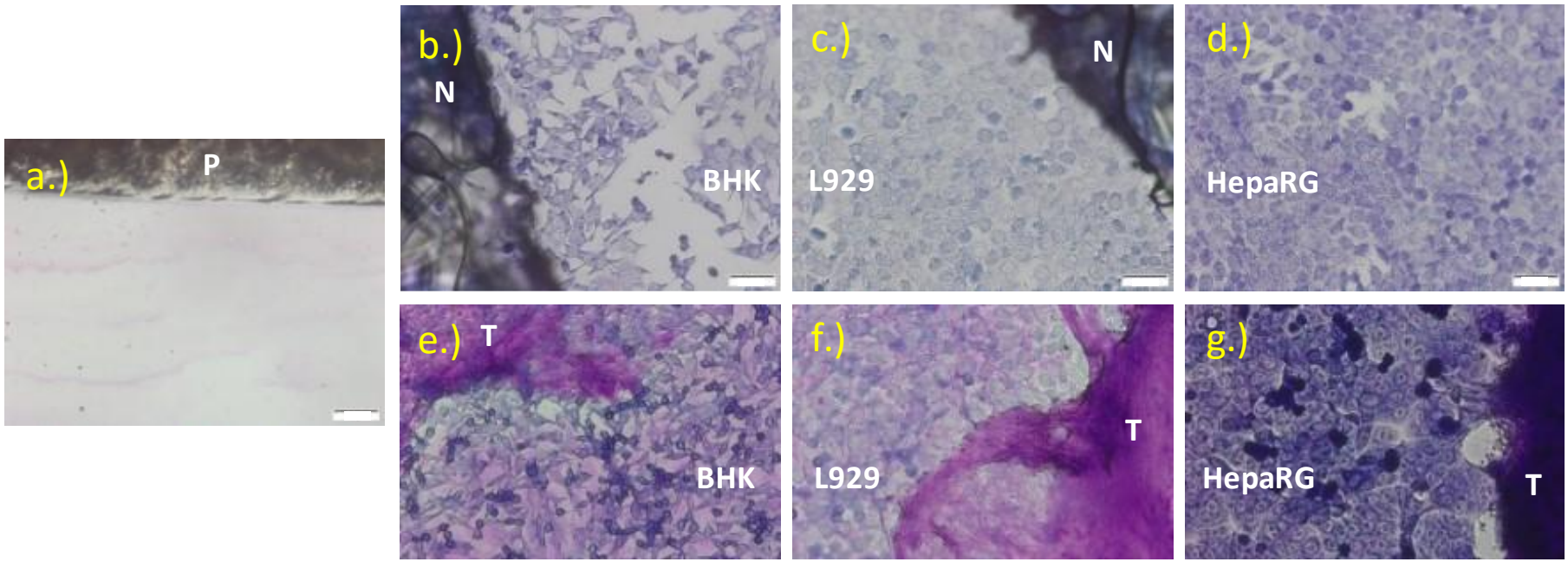

Figure 22. Contact cytotoxicity assessment of decellularised porcine liver with BHK, L929 and HepaRG cells. BHK = (b.) & e.)), L929 (c.) & f.)) and HepaRG (d.) and g.)) cells. a.) = positive control, b.)-d.) = negative control (steristrips), e.)-g.) = decellularised porcine liver. All cell types grow up to, and in contact with, both negative controls and decellularised porcine liver samples, with no morphological changes found, indicating a lack of cellular inhibition. P = cyanoacrylate glue, N = negative control, T = Decellularised porcine liver tissue. Scale bars represent 50 µm. n=3

(Figure 22 ~~Figure 21~~ and ~~-~~Figure 23~~Figure 22~~). All cell types cultured with cyanoacrylate adhesive (positive control) showed a non-viable morphology and a lack of cell growth surrounding the tissue perimeter, indicating cell death (~~Figure 21~~Figure 22, a.)). BHK, L929 and HepaRG cultured with Steristrips (negative control, ~~Figure 23. Contact cytotoxicity assessment of decellularised porcine liver with BHK, L929 and HepaRG cells. BHK = (b.) & e.)), L929 (c.) & f.)) and HepaRG (d.) and g.)) cells. a.) = positive control, b.) - d.) = negative control (steristrips), e.) -g.) = decellularised porcine liver. All cell types grow up to, and in contact with, both negative controls and decellularised porcine liver samples, with no morphological changes found, indicating a lack of cellular inhibition. P = cyanoacrylate glue, N = negative control, T = Decellularised porcine liver tissue. Scale bars represent 50 µm. n=3~~

~~Figure 24. Extract cytotoxicity assessment of decellularised porcine liver scaffolds with BHK, L929 and HepaRG.Figure 23Figure 21~~Figure 22 b.), c.) and d.)), as well as those with test samples (~~Figure 21~~Figure 22 e.), f.) and g.)) displayed normal morphological characteristics, growing up to, and in contact, with decellularised tissues. No difference in cell morphology was found between test samples and negative control samples. Potential for the decellularised tissues to leak toxic components was assessed through measurement of BHK, L929 and HepaRG ATP production in conditioned media using an ATP assay. Leakage of ATP occurs with increased membrane permeability, indicates increased toxic components within the media (Figure 23~~Figure 22~~).

No significant difference in cellular response was seen between scaffold extracts and negative controls (Figure 23~~Figure 14~~, 2-way ANOVA, $p<0.05$). A significant reduction of ATP within the positive control samples, compared to test samples indicated a lack of toxic components leached from decellularised porcine liver scaffolds.

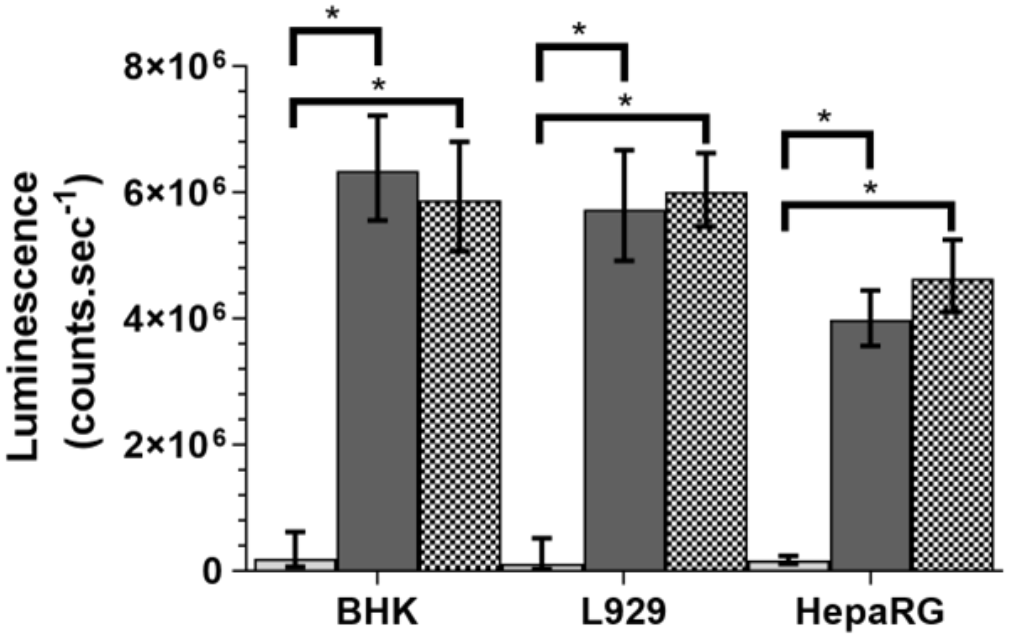

Figure 23. Extract cytotoxicity assessment of decellularised porcine liver scaffolds with BHK, L929 and HepaRG. Retention of ATP from BHK, L929 and HepaRG cells exposed to decellularised porcine liver tissue extract (grey bars) were not significantly different to levels in the same relative cell types cultured in standard culture media (green bars). Significant reductions were seen after exposure to DMSO supplemented media (red bars) (2 way ANOVA, $p<0.05$). n=3

~~*Figure 23. Total and denatured collagen content in decellularised (grey) and*~~

~~1.~~3.3.5 Was collagen retained within the scaffold after decellularisation?

Collagen content of native and decellularised porcine liver tissue was determined using tissue hydrolysis and hydroxyproline assay (See Sections 2.2.14.1 and 2.2.14.2). Hydroxyproline is a major constituent of collagen, occurring at a known frequency in the amino acid sequence. Oxidation of hydroxyproline forms pyrroles that react with p-dimethylaminobenzaldehyde and result in formation of a red chromophore that can be measured spectrophotometrically, the absorbance of which can be compared against a standard curve of known hydroxyproline concentrations. Quantification of hydroxyproline content in test samples was determined using a linear

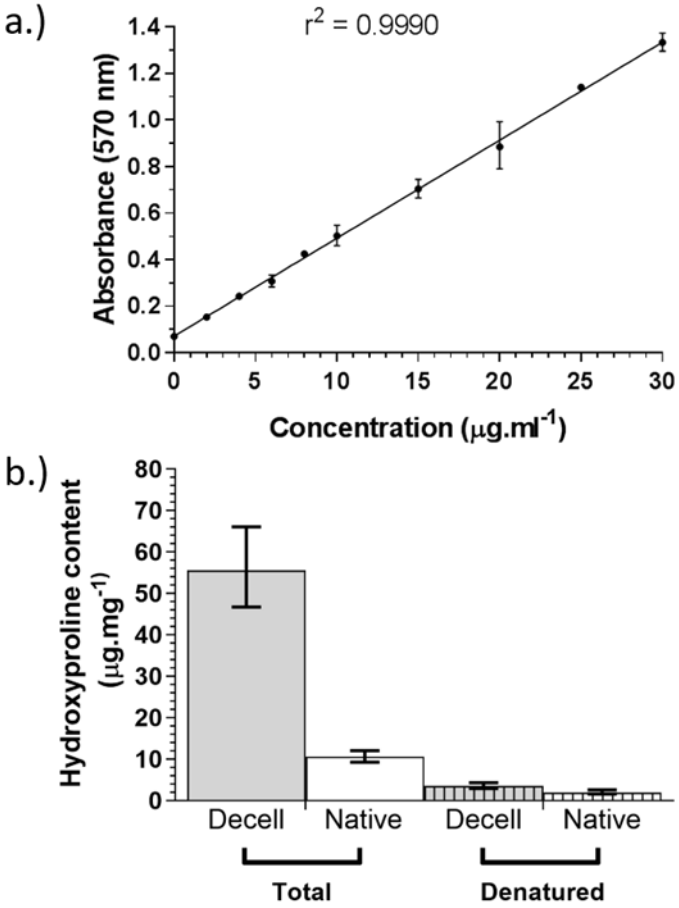

Figure 24. Total and denatured collagen content in decellularised (grey) and native (~~r~~white~~ed~~) porcine liver per mg dry weight tissue.
Validation of the accurate measurement of hydroxyproline content in decellularised porcine liver from known concentrations of trans-4-hydroxy-L-proline (a.)) and subsequent quantification of total and denatured hydroxyproline content (b.)). n=3

regression of a trans-4-hydroxy-L-proline standard curve (Figure 24a.)). Hydroxyproline content of native and decellularised porcine tissue was 10.63 ±2.04 and 55.77 ±3.60 ug.mg^{-1} dry weight respectively (n=6 ± 95 %

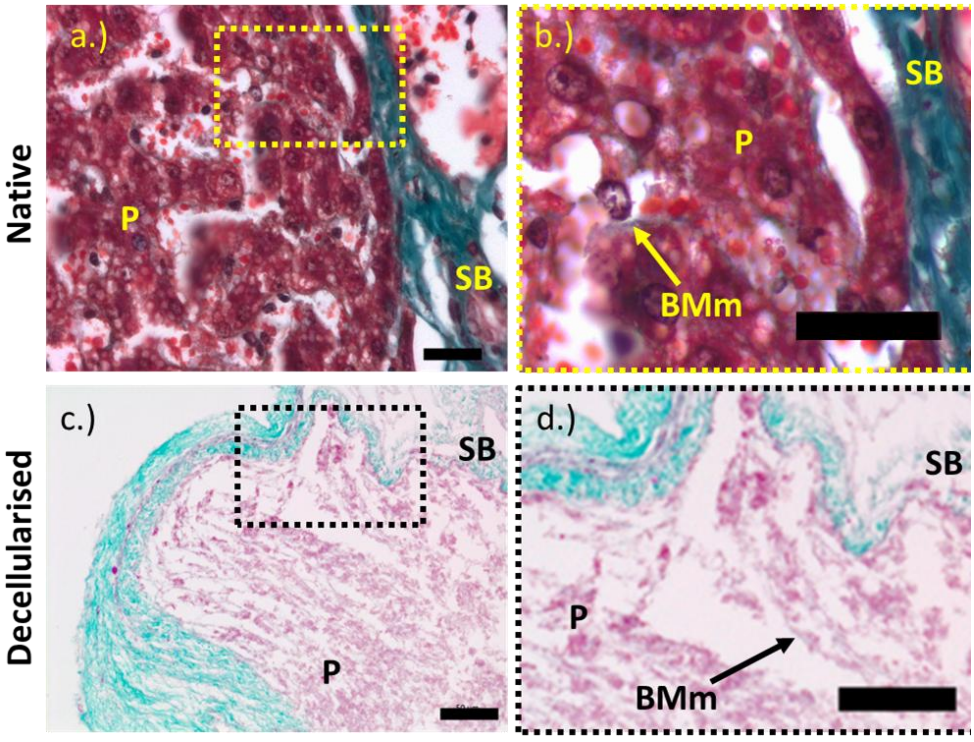

Figure 25. Identification of collagen fibre location in native ((a.) and b.)) and decellularised (c.) & d.)) porcine liver tissue using Masson's Trichrome stain. Collagen = green, from background (red – erythrocytes and cytoplasm) and nuclear staining (brown). SB = septal bands, P = parenchyma and BMm = basement membrane like membrane, SB = sinusoidal band, P = parenchyma. Black bar = 20 µm. Square indicates area examined under higher magnification.

confidence interval) (Figure 24~~,b.))~~,b.)),

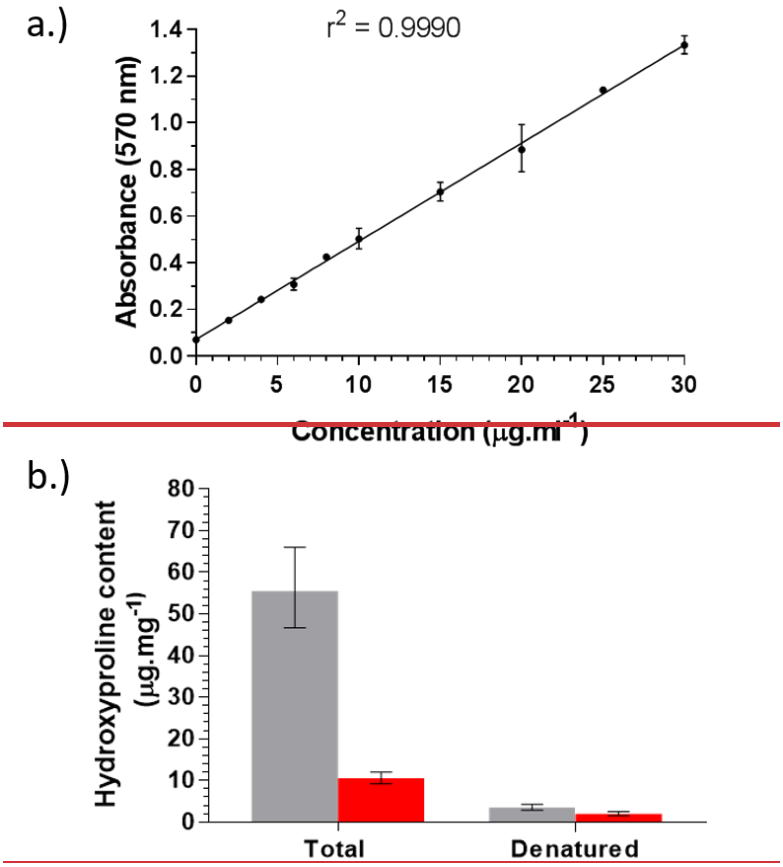

indicating that a greater ~~amount~~ percentage of collagen was found per mg tissue in decellularised tissue compared to native tissue. Denatured collagen content of native and decellularised porcine liver was determined by selectively digesting denatured collagen using an α-chymotrypsin enzyme, and found to be 1.25 ±0.46 and 5.41 ±0.64 ug.mg^{-1} (dry weight) respectively (n=6 ± 95 % confidence interval) (Figure 24~~b.))~~,b.)) A significant difference in total, and denatured, hydroxyproline content was calculated (Student's t-test; $p<0.05$). Relative amounts of denatured collagen compared to total collagen were 19.21% (native) and 6.45% (decellularised) and indicated that the relative amounts of denatured collagen were higher in native porcine liver tissues than that seen in decellularised porcine liver tissues. Results show that the application of decellularisation procedures to native tissue results in a decrease of denatured collagen, compared with non-denatured collagen. All results indicated the retention of liver collagen, although location and type of collagen cannot be obtained using the hydroxyproline assay. To identify collagen location within liver

sections, sections of native and decellularised liver were stained with Masson's Trichrome (Section 2.2.8.3) and visualised under ~~Koehler~~ brightfield illumination (Section 2.2.5.1). In native liver sections, dense collagen fibres (septal bands) were identified surrounding lobules, however, finer collagen fibres (BMm) were difficult to isolate (Figure 25a.) and b.)). Masson's trichrome staining of decellularised tissue also showed similar staining patterns within the septal bands, albeit at a lower intensity with a lack of staining seen in liver parenchyma. The absence of positive staining may have been due to the absence of collagen or due to the lack of staining intensity. Another histological collagen stain was therefore evaluated.

Successful staining of collagen and elastin fibres using picrosirius red and millers elastin has been achieved in other decellularised tissue types, including decellularised pulmonary valves (Luo et al., 2014a). This staining combination was applied to native and decellularised porcine liver sections (Section 2.2.8.4) and visualised using ~~Koehler illumination~~brightfield microscopy (Section 2.2.5.1). Both native and decellularised sections of porcine liver showed intense staining of collagen at the septal bands. Fine basement membrane like membranes in native and decellularised porcine liver tissue were again difficult to isolate (Figure 26~~a.) and b.))~~a.)& b.)). In native tissue, elastin was located in the hepatic arteries, with fine fibres dispersed throughout the septal bands (Figure 26a.)), with some retention of elastin seen in similar regions of

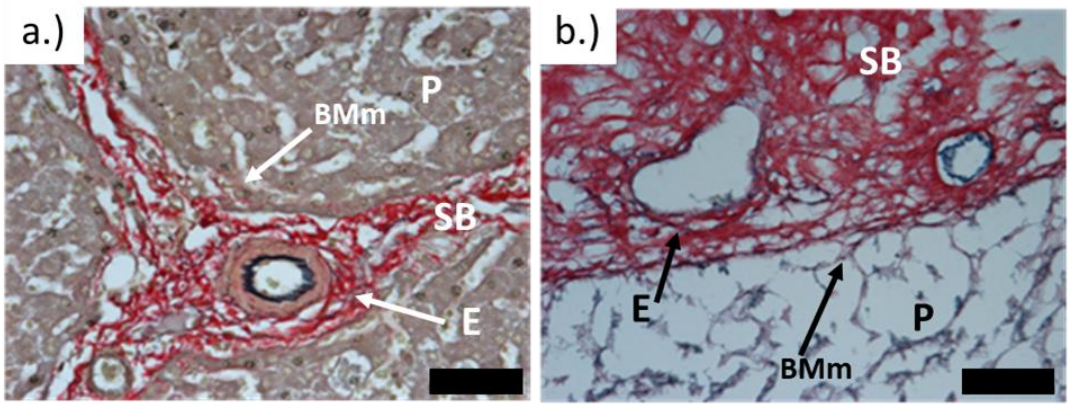

Figure 26. Native (a.)) and decellularised (b.)) porcine liver tissue stained with Sirius red / millers elastin stain to identify presence and location of total collagen and elastin. Specific identification of elastin and collagen was difficult to differentiate in native and decellularised porcine liver tissue. SB = septal bands, E = elastin, P = parenchyma and BMm = basement membrane like membrane. Red = collagen, elastin = black. Scale bars = 50 µm.

decellularised porcine liver, albeit

with less intensity of staining seen (Figure 26a.)). Histological staining of the fine collagen fibres located within the parenchyma was difficult, therefore, was immunohistochemical staining was performed. ~~(Figure 17a.)). Histological staining of the fine collagen fibres located within the parenchyma was difficult, therefore, immunohistochemical staining~~

Sections of native and decellularised porcine liver were labeled with primary antibodies against collagen I, III and IV, which were subsequently labelled with a species-specific secondary antibody, and a brown diaminobenzidine (DAB) tag (Figure 27). Collagen I and III in native tissue sections were located in a thin line, adjacent to hepatocytes within the parenchyma and throughout septal bands. In decellularised tissue sections, collagen I was retained in similar regions, albeit with lower intensity. Collagen III was retained at the same intensity within the parenchyma and septal bands. Collagen IV in native tissue was present adjacent to hepatocytes within the within the parenchyma.and lining the hepatic arteries and portal veins within the portal triads. Collagen IV was also present throughout the cholangiocytes within the bile duct. After decellularisation procedures were applied, the majority of collagen IV was lost, particularly within the parenchyma. A small amount of collagen IV was retained in the hepatic arteries and portal veins.

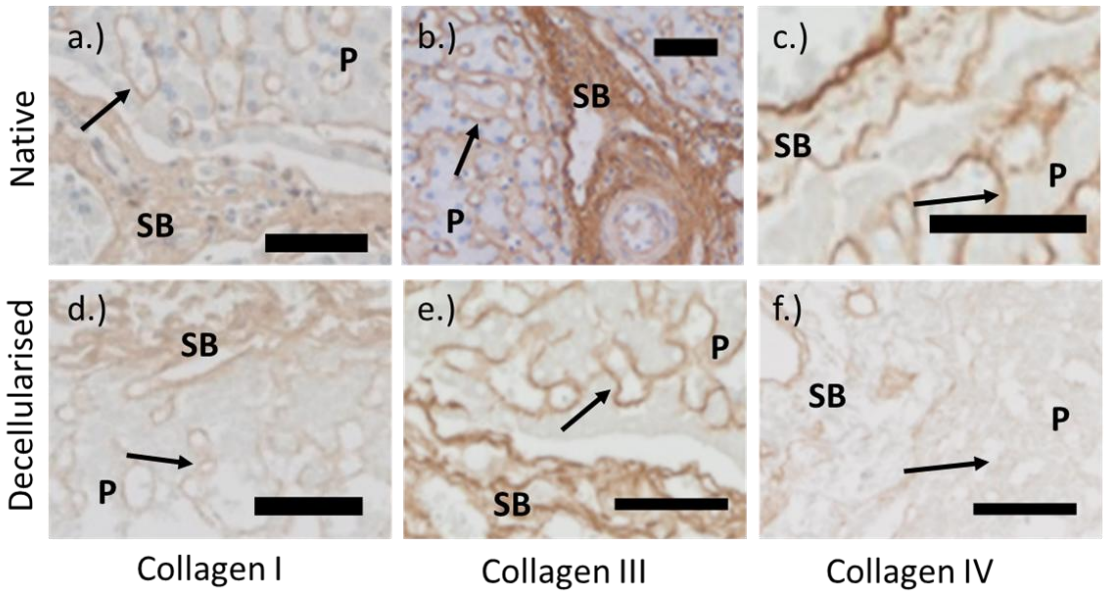

Figure 27. Presence and location of collagens I, III and IV in native and decellularised porcine liver tissue. Both collagen I (a.)) and III (b.)) were retained following decellularisation (d.) & e.)) in the septal bands (SB) and basement membrane like membrane (black arrows) within the parenchyma. Collagen IV was retained after decellularisation, albeit at a lower intensity at the edges of the lobular tissue and in the endothelial lining of the vasculature (f). P = parenchyma, SB = septal band. Scale bars = 50 μm

Reticulin staining (detailed in Section 2.2.8.5) was used to stain fine collagen III (reticular) fibres within the parenchyma of native and decellularised porcine liver (Figure 28). Visualisation using brightfield microscopy (detailed in Section 2.2.5.1) revealed vast variability between staining batches (Figure 28 a.)-c.)) indicating that effective comparison of staining patterns must be performed within individual batches. Finer reticulin fibres within the parenchyma could be identified through use of non-buffered formalin, allowing more effective comparison. In native tissue, reticular fibres were adjacent to hepatocytes, traversing sinusoids in the location of the BMm. Positive staining was also found within nuclei indicating further optimisation of the stain is required. In decellularised tissues, reticular fibres were also adjacent to hepatocytes, although shorter in length (Figure 28d.) & e.)).

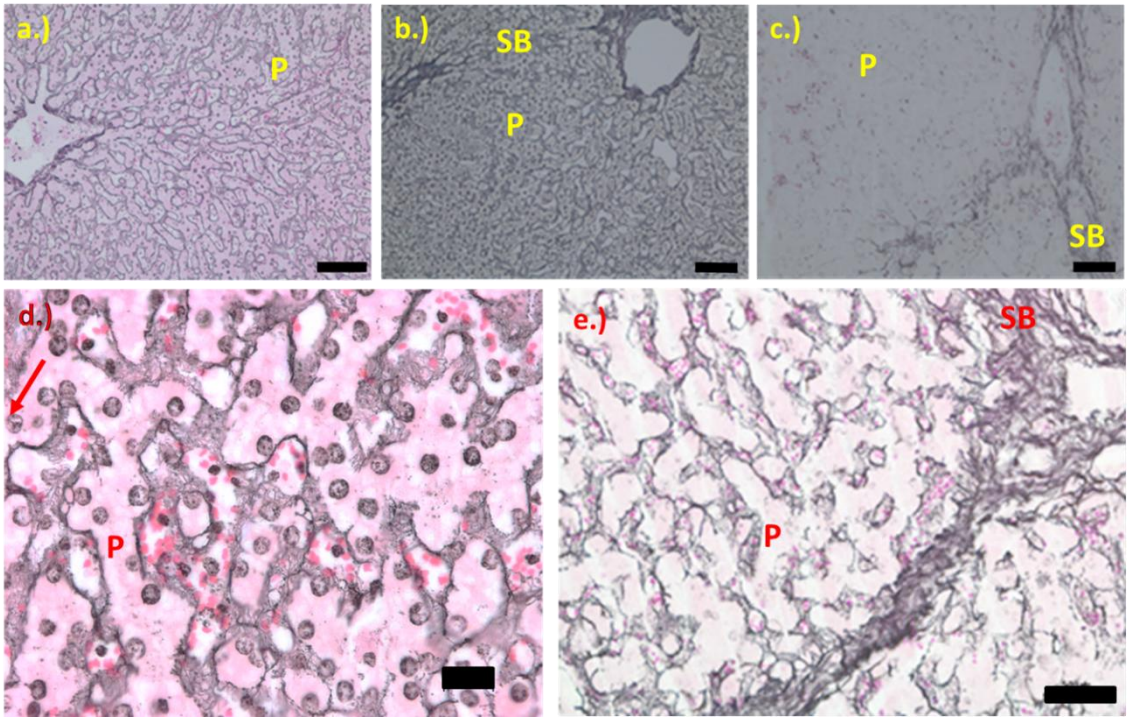

Figure 28. Reticular staining of native and decellularised porcine liver. Variation of reticular staining seen during development of staining technique (a.) to c.)) indicates significant batch variation, with batch comparison of reticular fibre retention between native (d.)) and decellularised (e.)) porcine liver showing retention of reticular fibres within the septal bands (SB) and between parenchymal cords (P). Black = Reticular fibres and nuclei (red arrow), pale pink = matrix components excluding reticular fibres, red blood cells red / dark pink. P = parenchyma, SB = septal band. Scale bars a.) b.) & c.) = 100 µm, d.) = 20 µm and e.) = 50 µm.

Figure 24. Identification of collagen fibre location in native ((a.) and b.)) and decellularised (c.) & d.)) porcine liver tissue using Masson's Trichrome stain. Collagen = green, from background (red – erythrocytes and cytoplasm) and nuclear staining (brown). SB = septal bands, P = parenchyma and BMm = basement membrane like membrane, SB = sinusoidal band, P = parenchyma. Black bar = 20 µm.

Figure 25. Native (a.)) and decellularised (b.)) porcine liver tissue stained with Sirius red / millers elastin stain to identify presence and location of total collagen and elastin. Specific identification of elastin and collagen was difficult to differentiate in native and decellularised porcine liver tissue. SB = septal bands, E = elastin, P = parenchyma and BMm = basement

3.3.6 ~~was performed.~~

~~Sections of native and decellularised porcine liver were labeled with primary antibodies against Collagen I, III and IV, which were subsequently labelled with a species-specific secondary antibody, and a brown diaminobenzidine (DAB) tag. Collagen I and III in native tissue sections were located in a thin line, adjacent to hepatocytes within the parenchyma and throughout septal bands. In decellularised tissue sections, collagen I was retained in similar regions, albeit with lower intensity. Collagen III was retained at the same intensity within the parenchyma and septal bands. Collagen IV in native tissue was present adjacent to hepatocytes within the within the parenchyma.and lining the hepatic arteries and portal veins within the portal triads. Collagen IV was also present throughout the cholangiocytes within the bile duct. After decellularisation procedures were applied, the majority of collagen IV was lost, particularly within the parenchyma. A small amount of collagen IV was retained in the hepatic arteries and portal veins.~~

~~Reticulin staining (detailed in Section 2.2.8.3) was used to stain fine collagen III (reticular) fibres within the parenchyma of native and decellularised porcine liver (Figure 27). Visualisation using Koehler illumination (detailed in Section 2.2.5.1) revealed vast variability between staining batches (Figure 27 a.)-c.)) indicating that effective comparison of staining patterns must be performed within individual batches. Finer reticulin fibres within the parenchyma could be identified through use of non-buffered formalin, allowing more effective comparison. In native tissue, reticular fibres were adjacent to hepatocytes, traversing sinusoids in the location of the BMm. Positive staining was also found within nuclei indicating further optimisation of the stain is required. In decellularised tissues, reticular fibres were also adjacent to hepatocytes, although shorter in length (Figure 27 d.) & e.)).~~

Was glycosaminoglycan retained in decellularised porcine liver tissue?

GAG content of native and decellularised porcine liver was determined by digestion of tissues with papain, and subsequent quantification of the GAG containing supernatant using a dimethylene blue (DMMB) assay (Section 2.2.14.4). GAG content was quantified using a linear regression of chondroitin sulphate B standard curve (Figure 29a.)). GAG content of native and decellularised porcine liver was 22.5 ±10.10 and 0 $\mu g.mL^{-1}$ respectively (Figure 29b.)). A significant difference was found between native and decellularised porcine liver GAG content. (Student's t-test, $p<0.05$, n=6 ± 95% confidence interval).

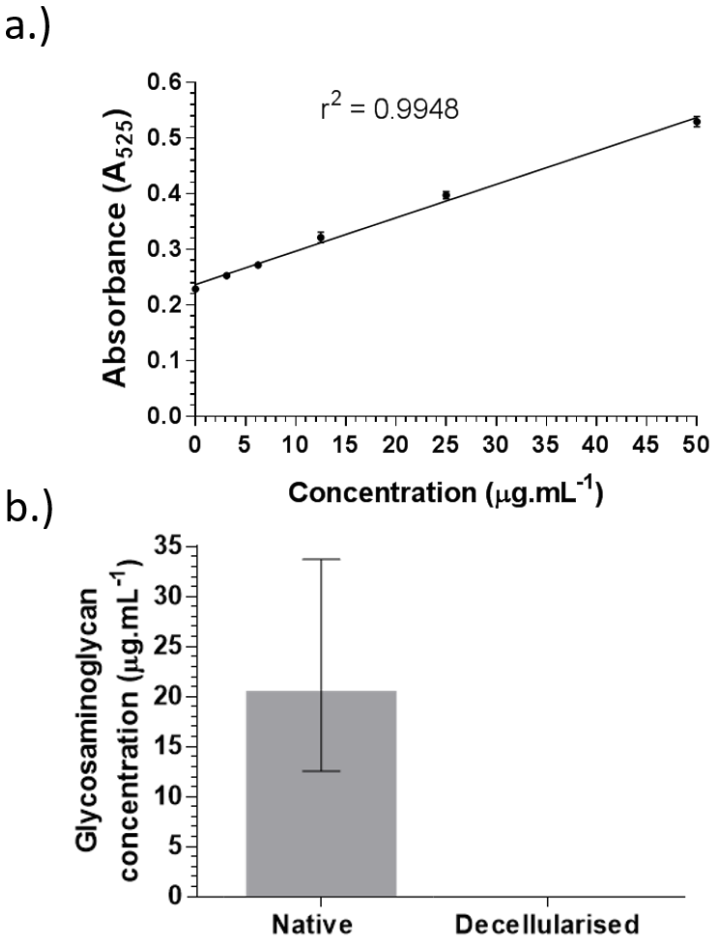

Figure 29. Reduction of glycosaminoglycan content in porcine liver after decellularisation. Standard curve of absorbance (595nm - 525 nm) of known concentrations of chondroitin B sulphate (a.) and calculation of sGAG concentration in native (grey bar) and decellularised (red bar) porcine liver b.).

~~GAG content of native and decellularised porcine liver was determined by digestion of tissues with papain, and subsequent quantification of the GAG containing supernatant using a dimethylene blue (DMMB) assay (Section 2.2.14.4). GAG content was quantified using a linear regression of chondroitin sulphate B standard curve (Figure 28 a.)). GAG content of native and decellularised porcine liver was 22.5 ±10.10 and 0 μg.mL^{-1} respectively (Figure 28 b.)). A significant difference was found between native and decellularised porcine liver GAG content. (Student's t-test, p<0.05, n=6 ± 95% confidence interval).~~

3.3.7 Did porcine liver retain attachment and growth factors after decellularisation?

Sections of native and decellularised porcine liver were labeled with primary antibodies against laminin and fibronectin, which were subsequently labeled with a

species-specific secondary antibody, and a brown DAB visually identifiable tag (Section 2.2.9.5, Figure 30). Laminin within native tissue was located within hepatocytes, hepatic arteries, and a small amount within portal veins. Decellularised porcine liver retained laminin~~fibronectin~~ within hepatic arteries and portal veins only. Fibronectin was located to varying amounts within hepatocytes of native porcine liver tissue, however, no repeatable pattern of staining was found. Fibronectin was not retained within decellularised porcine liver except for a few small areas (Figure 30).

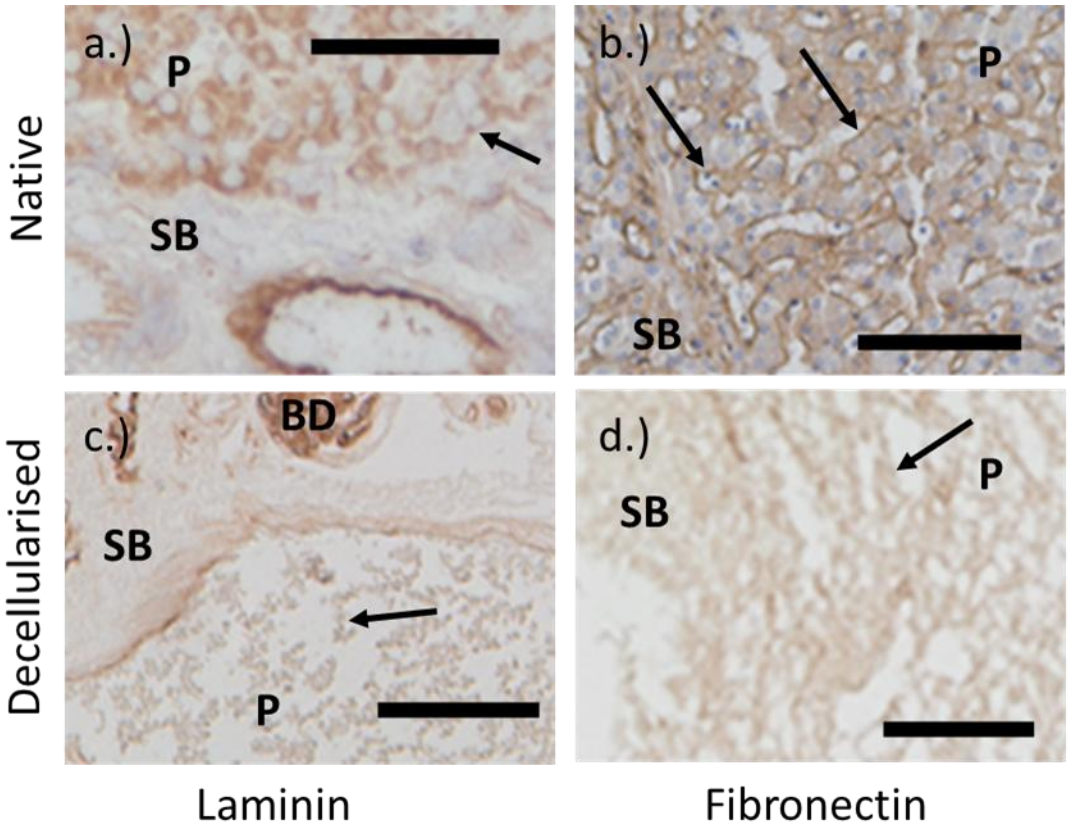

Figure 30. Laminin and fibronectin labelling of native and decellularised porcine liver. Native tissue showed the presence of laminin in the parenchymal hepatocytes and in the vasculature (a.), black arrow), and fibronectin was found in the BMm adjacent to hepatocytes in the parenchyma (b.), black arrow). Decellularised porcine liver shows loss of laminin (c.)) and fibronectin (d.)) from the parenchyma and BMm, except in a few areas at the edges of the parenchyma adjacent to the septal bands (black arrows). Some laminin was also retained within the vasculature of the portal triad (black arrows). P = parenchyma, SB = septal band. Black arrows = positive staining. Scale bars a.), c.) & d.) = 50 µm. and b.) = 100 µm.

3.4 Discussion

The aim of this Chapter was to create a porcine liver scaffold, depleted of cellular and nuclear components, with minimal negative effects upon viability when in contact with cells. Although definitive criteria for a decellularised scaffold do not currently exist, all the guidance to prevent adverse tissue remodelling, or immune, responses upon implantation were achieved in this Chapter using sections of porcine liver 10 mm in diameter and 7mm in depth decellularised using low concentration SDS (0.1 % v/v). As mentioned in Chapter 1, the decellularised tissue created in this Chapter were developed to study methods to maximise cell attachment *in-vitro*, however the alternative application of the decellularised liver tissue do not stop within the laboratory. These scaffolds may be implanted directly into, or macerated / freeze dried and combined with a hydrogel to be injected into, failing or damaged livers to support the native remodelling response and support some native liver function to allow liver regeneration to take place. The decellularised porcine liver developed in this Chapter, therefore was developed to the same standards as those required for subsequent implantation. Ideally, a decellularised liver scaffold would contain the complexity of native tissue physiological and biological components, to allow cells to attach to the scaffold and move to areas devoid of cells until the tissue is repopulated. Once repopulated, the scaffold should provide key environmental triggers to allow sufficient liver function, and cell viability, to be maintained. Balancing tissue retention with sufficient removal of nuclear and cellular components is a balance with multiple facets that must be considered including tissue size, detergent concentration, temperature and time. Minimising exposure whilst ensuring sufficient decellularisation must take all these factors into account.

Porcine liver contains denser septal bands than that seen in other species, whereas all species have fine collagenous structures within the parenchyma (Bancroft and Gamble, 2002). This presents a challenge in effective decellularisation of porcine tissue, with the requirement to remove sufficient nuclear components in septal bands whilst also retaining finer structures in the parenchyma. One cycle SDS (0.1 % v/v) has proven sufficient to remove nuclear components in both parenchyma and septal bands, and still results in retention of basement membrane like structures, such as reticular fibres, within the parenchyma (Figure 15 and Figure 28). Successful decellularisation of rat liver has been achieved within 80 min using low concentration SDS (0.1 % v/v) (Hussein et al., 2013b) and 60 min if higher concentrations detergent are used (1 % SDS v/v) (De Kock et al., 2011). Further development with the use of liver tissue from non-porcine liver would

require further adaptation of the Leeds method, and primarily focusing on reduction of tissue degradation. This may be achieved through shorter exposure times and/or lower SDS concentration to remove cellular and nuclear components from the septal bands, thereby minimising protein loss further.

Alternative methods for decellularisation have been reported, in particular the use of perfusion, rather than immersion and agitation. Perfusion of reagents through the native vasculature is not always possible in smaller tissues, even though immersion and agitation is not as efficient at removing nuclear contents (Kajbafzadeh et al., 2013). Investigations comparing methods of solution delivery (perfusion, or immersion and agitation) were compared using a variety of detergents and detergent concentrations including SDS, Triton X-100, EDTA and PAA. In each group, perfusion decellularisation was more efficient than immersion and agitation, showing better protein retention when perfusion decellularised for the same time lengths (Kajbafzadeh et al., 2013). Although the reason to decellularise smaller discs was to investigate cell repopulation; perfusion of an entire liver, or liver lobe, may have yielded better retention of BMm proteins, which could then have been trimmed into smaller sample sizes for subsequent seeding. This would also allow for scaling up of tissue production. Risk of contamination resulting from this modification would increase, although could be minimised through preparing discs of decellularised tissues before application of sterilant.

Perfusion of liver tissue has been reported using either the portal vein alone (Ren et al., 2013, Uygun et al., 2010, Hussein et al., 2013b, Park and Woo, 2012), via the hepatic artery and portal vein, and/or systemically alongside decellularisation of other organs (Park and Woo, 2012, Kajbafzadeh et al., 2013). Systemic perfusion decellularisation is often employed in rats due to the small organ sizes. Systemic perfusion of adult rats using SDS (1 % v/v) via the carotid artery at a rate of 50 $mL.min^{-1}$, and via the portal vein at a rate of 17 $mL.min^{-1}$, showed successful removal of cellular and nuclear components within multiple tissue types within 14 hr. Stomach, intestine, prostate, uterus and bladder decellularised the quickest (three hr), followed by spleen (seven hr) liver (ten hr), kidney and heart (14 hr) (Park and Woo, 2012). The use of perfusion through both the hepatic artery and portal vein was shown to decellularise the liver quicker than the kidney and heart, even though flow rates were reduced in the liver. Perfusion rates were reduced in the liver due to organ swelling observed at higher flow rates indicating the importance of flow rate (Park and Woo, 2012). A low

concentration of SDS has been used to perfuse rat livers through the portal vein within 60-80 min, with 30 min perfusion displaying graded loss of cellular material across the lobule and complete loss within 80 min. Even though substantial thinning of parenchymal cords were seen at 80 min, this was seen across lobules rather than the tissue. It is thought that slightly reduced time in perfusion may have created more ideal retention of tissue architecture (Hussein et al., 2013b).

Successful decellularisation involves a fine balance between successful remove of nuclear and cellular components and minimisation of tissue damage. This is especially prevalent in tissues with differing levels of tissue density. The BMm within the parenchyma is noted for being a fine, attenuated network that allows the bidirectional transport of molecules between the blood and hepatocytes. Septal bands are, however, much denser, therefore a greater amount of degradation was expected, and observed, within the parenchyma, when compared to the septal bands (Figure 13). Similar patterns have been seen with the application of immersion and agitation in both SDS based and Triton X-100 decellularised porcine liver (Mattei et al., 2014). In agreement with Gilbert and colleagues (2006), literature suggests that higher detergent concentrations are not the only factor in successful decellularisation, with SDS use associated with effective membrane solubilisation and increased risk of tissue degradation. The use of proteases, nucleases and/or hyper- and hypo-tonic solutions, such as those developed in this Chapter, can minimise risk of degradation in SDS based methods, akin to those seen with Triton X-100 based methods (Shirakigawa et al., 2012). Furthermore, the lack of buffered solutions and possible effect of agitative speed may have also caused greater levels of tissue degradation. Comparison of ionic, non-ionic and detergent-free solutions has been investigated (Mattei et al., 2014), with results indicating that detergents are required for successful removal of nuclear components. Increasing time of exposure from one cycle to three cycles resulted in increased loss of degradation, which was supported in both non-ionic and ionic detergent based methods in a time dependant manner (Shirakigawa et al., 2012, Mattei et al., 2014). These are, however, reported to occur slower when using non-ionic detergents, as opposed to ionic based. The additional application of protease inhibitors and low concentration SDS (0.1 % v/v), as used in the modified Leeds method developed in this Chapter, has shown successful removal within 24 hours exposure to detergent, although further development should focus on reducing SDS exposure further, with a quantitative comparison of total collagen from porcine liver decellularised with one, two and three cycles of SDS expected to show the level of degradation numerically.

Although successful decellularisation was achieved in this Chapter using three cycles SDS (0.1 % v/v), the exposure of reagents resulted in significant histoarchitectural degradation to the parenchymal matrices and flattening of lobule structure. Better retention of overall architecture was seen using one cycle SDS (0.1 %)(Figure 13). Similar results have been seen with porcine liver decellularised with 0.1 % SDS for 72 hours, equivalent to three cycles SDS using the Leeds method, at lower temperatures (4 °C) (Hussein et al., 2013a). Results confirmed that exposure for 72 hr is too long for successful retention of liver architecture even when temperatures are reduced. Reduced time of exposure has been explored in other species (Shirakigawa et al., 2012), with entire rat liver closer in size to the tissue dimensions reported within this chapter than seen in an entire human liver lobe. Six hr exposure of rat liver perfused with greater concentrations of SDS (1 %) showed quicker decellularisation than that seen in Triton X-100 (1 % v/v), with increases in Triton X-100 concentration (0.5 % - 4 %) showing a concentration dependant decrease in decellularisation time (Shirakigawa et al., 2012). Furthermore, it was reported that six hr exposure using SDS (1 % v/v) resulted in significant loss of the vascular network, whereas the use of 4 % Triton X-100 only achieved successful retention of architecture, but only with additional use of DNase and RNases.

Excessive tissue exposure maximises the risk of tissue degradation (Crapo et al., 2011) therefore the removal of DNA is not the only determinant of successful degradation. The fine reticular fibres present within the parenchyma that support organisation of the hepatocytes into cords is most likely to degrade as a result of exposure to the procedures and chemicals used during decellularisation. Optimal decellularisation would retain the reticular fibres to provide a surface upon which hepatocytes can re-establish after seeding. Retention of native vasculature would also provide a route upon which nutrients can be disseminated throughout the tissue, with biliary channel retention aiding in re-establishment of liver function. Greater levels of degradation were ~~also~~ seen with thinner samples (2-4 mm) than thicker samples (9-11 mm) (Figure 14), making tissue dimensions important during method development. Results indicate that one cycle SDS (0.1 % v/v) is sufficient to remove nuclear components up to 11 mm in depth (Figure 13 and Figure 15), although the degree of damage to both parenchyma and septal bands were greater with smaller depths. Sheets of porcine liver have been decellularised from 5 mm in depth, with results showing loss of parenchyma, irrespective of detergent used (Mattei et al., 2014). Samples of porcine liver were

decellularised using SDS (0.1 % v/v) for one, two and three days with results showing increased levels of degradation in parenchyma and lobular architecture, however, the level of destruction seen was greater than that reported in this Chapter. Samples of porcine liver with greater depth than that applied in this Chapter (max 11mm) have also been decellularised, although this occurred in tissues perfused with, rather than immersed in, detergent solutions (Barakat et al., 2012) or with liver from different species (Park and Woo, 2012, Hussein et al., 2013b, Ren et al., 2013, Kajbafzadeh et al., 2013). Results within this Chapter suggests that tissue depths of a minimum of 5mm are required to retain parenchymal hepatocyte cords after decellularisation. Another study (Hussein et al., 2013a) investigated the decellularisation of porcine liver discs at 3 mm in depth. Even though a 0.1% solution of SDS was used for 72 hr at 4 °C, substantial loss of structure was seen. Thin slices (3mm) of porcine liver decellularised using 2% Triton X-100 for longer times (five days) (Lang et al., 2011) has also displayed detrimental changes to tissue structure with loss of overall lobular structure prevalent. In addition, defining whether decellularisation was achieved was not possible as tDNA, and not dsDNA, was quantified (Lang et al., 2011). When re-seeding decellularised tissues, retention of cell viability may be limited to rates of oxygen and nutrient diffusion across the entire disc, therefore thinner tissue sections may be advantageous over thicker pieces even though they are more difficult to handle. —Tissue retention was graded across the disc, with better tissue retention seen in central, as opposed to peripheral, areas. This may be advantageous in providing easier access for cells to nutrients and oxygen supply. Decellularisation of thicker tissues, however, provides a mechanism to achieve better tissue retention when more degraded tissue is removed. Graded degradation is attributed to rates of reagent diffusion across the discs. Investigations of diffusion rates in alginate, adipose, fibrin and gelatin scaffolds show that the relationship between diffusion and size depends on the material through which the molecule is diffusing, as well as the molecular size of the scaffold. Cell presence was seen to decrease diffusivity rates. When applied to the process of decellularisation, this could mean that diffusion rates increase as cells are removed leading to increased tissue degradation at peripheral areas when decellularised using immersion. Further investigation into methods that may reduce degradation are required, including reduction of time or temperature, or the application of graded concentration of detergents. Histological evaluation and grading of tissue retention, alongside measurement of distance across the disc would help guide future work towards promoting tissue retention, whilst

benchmarking against the guidance provided (Crapo et al., 2011). Once diffusion rates were calculated to

maximise tissue retention and minimise protein loss, the necessary time in detergent required to achieve decellularisation whilst minimising protein loss could be established to aid definition of tissue sizes and detergent concentrations.

The greatest amount of laminin was lost from the parenchyma, with some retention within portal triads and septal bands, otherwise known as Zone I of the acinus. Other studies have reported similar patterns of retention in porcine (Mirmalek-Sani et al., 2013, Baptista et al., 2011, Barakat et al., 2012) and also in other species (Yagi et al., 2013, Baptista et al., 2011, Jiang et al., 2014). Although prolonged exposure to trypsin/EDTA is associated with loss of laminin, fibronectin and GAGs in pulmonary valves, the use of EDTA alone is not associated with such loss. EDTA binds divalent cations that are necessary for cell attachment to collagen and fibronectin, and its use facilitates cell removal. Polymerisation of laminin types, however, are calcium dependent. Damage created by removal of these cations through the use of EDTA may, therefore cause removal of collagen, laminin, and fibronectin, either directly, or through increasing susceptibility to other decellularising agents. The structural changes imposed through removal of these cations may also affect protein folding, causing reduced effective visualisation through impaired antibody binding. Similar patterns of retention within Zone 1 of the acinus were noted with collagen IV also. Laminin provides bioactive sites for cross linking collagen IV, therefore, the loss of collagen IV alongside laminin is not unexpected. Retention of laminin within zone 1 may relate to either greater original levels of laminin present in the septal bands of native tissue, or a difference in isoforms of these components in the septal bands compared to those found in the lobules. Some laminin isoforms are essential for organ development; however, some isoforms are not (Schéele et al., 2007) and laminin is usually absent from the lobules of mature liver, except during times of regeneration. Further analysis of the types of isoforms in native porcine tissue may identify different isoforms that are more susceptible to degradation than others and may explain the pattern of laminin loss from the parenchyma seen post decellularisation. Laminins promote cell adhesion and migration (Section 1.2), and its loss may result in reduced cell attachment and migration through the lobule. To the contrary however, this is not seen within the literature. Numerous studies have reported laminin loss with various cell types attaching to, and remaining viable on the scaffold, including HepG2

(Mirmalek-Sani et al., 2013), mesenchymal stem cells (Jiang et al., 2014) and foetal liver cells (Barakat et al., 2012, Baptista et al., 2011). Although cell attachment and viability does not seem to be affected by the loss of laminin, its effect on cell function or the time required to achieve full function has yet to be determined. As laminins are absent in the lobules of mature liver, it is thought that their absence may increase cell function rather than cell proliferation and/or movement.

Application and development of the Leeds method to porcine liver tissue resulted in the loss of fibronectin, a protein involved in cell differentiation (McClelland et al., 2008). Fibronectin loss has also been seen with development of the Leeds method on other decellularised tissues (aortic wall) to a lesser extent, therefore some loss was expected. This may be attributed to the use of SDS, with the work of Mattei and colleagues (2014) showing fibronectin loss with methods using SDS and not Triton X-100. Loss of fibronectin is also seen with other species such as sheep (Kajbafzadeh et al., 2013) and rats (Uygun et al., 2010, Ren et al., 2013), although not as great as that seen within this Chapter (Figure 30). Antibody staining of native tissue from various species would identify whether the variations observed after decellularisation were attributed to variations between species. Better retention of fibronectin has been seen with the use of Triton X-100 over SDS (Kajbafzadeh et al., 2013), and with the use of perfusion-based methods of decellularisation in rat tissue vein (Uygun et al., 2010). Fibronectin loss has also been noted in Triton X-100 based decellularisation methods (Baptista et al., 2011), although the patterns of loss differs. Perfusion of porcine liver with 0.25% and 0.5% SDS (Barakat et al., 2012) were associated with similar patterns of fibronectin loss as seen within this Chapter, however, decellularisation using Triton X-100 displayed loss of fibronectin in the septal bands, and retention in the parenchyma (Baptista et al., 2011). Decellularisation of Sprague-Dawley rats with either Triton X-100 (1%) or SDS (1%) reported comparatively greater amounts of fibronectin were removed from rat livers treated with SDS (Ren et al., 2013). As with livers decellularised with either SDS or Triton X-100 were perfused for the same time (2 hr), and SDS is more effective in removing nuclear components than Triton X-100 (Gilbert et al., 2006), the increased loss is not entirely reflective of the solutions used, but also the time of exposure. No significant difference in hepatocyte engraftment efficiency was noted between SDS or Triton X-100 treated rat livers implying that the loss of fibronectin does not affect cell engraftment. Production of albumin and urea, as well as increased rates of ammonia elimination were significantly higher in those cells seeded in Triton X-100 decellularised tissue, which may

be attributed to the increased retention of fibronectin between the two detergents (Ren et al., 2013). Future development of perfusion-based decellularisation methods or altering the type of detergent used would, therefore, prevent loss of fibronectin in porcine tissue. As mentioned previously (Section 1.2), fibronectin is associated with hepatocyte differentiation, therefore its loss may result in retention of a proliferative or non-differentiated phenotype, rather than affect cell attachment. If cell adhesion and migration is hindered by the loss of fibronectin, supplementation of matrices with foetal or human fibronectin has been shown to aid cell adhesion and migration (Hsiao et al., 2017). Fibrillar collagens I and III were retained throughout the tissue, whereas non-fibrillar collagen IV was lost, which may be attributed to differences in protein structure. Structural collagen rods are tightly bound, lying adjacent to each other to form a helical structure with multiple crosslinks between fibrils. Collagen IV rods on the other hand are bound in a head:head configuration with associated hinge like regions and lateral aggregation that provide flexibility. The loose, interconnecting network of collagen IV rods are therefore more exposed to the degradative effects of the decellularising agents when compared to the helical fibrillar collagens.

Reticular fibres are not often investigated after liver decellularisation however, the vital role in supporting hepatocytes and sinusoidal structure during fibrosis and/or cirrhosis cannot be minimised (Wen et al., 2016). The remodelling of reticular tissue has been shown in rat and human liver, involving upregulation of matrix metalloproteinases (MMP-2, MMP-9) and tissue inhibitors of MMPs (TIMP-1) early in the formation of fibrotic lesions (Wen et al., 2016) and indicate high levels of degradation and formation. As reticular fibres provide cell support and arrangement of cell location, its retention is thought to be critical for the formation of cell cords and plates, and liver tissue regeneration. Reticular fibres were retained in the protocols used in this study, the retention of which is attributed to the use of aprotinin and EDTA, which inhibit MMPs. MMPs are made by many cell types including hepatocytes (Calabro et al., 2014) and are released upon cell death. The use of aprotinin and EDTA may therefore inhibit degradation of the fine reticular fibres adjacent to the hepatic cords. Only three other studies have reported retention of reticular fibres (Baptista et al., 2011, Nari et al., 2013, Mattei et al., 2014). Decellularisation using three cycles Triton X-100 reportedly retained reticular fibres, however, the level of non-specific staining, and low magnification of images made confirmation of the presence and/or location of reticular fibres questionable (Mattei et al., 2014). Use of Wilde's silver stain,

as opposed to Gordon and Sweets silver stain on rabbit livers decellularised with SDS (0.1% v/v) and Triton X-100 (3% v/v) also indicated retention of reticular fibres,

> however, application of this silver stain was too aggressive for sufficient decellularised tissue to remain on the slide. As a result, accurate location of reticular staining was not identified. Furthermore, the retention of reticular fibres assessed through SEM (Baptista et al., 2011) does not exclude other collagen fibres or proteins associated with the BMm, merely the presence of a mesh within vessels of the portal triad. Further development in the application of silver stains is essential to assess retention of these specific fibres and as a result, has not been effectively shown in other literature of decellularised tissues, let alone to the same standard or level seen in this Chapter.

Although SDS is associated with protein denaturation, the comparison of total and denatured collagen from decellularised tissue indicates no comparative increase in denatured collagen:collagen as a result of denaturation resulting from the developed protocol (Section 2.2.14). This has been seen in other tissues decellularised using methods based on the same Leeds method. Decellularisation of human aorta's ~~large diameter vascular grafts~~ using 0.1% SDS and PAA for example, reported no significant increase in the ratio of denatured collagen:collagen content between native and decellularised tissues (Aldridge et al., 2018). As a result, it is thought that low concentration of SDS ~~has not~~ does not cause excessive amounts of collagen degradation. This is in alignment with the quantification of hydroxyproline content from low concentration SDS decellularised human aorta ~~ic heart valves~~ (Aldridge et al., 2018), human aortic and pulmonary valves (Vafaee et al., 2018) porcine super-flexor tendon (Jones et al., 2017) or human dermis ~~skin~~ (Hogg et al., 2015). Retention of collagen after decellularisation with low concentration SDS (0.1% v/v), however, is also associated with loss of glycosaminoglycan (GAG) as seen in this Chapter (Figure 29).

GAGs are thought to be involved in the regulation of cell signalling and adhesion, as well as tissue regeneration. Complete loss of GAG content was seen after decellularisation of porcine liver using 0.1% (v/v) SDS (Figure 29). Decellularisation of rat liver has displayed differing results, with an SDS based decellularisation method showing an increase in GAG content (0.57 ± 0.069 % vs 0.399 ± 0.012 % in decellularised and native tissue respectively) (Hussein et al., 2013b), and a Triton X-100 based method showing retention of 83.8 % native SDS (Lee et al., 2014). This suggests that there is another cause for the

loss of GAGs seen in porcine tissue as opposed to rat tissue. Loss of GAG has also been seen in porcine liver tissue decellularised with PBS, water or salt, either with or without the inclusion of peracetic acid (PAA) (Lang et al., 2011). GAG content was lower in methods using a PBS or salt solution containing PAA, as opposed to without PAA indicating that the use of PAA is associated with GAG loss. Loss of GAGs has also been reported in decellularised pulmonary valve (Luo et al., 2014b) and tendon (Jones et al., 2017) where all methods include use of peracetic acid as a ~~terminal~~ sterilant. GAG quantification of tissues decellularised with, and without, the use of peracetic acid could be performed to confirm this hypothesis. The increased risk of microbial contamination as a result of not using peracetic acid is too great to consider, although other methods such as gamma irradiation may be investigated. Even though GAGs are lost using PAA, studies have shown that scaffolds still supported fibroblast attachment (71.50 ±1.95%), indicating that other attachment factors may supersede the effects of GAG loss, although any effects seen from the loss of GAG content may still effect cell signalling (Hussein et al., 2013a).

This study used three cell types (L929, BHK, HepaRG) in testing for direct and indirect toxicity of decellularised porcine liver scaffolds, with cells lacking abnormal changes in cell morphology and showing no significant changes in metabolic activity when compared with negative controls. Cytotoxicity studies of scaffolds treated with 0.1 % SDS and PAA indicated an increase in fibroblast metabolic activity with scaffold conditioned media, thought to be resulting from increased proliferation (Hussein et al., 2013a). Subsequent staining of the fibroblasts with Ki-67 showed increased proliferation after the addition of conditioned media. Although the results in this chapter did not show a significant increase in metabolic activity, an increase in HepaRG activity was seen, albeit not significantly greater. Antibody staining with Ki-67 may indicate whether this is resulting from an increase in cellular proliferation. To minimize structural damage, porcine liver discs were rolled in 2L indented cell culture bottle. In addition, speeds were limited to 6 RPM to provide full disc rotation and minimise potential damage to internal structures. Although structural retention in this Chapter surpasses those reported by others (Baptista et al., 2011, Lang et al., 2011, Mattei et al., 2014), the retention of BMm proteins, including fibronectin and laminin were still reduced and GAGs were lost. Further development of the decellularisation protocol may include:

1. reducing SDS exposure through further reductions in concentration and/or time.
2. application of perfusion to maximise efficiency and minimise protein loss, particularly fibronectin.
3. investigation of other ~~terminal~~ sterilant's to minimise loss of glycosaminoglycans.

Although the total loss of GAG and reduction in BMm proteins within the parenchyma seen in this Chapter may indicate a possible reduction in cell attachment or viability, assessment of cell behaviour after seeding is currently limited. The retention of collagen IV was specifically limited to the endothelial tissue which may provide a future avenue of cell attachment should limited attachment be seen within the parenchyma.

Future questions regarding successful cell seeding include whether cells attach to, and remain viable on, the decellularised porcine liver created in this Chapter, whether cells remain on the surface or penetrate the tissue, and whether the cells proliferate or differentiate. Some of these will be investigated in Chapter 5 once baseline cell characteristics are defined in Chapter 4.

~~2.~~4 Characterisation of Huh7 and HepaRG cells

4.1 Introduction

After successful production of decellularised porcine liver discs that retain key cell attachment components, lobular ~~histioarchitecture~~histoarchitecture, and vascular features, the next step was to identify suitable cell types for seeding on the decellularised porcine liver discs. A high initial proliferative and migratory capacity would therefore be essential, followed by a signal or time bound event that initiates and/or maintains differentiation thereafter at similar levels to that seen *in vivo*.

Cells lines are considered advantageous compared to primary cells due to the ready availability, high proliferation capacity, and stable metabolism. When cultured on decellularised matrices, mono-culture provides a way to study interactions between individual cells and the matrices, whereas co-culture also allows for the study of relationship between cell types (Paschos et al., 2014). Two cell types were initially chosen to develop seeding methods: Huh7 (a highly proliferative cell type) and HepaRG (a cell line with progenitor like phenotype that differentiates into two distinct cell types; hepatocyte-like and cholangiocyte-like cells). Induction of differentiation in both cell types can occur using dimethylsulfoxide (DMSO).

4.1.1 Identification of, and differences in, cell morphology between phenotypic states

Proliferative and differentiated phenotypes can be identified in both Huh7 and HepaRG through cell morphology and protein markers expressed; with proliferative cell types larger and more uniform in morphology and expressing phenotypic markers such as CD24 and CK19, whereas differentiated hepatocyte phenotypes show reductions in cell size, increased cytoplasmic granularity and expression of functional proteins such as albumin and CYP3A4. Both cell types have well established and characterised culture protocols (Godoy et al., 2010, Gripon et al., 2002, Parent et al., 2004) that allow for identification of phenotype specific protein expression through cell morphology. Identification of proliferative and differentiated morphologies was undertaken using microscopy. Both HepaRG and Huh7 cell types proliferate when seeded subconfluently. HepaRG cells stop proliferating when in contact with other cells, whilst Huh7 cells do not (Nakabayashi et al., 1982, Guillouzo et al., 2007). Both cell types, however, fully differentiate upon the addition of DMSO (1.8-2%) supplemented media

(Godoy et al., 2010, Gripon et al., 2002, Parent et al., 2004). When cultured as a monolayer, Huh7 phenotypes can be identified morphologically through differences in cell size, as well as cytoplasmic granulation. Proliferative cells are larger in size with low cytoplasmic granularity. Huh7 cells form a pavement like arrangement after differentiation has occurred (Figure 31). Differentiated Huh7 are comparatively smaller in size with large prominent nuclei and darker, granulated cytoplasm. When seeded at appropriate densities, full cell differentiation can occur within nine days (Godoy et al., 2010).

Two distinct growth phases were identified in HepaRG cell morphology when cultured on tissue culture plastic. Proliferative HepaRG are small, round cells that are uniform in size with clear cytoplasm. HepaRG continue to proliferate until in contact with other cells. The addition of DMSO supplemented media induces differentiation into two distinct cell populations; large, flat, polygonal cells with homogenous cytosol and non-clear nuclei, and smaller cells with dark granulated cytosol, prominent nuclei and refractile borders (Gripon et al., 2002, Parent et al., 2004, Marion et al., 2010) (Figure 31).

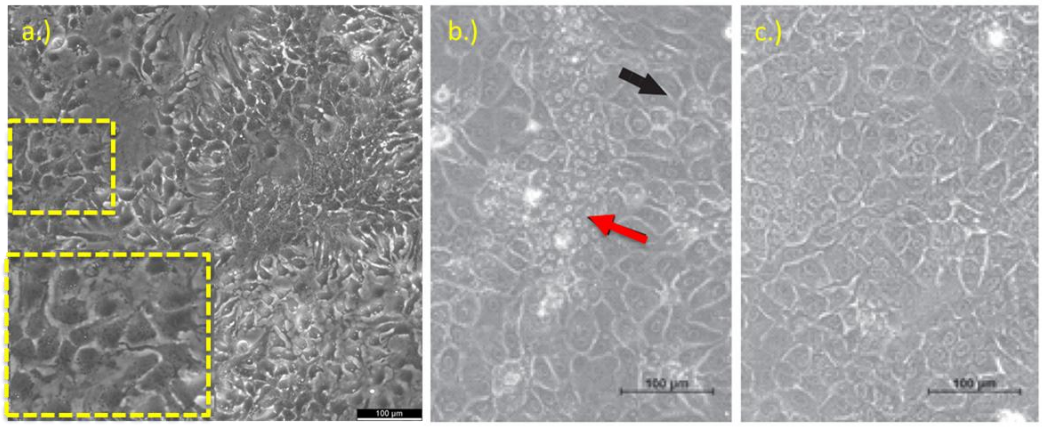

Figure 31. Huh7 and HepaRG cell morphology. Huh7 (a.)) show pavement like cell arrangement after differentiation, whereas HepaRG show two different morphologies, large polygonal cells with non-clear nuclei (b.) black arrow) and smaller cells with dark granulation and prominent nuclei (b.) red arrow). Non-differentiated HepaRG (c.)) are uniform in size with clear cytoplasm. . Scale bars = 100 µm. Images adapted from www.cytion.com/HuH7-Cells/300156 and (Gutmann et al., 2023). Square indicates area examined under a higher magnification.

4.1.2 Evaluation of protein expression to relate morphological changes to cell phenotype

Expression of specific protein markers is an effective means by which to identify cell phenotype. Two separate phases should be identified with proliferative markers present during cell proliferation and absent when cells are differentiated. Functional

markers should only present when cells are differentiated and be absent when proliferating. In addition, markers of cell:cell contact should only be present for cells in close contact. Expression of different markers for cell proliferation, contact and hepatocyte function were therefore investigated; Ki67 and PCNA for cell proliferation, EpCAM as a progenitor cell marker, albumin and CYP3A4 for cell function. Nestin was also added during assessment of HepaRG cells as this intermediate filament protein is associated with neuroepithelial progenitor cells. Immunofluorescence staining and Western blots were performed to identify the presence and location of expressed proteins. Immunofluorescent staining revealed protein localisation, whereas Western blots provided a method to detect bulk population protein expression. ~~The use of immunofluorescent staining provides the location of protein expression, whereas the use of Western blotting provides a visual quantity of protein content.~~ Identification of proliferating and differentiating cell morphology's after seeding cells on decellularised biological matrices is difficult due to surface topology and depth of cell penetration, therefore identification of protein markers expressed during both phases of monolayer cell culture will aid in identification of proliferative and differentiated cell phase when seeded on decellularised porcine liver matrices.

4.2 Aims and Objectives

4.2.1 Aims

The aim of this Chapter was to identify individual or combinations of suitable protein markers to identify and differentiate between dividing, fully-differentiated and/or semi-differentiated Huh7 and HepaRG cell phenotypes when cultured on tissue culture plastic.

4.2.2 Objectives

~~• To identify Huh7 and HepaRG phenotype through alterations in cell morphology when cultured in monolayer.~~

~~• To identify protein markers expressed in proliferative and/or differentiated Huh7 phenotypes through immunofluorescent staining and/or Western blots.~~

~~• To identify protein markers expressed in proliferative or differentiated HepaRG phenotypes through immunofluorescent staining and/or Western blots.~~

~~Objectives~~

~~To culture Huh7 and HepaRG in monolayer using standardised methods.~~

- To culture Huh7 and HepaRG cells in monolayer using standardised methods.

~~• To identify cell phenotype and type through assessing changes in cell and nuclear size, and cytoplasmic granularity~~

- ~~Use Western blots and immunofluorescent staining to comparatively identify increased and decreased expression of protein markers for cell adhesion, proliferation and hepatocyte function during proliferative and differentiated phenotypes.~~ To morphologically characterise differences in cell shape, size, and nuclear size and cytoplasmic granularity to identify and differentiate between proliferative and differentiated phenotypes.

- To use Western blots and immunofluorescent staining to identify and compare proteins expressed in dividing and differentiated Huh7, identified as such using morphological characteristics.
- To use Western blots and immunofluorescent staining to identify and compare proteins expressed in dividing, semi-differentiated and fully-differentiated HepaRG, identified as such using morphological characteristics.

~~1.~~ 4.3 Results

~~2.~~ 4.3.1 Identification of Huh7 morphology across a nine-day differentiation culture period

Huh7 were seeded as described in Section 2.2.16, images were taken from three regions of each well as described in Sections 2.2.5.2, 2.2.5.3 and Figure 33. Reduction in length of Huh7 nuclei and cytoplasm when cultured over nine days. Huh7 were seeded in wells, with images of cells taken at three different locations: P1, P2 and P3 (a.)). Nuclear and cell lengths were measured in triplicate, at each location and averaged (b.)). Values were plotted against number of days in culture (c.) and d.)). Results show nuclei and cell lengths increased between days one and three, decreased at day five and increased once more at day seven. At day nine lengths decreased slightly once P1 = Green, P2 = Red, P3 = Blue. n=3

Figure 34. Decrease in proliferation markers and increase in differentiation markers through nine days of Huh7 cell culture. GAPDH (housekeeping gene) decreased slightly over nine days. PCNA decreased over the culture period, whereas, albumin levels increased. CYP3A4 expression remained constant throughout. Red dashed box = Supplementation of standard media with DMSO (1.8 %-2 % v/v). All experiments imaged three times and repeated in triplicate, with representative images shown.

Figure 33. Reduction in length of Huh7 nuclei and cytoplasm when cultured over nine days. Huh7 were seeded in wells, with images of cells taken at three different locations: P1, P2 and P3 (a.)). Nuclear and cell lengths were measured in triplicate, at each location and averaged (b.)). Values were plotted against number of days in culture (c.) and d.)). Results show nuclei and cell lengths increased between days one and three, decreased at day five and increased once more at day seven. At day nine lengths decreased slightly once P1 = Green, P2 = Red, P3 = Blue. n=3. At day one, Huh7 were found in isolated or small groups (Figure 32), which subsequently formed larger clusters with extended protrusions that adhered to neighbouring cells (Figure 32). Polygonal morphology was present before monolayer formation, seen at day five. Huh7 reduced in size and displayed increased cytoplasmic granularity. By day nine, cells were smaller, spherical and uniform with granular cytoplasm (Figure 32). Huh7 reduced cellular and nuclear diameter after addition of DMSO supplemented media, before cells formed a monolayer (Figure 32 and Figure 33). The greatest difference in size occurred between days one and three, immediately after DMSO supplemented media was added and when non occupied surface area was largest, and after between days seven and nine. ~~The decrease in cellular and nuclear diameter plateaued between days three and five, and c~~Cytoplasmic granularity increased from day five onwards (Figure 32 and Figure 32). Protein expression and location was analysed using Western blots and immunohistochemistry respectively.

~~3.~~4.3.2 Identification of suitable markers to differentiate Huh7 phenotype across nine-day culture period.

Huh7 were cultured as previously described in Section 2.2.16 with six well plates used instead of 12 well plates and volume of media added was greater (3 mL instead of 2 mL). Protein lysates were generated. quantified and Western blots performed using antibodies for GAPDH (housekeeping gene), the proliferation marker PCNA, and two functional hepatocyte proteins; albumin and CYP3A (See Sections 2.2.9).

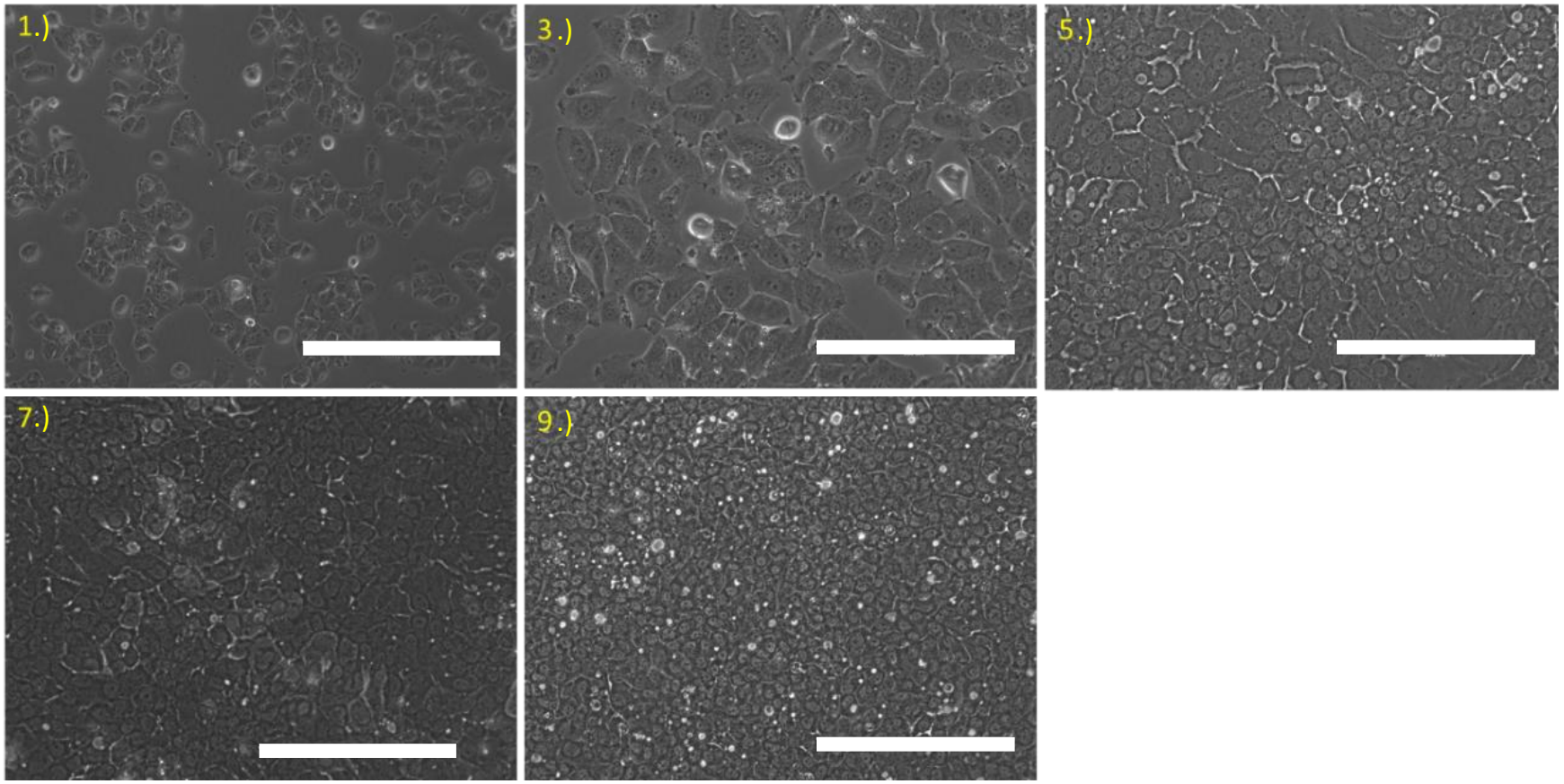

Figure 32. Progression of morphological changes through Huh7 cell differentiation. Huh7 show an increase in cell number up to day five where confluent. Huh7 decrease in cell size, with cytoplasm becoming more granular and darker. Numbers correspond to days in culture and scale bars = 200 µm at days one, five, seven and nine, Scale bar = 100 µm at day 3. All experiments imaged three times and repeated in triplicate, with representative images shown.

a.)

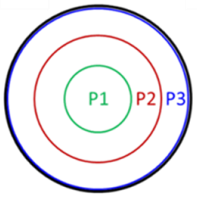

b.)

Day	P1 (µm)		P2 (µm)		P3 (µm)		Combined (µm)	
	Nuclear	Cellular	Nuclear	Cellular	Nuclear	Cellular	Nuclear	Cellular
1	5.52	5.86	5.81	6.01	5.94	6.08	5.76	5.98
3	7.12	6.58	7.98	7.75	7.83	7.84	7.64	7.39
5	5.55	5.90	5.28	5.56	5.02	5.70	5.28	5.72
7	8.57	9.06	8.84	9.41	9.63	10.20	9.01	9.55
9	6.99	7.59	7.77	8.12	6.59	6.98	7.12	7.56

c.)

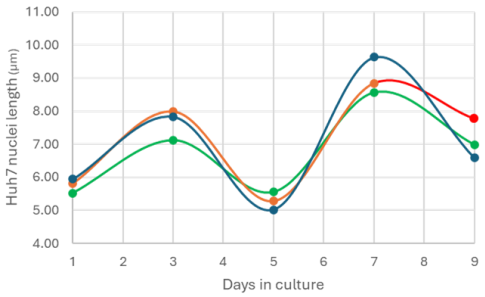

d.)

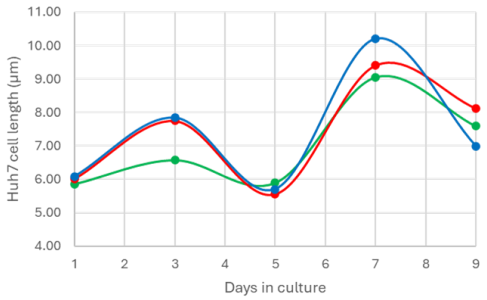

Figure 33. Reduction in length of Huh7 nuclei and cytoplasm when cultured over nine days. Huh7 were seeded in wells, with images of cells taken at three different locations: P1, P2 and P3 (a.)). Nuclear and c~~C~~ell~~ytoplasm and nuclei~~ length~~s were~~ ~~was~~ measured in triplicate, at each location and averaged (b.)). Values were plotted against number of days in culture (c.) and d.)). Results show nuclei and c~~ytoplasm~~ ell lengths increased between days one and three, decreased at day five and increased once more at day seven. At day nine lengths decreased slightly once ~~were greatest in length at day one,~~

Immunofluorescent labelling of Huh7 was performed using antibodies for Ki-67, albumin and EpCAM (Section 2.2.9). PCNA content from protein lysates significantly reduced after day one, and reduced further thereafter (Figure 34). Decreased expression of PCNA in Western blots correlated well with the decrease in Ki-67 expression in immunofluorescent labelled images (Figure 35), and inversely correlated with the increase in cell number seen between days one and five (Figure 32). The functional protein albumin showed an inverse correlation with PCNA, with albumin almost absent within the cells at days1 and 3, and increased at day five onwards. Results from Western blots (Figure 34) support that seen with immunofluorescent labelling (Figure 35 to Figure 38). CYP3A4 was present at all time points within the total protein lysed from Huh7 cells, although immunofluorescent labelling indicated that CYP3A4 was greatest at day one, with large amounts of protein seen in the cytoplasm at day one, which decreased until day 5. At days seven and nine, intense nuclear CYP3A4 staining was seen in a small number of cells. Morphologically, proliferative Huh7 (Figure 32- day one)

were larger in cytoplasmic and nuclear diameter (Figure 32) with extended morphology and clear cytoplasm.

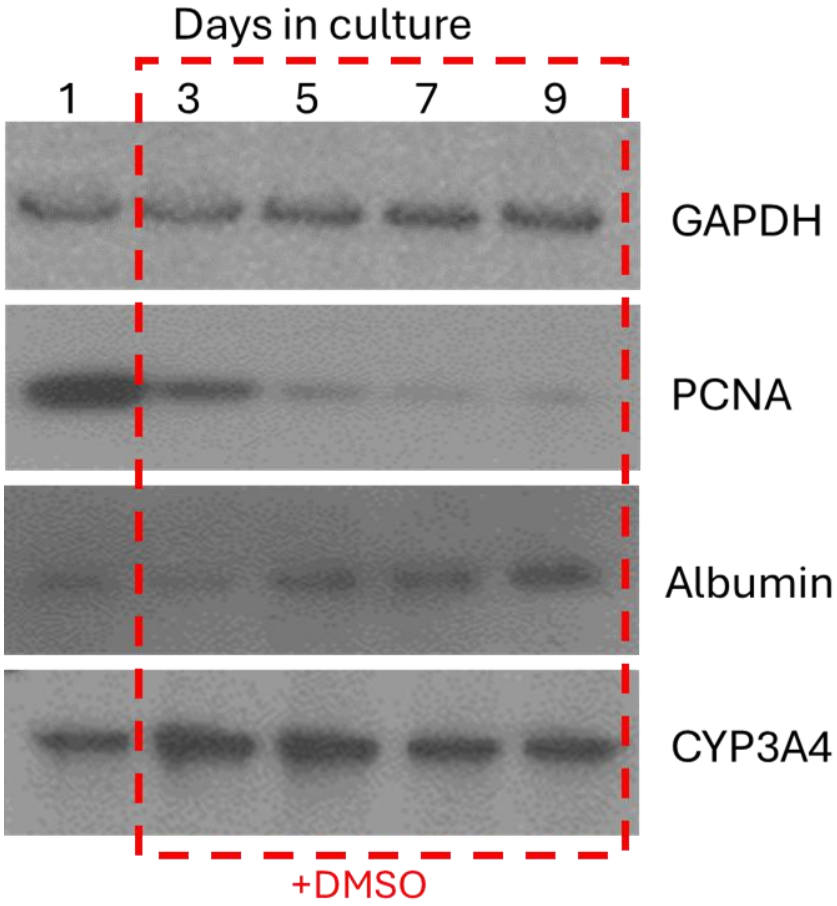

Figure 34. Decrease in proliferation markers and increase in differentiation markers through nine days of Huh7 cell culture. GAPDH (housekeeping gene) decreased slightly over nine days. PCNA decreased over the culture period, whereas, albumin levels increased. CYP3A4 expression remained constant throughout. Red dashed box = Supplementation of standard media with DMSO (1.8 %-2 % v/v). All experiments imaged three times and repeated in triplicate, with representative images shown.

Both proliferation markers, PCNA protein content, and Ki-67 expression in nuclei, were present. Diffuse albumin fluorescence was seen at day one, which reduced at day three before rising at day five onwards. Albumin protein content, however, was low at day one and increased thereafter (Figure 34). CYP3A4 expression was also present at day one, and decreased at day three before rising again thereafter, whereas protein content was high

throughout. Furthermore, expression of the cell adhesion marker EpCAM was not seen at day one and increased in intensity at cellular surfaces across the remaining culture period. At day nine, cells were smaller in both nuclear and cytoplasmic diameter, with darker cytoplasmic granularity (Figure 34 - day nine). PCNA protein content and

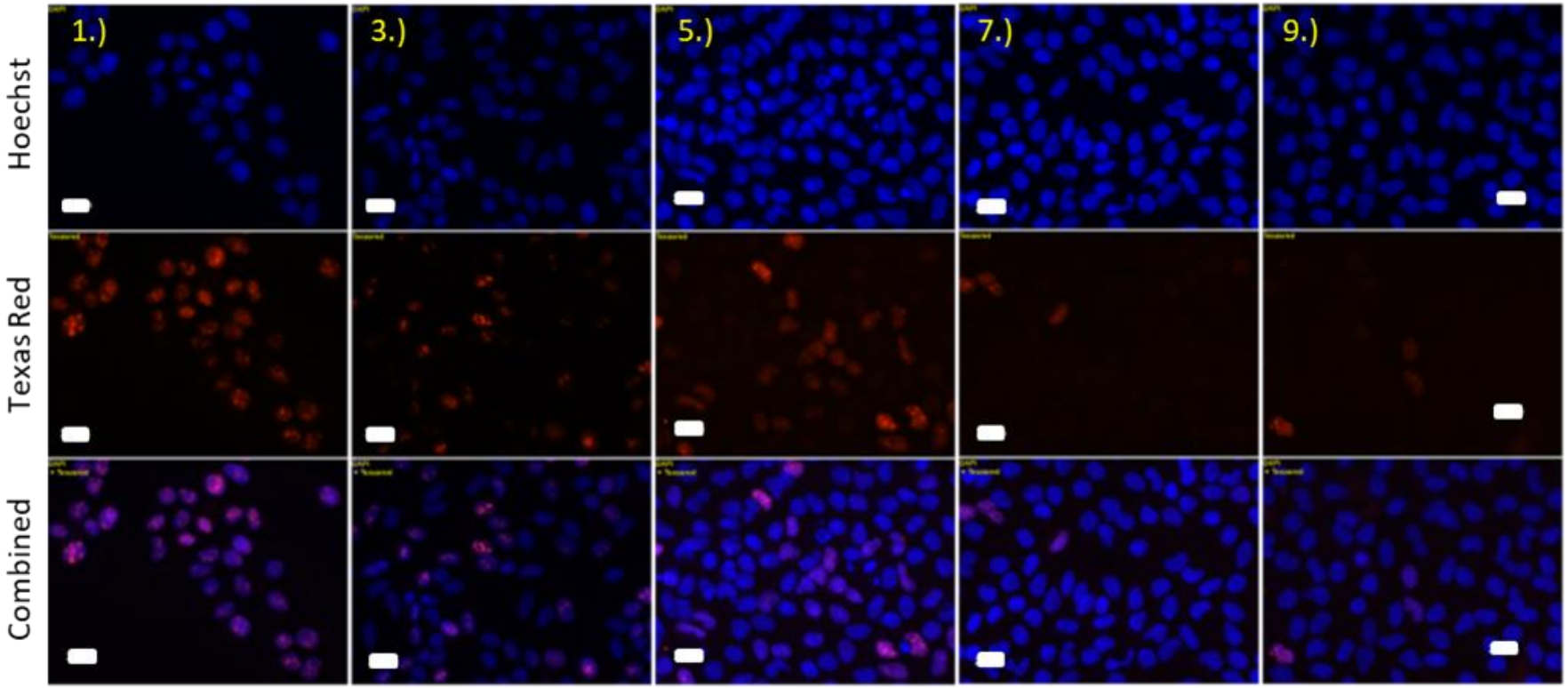

Figure 35. Immunofluorescent staining of Huh7 cells labelled with antibodies to Ki-67. Labelling was greatest at day one and reduced thereafter. Red = Ki-67 protein, Blue = nuclei. Yellow numbers = days in culture. Scale bars = 20 µm. All experiments imaged three times and repeated in triplicate, with representative images shown. n=3

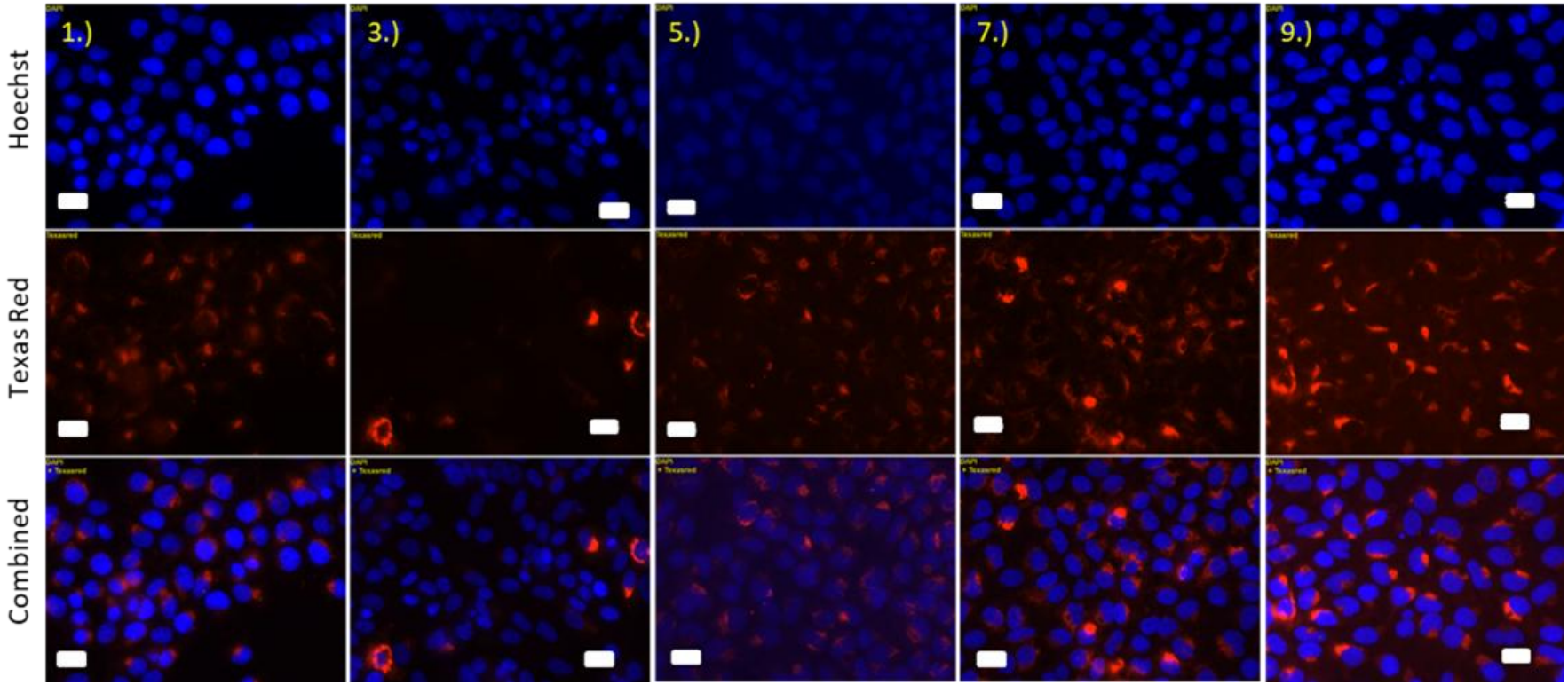

Figure 36. Albumin expression in Huh7 cells seeded for nine days. A decrease in albumin expression was seen from day one to day three, however, albumin expression increased from day three onwards. Albumin expression was limited to the cytoplasm only. Red = albumin protein, Blue = nuclei. Yellow numbers = days in culture, white bars = 20 µm. All experiments imaged three times and repeated in triplicate, with representative images shown. n=3

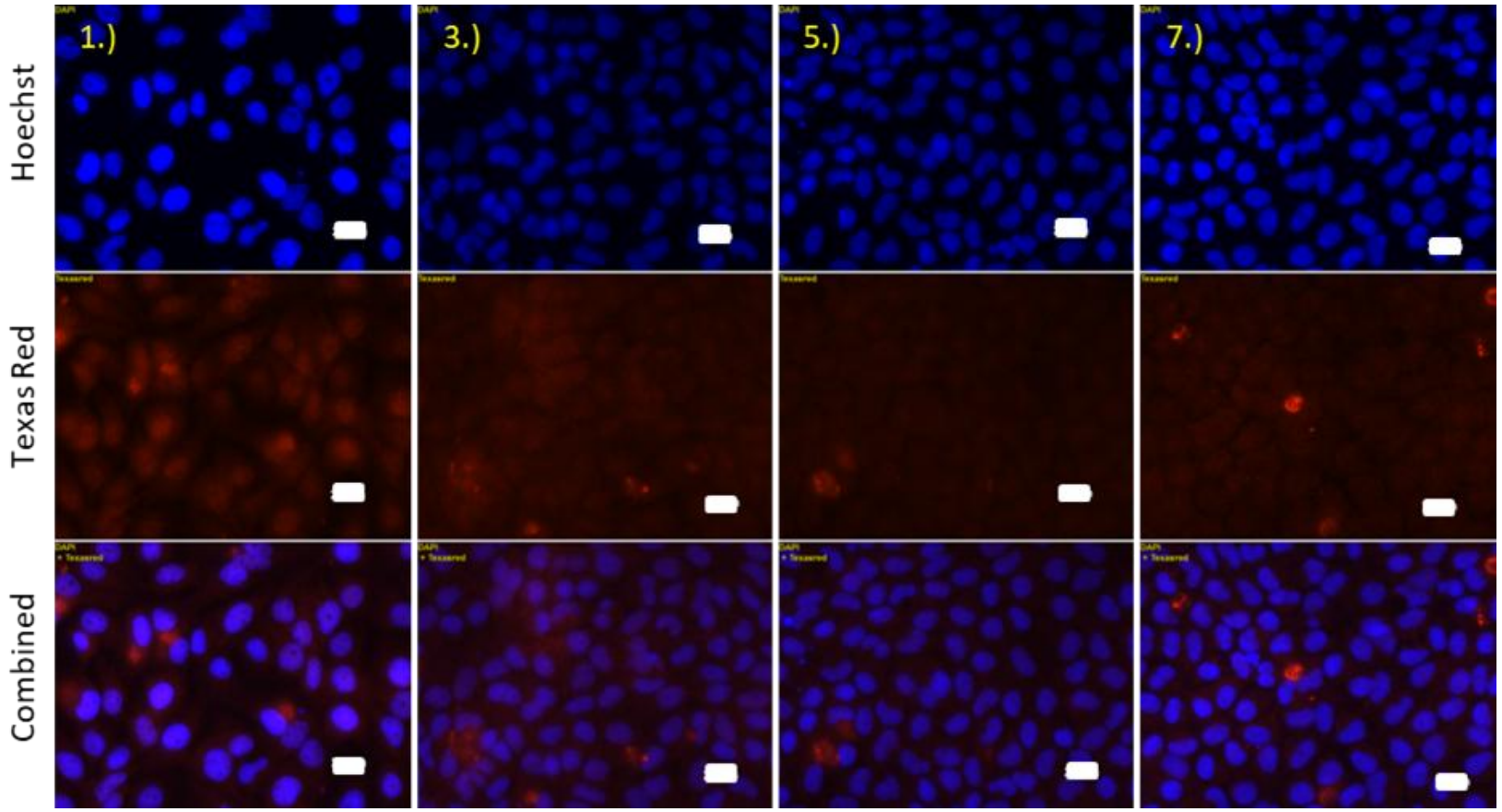

Figure ~~363~~7. CYP3A4 expression in Huh7 cells seeded for seven days. Large amounts of cytoplasmic staining were present at day one. Which decreased in intensity until day 5. At day seven, intense nuclear staining was seen in isolated cells. Red = CYP3A4 protein, Blue = nuclei. Yellow numbers = days in culture, Scale bars = 20 µm. All experiments imaged three times and repeated in triplicate, with representative images shown. n=3

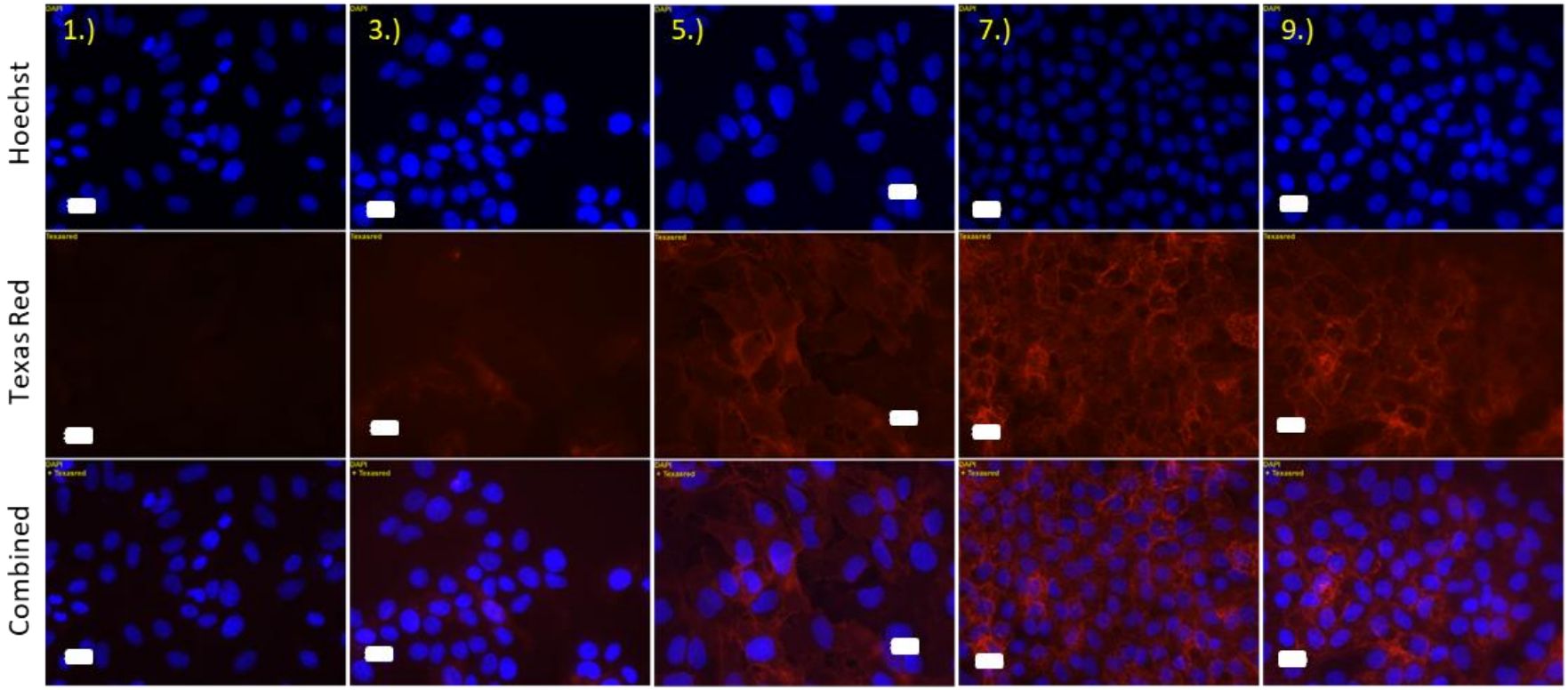

Figure 38. Expression of EpCAM in Huh7 seeded for nine days. EpCAM expression increased across the entire culture period, located at the cell surface. Red = EpCAM protein, Blue = nuclei, yellow numbers = days in culture. Scale bars = 20 µm. All experiments imaged three times and repeated in triplicate, with representative images shown. n=3

~~nuclear diameter (Figure 32) with extended morphology and clear cytoplasm. Both proliferation markers, PCNA protein content, and Ki-67 expression in nuclei, were present. Diffuse albumin fluorescence was seen at day one, which reduced at day three before rising at day five onwards. Albumin protein content, however, was low at day one and increased thereafter. CYP3A4 expression was also present at day one, and decreased at day three before rising again thereafter, whereas protein content was high throughout. Furthermore, expression of the cell adhesion marker EpCAM was not seen at day one and increased in intensity at cellular surfaces across the remaining culture period. At day nine,~~ Ki67 expression were not seen, whereas albumin protein content and expression was increased, when compared to results of Western blots and Immunofluorescent labelling seen at day one.

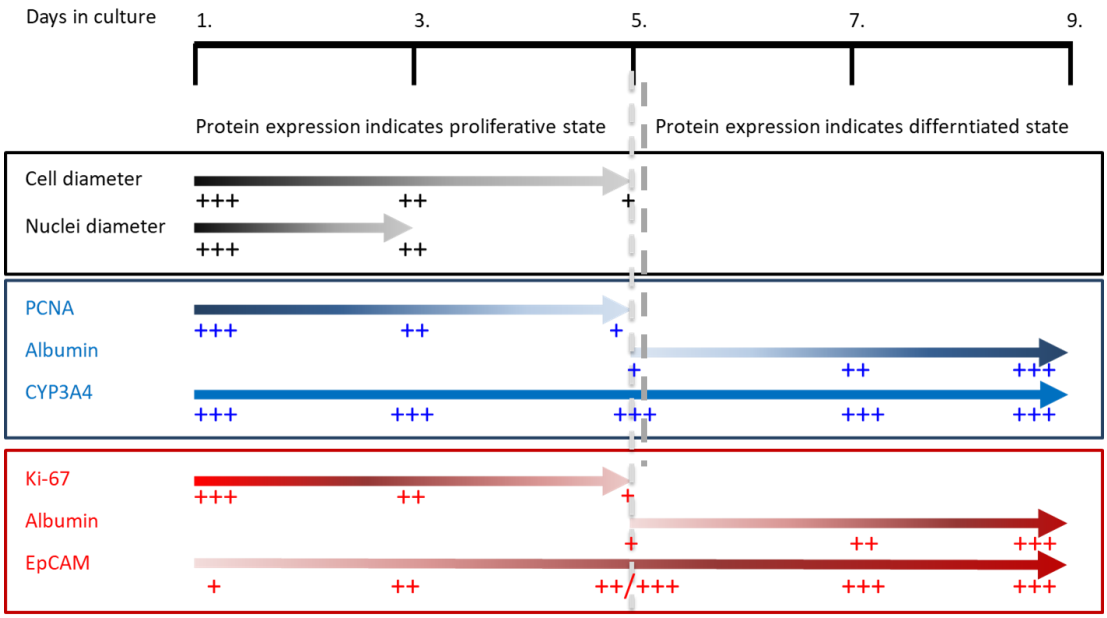

Figure 39. Summary of markers expressed from Huh7 cells during proliferative and differentiated stages. Huh7 at day one in culture, are larger in cellular and nuclear diameter, showing positive expression of ~~proliferative~~ markers of cell division PCNA and Ki67 and cytoplasmic CYP3A4. Differentiated cells express albumin and nuclear CYP3A4, as well as albumin and EpCAM. Black = Data retrieved using microscopic imaging, blue = data retrieved using Western blots, and red = data retrieved using immunofluorescent labelling. Dotted grey line represents the point at which the combination of protein expression can differentiate between a proliferative and a differentiated state. Number of arrows correlate with intensity of expression.

In summary, proliferative phases of the cell cycle can be identified through high levels of ~~proliferation~~ cell division (PCNA / Ki67) and low levels of cytoplasmic albumin, whereas differentiated states can be identified through low levels of proliferative markers (PCNA / Ki67) and high levels of albumin protein content and cytoplasmic expression, which is also associated with increased cell adhesion (Figure 39). CYP3A4 content and expression

cannot be used to differentiate between states of cell division or ~~proliferative and~~ differentiation (Figure 39)~~ed states~~.

~~4.~~4.3.3 Identification of HepaRG morphology across the 28-day culture differentiation period

HepaRG were seeded as described in Section 2.2.16, images were taken from three regions of each well as described in Figure 33. When cultured subconfluently on tissue culture plastic, HepaRG are elongated and oval, forming cell groups / clusters within 24 hours of seeding (Figure 40a, day one). HepaRG increase in number and adopt a more rounded morphology after contact with neighbouring cells (Figure 40a, day ten)~~., ,~~ at which point, differentiation begins and cells adopt one of two morphology's (Figure 40a, day 14). HepaRG become either ~~reduce~~ smaller in size, displaying granulated cytoplasm and prominent (hepatocyte-like), or a flattened, cuboidal morphology ~~with~~ and comparatively larger cell size (biliary-like) (Figure 40, day 14 onwards). At day one, HepaRG were elongated (Figure 40a -day one) and often found adjacent to other HepaRG in small groups or clumps. Increasing~~ed~~ cell numbers were seen ~~between~~ up to day five, with groups becoming larger in size. HepaRG became more rounded and adopted a polygonal morphology, before forming a confluent layer by day 14 (Figure 40a.) -day 14). Two different cell morphologies were seen at day 14; comparatively larger cells with a raised morphology and prominent nucleoli (Figure 40a-day 14, C), and comparatively smaller, more rounded cells with darker, more granular cytoplasm (Figure 40a-day 14, D). By day 17, two distinct cell morphologies were identified, with regions of smaller, rounded cells with cytoplasmic granulation, and larger polygonal cells with raised morphology and clearer cytoplasm (Figure 40b, a.) & b.) respectively). Loosely attached cells could also be seen (Figure 40b, c.)). Different morphological cell regions were easily identified from 14 days onwards, with larger numbers of loosely attached cells seen with cells cultured in DMSO supplemented media than those seen in standard media (Figure 40b-days 17-28). A decrease in the length of nuclei and cytoplasm was seen within the first seven~~14~~ days of culture (Figure 41). After the supplementation of media with DMSO (1.8 – 2%), two cells were formed: one slightly smaller in nuclear and slightly larger in cytoplasmic length (hepatocyte like cells) than the other (cholangiocyte-like cells). Cell~~Both nuclear and cytoplasmic~~ length increased between day 14 and day 21, and ~~decreased at day 24. Length of nuclei and cytoplasm increased at day 28~~plateaued thereafter (Figure 41).

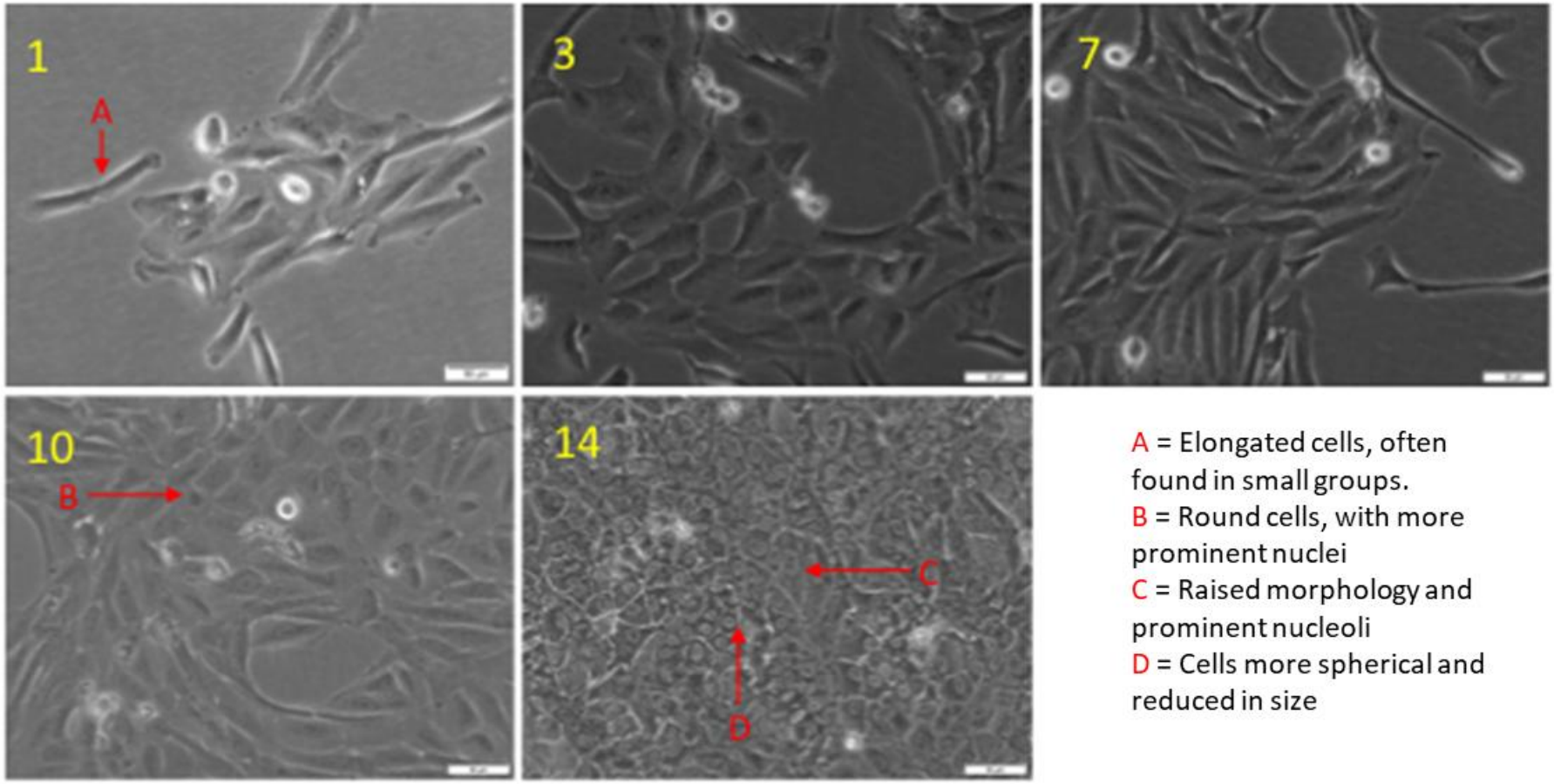

Figure 40a. Progression of morphological changes through HepaRG differentiation. HepaRG were initially elongated and found in small groups at day one and increased in number until confluency was achieved between days ten and 14 . HepaRG at day ten were less elongated and more rounded (B). At day 14, cells formed one of two morphologies, displaying either prominent nucleoli and a raised morphology (C) or reduced in size and more spherical (D). Scale bars = 100 µm. All experiments imaged three times and repeated in triplicate, with representative images shown. n=3

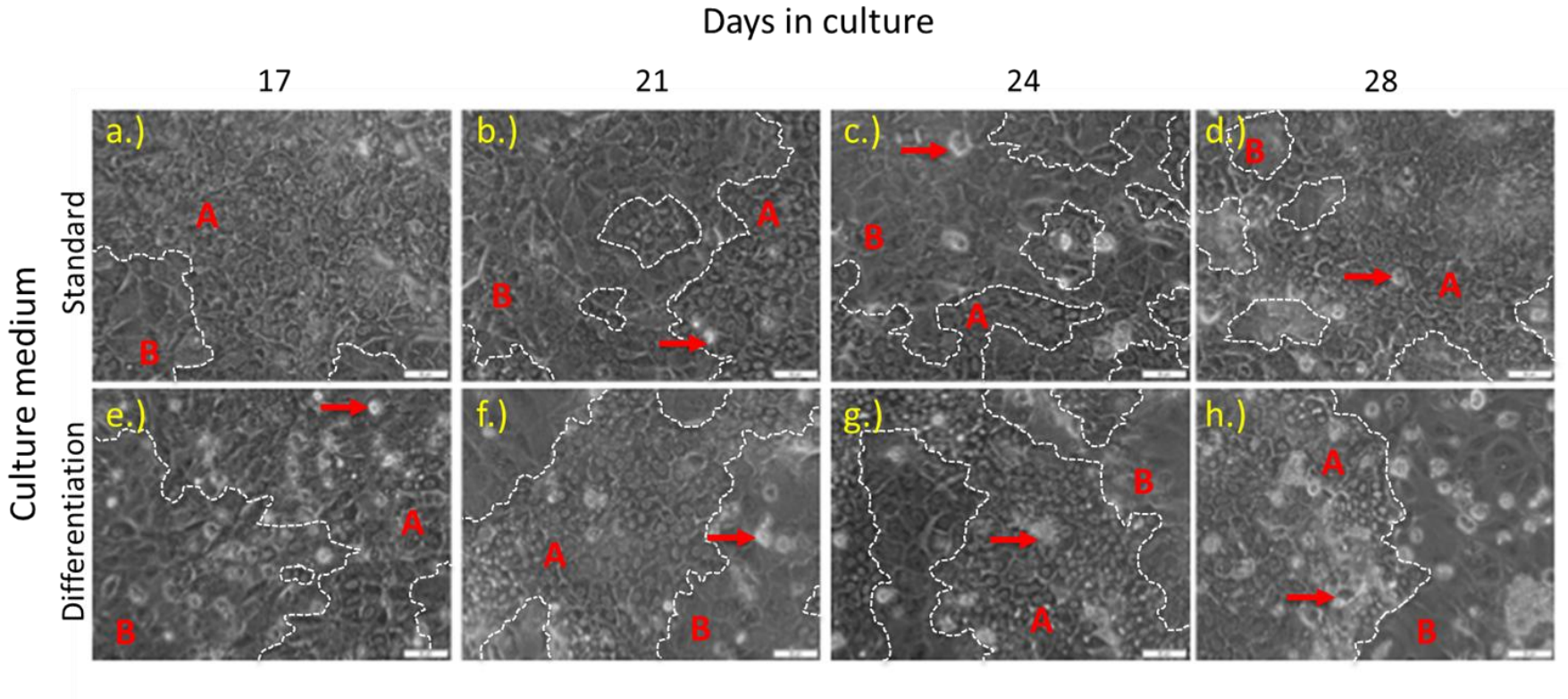

Figure 4~~0~~~~39~~b. Progression of morphological changes through HepaRG differentiation. Two distinct morphologies can be seen from day 17 onwards; smaller more rounded cells with dark granulated cytoplasm (A) and larger, more polygonal cells with clearer cytoplasm and raised morphology (B). Red arrows = loosely attached cells. Images a.) - d.) were cultured using standard media, images e.) - h.) = HepaRG cultured using DMSO supplemented media (1.8 % - 2%). Scale bars = 200 µm All experiments imaged three times and repeated in triplicate, with representative images shown. n=3

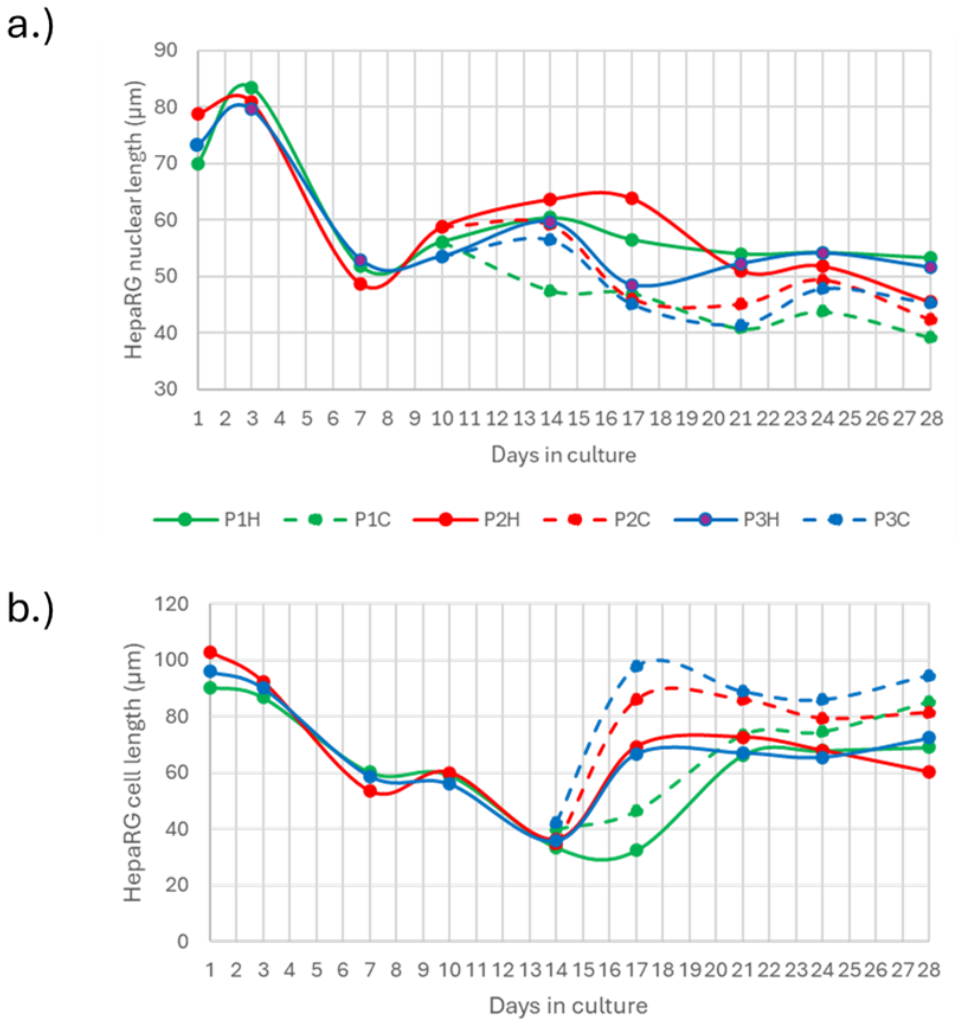

Figure 41. Variation in length of nuclei and cytoplasm in HepaRG cultured over 28 days. HepaRG were seeded in wells, with images of cells taken at three different locations (See Figure 35). Nuclei (a.) and cell ~~cytoplasm~~ (b.)) lengths were measured in triplicate. Nuclei length (a.)) initially increases at day 3 and subsequently decreases until day ~~decreases between days one and~~ 7~~14~~, after which levels plateau. Cell size decreases until day 14, increasing in size up to day 17 and plateauing thereafter. T~~t~~wo cell types form; hepatocyte like cells were ~~smaller~~ larger in nuclei and smaller in cell length (solid lines), whereas cholangiocyte like cells (dashed lines) showed smaller nuclei and larger cell

~~5.~~4.3.4 Identification of suitable markers to differentiate HepaRG phenotype across 28-day culture period

HepaRG were cultured as previously described in Section 2.2.16, with six well plates used instead of 12 well plates with greater volume of media added (3 mL instead of 2

mL). Protein lysates were generated and quantified using a BSA assay (See Section 2.2.25), with Western blots performed using antibodies for GAPDH (housekeeping gene), a progenitor cell marker nestin, and two functional hepatocyte proteins; albumin and CYP3A (See Section 2.2.26). Immunofluorescent labelling of Huh7 was performed using antibodies for Ki-67, albumin, CYP3A4 and EpCAM for cell adhesion (Section 2.2.9).

Western blots initially showed high levels of nestin content at days one to seven, with a reduction seen at day seven, which decreased at day 14 and raised once more at day 21 (Figure 42). After this, nestin content

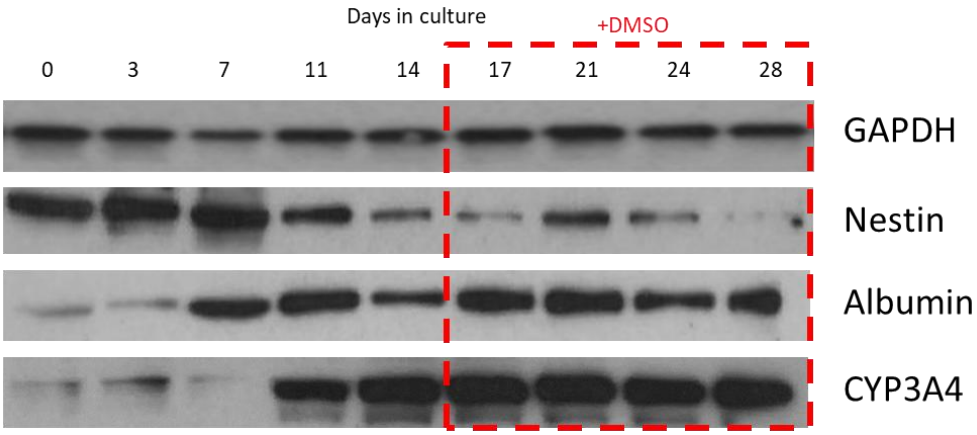

Figure 42. Decrease in epithelial markers and increase in differentiation markers through 28 days of HepaRG culture. GAPDH (housekeeping gene) remained steady throughout the culture period, Nestin decreased from day 11 onwards, albumin and CYP3A4 increased from day seven and 11 respectively. Red dashed box = Supplementation of standard media with DMSO (1.8 %-2 % v/v). All experiments imaged three times and repeated in triplicate, with representative image shown. n=3

decreased once more (2), indicating a loss of neuroepithelial / progenitor protein content. Loss of nestin content corresponded with increased cell:cell contact and morphological differentiation forming hepatocyte-like like and biliary-like cell types (Figure 40a). Albumin content

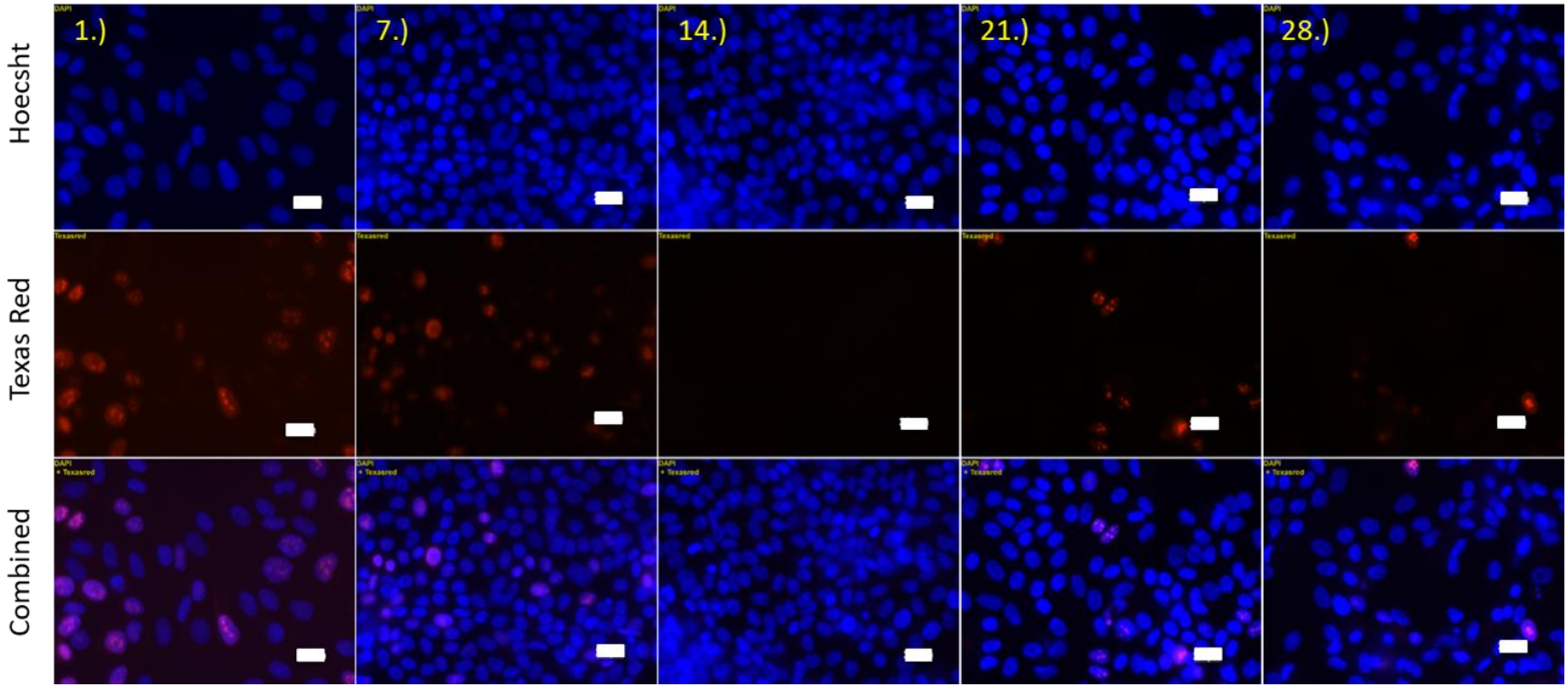

Figure 43. Ki-67 immunofluorescent staining observed in HepaRG cultured in tissue culture plastic for up to 28-days. Greatest Ki-67 staining was seen at the start of cell culture, and reduced until day 14 after which minimal cell proliferation is seen. Numbers correspond to days in culture. Red = Ki-67 protein, Blue = nuclei, yellow numbers = days in culture. Scale bars = 20 µm. All experiments imaged three times and repeated in triplicate, with representative images shown. n=3

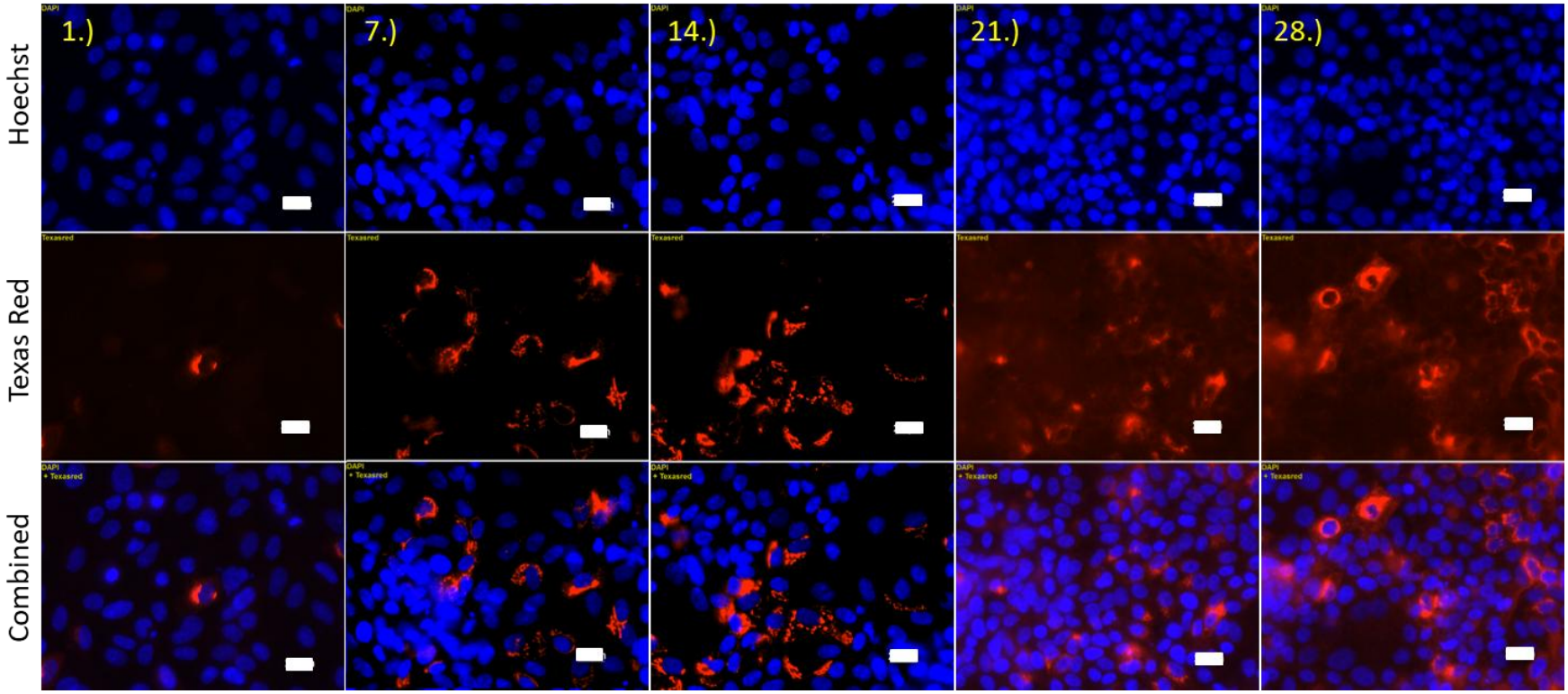

Figure 44. Albumin labelling of HepaRG cultured on tissue culture plastic for up to 28-days. Albumin staining was almost absent at day seven and increased over the entire culture period. Red = Albumin protein, Blue = nuclei, yellow numbers = days in culture. Scale bars = 20 µm. All experiments imaged three times and repeated in triplicate, with representative images shown. n=3

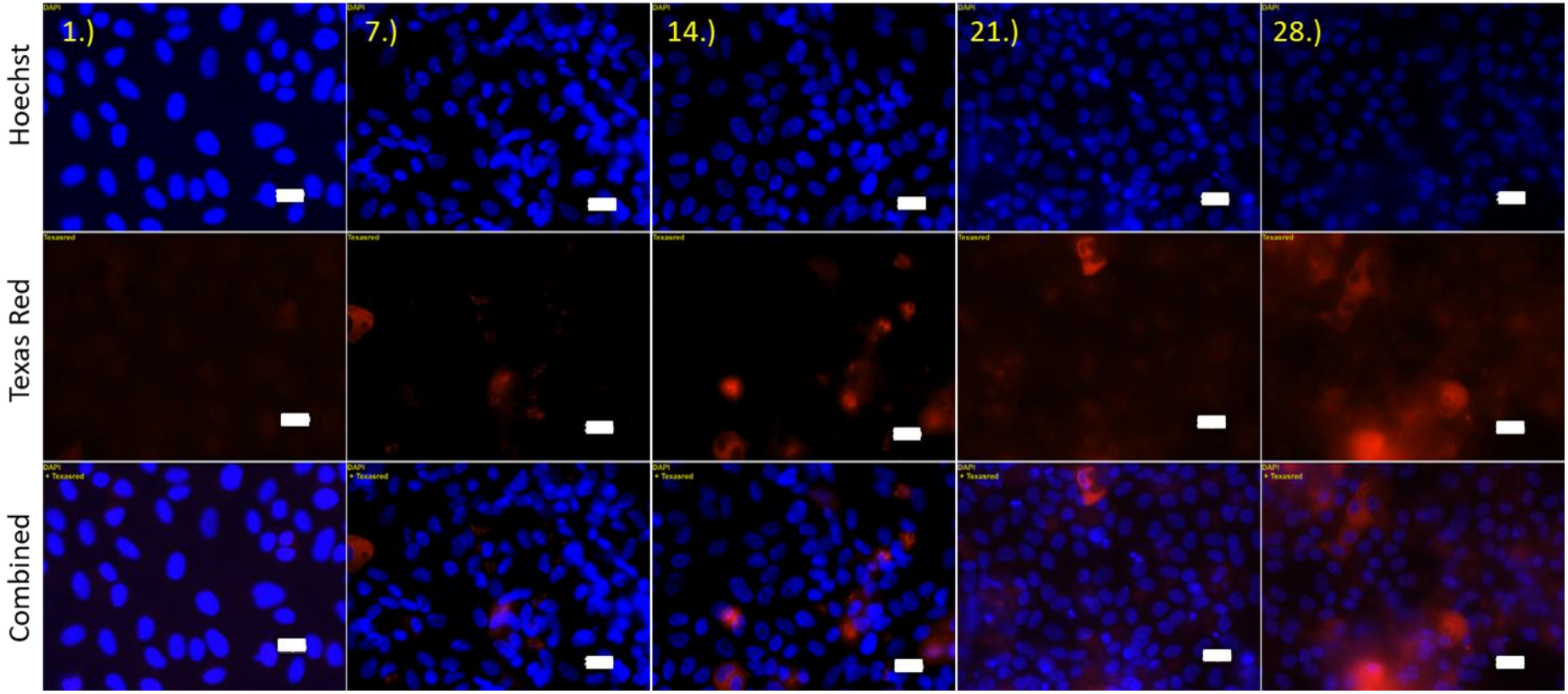

Figure 45. CYP3A4 immunofluorescent staining of HepaRG cultured on tissue culture plastic for up to 28-days. CYP3A4 staining was low at day one and increased in number until 28 days in culture. Red = CYP3A4 protein, Blue = nuclei, yellow numbers = days in culture. Scale bars = 20 µm. All experiments imaged three times and repeated in triplicate, with representative images shown. n=3

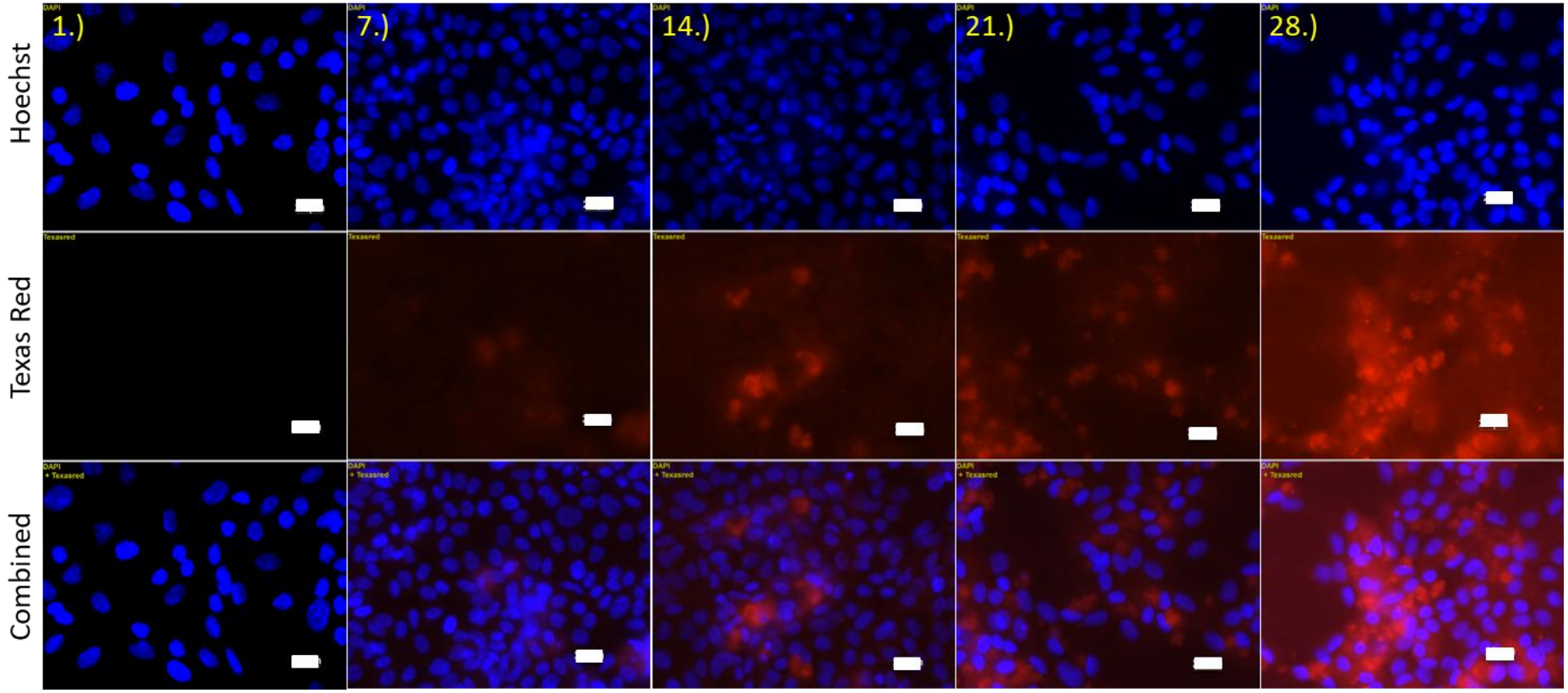

Figure 4613. EpCAM immunofluorescent staining of HepaRG cultured on tissue culture plastic for up to 28-days. EpCAM staining is absent at day one, and slowly increased over the 28-day culture period. The greatest amount of EpCAM seen occurs at 28 days in culture. Red = EpCAM protein, Blue = nuclei, yellow numbers = days in culture. Scale bars = 20 µm. All experiments imaged three times and repeated in triplicate, with representative images shown. n=3

substantially increased from day seven onwards, whereas CYP3A4 protein increased from day 11 onwards. Both remained high throughout the remaining culture period (Figure 42). Increased albumin content was seen just after HepaRG adhered to neighbouring cells and formed clusters (Figure 40a, days three - ten). Increased CYP3A4 content was associated with the loss of HepaRG uniformity and development of two different cell types (Figure 40, Figure 42 and Figure 45, between days ten and 14). Immunohistochemical staining of HepaRG showed nuclear expression of the cell division ~~proliferation~~ marker Ki-67 at day one, which decreased until day seven and remained low for the remaining culture period (Figure 43). Cytoplasmic albumin expression was low at day one and increased up to day 14, after which staining remained cytoplasmic, with a diffuse level seen outside of the cell cytoplasm (Figure 44). CYP3A4 staining was not originally present, although some cytoplasmic, diffuse staining was seen at day seven and increased thereafter (Figure 45). EpCAM expression

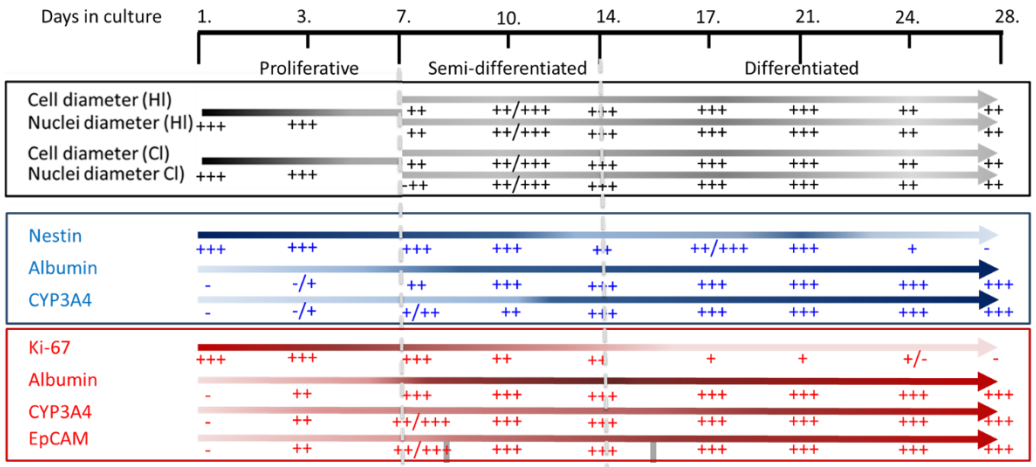

Figure 47. Summary of HepaRG findings. Proliferative phases showed an initial high nuclear and cell length, which reduced in semi differentiated states, and increased slightly when cells entered the full differentiated state. Nestin protein content and Ki-67 expression was high at proliferative phases and reduced in full differentiated states. Albumin and CYP3A4 protein content and expression increased in semi differentiated states, and increased further in differentiated states. Results indicate proliferative/ epithelial markers in proliferated states and functional markers present in differentiated states. Semi differentiated states showed combinations of both proliferative/epithelial and differentiated markers. Grey dashed line indicates regions where the combination of protein expression can aid in the identification of proliferative, semi differentiated and differentiated states.

was also diffuse and remained low between days one and seven (Figure 46). Increased EpCAM expression was seen across the remaining culture period (Figure 46), although was not limited to the cell surface as seen previously in Huh7 cells (Figure 38).

In conclusion, early proliferative phases of HepaRG were identified through the expression of nestin and Ki-67, and lack of expression of albumin, CYP3A4 and EpCAM as seen between days 0 and seven. The transfer from ~~proliferative~~ cell division to a partially differentiated stage was identified through the additional expression of albumin, as well as nestin and Ki-67, as seen between days seven and 11. Further progression to a differentiated phase was identified through the expression of albumin, CYP3A4 and EpCAM, and absence of nestin and Ki-67 as seen at days 17 onwards.

~~1.~~ 4.4 Discussion

Results from this chapter have shown that HepaRG and Huh7 cells are able to ~~proliferate~~ divide and become functional~~and differentiate~~, with different morphologies and markers expressed in each stage. Proliferative Huh7 cells displayed larger nuclei and cell lengths, with clear cytoplasm, which when differentiated resulted in cells with smaller nuclei and cytoplasmic granulation. Huh7 display different morphologies when cultured with and without serum (Nakabayashi et al., 1982). When cultured in serum, Huh7 form multi layered islands, growing over on top of each other, with peripheral cells flattened. When cultured without serum and supplemented with LAH (lactalbumin hydrolysate, 0.4 %), however, Huh7 form a pavement like cell arrangement, and form a confluent layer on the culture plate. Serum free culture conditions also decreased cell doubling times. Within this study, Huh7 initially formed small groups (Figure 32– day one), which increased in number, and decreased in size until the end of the culture period. At day nine, Huh7 formed a monolayer of smaller cells with granulated cytoplasm and pavement like morphology, similar to that seen in other studies (Liu, 2022, Sainz et al., 2009). The differentiating factors between culture at days one and nine, is time, the addition of DMSO and increased contact with neighbouring cells. When comparing results seen in this Chapter, with those reported by Nakabayashi et al (1982), the additional use of serum results in cells that are not cell contact inhibited, however, is rectified through the use DMSO which induces cell differentiation similar to that seen with serum free, media containing

selenium and LAH. Although the individual cause for the ~~difference~~ altered~~in~~ morphological differences seen in ~~proliferative~~ dividing cells cultured with and without serum was not investigated, cells cultured without serum showed an increased ~~proliferation~~ rate of division. Cell culture using a synthetic medium, containing selenium and amino acids, may therefore provide increased rates of proliferation to that seen within this Chapter. Although non-essential amino acids were added to Huh7 culture media within this chapter, cell culture using synthetic medium without serum, and containing selenium may enhance Huh7 replication rates, if required. The addition of DMSO (1.8 - 2 %) resulted in significant reductions in the length of cells and nuclei, with cells increasing in number up until formation of a tightly packed cell monolayer after eight days exposure. Results are supported by the work of others (Sainz and Chisari, 2006), with ~~1.5 fold~~1.5-fold per day (average) increase in cell numbers seen within the first six days of DMSO supplementation, after which Huh7 showed growth arrest. Throughout the 20-~~-~~day post differentiation monitoring, 92% cells did not divide, and were stopped at G0 / G1 of the cell cycle. Furthermore, real time reverse transcriptase PCR analysis revealed amplification of liver specific genes after six days expression, including albumin, HNF-4α and α1-antitrypsin, with increases in albumin levels seen to rise within 24 hours culture post-supplementation with DMSO. Clear distinction between proliferative and differentiated cell states were seen through morphology alone, in line with results reported in the literature (Sainz et al., 2009, Nakabayashi et al., 1982). This allowed further identification of phenotype specific protein markers to be found.

Several different markers of cell ~~proliferation~~ division and function~~and differentiation~~ were investigated, with clear differentiation identified using PCNA / Ki-67 for ~~proliferative~~ dividing cell morphologies and albumin for ~~differentiated~~ functional cell morphologies. PCNA is highest at day one, decreases until day five where cells shrink and begin to show a condensed granular cytoplasm. It is at this point where cells also increase albumin production until the end of the experiment at day nine. This was expected and accurately displays a loss of cell ~~proliferation~~ division alongside an increase in hepatocyte function. As mentioned previously, Sainz and colleagues (2009) reported increased ~~proliferation~~ rates of cell division~~rates~~ within the first six days after DMSO application, with 1.5-~~-~~fold increase in cell numbers reported. Furthermore, upon the addition of DMSO, increased production of albumin was reported. Increased expression of cell adhesion marker EpCAM was associated with increased albumin expression and increased cell:cell contact seen morphologically. The Hippo pathway is critical in the inhibition of cell and tissue growth and determination of organ size. Recently, data has

suggested that the Hippo pathway is also involved in tumour metastasis and invasion (Li et al., 2021). Cell signalling resulting from external factors, leads to the binding of YAP/TAZ, the non-phosphorylated version of which traverses the nuclear membrane and binds to transcription factors with DNA binding domains, such as TEADs, and leads to activation of the cell migration and/or invasion (Li et al., 2021). The phosphorylation cascade (MST1/2-LATS1/2-YAP/TAZ) is activated in response to differing signals, such as cell:cell contact, cell polarity and/or alterations in ECM stiffness (Meng et al., 2016).

Immunofluorescent co-labelling using antibodies to YAP and TAZ would further support ~~proliferation~~ the cell division observed in this Chapter (Figure 32). CYP3A4 expression was displayed throughout the entire culture period, in both proliferative and differentiated states. CYP3A4 is a drug metabolising enzyme associated with functional, differentiated hepatocytes and not actively ~~proliferating~~ dividing cells. Two studies have looked at CYP3A4 expression over the entire culture period, both of which report increases in CYP3A4 expression, but differ in the levels reported (Sivertsson et al., 2010, Choi et al., 2009). One study (Sivertsson et al., 2010) reported increased CYP3A4 expression over four weeks of cell confluence, and that the supplementation of media with DMSO did not show any increase CYP3A4 protein expression. In contradiction, a different study (Choi et al., 2009) reported that the addition of DMSO (1%) to media for 20 days resulted in a 155-fold increase in CYP mRNA expression when compared with baseline levels observed before addition of DMSO (Choi et al., 2009). Although protein and mRNA expression increased in both studies (Choi et al., 2009, Sivertsson et al., 2010), results from this study indicated that protein content was high throughout the culture period (Figure 34), whereas expression at the membrane surface was low throughout (Figure 37). Due to the expression in both proliferative and differentiated states, CYP3A4 was considered an unsuitable marker for identification of Huh7 cell phenotype. The repeated splitting of cell lines can lead to phenotypic drift and result in variation of cell morphology, activity and function which may explain this observation. When seeded at 32 x10^3 cells.mm^2, HepaRG increase in cell number until they become confluent, with DMSO added at day 14, which corresponded slightly after cell confluence was achieved. In a proliferative phase, cells display a more epithelial morphology: elongated and often found in groups, after which

cells adopt a more polygonal or rounded phenotype. Two cell types are formed; one adopting a more raised morphology and larger size, and a second type of cell group that are morphologically smaller and rounder with granular cytoplasm. These two cell types were maintained thereafter. HepaRG cultured with DMSO

displayed higher levels of cell detachment, than those cultured in standard media. Results reflect those reported in the literature (Parent et al., 2004, Cerec et al., 2007, Gripon et al., 2002). Parent *et al.* (2004) reported the presence of an early proliferative phase at day two where HepaRG were extended and showed a typical epithelial morphology. Late stages of ~~proliferation~~ Cell division were seen at days four~~4~~ to five ~~5~~, signified by high cell:cell contact. HepaRG subsequently enter a stationary or intermediate phase between days seven and 14, where cells formed either smaller cells with granular cytoplasm or more polygonal cells with clear cytoplasm. At day 14, DMSO (2%) was added and resulted in clearer distinction between the two cell types as culture continued. The time points at which the literature report the change in cell morphology differs slightly, and not in order. The delay in reaching confluence may be attributed to differing seeding densities within each study, with 27 $x10^4$ cells.mm^2, Cerec et al. (2007), 53 $x10^4$ cells.mm^2, (Parent et al., 2004) compared to the work from this Chapter (approx. $32x10^3$ cells.mm^2). Excluding original seeding density, all studies confirm that two-week exposure to DMSO (2%) signifies the point at which full differentiation occurred. Clear morphological differences can be seen between proliferative and differentiated cell states.

During initial stages of HepaRG culture, cells contained nestin and expressed Ki-67, indicating that cells are still in a progenitor like ~~e,~~ ~~proliferative~~ dividing state. After seven days in culture, cells become confluent and expressed functional markers such as albumin, and lost epithelial marker nestin, followed by cell division~~proliferation~~ marker Ki-67 at days seven and 14 respectively (Figure 44, Figure 45 and Figure 46). CYP3A4 content increased later, at day 11 (Figure 47). This coincided with increased cell:cell contact (Figure 42) and EpCAM expression (Figure 46). Although comparison of HepaRG cultured longer than 14 days with and without DMSO showed similar morphologies, HepaRG cultured with DMSO resulted in more defined cell groups and greater cell detachment compared to those cultured without (Figure 42). When compared to research of others (Parent et al., 2004), day two of culture showed 90% HepaRG were actively proliferating (BrdU labelling index), which reduced to 20% at day seven after confluency was reached and absent after 14 days culture in DMSO

supplemented (2 %) media. Further analysis of HepaRG ~~proliferation~~ division using BrdU labelling would provide a numerical value of cell ~~proliferation~~ division allowing absence to be defined further. Although Ki-67 staining was low at day 28 (Figure 43), and absent in other studies by Parent and colleagues (Parent et al., 2004), this variation may be explained by initial seeding number (32 $x10^3$ cells.mm^2 vs 53 $x10^4$ cells.mm^2 respectively) or other factors such as relative volume of media components

or culture temperature. Comparison of differences performed between these studies may account for the alteration in times. Albumin expression has been reported to increase from proliferative, through transient and differentiated states (Parent et al., 2004, Gripon et al., 2002), with CYP3A4 expression increasing from transient to differentiated states only (Gripon et al., 2002). Increased functional content and/or expression matches that seen within this Chapter, with albumin expression increasing earlier (day seven) than CYP3A4 (day 11)(Figure 44 and Figure 46).

Although slight differences were seen between results in this Chapter and the literature, both Huh7 and HepaRG cells have been shown to proliferate and differentiate, with research defining clear expression patterns and content of key proteins that will allow further exploration of how 3D culture affects this behaviour. Further work therefore, will focus on seeding these two cell types on / in to the decellularised porcine liver matrices created in Chapter 3.

~~2.5~~ Development of seeding procedures for decellularised porcine liver discs

5.1 Introduction

Having created a decellularised porcine liver matrix, and characterised the markers expressed throughout both proliferative and differentiated stages of the Huh7 and HepaRG cell cycle, the following work focused on methods used to maximise cell attachment on, and cell migration into, the decellularised porcine liver matrices. Seeding methods differ greatly across the literature and the approaches taken are broadly differentiated by variations in seeding density, method of cell attachment, method of cell culture and investigative need. As perfusion-based systems are best applied in larger tissues, all investigated methods focused on variations in immersive and agitative techniques. Increasing cell densities were seeded on decellularised porcine liver to ascertain the maximum seeding density required to maximise cell attachment and maintain cell viability. Assessment of cell attachment was assessed using haematoxylin and eosin staining of seeded matrix sections throughout the entire decellularised disc (Section 2.2.8.1). Cell viability was ascertained using a Live / dead immunofluorescent dye, in which live cells actively retained a green fluorescent protein, whereas dead / dying cells were labelled red (Section 2.2.9.8). Various methods were applied to increase the number of cells attached to the decellularised porcine liver matrix. As surface area to volume ratio of the decellularised porcine liver discs are ~~high~~low, cell repopulation at the centre of the disc would take a long time. Initially, studies focused on increasing the number of cells within the centre of the disc through direct application using a pipette tip of cells on either the uppermost surface or the inner surface of a sliced decellularised disc, or cells were injected within the matrices, again, using a pipette tip. Cells were also seeded across the entire disc surface through immersion in cell suspension. Time course experiments were performed where both seeding and culture times were varied across ranges of 20 min to 24 hr, and two to 35 days respectively.. Culture methods were limited to static culture (37 °C, 5% CO_2 (v/v) in air), immersion in cell suspension or media with flow applied by rotation at 37 °C in either a universal at 35 RPM, or a cell spinner at 40 RPM . The three main avenues of research detailed above were applied through an iterative process that continuously developed and advanced knowledge contemporaneously. Consequently, this Chapter is written to reflect the process developed across this time.

5.2 Aims and Objectives

5.2.1 Aims

The aim of this Chapter was to investigate various methods of seeding and culturing cells to increase HepaRG and Huh7 cell attachment on to, across, and within decellularised porcine liver scaffolds.

5.2.2 Objectives

- To identify whether cell viability is maintained without the addition of DMSO to cell culture media when seeded on decellularised porcine liver grafts.
- To assess whether increasing time during cell seeding and/or culture will affect cell attachment and/or location.
- To investigate the variation in cell location after application of dynamic culture.
- To determine the cell seeding density that results in the greatest number of attached viable cells and lowest number of non-viable cells.
- To evaluate the use of cellular injection to increase cell attachment within the decellularised porcine liver scaffolds.
- To compare cell attachment to decellularised porcine liver scaffolds at varying levels of scaffold degradation.

~~**Experimental approach**~~

~~**investigations began using HepaRG cells and subsequently moved to the use of Huh7 cells. The following questions were initially investigated using HepaRG cells:-**~~

~~1.**Do HepaRG cells attach to, and remain viable on, decellularised porcine liver matrices without DMSO?**~~

~~2.**Does the application of flow increase HepaRG number and/or coverage?**~~

~~3.**Does an increase in seeding time lead to increased numbers of attached cells?**~~

~~4.**What is the maximum seeding density that HepaRG can be seeded?**~~

~~5.**Are HepaRG cells retained after injection into decellularised porcine liver matrices?**~~

~~6.**Does the method of flow affect cell attachment?**~~

~~**Information gained from the HepaRG culture was applied to Huh7 culture, with further questions identified below:**~~

~~1.**Can Huh7 cells be injected inside the decellularised porcine liver matrices?**~~

2. How can we increase the number of cells initially attaching to the decellularised porcine liver matrices?

3. Is there a difference in the number of cells attached to damaged matrices, compared to better retained matrices?

4. Does the method of flow affect cell attachment?

5. Do Huh7 cells remain functional when cultured on decellularised porcine liver matrices over 28 days?

5.3 Results

5.3.1 HepaRG cells

5.3.1.1 Do HepaRG cells attach to and remain viable on, decellularised porcine liver matrices without DMSO?

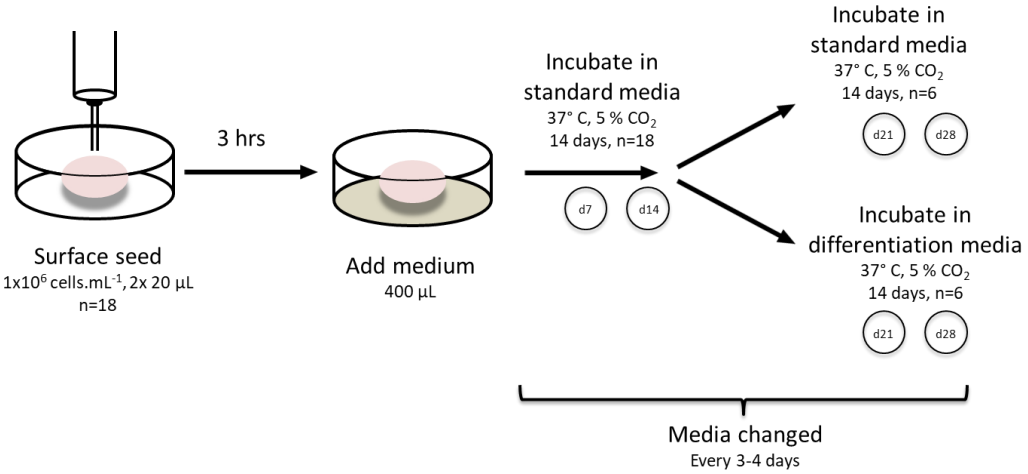

Figure 48. Experimental outline to ascertain whether HepaRG cells attach to, and remain viable, after seeding on decellularised porcine liver discs. HepaRG were pipetted on decellularised porcine liver matrices (n=18) and for three hr. Standard media was added to allow for cell attachment. Seeded discs were incubated for 14 days in standard HepaRG media, followed by 14 days in either standard or differentiation media. Media was changed every three to four days. Discs (n=3) were removed at days seven, 14, 21, and 28 for each condition.

As inducing differentiation of HepaRG cells on tissue culture plastic required DMSO, the first approach was to ascertain whether DMSO was required for HepaRG seeded on decellularised porcine liver matrices. HepaRG were seeded and cultured on decellularised porcine liver disc up to 28 days to ascertain whether cells attached to, and remained viable on, decellularised porcine liver discs (Section 2.2.20). Media was changed every three to four days and assessment of cell viability was performed using Live / dead stain every seven days and imaged using a confocal microscope (Sections ~~2.2.9.8~~2.2.9.8 and 2.2.5.4), as summarised in ~~Figure 47~~Figure 48. After seven days in culture with standard culture medium, HepaRG attached to the decellularised porcine liver discs with most of the uppermost tissue surface covered with medium to large, round viable cells that fluoresced ~~viable cells that fluoresced~~ green, indicating HepaRG viability (~~Figure 48~~Figure 49a~~b~~.L~~)~~, ~~L)~~. Small, round, uniformly red fluorescing cells were present indicating some non-viable cells present (~~Figure 48~~Figure 49a.)D~~), D)~~. After 14 days in standard culture media most remaining cells fluoresced red (~~Figure 48~~Figure 49b.), D) and comparatively few fluoresced green (~~Figure 48~~Figure 49b.), L).Few cells fluoresced both green and red which would indicate progressive loss of cell viability (~~Figure 48~~Figure 49~~-~~b.) Y). Similar results

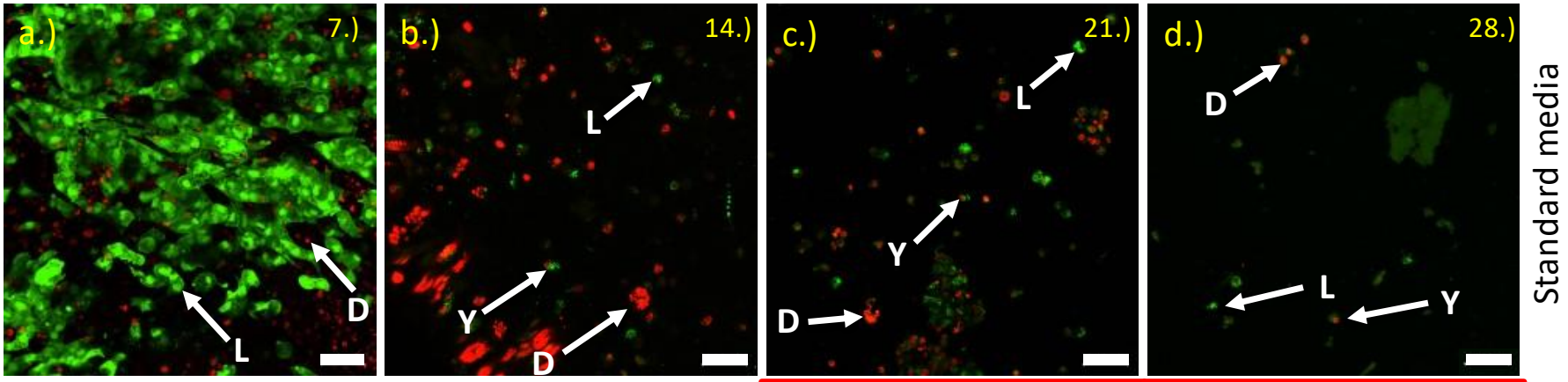

Figure 49. HepaRG viability after seeding on decellularised porcine liver discs up to 28 days. *Majority of cells cultured in standard media were viable at day seven, and lost viability by day 14 (a.)) Attached cell number decreased for the remaining culture period (c.) and d.)). When differentiation media was added after 14 days, cells initially remained viable (e.)), and become smaller in length and more spherical after 14 days culture (f.)). Images enclosed in a red box (e.) & f.)) indicate cells exposed to DMSO supplemented (differentiation) media before imaging. All experiments were performed in triplicate and imaged three times. Green = Viable cells (Calcein AM, 530 nm) Red = non-viable (Ethidium homodimer, 645 nm). Scale bar represents 50 µm. L = living cells, D = dead cells, Y = dying cells. n=3.* ~~*Majority of cells cultured in standard media were viable at day seven,*~~

were seen at 21 and 28 days in standard

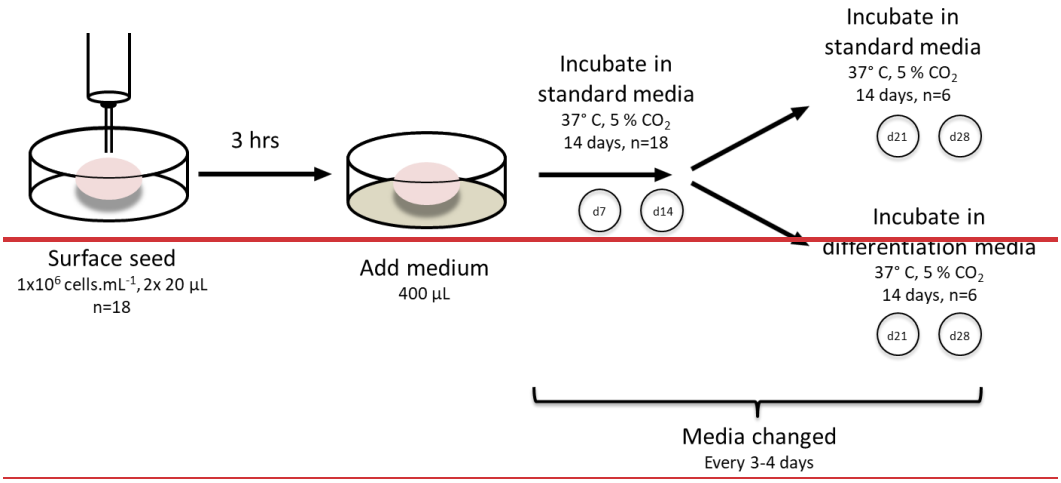

culture media (~~Figure 48~~Figure 49c.)&d.)). After 14 days in standard ~~reduced in cell size(Figure 48 f.), V), with some cells fluorescing both red and green indicating reduction in cell viability (Figure 48 f.) L). Results indicated that cells attached to the decellularised porcine liver discs and retained viability until seven days culture, but viability of most cells was not maintained beyond this point. It was postulated that this could have occurred for several reasons. Following on from experiments performed in Chapter 3 (Figure 21), matrices were shown to retain L929, BHK and HepaRG cell morphology so matrix toxicity was unlikely. Furthermore, HepaRG cells increased, although not~~ media and seven days in differentiation media (Figure 49~~Figure 48~~e.)). ~~,~~, overall cell numbers were similar to that seen after 14 days in standard culture media (Figure 49~~Figure 48~~b.)). ~~,~~ however, more viable cells were present, than non-viable cells (Figure 49~~Figure 48~~e.), L vs D). After 14 days in standard culture media and 14 days in differentiation media, viable cells became more circular and reduced in cell size (Figure 49f.), V), with some cells fluorescing both red and green indicating reduction in cell viability (Figure 49f.) L). Results indicated that cells attached to the decellularised porcine liver discs and retained viability until seven days culture, but viability of most cells was not maintained beyond this point. It was postulated that this could have occurred for several reasons. Following on from experiments performed in Chapter 3 (Figure 22), matrices were shown to retain L929, BHK and HepaRG cell morphology so matrix toxicity was unlikely. Furthermore, HepaRG cells increased, although not significantly, ATP production when cultured with decellularised porcine liver matrix conditioned media (Figure 23). The loss of cell viability seen after seven days culture may be attributed to sub-optimal culture conditions. Maintenance of cell viability is dependent on multiple factors including oxygen concentration, media pH and sufficient glucose levels (Raza et al., 2017). Furthermore, HepaRG viability and function is thought to be enhanced by the application of flow (Sassi et al., 2021, Ong et al., 2017). This

suggests that the culture conditions used in the first investigation of HepaRG (Section 5.3.1.1) were insufficient to maintain viability, and could be attributed to increased media acidity, decreased glucose availability, or insufficient oxygen diffusion throughout the scaffolds When cultured on tissue culture plastic, HepaRG ~~proliferate~~ divide until they contact other cells, where partial differentiation reportedly occurs (Gripon et al., 2002). It is postulated that a lack

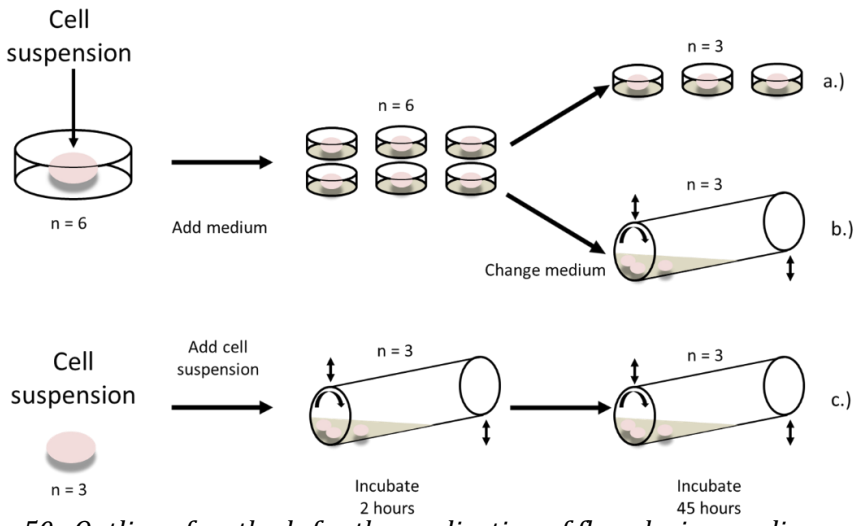

Figure 50. Outline of methods for the application of flow during seeding and culture of HepaRG on decellularised porcine liver discs. Six discs were statically seeded with HepaRG, with three discs. immersed in 200 µL standard media and statically cultured (a.)), and three discs immersed in standard culture media (4mL) and dynamically cultured in a rotating universal (b.)). Three further discs were immersed in a universal containing cell suspension at 37 °C (4 mL, 3.75 x10⁶ cells.mL⁻¹, 35 RPM) for two hours, and cultured dynamically at 37 °C (35 RPM, c.)). After 45 hours, all discs were removed from the media, fixed in 10 % neutral buffered formalin for 24 hours, processed &, stained with Haematoxylin and eosin.

of cell:cell contact occurred after seeding HepaRG on decellularised porcine liver matrices, resulting in cells unable to reach confluence, and resulted in cell death.

~~6.~~ 5.3.1.2 Does the application of flow increase cell number and/or coverage?

The previous experiment involved seeding decellularised porcine liver discs on the uppermost surface. To enhance cell coverage and increase cell:cell contact, HepaRG would require seeding on the entire surface, and preferentially within the disc. Investigations into the application of

flow were therefore made, see Figure 50. Discs were seeded statically (n=6), and cultured either statically (n=3) or under flow (n=3, 4mL), as outlined in Sections 2.2.20, 2.2.21). Discs (n=3) were seeded and cultured dynamically, with cell density in suspension at 3.75 x10⁶ cells.mL⁻¹.

Sections of seeded discs were stained with H&E to ascertain cell presence and location, visualised using brightfield microscopy (Sections 2.2.8.1 and 2.2.5.1). Results show few HepaRG attached at the external periphery on one side of statically seeded discs (See Figure 51a.) black arrows). A small amount of tissue penetration was noted ~~Sections of seeded discs were stained with H&E to ascertain cell presence and location and visualised using Köehler (Sections 2.2.8.1 and 2.2.5.1). Results show few HepaRG attached at the external tissue periphery on one side of statically seeded discs (See Figure 50a.), black arrows) a small amount of tissue penetration was noted~~(Figure 51a.) red arrows). No difference in HepaRG location was noted between statically seeded discs, that were subsequently cultured statically (Figure 51a~~a~~.) or dynamically (data not shown). ~~, red arrows). No difference in HepaRG location was noted between statically seeded discs, that were subsequently cultured statically (Figure 53 a.), or dynamically (data not shown).~~ Similar depth of HepaRG were attached at the matrix periphery when seeded and cultured dynamically (Figure 51~~-54~~c.), black arrows), however, isolated areas of the seeded matrices displayed increased number of HepaRG medial to the tissue periphery (Figure ~~55~~51c.) & d.) red arrows). HepaRG seeded and cultured dynamically

~~illumination (Sections 2.2.8.1 and 2.2.5.1). Results show few HepaRG attached at the external tissue periphery on one side of statically seeded discs (See Figure 50a.), black arrows) a small amount of tissue penetration was noted (Figure 50a.), red arrows). No difference in HepaRG location was noted between statically seeded discs, that were subsequently cultured statically (Figure 51a.), or dynamically (data not shown). Similar depth of HepaRG were attached at the matrix periphery when seeded and cultured dynamically (Figure 52c.), black arrows), however, isolated areas of the seeded matrices displayed increased number of HepaRG medial to the tissue periphery (Figure 53c.) & d.), red arrows). HepaRG seeded and cultured dynamically~~ showed a repeated pattern of attachment location, with increased quantity of

HepaRG seen at the tissue edges in comparison to the centre of the disc (~~Figure 55~~Figure 51~~Figure 56~~54c.)). Although HepaRG penetration increased when seeded and cultured

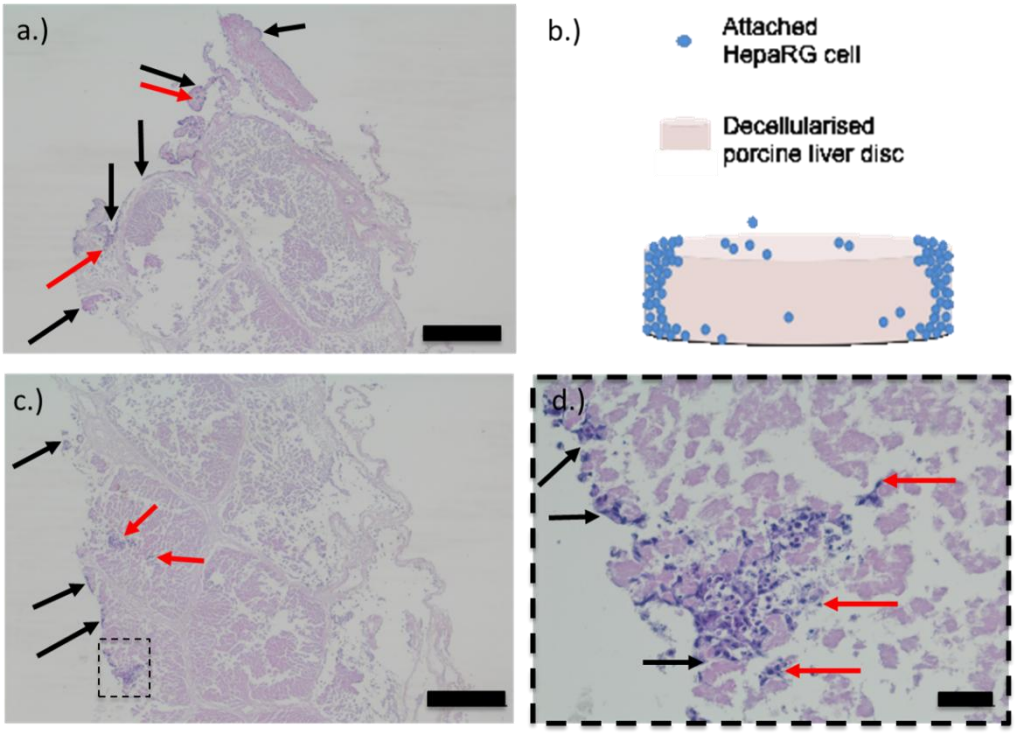

Figure 51. ~~Figure 50.~~ HepaRG penetration in decellularised porcine liver discs seeded statically and dynamically.
-HepaRG attached to peripheral areas of the decellularised porcine tissue seeded and cultured statically (a.), with increased cell penetration into the tissue seen when seeded and cultured dynamically (c.) & d.)).Diagram of cell distribution across the entire discs after dynamic seeding and culture outlines cell presence across the disc periphery b.). Black arrows show cells at tissue periphery, red arrows show cells within decellularised porcine liver disc. Purple = cell nuclei, pink = cell cytoplasm and/or tissue matrices. Scale bar = 200 µm in a.) and c.), 50 µm in d.). All experiments performed in triplicate and imaged three times. d.) represents area

dynamically, effective cell distribution was not achieved. Through observation of the discs during rotation, immersed discs slid from side to side, rather than rotating within the solution. A second experiment was therefore performed repeating dynamic methods outlined in ~~Figure 51Figure 50~~Figure 50 (c) to increase cell coverage by providing an environment in which discs rolled inside the suspension, rather than sliding. The same procedure outlined in the previous experiment was performed, incorporating a larger volume of cell suspension and culture media (6 mL) within the universal. Cell viability was assessed through Live / dead staining of seeded discs (Sections 2.2.9.8), with cell location assessed from H&E--stained sections of seeded discs (Section 2.2.8.1). Live/dead staining showed the presence of viable cells on multiple surfaces of the decellularised porcine liver matrices. Lower numbers of cells fluoresced red indicating the presence of a smaller number of non-viable cells. In addition, H&E staining showed the presence of a thin layer of cells covering the majority of tissue periphery. All peripheral

surfaces of the matrices s

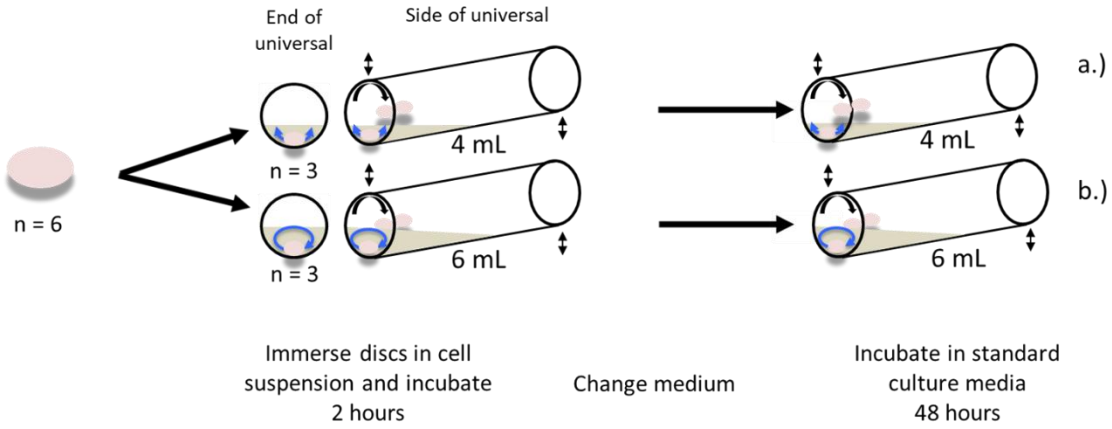

Figure 17. Comparison of the change in cell suspension and media volume to enhance disc movement. Decellularised porcine liver discs were immersed in either 4 mL cell suspension (3.75 x10⁶ cells.mL⁻¹, n=3) (a.)) or 6 mL cell suspension (3.75 x10⁶ cells.mL⁻¹, n=3)(b.)) and incubated for two hours (37 °C). Media was changed for the same amount of standard

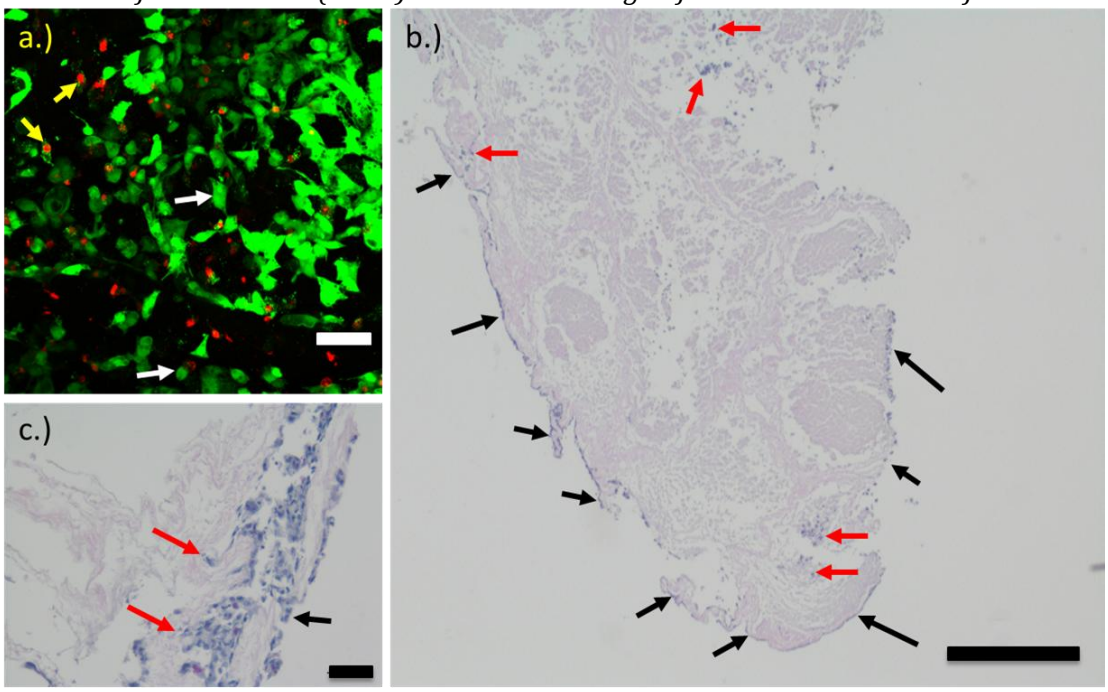

Figure 14. Viability and distribution of HepaRG seeded with increased volume of cell suspension and culture media. Majority of cells seeded with 6 mL cell suspension remained viable (a.) white arrows)with some non-viable cells present (a.), yellow arrows). HepaRG were located around the tissue periphery (b.) & c.), black arrows), with some cell penetration seen (b.) & c.) red arrows). Green = viable cells, Red = non-viable cells (a.)). Purple = cell nuclei, pink = cell cytoplasm and/or tissue matrices (b.) & c.)). Scale bar = 50 µm on a.)& b.) and 500 µm on c.). White arrows = viable cells, yellow arrows = non-viable

~~s~~howed higher cell numbers on discs rotated in 4mL media compared with those rotated in 6 mL media, although cells were present more medially.

5.3.1.3 Does increasing time in cell suspension, increase cell attachment?

Although the increase distribution of HepaRG was seen across the tissue periphery, the thickness of cell layers formed on the disc periphery were still low. It was hypothesised that increasing the time in which HepaRG were exposed to the decellularised disc would result in increased

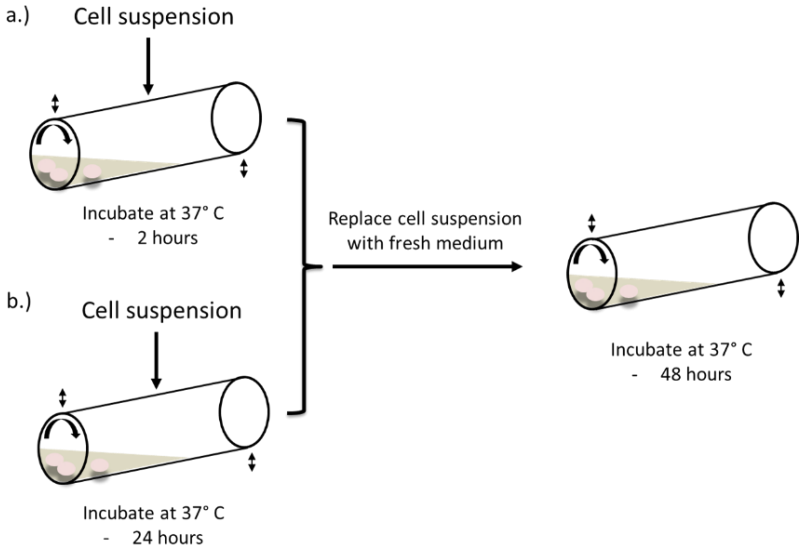

Figure ~~5559575~~2. Outline of dynamic HepaRG cell seeding and culture protocol across the entire periphery of decellularised porcine liver discs. Six decellularised porcine liver discs were immersed in two universals (n=3 per universal) containing cell suspension (4 mL, 3.75 x10^{6} cells.mL^{-1}). Seeded discs were dynamically incubated (35 RPM) at 37 °C for either two (a.)) or 24 hr (b.)) before replacing cell suspension with standard culture medium (4mL). Seeded discs were dynamically incubated (35 RPM) for 48 hr.

cell:matrix contact and, therefore, chance of successful attachment.

~~Although increased distribution of HepaRG was seen across the tissue periphery the thickness of cell layers formed on the disc periphery were still low. It was hypothesised that increasing the time in which HepaRG were exposed to the decellularised disc would result in increased cell:matrix contact and, therefore, attachment.~~ Discs were seeded and cultured dynamically based on methods outlined in Sections 2.2.20 and 2.2.21, with the following modifications. Discs were seeded with HepaRG for either two or 24 hr in cell suspension and cultured in media for 48 hr (Figure 52~~Figure 57~~). HepaRG cell viability was assessed using Live/dead stain (Section 2.2.9.8), before assessment of cell location using H&E stained tissue sections taken at multiple tissue depths (Section 2.2.8.1 and 2.2.5.1)

Discs seeded for two hr displayed multiple viable cells with largely elongated morphology (Figure 53~~Figure 54~~a.), L-e), and grouped cells with a

more rounded morphology (Figure 53~~Figure 54~~a.), L-r). Non-viable cells were not visible in discs seeded for two hr. H&E staining also revealed cells with two morphologies; one with extended morphology that were predominantly attached to septal bands (Figure 53~~Figure 54~~b.), black arrows), and another with more rounded morphology (Figure 53~~Figure 54~~b.~~).)~~ red arrows), often attached to parenchyma. A larger number of both viable and non-viable cells were seen in discs seeded for 24 hr (Figure 53~~Figure 54~~a.) & c.)). H&E staining confirmed

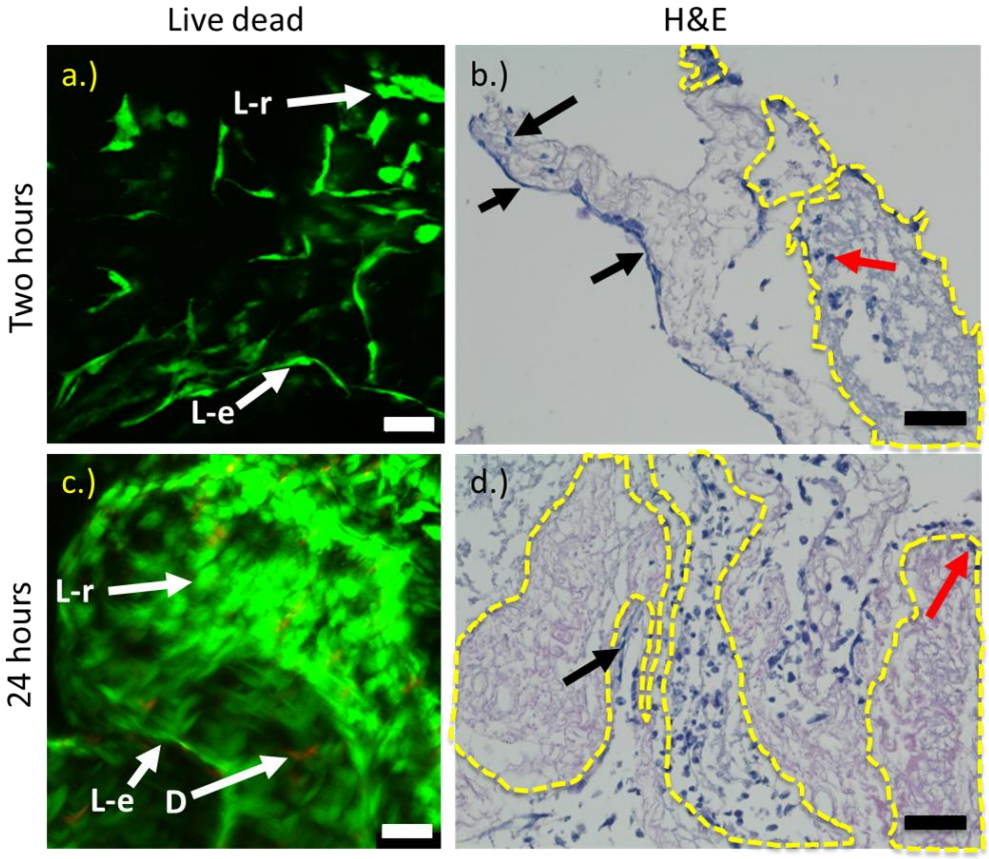

Figure ~~565453~~. HepaRG penetration in decellularised porcine liver discs immersed in suspension up to 24 hours. Majority of cells remained viable after seeding for two & 24 hr (a.) & c.) respectively), with attachment to both parenchyma and septal bands seen (b.) & d.) respectively). Green = viable cells, red = non-viable cells, purple = nuclei, pink = tissue matrix, L-e = viable, elongated cells,, L-r = viable rounded cells, D = dead cells. Black arrow = elongated cell attachment to septal bands, red arrow = rounded cell attachment to parenchymal tissue. Scale bar= 50 µm on a.), c.) & d.), scale bar = 200 µm on b.). n=3

the increased cell attachment in discs seeded for 24 hr (Figure 53~~Figure 54~~d.)) as opposed to two hours (Figure 53~~Figure 54~~b.)). A mixed morphology was seen in discs seeded for two and 24 hr, with parenchyma associated with HepaRG of a more rounded morphology (Figure

53~~Figure 54~~d.), red arrows) whereas HepaRG at the septal bands were elongated and flat (Figure 53~~Figure 54~~D. black arrows). Extending the seeding time to 24 hr resulted in a greater number of cells becoming attached compared to those seeded for two hr. The number of both viable

and non-viable cells increased when seeding time was extended, with the number of viable cells greater than the number of non-viable cells in discs seeded for 24 hr. Cells were also present deeper within the tissue periphery of the decellularised porcine liver discs in discs immersed for 24 hours, versus those immersed for two hr (Figure 53~~Figure 54~~b.)&d.)).

~~1.~~ 5.3.1.4 What is the maximum density at which cells can be seeded on to the decellularised porcine liver discs?

Further optimisation involved seeding of increased cell densities and monitoring of cell viability and metabolic activity through Live / dead staining (see Section 2.2.9.8~~).)~~ and quantification of glucose uptake (See Section 2.2.15). HepaRG were dynamically seeded (24 hr) onto decellularised porcine liver scaffolds at different cell densities (6mL, 0.5 x10^6, 1 x10^6, 2 x10^6, 3 x10^6, 4 x10^6, 5x10^6 & 6x10^6 cells.mL^{-1}) and cultured for 48 hr in standard culture medium). Viable cell number increased up to a seeding density of 4 x10^6 cells.ml^{-1} (Figure 54~~Figure 59~~, a.) - e.)), after which, the number of viable cells decreased (~~Figure 59,~~Figure 54 f.) & g.)). Although non-viable HepaRG were sparsely present at seeding densities up to 4 x10^6.cells.ml^{-1} ~~these significantly~~non-viable cell numbers increased at densities of 5 x10^6 cells.ml^{-1} and above. HepaRG displayed two different morphologies throughout all seeding densities; either long and elongated, or smaller and rounded. Glucose quantification analysis indicated that glucose uptake increased with increasing cell density, peaking at between 3 x10^6 cells.mL^{-1} and 4 x10^6 cells.mL^{-1}. Glucose uptake decreases with seeded cell densities above 4 x10^6 cells.mL^{-1} (Figure 55~~Figure 56~~). The most efficient seeding density was determined through the proportion of viable to non-viable cells after cell seeding (Figure 55~~Figure 59~~), and the greatest quantity of glucose uptake when increasing seeding densities were investigated (Figure 60~~Figure 60~~). As the number of attached, viable cells was highest at 4x10^{-6} cells.mL^{-1}, the number of non-viable cells increased at 5x10^6 cells.mL^{-1} and above, and the highest rate of glucose uptake was seen at 3x10^6 cells.mL^{-1} and 4x10^6 cells.mL^{-1} ,

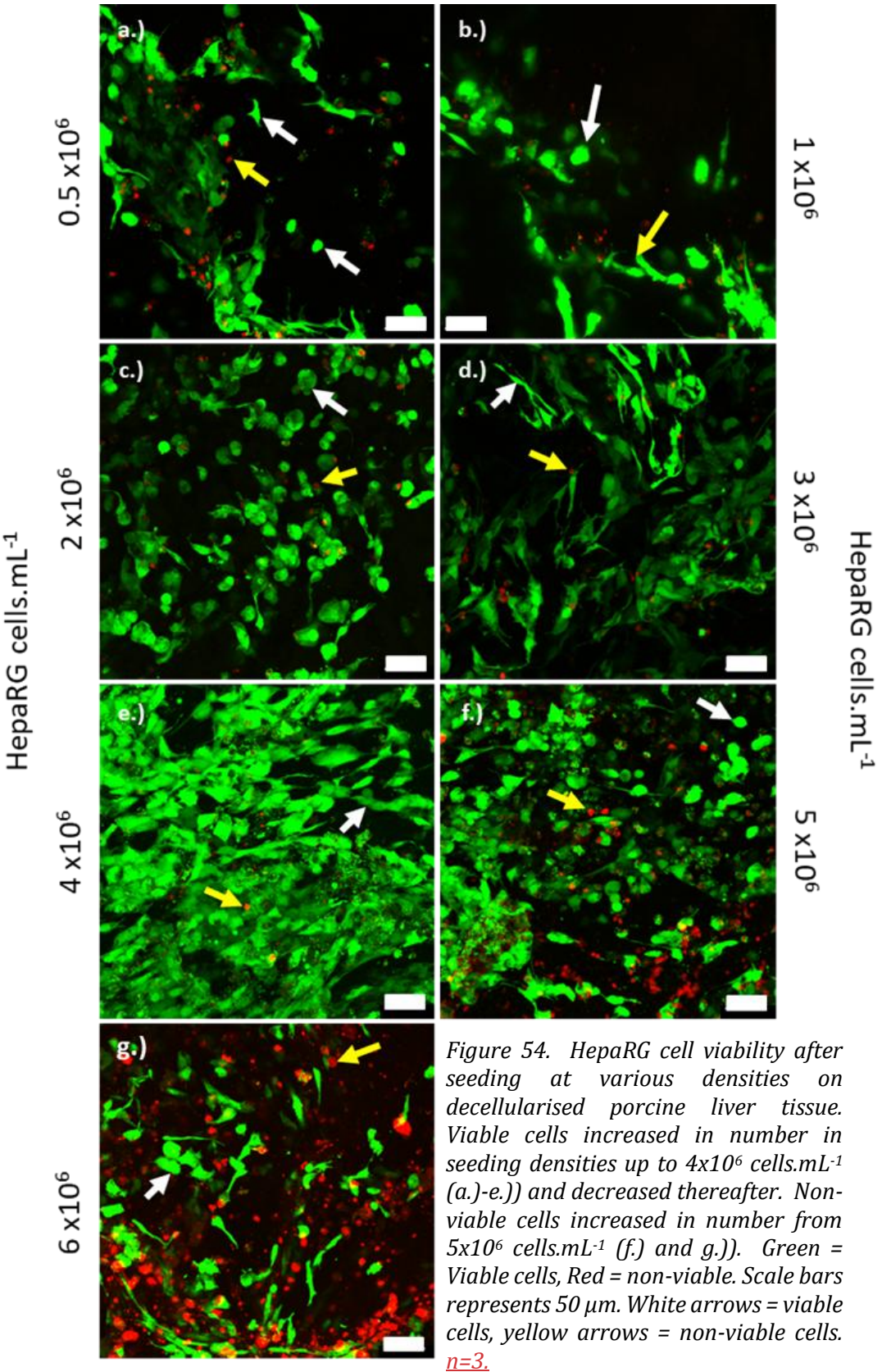

Figure 54. HepaRG cell viability after seeding at various densities on decellularised porcine liver tissue. Viable cells increased in number in seeding densities up to 4x10⁶ cells.mL⁻¹ (a.)-e.)) and decreased thereafter. Non-viable cells increased in number from 5x10⁶ cells.mL⁻¹ (f.) and g.)). Green = Viable cells, Red = non-viable. Scale bars represents 50 µm. White arrows = viable cells, yellow arrows = non-viable cells. n=3.

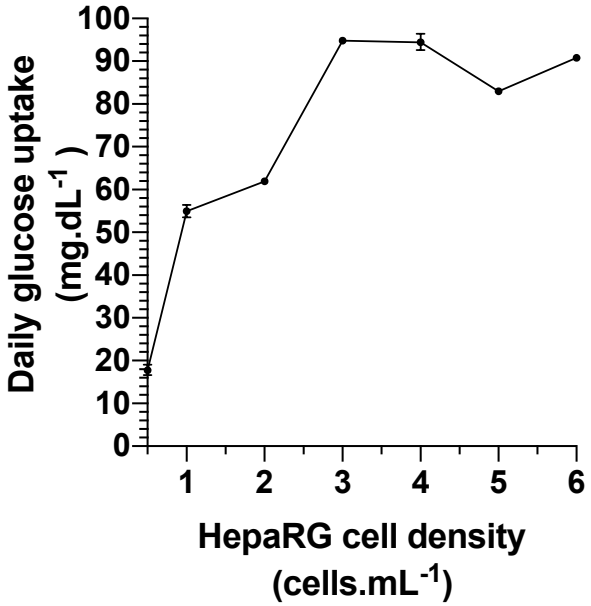

Figure ~~60~~5. Glucose uptake of various seeding densities of HepaRG cells, seeded on decellularised porcine liver. Glucose uptake increases as cell density increases, peaking at between 3x10⁶ and 4x10⁶ cells.mL⁻¹. Glucose uptake decreases when cells are seeded greater than 4 ~~-~~x10⁶ cells.mL⁻¹. n=3, measured in triplicate.

it was determined that the most efficient seeding density was 4x10⁶ cells.mL⁻¹. This seeding density was used for all further experiments.

5.3.1.5 Are HepaRG cells retained after injection into decellularised porcine liver matrices?

The injection of HepaRG within the decellularised porcine liver discs did not result in sufficient cell attachment within the disc. Decellularised porcine liver discs have been shown to display better retention of tissue ~~histioarchitecture~~histoarchitecture within the medial disc areas compared with those seen at external surfaces, with peripheral areas showing increased damage to the matrix, and greater gap sizes between structures (Figure 11). It was hypothesised that the increased retention of tissue structures would lead to increased rates of HepaRG cell attachment and cell attachment is increased at the tissue periphery due to larger spaces for attachment to occur. Further experiments therefore investigated whether HepaRG showed greater cell attachment where tissue spaces were largest by injecting the cells into the tissue discs. Decellularised porcine liver discs

(n=12) were injected with HepaRG in a 24 well plate at one location on the surface of the disc (peripheral) and seeded for two hr, as outlined in Section 2.2.20. (Figure 56). To not overload the limited space available at the injection site, and reduce the risk of cell clumping, lower than optimal cell densities were injected ($2x10^5$ cells, 50 µL). Discs were placed in either a 24-well culture plate (n=6) and cultured statically (400 µL media, Figure 56, a.)), or in a universal (n=6) with 6 mL standard culture media and cultured dynamically (35 RPM, Figure 56, b.)) (Sections 2.2.16.3 and 2.2.17.2). Seeded

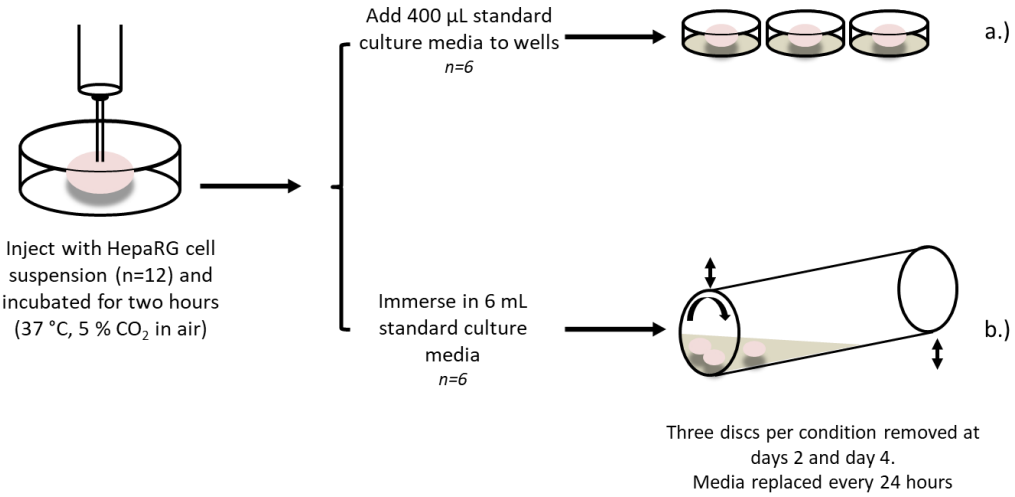

Figure ~~5~~6~~61~~. Injection of HepaRG into decellularised porcine liver discs. Discs were injected with cell suspension ($2x10^5$ cells, 50 µL) and left to statically attach. Six discs were transferred and statically cultured (a.)), and remaining discs were dynamically cultured (b.)). Seeded discs were cultured at for up to four days before media was replaced. Discs (n=3) were removed after two- and four-days culture for each condition, with media retained to assess activity and discs retained to assess cell location.

discs were seeded for two hr and cultured for 72 hr, with media changed every 24 hr. Cell activity was quantified from media retained after disc removal and cell location was determined on H&E stained tissue sections of seeded discs, visualised with ~~Köehler illumination~~brightfield microscopy (Sections2.2.8.1 and 2.2.5.1).

~~M~~Minimal numbers of HepaRG were seen attached to the medial areas, and the peripheral entrance of the injection site at both days two and four. At day two, few HepaRG were seen at the injection site (Figure 57a.)). HepaRG were also seen within the vascular structures (Figure 57b.)) and at the disc periphery adjacent to the injection site. At day four, few HepaRG remained at the periphery of (Figure 57d.)), and within the injection site (Figure 57e.)). To assess whether cell metabolic activity, glucose uptake was quantified from retained culture

media. Results showed that HepaRG injected and statically cultured showed increased metabolic activity compared with dynamic culture, but this activity level was not maintained for 72 hr. HepaRG injected and dynamically cultured showed little glucose uptake, which reduced further at day three. HepaRG do not appear to attach in large numbers to the inner areas of the decellularised porcine liver discs after injection. Two main causes were proposed.

1. As a result of increased pressure within the disc, or fluid movement resulting from cell injection, HepaRG did not have enough time to attach to the matrices before being displaced.
2. or HepaRG preferentially bind to more damaged tissues such as tissue seen at the external tissue or discs that have been excessively exposed to decellularisation reagents and resulted in increased matrix damage

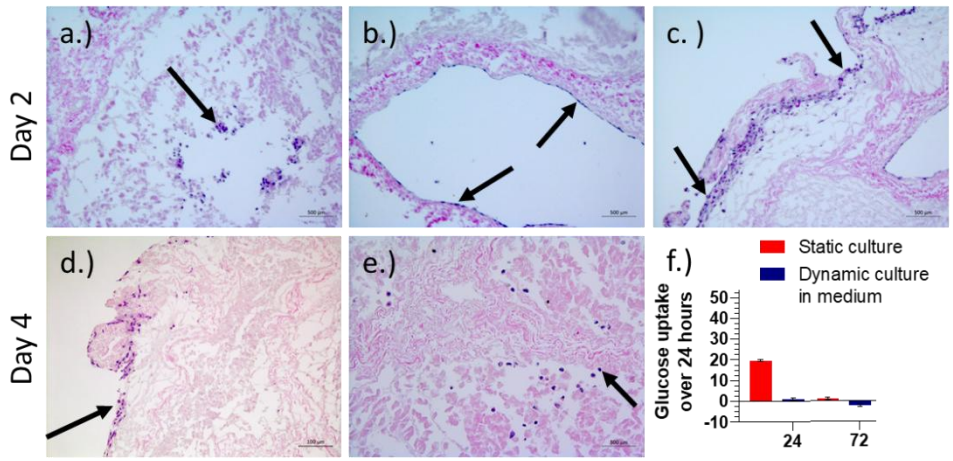

Figure 57. HepaRG attachment after injection site of decellularised porcine liver discs. Within two days culture, clumps of HepaRG were present at the injection site (a.)), with HepaRG monolayers present at the vascular surfaces (b.)). After four days culture, layers of HepaRG were seen at the peripheral tissue edges (c.) and d.)). Isolated HepaRG were also seen in the tissue surrounding injection sites. Metabolic activity was highest within the first day of static culture only. n=3.

To test this theory, HepaRG attachment capability was investigated using the differential gradients of matrix retention already observed across the discs after decellularisation in Chapter 3 (Figure 12). To understand whether greater number of cells attach to the medial or peripheral surfaces of the decellularised porcine liver discs when given enough space and time to attach, decellularised porcine liver discs (n=3) were transversely bisected (Figure 58a.)) and immersed in cell suspension (3.75 x10^6 cells.mL^{-1}, 37 °C) overnight, before being transferred into either a 24 well plate containing 400 µL standard culture media (n=3, Figure 58b.)) or a cell spinner containing 75 mL standard culture media (n=3, Figure 58c.)). Discs were cultured for 14 days, with media changed every day for seeded discs statically cultured and three to four days for seeded discs cultured dynamically (Figure 58). Internal dissected surfaces were differentiated from external dissected surfaces by a darker colouration and sharper edges to the cut surface. External surfaces were lighter in colour and had more rounded edges. When

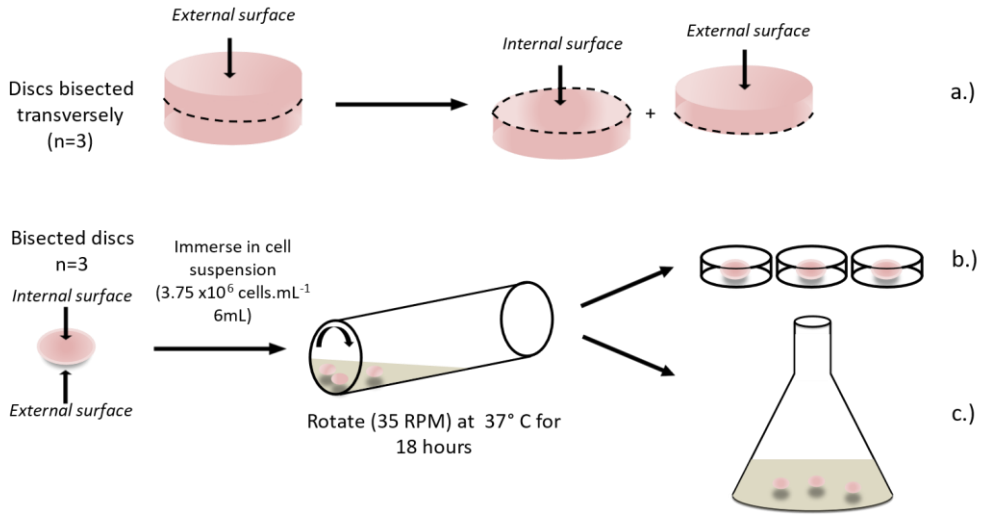

Figure ~~–~~5~~8~~~~63~~. HepaRG attachment to internal and external regions of decellularised porcine liver discs. Three decellularised porcine liver discs were transversely bisected and immersed in 6 mL cell suspension, rotating for 18 hours in two universals (3.75 x10^6 cells.mL^{-1}, 37 °C, 35RPM, n=3 discs per universal). Discs were transferred into either a 24 well plate (n=3, one disc per well, B) with 400 µL standard culture media added, or immersed in 75 mL standard culture media (n=3). Discs were statically (n=3, 37 °C, 5 % CO_2 in air) or dynamically (n=3, 37 °C, 35 RPM) cultured for up to 14 days. Media was changed every day and three – four days for those cultured statically and dynamically respectively. Three discs were removed after 14 days for further

orientated and embedded perpendicularly, and viewed microscopically, external surfaces showed greater ECM damage and tissue detachment, with greater spaces within canaliculi and at septal bands than those seen at internal surfaces. No ~~significant~~ appearance of changes in ~~difference in~~ the number of attached HepaRG was noted between internal/medial (Figure 59a.) & d.), red arrows) and

external/peripheral surfaces (Figure 59a.) & d.), black arrows). Thin layers of HepaRG were seen on the periphery of statically (Figure 59b.)) and dynamically cultured discs (Figure 59) every day for seeded discs statically cultured and three to four days for seeded discs cultured dynamically (Figure 58). Internal dissected surfaces were differentiated from external dissected surfaces by a darker colouration and sharper edges to the cut surface. External surfaces were lighter in colour and had more rounded edges. When orientated and embedded perpendicularly, and viewed microscopically, external surfaces showed greater ECM damage and tissue detachment, with greater spaces within canaliculi and at septal bands than those seen at internal surfaces. No appearance of changes in the number of attached HepaRG was noted between internal/medial (Figure 59a.) & d.), rede.)), although HepaRG were present further below the surface in dynamically cultured discs, compared with those seeded statically. HepaRG formed more defined cell layers when attached to internal areas of the discs

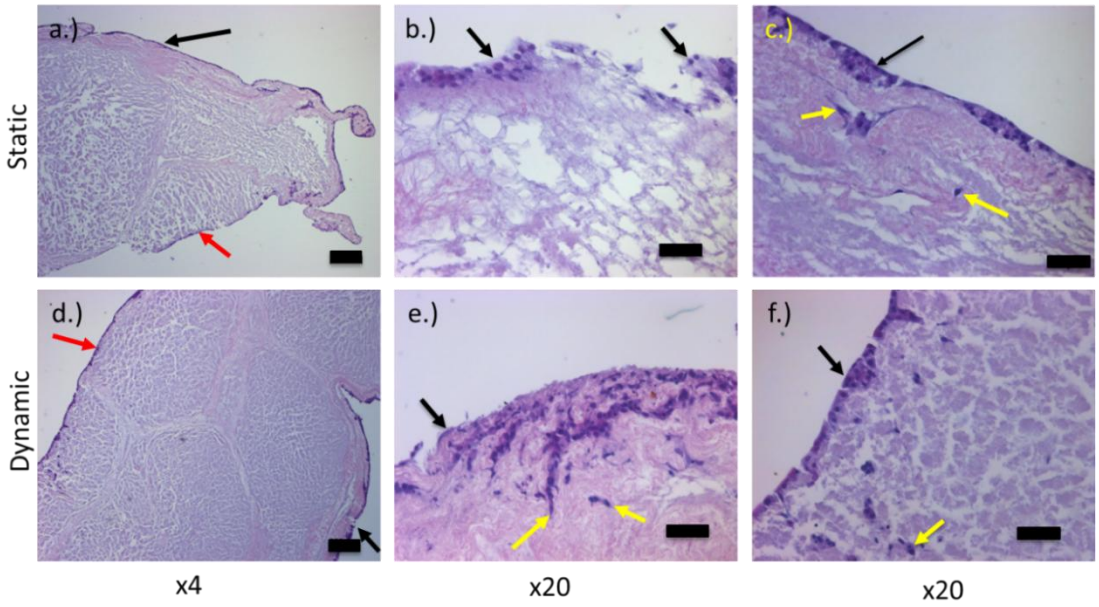

Figure 59. Patterns of HepaRG attachment after seeding on decellularised porcine liver discs. Discs were stained with H&E and imaged using a Zeiss Axio Imager M2 microscope with images taken using a AxioCam MCr5 digital camera and Zen software. a.) & d.) were taken using a x4 lens, b.),c.),e.) & f.) were taken using a x20 lens. Purple = cell nuclei, pink = cell cytoplasm/tissue matrix. No preference for internal (red arrows) or external (black arrows) disc surfaces were noted. Yellow arrows denote cells inside matrices. HepaRG cultured dynamically (d.) to f.)) show better cell penetration than those cultured statically (a.) to c.)). n=3

(Figure 59c.)&f.)), whereas more haphazard cell arrangements were seen on those attached to more external/peripheral regions (Figure 59b.)&e.)). Although cells

did not preferentially bind to matrices that were better retained, or more degraded, results supported previous work that indicated an application of flow during culture increased cell penetration into the tissue (Figure 59c.) & d.)). Fourteen days of either static or dynamic culture did not result in an increased cellular presence within the medial aspects of the matrix than that seen at four days.

5.3.1.6 Do cells require longer than 14 days to penetrate the decellularised porcine liver discs?

Previous experiments indicated that HepaRG were not present within the centre/ more medial of the decellularised porcine liver matrices after 14 days in culture and indicated that longer

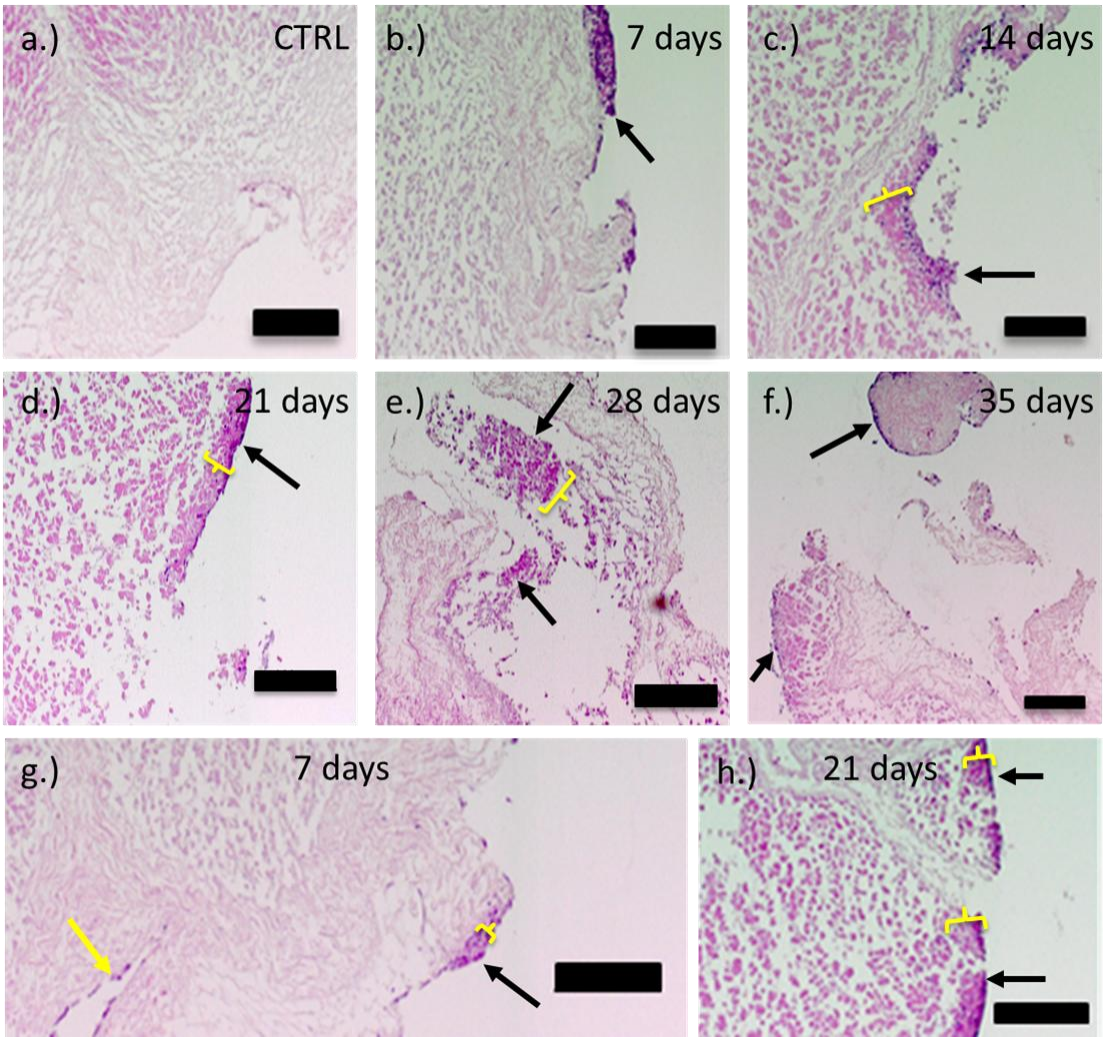

Figure 60. Monitoring HepaRG penetration over 35 days culture. HepaRG attach and penetrate decellularised tissue within seven days (b.)), with small amounts of cell movement seen at day 14 (c.)). HepaRG do not move any further at days 21 (d.)), 28 (e.)) and 35 (f.)). HepaRG form monolayers when in contact within the vasculature (yellow arrow, g.)) and penetrate parenchymal tissue (black arrow, g.) & h.)). Yellow parentheses indicate area of increased eosin staining a.) = no cell control tissue. Purple = cell nuclei, pink = cell cytoplasm/tissue matrix. a.) = negative control, b.) to f.) HepaRG seeded discs. Scale bar = 50 µm on a.), - d.), 100 µm on e.), f,) & g.), n=3

time frames may be required. Discs were seeded and cultured dynamically (Sections 2.2.20 and

2.2.21) with HepaRG for up to 35 days, with previous developments in application of flow, cell density, time for seeding, volume of media / cell suspension, applied (Sections 5.3.1.2, 5.3.1.3, 5.3.1.4,). HepaRG location and ~~proliferation~~ division ~~was~~ were ascertained through H&E stained, and Ki-67 labelled, HepaRG seeded discs (n=3 per timepoint), H&E staining indicated that HepaRG

primarily remained on the surface of the discs, with limited movement or ~~proliferation~~ division into the medial aspects. Increased cell presence in the medial aspects of the tissue were seen in areas of parenchymal matrix (Figure 60, black arrows). Some cells were also noted in vascular tissue, laid flat against the remaining endothelial tissue matrices (Figure 60g.), yellow arrow). Increased eosin uptake was seen in the regions where cells were attached (Figure 60, yellow parentheses).

Labelling of tissue sections cultured for up to 35 days with standard culture media (not supplemented with DMSO) and labelled with Ki-67~~an~~ antibody ~~to Ki-67~~ indicated that some cells showed ~~proliferation~~division up to day 14, after which ~~proliferation~~division stopped. Positively labelled cells

Figure ~~666~~1. HepaRG proliferation after seeding onto decellularised porcine liver discs over 35 days culture. a.) = Isotype control~~No cell control~~. Positive cellular staining for the proliferation marker was seen in HepaRG cultured for seven (b.)) and 14 (c.)) days (black arrows = Ki-67 labelled cells). Proliferation was seen with HepaRG attached to both septal bands (b.)) and parenchyma((c.)). At day 21 (d.)), 28 (e.)) and 35 days (f.)) culture, HepaRG are still attached, but not proliferating (red arrow = Ki-67 negative cells). Scale bars = 50 µm, n=3.

were identified by circular area

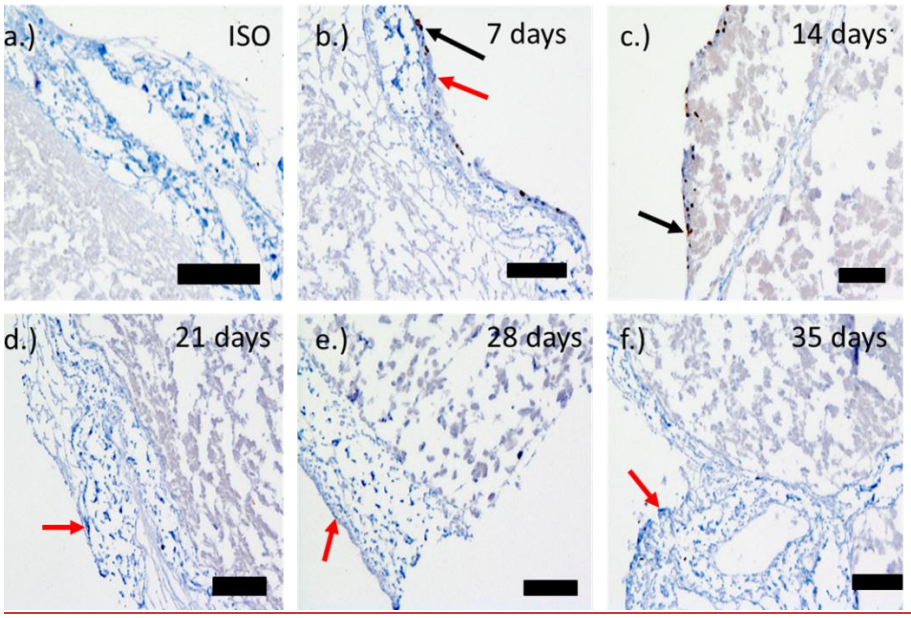

s of dark brown staining. Parenchymal tissue appeared as a faint brown background staining and septal bands were stained blue. Cellular material devoid of Ki-67 (non-dividing) were identified through the presence of dark blue circular regions. The maximum number of

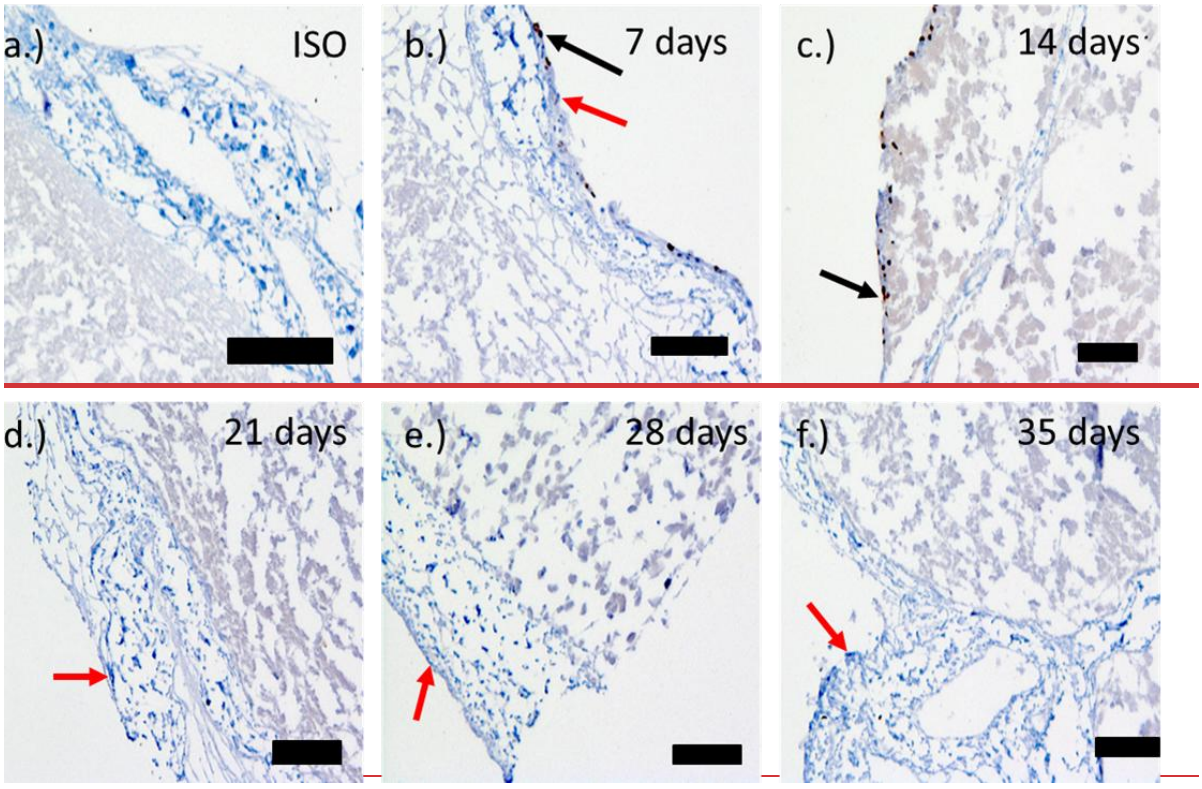

~~Labelling of tissue sections with an antibody to Ki-67 indicated that some cells showed proliferation up to day 14, after which proliferation stopped. The maximum number of proliferative~~dividing cells were seen at day 14 and within parenchymal areas of tissue matrix. Although cells remained on the tissue up to 35 days in culture with standard media, no further evidence of ~~proliferation~~ division ~~were~~ was seen. Although initially HepaRG showed the ability to repopulate the matrices, this was limited to 14 days in culture. Further research focused on a more differentiated cell line Huh7.

~~5.~~ 5.3.2 Huh7 cells

Following the development of conditions in seeding HepaRG cells onto decellularised porcine liver discs, the project progressed to Huh7 cells. Although HepaRG are a progenitor like cell type, Huh7 cells are a HCC transformed cell line.

5.3.2.1 Can Huh7 cells be injected inside decellularised porcine liver matrices?

As mentioned previously, the surface area to volume ratio of the decellularised porcine liver discs are high and previous experiments using HepaRG indicated that central disc repopulation re-population would take longer than 35 days Initial studies with Huh7, therefore, focused on achieving cells within the centre of the disc through injection. Decellularised porcine liver discs were aseptically injected with either 4 x10^6 cells.mL^{-1} (50 µL, n=9) or 50 µL media (n=9) using a 16-gauge (G) needle. Huh7 were allowed to attach for two hours in six 12 well plates (37 °C, 5 % CO_2) (See Figure 62). Discs were either injected with cell suspension (50 µL, 4 x10^6 cells.mL^{-1}) or media (50 µL)(Section 2.2.20) and cultured statically or dynamically (Sections 2.2.20 and 2.2.21). Cell location was assessed through microscope examination of sections of seeded discs, stained with H&E (Sections 2.2.8.1 and 2.2.5.1). Discs injected with Huh7 and cultured statically in media (Figure 62a) showed the presence of cell layers on one peripheral/external surface of the disc (black arrows, Figure 63a.) &b.)), with a small number of isolated Huh7 present within the septal band of one medial disc region (red arrow, Figure 63b.)). No Huh7 were found within the medial aspects of the parenchyma. Discs injected with Huh7 and culture dynamically in media only (Figure 63b.)) showed very small number of grouped Huh7 on one external surface only (Figure 63c.) &d.)). Discs injected with Huh7, and statically cultured in cell suspension (Figure 63c.)) displayed layered deposition of Huh7 on all peripheral surfaces, and at varying depths (Figure 63a.),b.) &c.), Black arrows). Huh7 were also present within areas of matrix medial to the external surfaces and/or surrounding the vessels

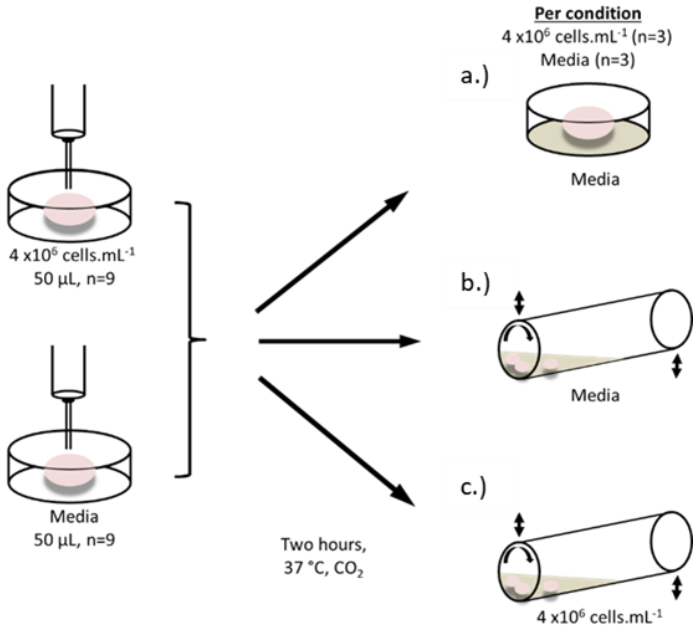

Figure 62~~68~~. Investigation of injecting Huh7 cells in decellularised porcine liver matrices. Discs of decellularised porcine liver matrix were injected with either Huh7 suspension (50 µL, 4 x10⁶ cells.mL⁻¹) or media and statically incubated for two hours. Three Huh7-seeded and three media-seeded discs were statically cultured in media (400 µL, a.)), or dynamically cultured in 6 mL cell suspension (b.), 4 x10⁶ cells.mL⁻¹) or media (c.)).

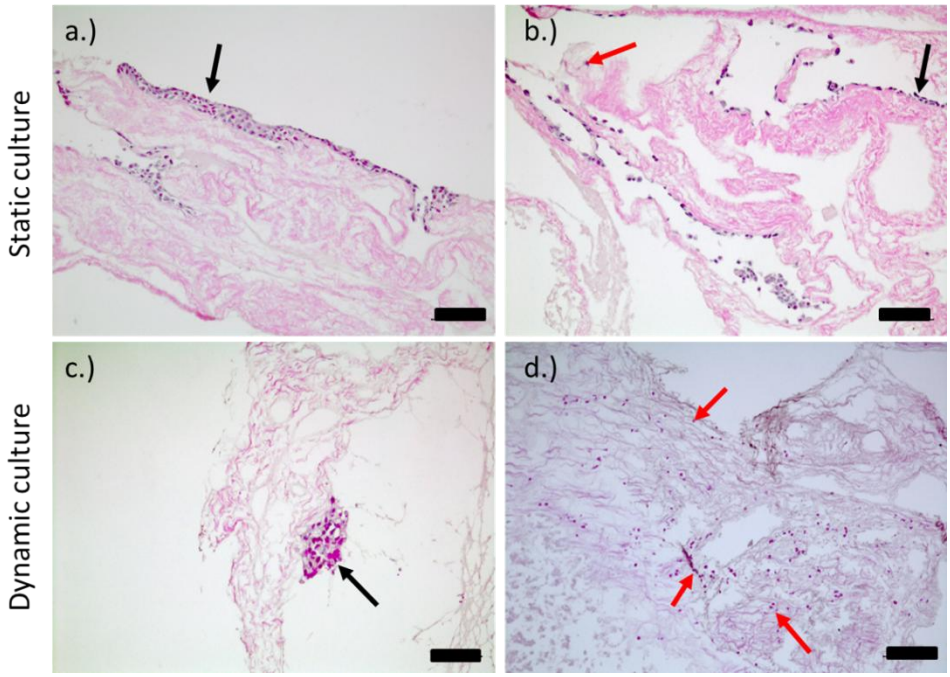

Figure 63. Comparison of Huh7 number and position after injection in decellularised porcine liver discs, seeded statically and dynamically. After injection, static culture resulted in the formation of cell layers across the uppermost peripheral surface (a.), and present to the peripheral surface (b.)). Dynamic culture in media resulted in formation of isolated cell groups at the disc periphery (c.), with isolated Huh7 throughout medial disc regions. (d.) red arrows). Purple = cell nuclei, pink = cell cytoplasm and/or tissue matrices. Black arrow = Huh7 cells on tissue surface, red arrow = Huh7 cells on internal surface. Scale bars = 200 µm on a.) and d.),100 µm on b.) & d.), 500 µm on c.). n=3

(Figure 63b.)&c.), red arrows). Unlike images seen in static culture, groups of HepaRG were also located within the retained vasculature (Figure 63c.)&d.), Red arrows). All discs that were not injected with, or immersed in, HepaRG suspension were bereft of cells (injected with media and either statically or dynamically cultured in media only), indicating an absence of cell contamination. Layers of HepaRG form on one surface when injected discs are statically cultured (Figure 64a.)), and multiple surfaces, with greater presence at medial regions, when dynamically cultured in cell suspension (Figure 64a.)). Further research therefore focused on increasing Huh7attachment on, and within, the decellularised discs through modification of the protocols used. Both static and

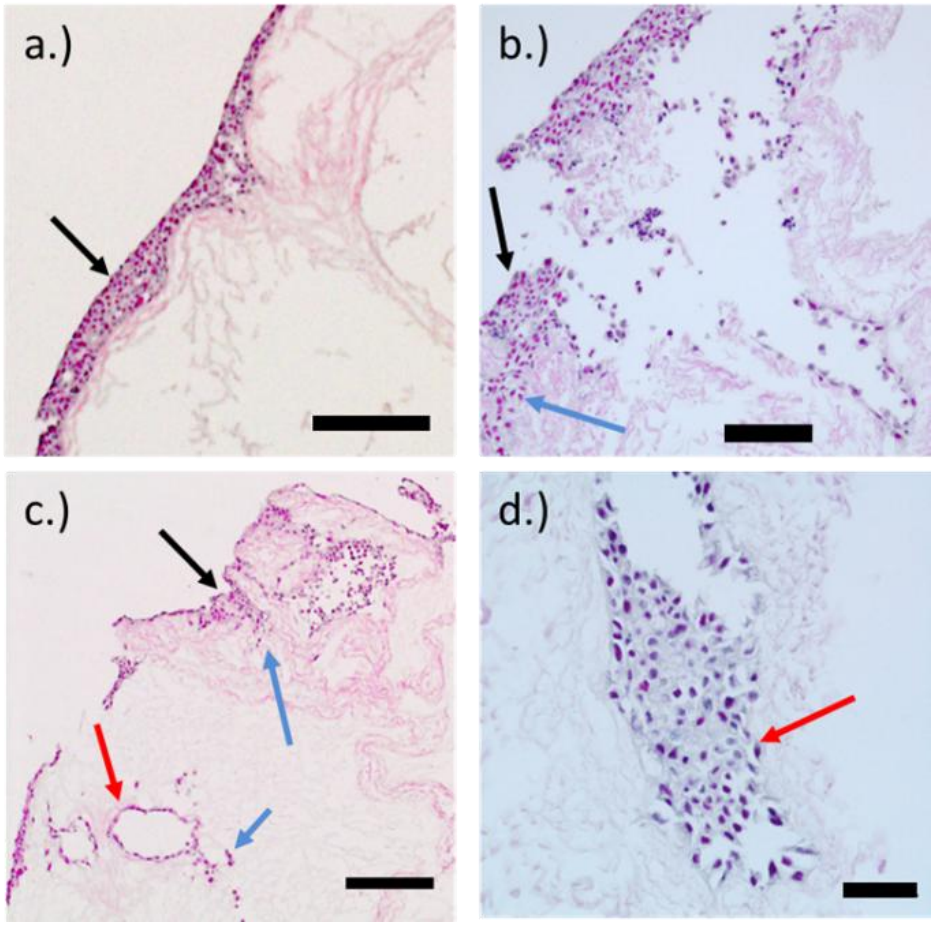

Figure 6419. Variation in Huh7 cell number and position after injection of Huh7 cell suspension, dynamically seeded and cultured on decellularised porcine liver discs. Cell layers formed on external surfaces (a.), b.) & c.)) (black arrows) on all peripheral areas of the discs, to varying depths. Cells were also present in deeper regions of the discs (c.) – blue arrows), and within the vasculature, either in layers (c.) red arrow) or in clumps (d.) red arrow). Purple = cell nuclei, pink = cell cytoplasm and/or tissue matrices. Black arrows = Huh7 cells on the tissue surfaces, Blue arrows = Huh7 cells on internal surfaces. Scale bars = 50 µm in b.), 100 µm in a.) & d.) & 200 µm in c.). n=3

.

dynamically cultured discs formed cell layers on external disc surfaces after injection, however, this was maximised when seeded and cultured in a similar manner (statically seeded and cultured or dynamically seeded and cultured)(Figure 64 and Figure 65).

~~1.~~ 5.3.2.2 Investigation to increase number of cells attached to decellularised porcine liver discs.

Following on from results observed with HepaRG cells, three different approaches were investigated to increase cell attachment and distribution within the decellularised porcine liver discs; through increasing cell density, increasing the number of sites injected and extension of time in culture. Huh7 were injected at one site as described in Chapter 2 (2.2.20) with either $4x10^6$ cells.mL^{-1} (40 µL, n=3), or $4x10^7$ cells.mL^{-1} (40 µL, n=3). Huh7 were left to adhere for four hr rather than two, and statically cultured for up to four days (Sections 2.2.21).

No ~~significant~~ apparent differences in layer depth were seen on peripheral surfaces between the two cell densities, although no cell attachment was seen at the injection sites. Huh7 layers of discs seeded with higher densities were more friable and prone to detachment upon sectioning (Figure 65b.), red arrow). Huh7 seeded at both densities were attached to the peripheral

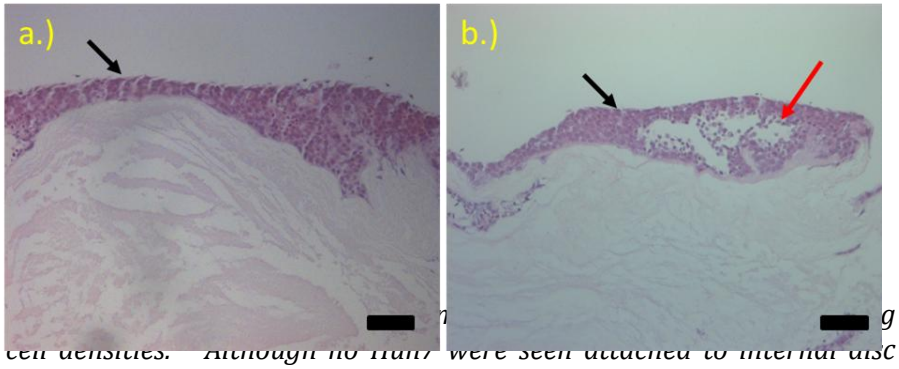

cell densities. Although no Huh7 were seen attached to internal disc regions, cell layers formed (black arrows) at the periphery of the injection sites on the decellularised porcine liver discs a.) & b.). Huh7 layers that formed on discs seeded with $4x10^7$ cells.mL^{-1} (b.)) were more fragile than those seeded with $4x10^6$ cells.mL^{-1} (a.)), often showing regions that were absent of cells within layers (red arrow, b.), or breaks in layer formation. Scale bars = 100 µm. Purple = cell nuclei, pink = cell cytoplasm and/or tissue matrices. Black arrows = Huh7 cells on the tissue surfaces, red arrows = Huh7 cells on internal surfaces. Scale bars = 100 µm. n=3

surfaces at varying thicknesses, forming thicker cell layers where parenchymal tissue

was present (Figure 65, black arrow). Bands of Huh7 cells were present on the uppermost surfaces and were not present far beneath the peripheral septal bands. The subsequent experiment focused on increasing cell number within the disc through increasing the number of injection sites or extending the culture period.

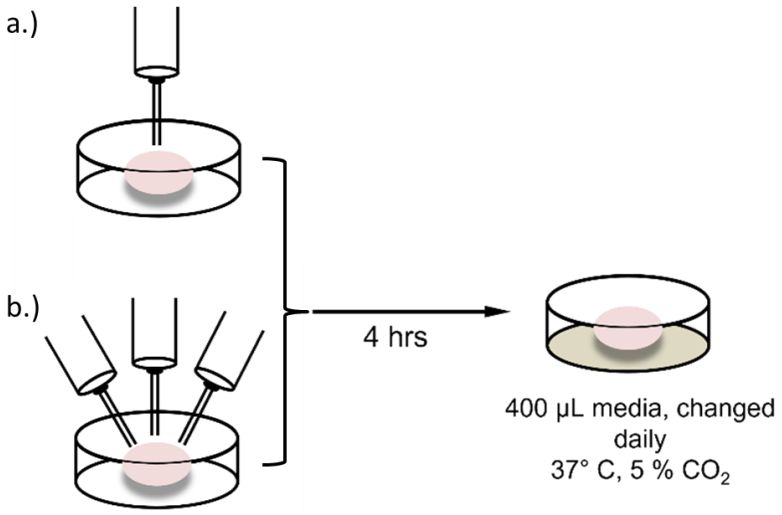

Figure 66. Investigation to increase Huh7 distribution and retention within decellularised porcine liver matrices. Discs of decellularised porcine liver tissue were injected with 4 x10^{7} cells.mL^{-1} (a.), n=9) once (a.) n=9), or three times (b.) n=9), in the centre of the upper disc surface. Seeded discs were incubated for

Huh7 (4x10^{6} cells.mL^{-1}) were injected at either one (Figure 66a.) n=9) or multiple sites (Figure 66b.)) on the surface of the decellularised porcine liver discs, as described in Chapter 2 (Section 2.2.20). Seeded discs were statically cultured (Section 2.2.21) for four, 21 and 28 days to assess initial cell attachment, long-term cell retention and distribution. Media was changed daily. After four days culture, an increase in cell location or density was not seen between discs injected at one or multiple sites, despite the increased total cell number injected at multiple sites (Figure 67a.) & b.)). Thicker layers of Huh7 formed on parenchymal tissue, with thinner layers formed at septal bands. Huh7 were not present below septal bands, except in areas where septae were fragmented or where the 3D lobular structure is not seen (one section only), thereby giving the impression of movement across one septal band. At day 21, Huh7 were present at similar locations as to that seen after four days culture, although isolated cells were also present in more medial sections of the decellularised matrices (Figure 67, c.) & d.)). Minimal cell numbers were seen at injections sites seen at days four (Figure 67a.) & b.) red arrows). Thicker Huh7

layers at day 21 were friable and prone to detachment upon sectioning (67c.)). At day 28, Huh7 were present along the peripheral surfaces, and within parenchymal tissue

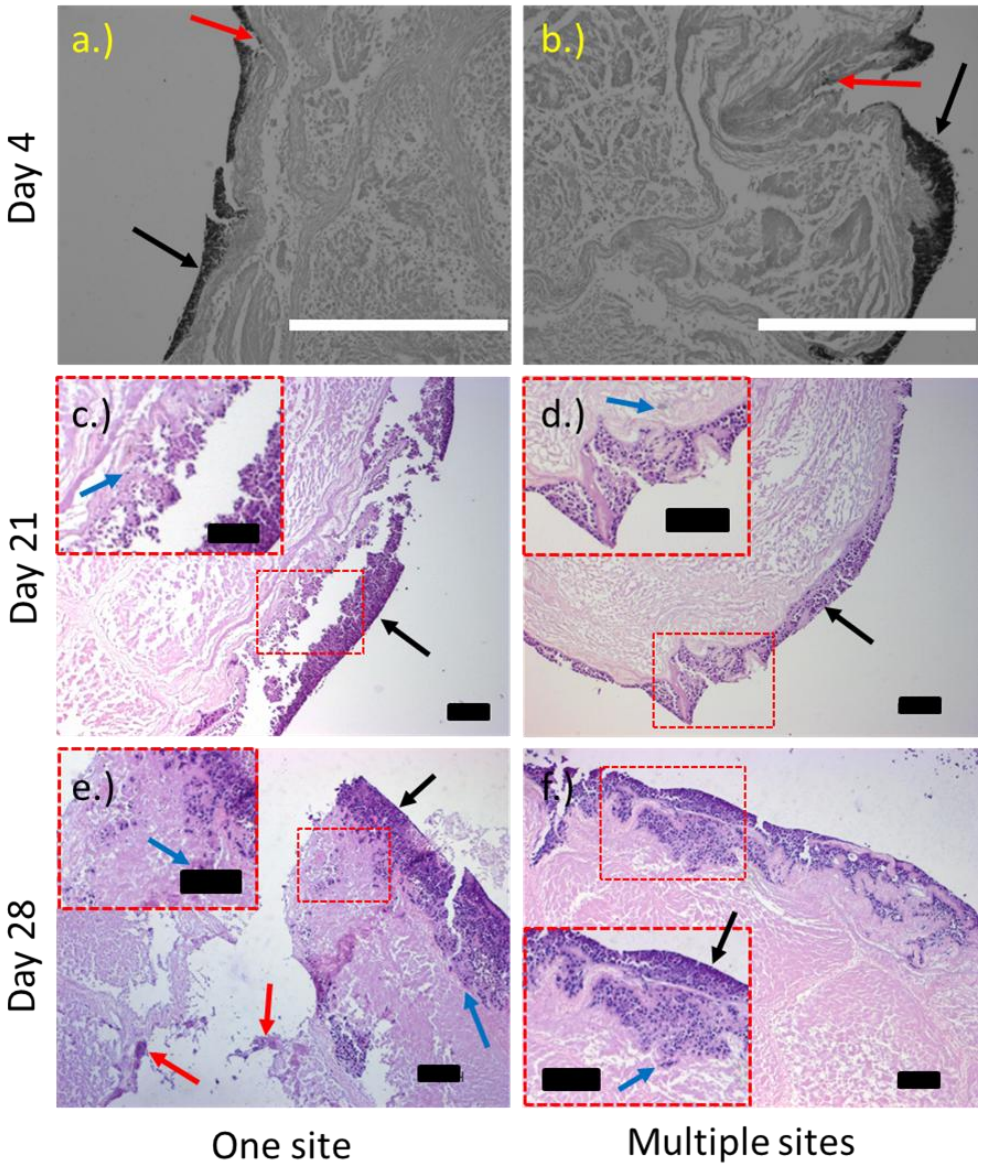

Figure 67. Injection of decellularised porcine liver discs with Huh7 cells to assess cell retention and distribution over 28 days culture. At day four, few Huh7 cells attached to the discs at injection sites (a.) & b.), red arrows), however cell layers were present on peripheral surfaces adjacent to the injection sites (a.) & c.), black arrows). At day 21, Huh7 layers were thicker on external surfaces (c.) & d.) black arrows), and often fragmented indicating fragility of cell attachment. Few cells were noted in underlying lobules (c.) & d.) blue arrows). At day 28 (e.) & f.), cells were present in peripheral and underlying parenchyma (black and blue arrows respectively) Clumps of cells were noted at larger injection sites only (e.)). Minimal differences were present in Huh7 retention or distribution between those injected at one site (a.), c.) & e.)), compared with those injected at multiple sites (b.), d.) and f.)). Scale bars = 100 µm Black = Huh7 cells, Grey = decellularised porcine liver matrices. White bars represent 100 µm (a.)&b.)). Purple = nuclei, pink = matrices (c.) to f.)). Black bars = 200 µm. n=3

beneath the outermost lobule (Figure 67e.) & f.)). Huh7 were either isolated, or found in small groups. Huh7 groups were also seen around

injection sites. Huh7 attached to, and populated parenchymal tissue, although at similar amounts in medial and peripheral regions. It was thought that Huh7 attachment was increased further through extension of seeding time from two to four hr. As tissue retention was greater, and cell attachment lower at the medial aspects of the disc, further investigations compared cell attachment in the medial aspects, or the peripheral areas.

~~1.~~ 5.3.2.3 Does the type of rotation affect cell behaviour and distribution in the disc?

Huh7 and HepaRG within this Chapter have been cultured in universals rotated to provide better nutrient exchange and oxygen gradients, however, other methods of enhancing cell attachment, as well as oxygen and nutrient exchange exist, including spinner flasks and bioreactors. Furthermore, the speed and/or direction of rotation could provide other areas of investigation to further enhance oxygen and nutrient exchange during culture (Huang et al., 2022). Comparison of Huh7 culture method was performed between rotating vessels, and spinner flasks. Decellularised porcine liver discs (n=3) were bisected before dynamic seeding of Huh7 through rotation, and cultured using universals (35 RPM, 37 °C) or spinner flasks (35 RPM, 37 °C, 5 % CO_2 (v/v)) (See Figure 68. Outline of protocol used to compare Huh7 attachment and location on decellularised porcine liver. Three decellularised porcine liver discs were transversely bisected (a.) and immersed in 6 mL cell). Huh7 deposition across

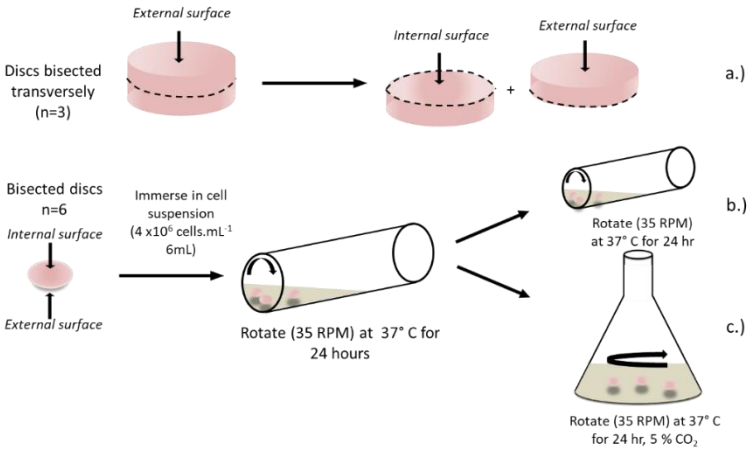

Figure 68. Outline of protocol used to compare Huh7 attachment and location on decellularised porcine liver. Three decellularised porcine liver discs were transversely bisected (a.) and immersed in 6 mL cell suspension, rotating for 24 hr in two universals (4 x10⁶ cells.mL⁻¹, 37 °C, 35RPM, n=3 discs per ~~universal). Discs were transferred into either a fresh universal containing 6 mL standard culture media (n=3, b.)), or immersed in 75 mL~~

~~*Figure 74. Outline of protocol used to compare Huh7 attachment and location on*~~

the entire tissue was seen though H&E stained sections at multiple levels throughout the discs (See Sections 2.2.7.4 and 2.2.8.1). Results showed the formation of thick layers of Huh7 on all peripheral, parenchymal surfaces in seeded discs cultured through rotation (Figure 69a.) & b.)), or using cell spinners (Figure 69,c.)).

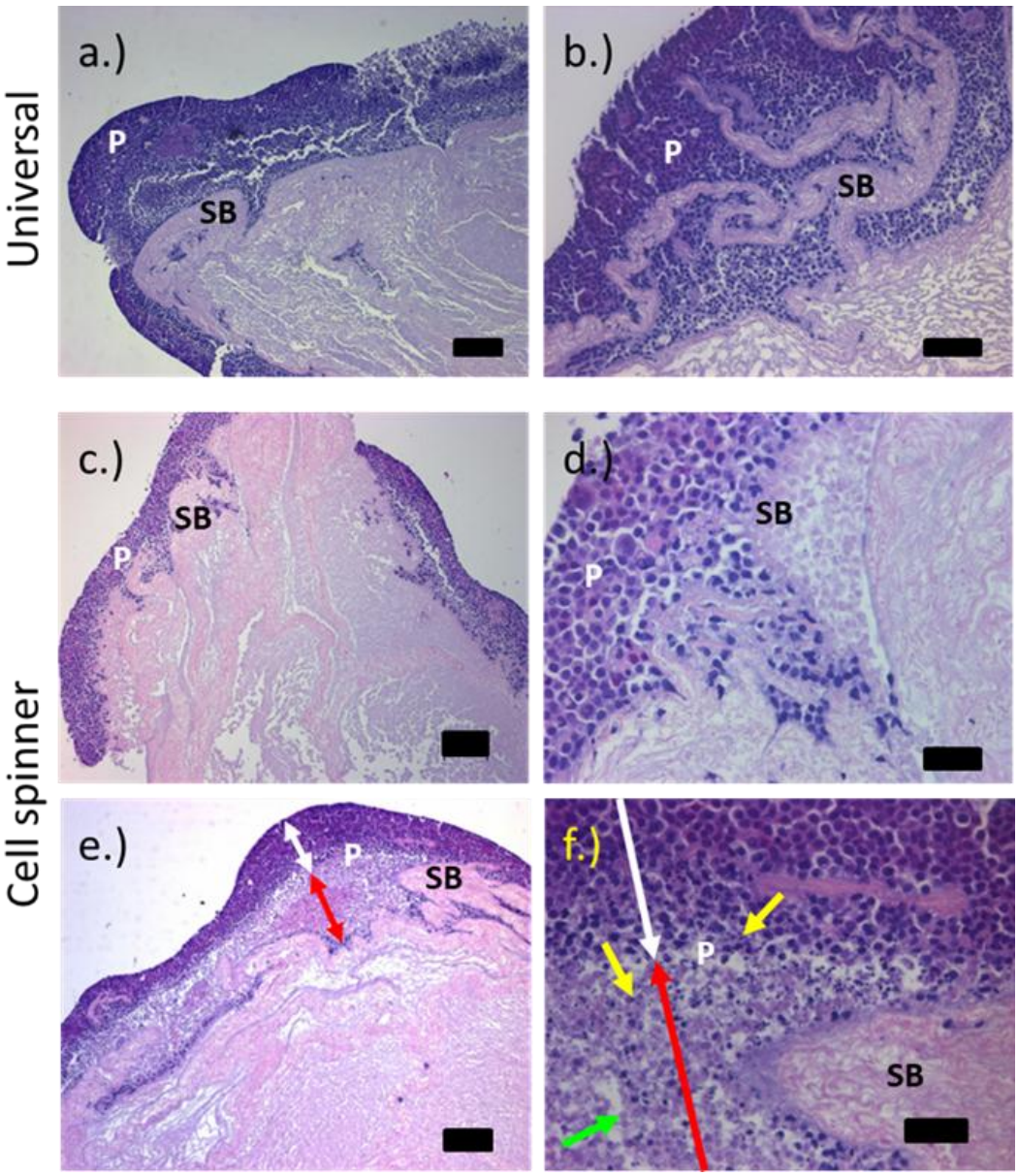

Figure 69. Comparison of dynamic culture conditions. Huh7 cells seeded and cultured in rotating universals (a.) & b.)) showed cell attachment to the parenchymal tissue in layers at the peripheral surfaces, and in underlying lobules. Similar patterns of cell distribution were seen when cell spinners were used (c.) and d.)), although ghost cells green arrow), and apoptotic cells (yellow arrows) were present where cell layers were thickest (e.) & f.)). Purple = cell nuclei, pink = cell cytoplasm and/or tissue matrices. Scale bars = 50 µm (d.) & f.)), 100 µm (b.) & e.)), 200 µm ((a.) & c.)). P = parenchyma, SB = septal bands. White arrows = Huh7 seeded in parenchyma, red arrows = Huh7 where cell death occurred. n=3

although apoptotic (yellow arrows) and ghost cells (green arrow) were present in those to f.)). ~~No significant difference in layer thickness was seen between~~ using cell spinners (Figure 69a.) red arrows shows layers where cell death occurred). ~~the two culture methods, although apoptotic (yellow arrows) and ghost cells (green arrow) were present in those cultured using cell spinners (Figure 73a.) red arrows shows layers where cell death occurred).~~

5.3.2.4 Investigation of cell attachment to damaged and better retained decellularised porcine liver matrices

Huh7 attachment was greatest at sites where tissue degradation was highest. This was thought to be attributed to either increased space for cell attachment, or from the cellular signalling response from attachment to damaged matrices. Future work was directed towards investigating cell response to damaged tissue. Subsequent investigations to assess cell attachment and response to damaged tissue took advantage of the graded degradation seen

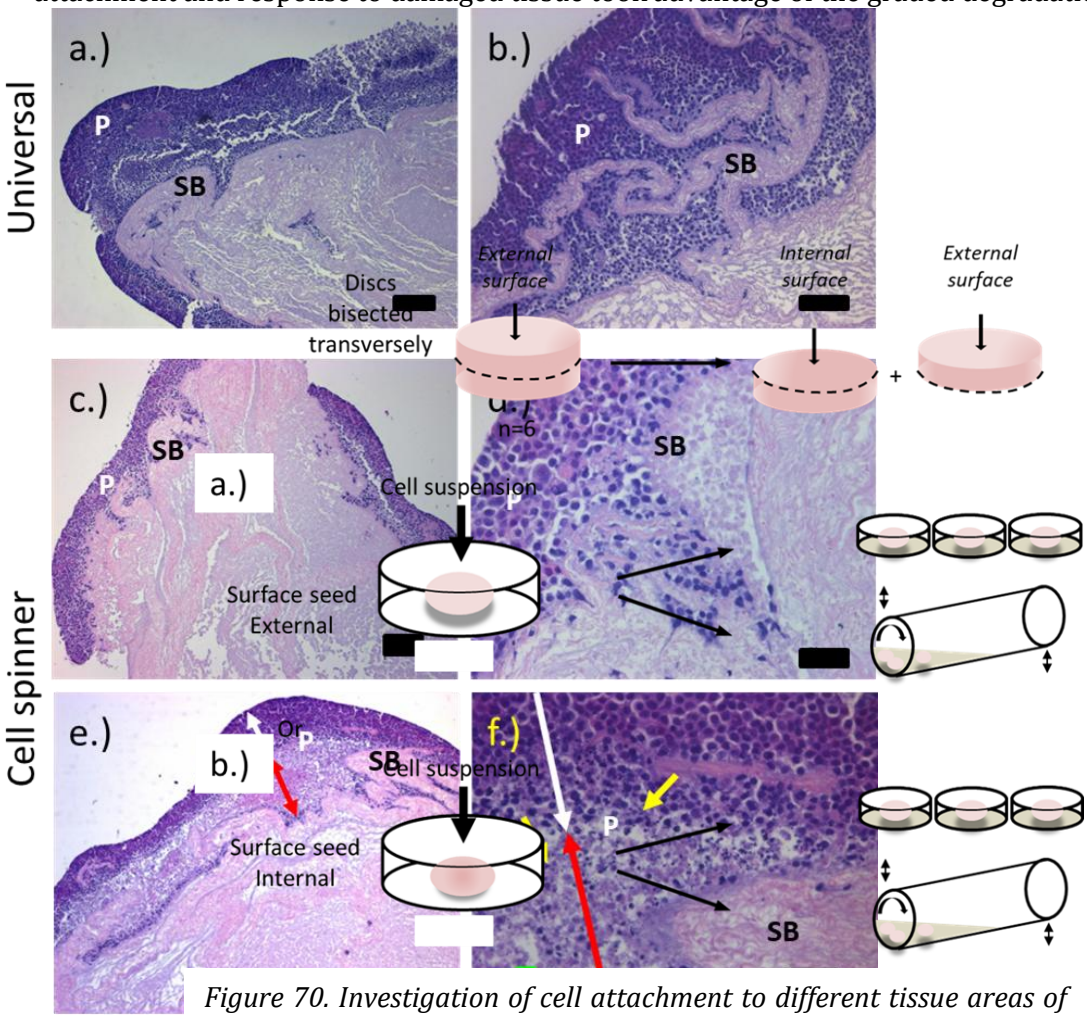

Figure 70. Investigation of cell attachment to different tissue areas of decellularised porcine liver matrices. Discs (n=6) were transversely bisected and seeded with Huh7 cells ($4x10^6$ cells.mL^{-1}, 40 µL) on either the external, or internal surfaces.

within the decellularised tissue (Figure 12), Decellularised porcine liver discs (n=6) were bisected transversely and statically seeded with Huh7 on either the external or internal disc surfaces (Section 2.2.20) for four hr. Seeded discs were cultured either statically or dynamically for 14 days, as outlined in Figure 70.

Huh7 location was assessed from sections of formalin fixed, seeded discs stained with H&E, (Sections 2.2.7.1, 2.2.16.1, 2.2.8.1 and 2.2.5.1). Thicker layers of Huh7 were present on external surfaces of the seeded discs, where tissue damage was greatest (Figure 71, a.) & b.), black arrows), when compared with the inner surfaces of the seeded discs (Figure 71, c.) & d.)). The application of dynamic culture resulted in Huh7 present within deeper regions of the periphery, at both external and internal surfaces (Figure 71b.) & d.)), with thinner cells bands noted at internal surfaces (Figure 71d.), blue arrow). Septal bands contained only minimal cell numbers, the greatest of which were seen at external surfaces of discs dynamically cultured (Figure 71c.), red arrow).

Transverse sectioning throughout the disc (detailed in Section 2.2.7.4) showed peripheral lobules containing largest cell numbers, with few cells present within septal bands (black arrows). Huh7 were present in deeper sections, thought to originate from lobules closer to the tissue periphery

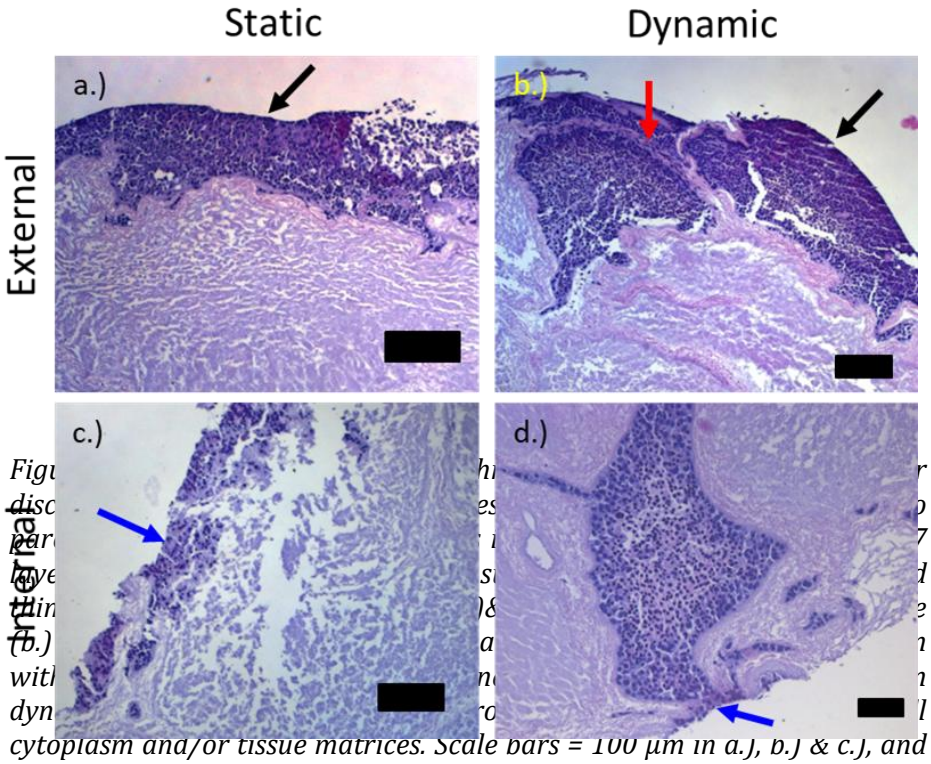

Figu… h… r
disc… es… p
par… i… 7
laye… s… d
thin…)&… e
(b.)… a… n
with… n… n
dyn… ro… l
cytoplasm and/or tissue matrices. Scale bars = 100 µm in a.), b.) & c.), and 200 µm in d.). n=3

(Figure 72). Viewing multiple sections of a 3D tissue is a limitation of this technique. Huh7 attached to the decellularised porcine liver parenchyma when the discs were bisected, but did not successfully attach when injected within the disc itself as demonstrated in previous experiments (Figure 66).

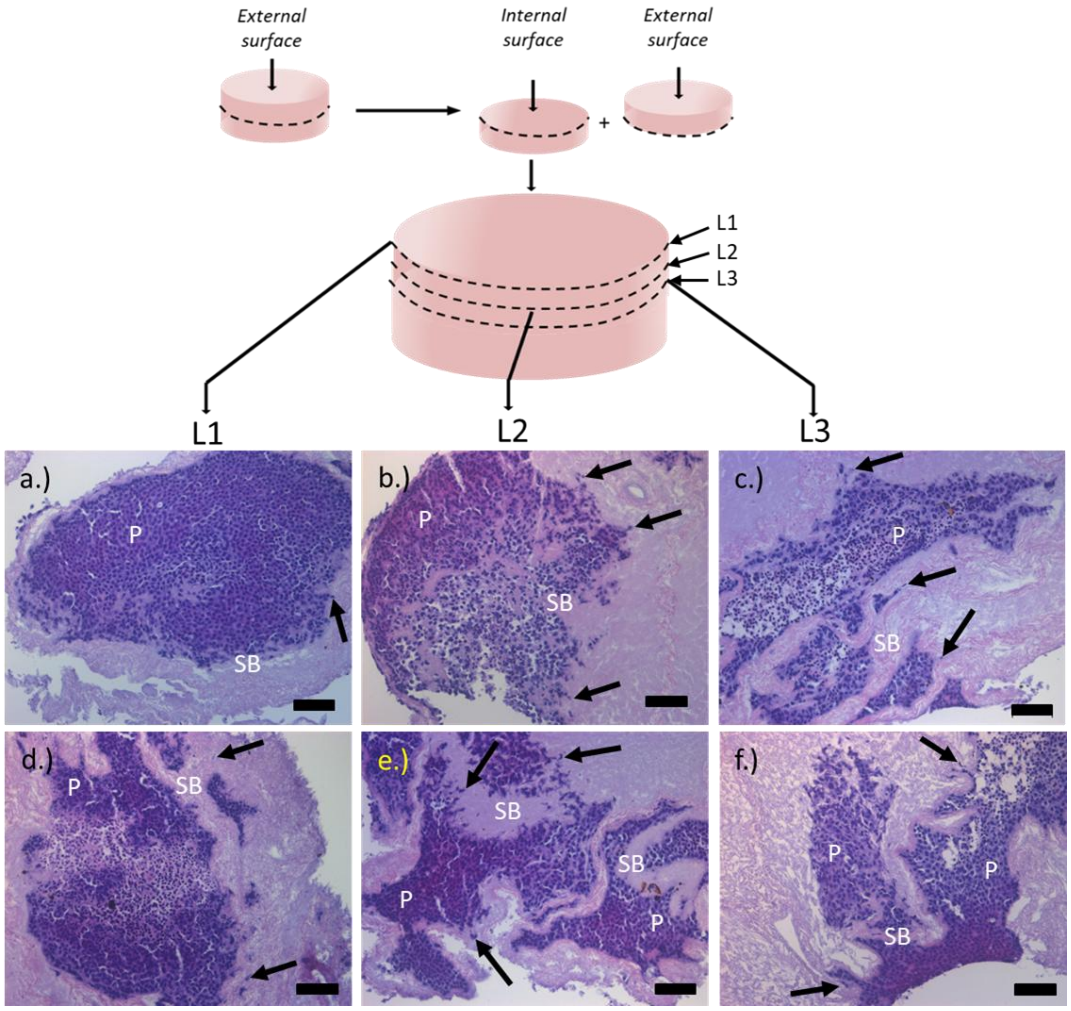

Figure 72. Huh7 attachment in transverse sections of seeded decellularised porcine liver discs, cultured for 14 days. Huh7 were present across the majority of the peripheral surface (L1, a.) & d.)) . Sections taken at deeper levels (L2, b.) & e.)) show a reduction in cell presence compared to those seen at the first level, with a further reduction seen within the third level (L3; c.) & f.)). Huh7 were attached to parenchymal tissue (P) with minimal Huh7 seen in septal bands (SB; (black arrows). Purple = cell nuclei, pink = cell cytoplasm and/or tissue matrices. Black bars represent 100 µm. Black arrows = cells penetrating septal bands. n=3

Deeper sections of seeded tissue indicate the movement of cells throughout the 3D lobules within 14 days, instead of being retained at peripheral surfaces. Huh7 are also able to attach and bind to more damaged / exposed tissue forming cell layers, with subsequent movement across the parenchymal tissue. Huh7 cells, however, have limited capability to permeate the septal bands that surround the parenchymal tissue, leading to further investigation. To

promote cell movement through the thicker septal bands, it was thought that breakdown of ECM collagen would result in loosening of the collagenous helical structure, thereby allowing cells to more easily occupy the space. A fine balance, however, would be required to minimise damage to the thinner reticular fibres within the parenchyma. Focus was placed on identification of a suitable method to open collagen fibres within the collagen bands and minimising damage to the overall lobular structure. Ingram et al (2007) investigated a novel approach to open the collagen structure of decellularised tendons using ultrasound sonication (Ingram et al., 2007). The study investigated the optimal power and pulse time required to allow for better cell penetration of tendons, with various amplitude's tested (90 W to 456 W) with repetitive pulse times of between one to three sec on, followed by one sec off, for a total of one min only. An intensity of 360W, with a pulse time of 1s resulted in a more porous structure with no reduction in collagen and GAG content or strength when compared with fresh tissue. The comparative volume of damaged collagen before and after sonification indicated retention of the collagen triple helical structure and maintenance in the distribution of collagens I and III, as determined by immunohistochemistry. In addition, subsequent seeding and culture of the sonicated scaffolds for three weeks resulted in cell distribution across the entire 1 cm^3 piece of decellularised tendon, albeit with a ~~significant~~ marked reduction in cell number and viability. Two methods to increase tissue porosity were investigated: enzymatic degradation of collagen using collagenase, versus sonication .

5.3.2.5 Experiment One: Sonication of decellularised porcine liver discs to provide better porosity for cell movement.

Experiment One explored the use of sonication. The ultra-sonicator available had a limited range of intensity, therefore, time was used as a variable whilst intensity remained constant. Decellularised porcine liver discs (n=9) were inserted into a universal containing 30 mL ice cold PBS. Decellularised porcine liver discs were pulse sonicated (one sec on and one sec off) at 300W for either two min (n=3), five min (n=3) or eight min (n=3). Collagen degradation and porosity was assessed through staining of formalin fixed sonicated discs with Picrosirius red (detailed in Section 2.2.8.4).

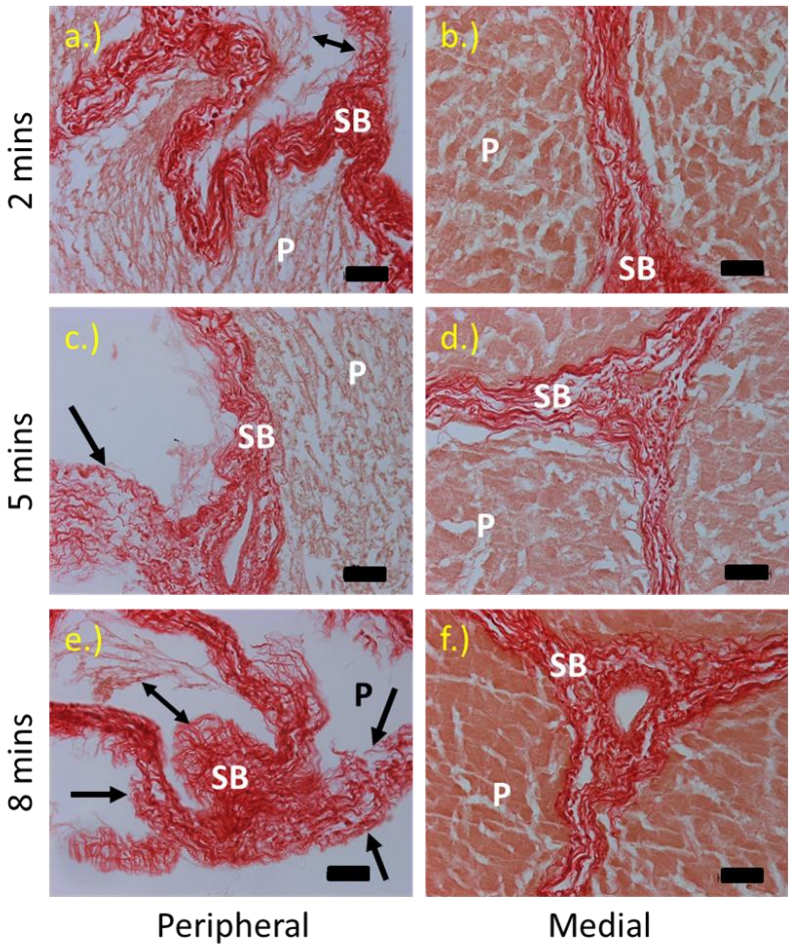

Figure 73. Assessment of damage to decellularised porcine liver discs after tissue sonication. Collagen bands show increasing amounts of damage to the reticular fibres within the parenchyma with increasing times under sonication. Greater damage was seen in peripheral regions of the decellularised porcine liver discs. Red = collagen dense material, pink = fine collagen material. SB = septal bands, P = parenchyma and black arrows = loss of parenchymal cord attachment to septal bands. . Black bars = 50 µm. n=3

Assessment of tissue degradation was made through comparing the thickness of, and spaces between, parenchymal cords, separation of the collagen within septal bands and loss of contact between parenchymal cords and septal bands. Increased damage as detailed was seen as time increased, in particular in parenchymal tissue (Figure 73). Increased detachment of the parenchyma from the septal bands was seen as damage increased (black arrows) and resulted in the separation of tissue strands and loss of

architecture, which was more pronounced in peripheral areas (Figure 73a.), c.) & e.)) than that seen in within the centre of the decellularised discs (Figure 73b.), d.) & f.)). As damage was greatest in discs sonicated for eight min, discs sonicated for two and five min were subsequently ~~sterilised~~ treated with peracetic acid (0.1 % for three hr) and seeded with Huh7. In brief, decellularised porcine liver discs (n=6) were bisected

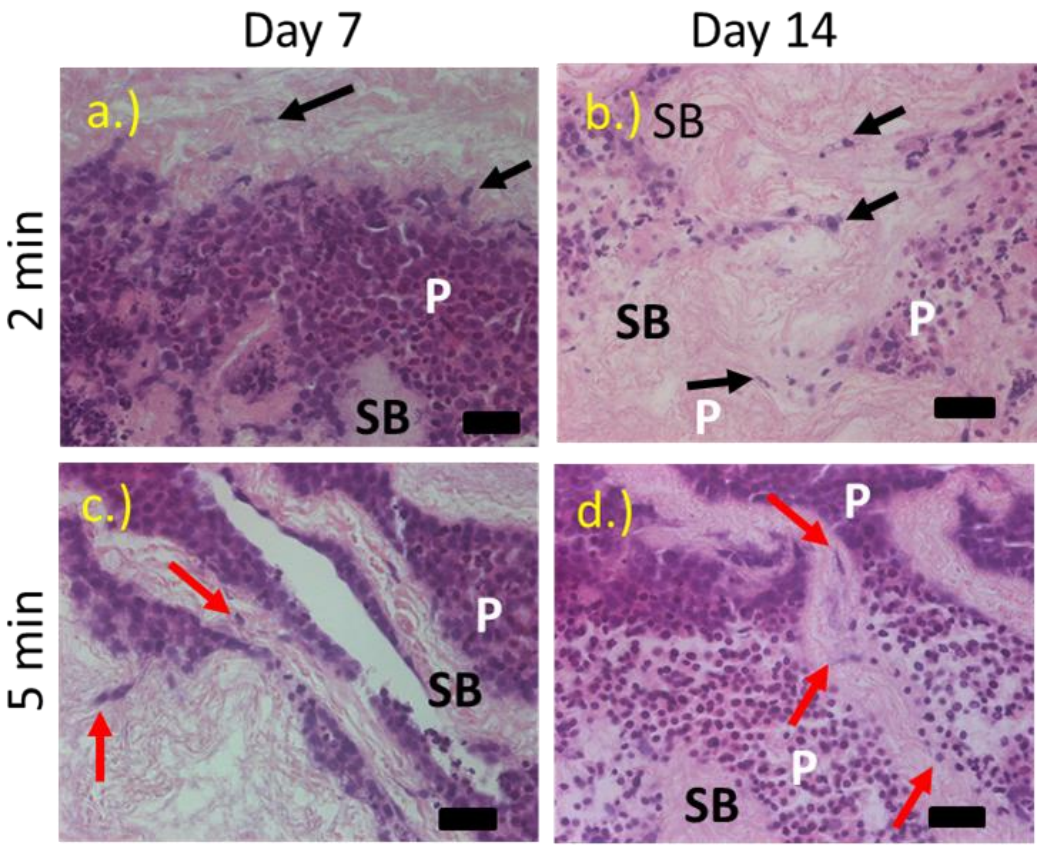

Figure 74. Huh7 distribution after seven and 14-day culture on sonicated decellularised porcine liver discs. Minimum Huh7 were present in septal bands sonicated for two min at both seven (a.)) and 14 days (b.))(black arrows), with more Huh7 present in bands at 14 days, compared with seven days. Huh7 were present at seven (c.)) and 14 days in discs sonicated for five min (d.)) also (red arrows). Greatest cell presence was seen when discs were sonicated for five min and cultured for 14 days. Scale bars = 50 µm. Purple = cell nuclei, pink = cell cytoplasm or decellularised matrices. SB = septal bands, P = parenchyma. Experiments were repeated in triplicate, with representative images shown. n=3

and seeded in cell suspension for 24 hr. Discs were dynamically

~~discs (n=6) were bisected and seeded in cell suspension for 24 hr. Discs were dynamically~~ cultured in standard media for up to 14 days, with 3 discs per universal. Three discs were removed per condition at day 7, with remaining discs removed at day 14. Media was changed daily. Assessment of cell presence within, and through,

septal bands was made on H&E stained, formalin-fixed sections of sonicated decellularised discs seeded with Huh7. Results showed the presence of Huh7 within external lobules, with small numbers of Huh7 within septal bands after seven days culture (Figure 74a.) & c.)). No ~~significant~~ apparent

difference in Huh7 movement within the septal bands was seen between two min and five min sonicated discs (Figure 74a.) & c.). Huh7 were seen at deeper areas of the septal bands after 14 days culture in discs sonicated for two and five min (Figure 74b.) & d.)), compared to those cultured for seven days (Figure 74a.) & c.). No cells were present in central disc regions (Data not shown).

5.3.2.6 Experiment Two: Collagenase treatment of decellularised porcine liver discs to provide better porosity for cell movement.

Decellularised porcine discs were exposed to three different concentrations of collagenase (0.1 mg.mL^{-1}, 0.01 mg.mL^{-1} and 0.001 mg.mL^{-1}) for 30 min at room temperature. Collagen degradation and porosity was assessed through staining of formalin fixed sonicated discs with

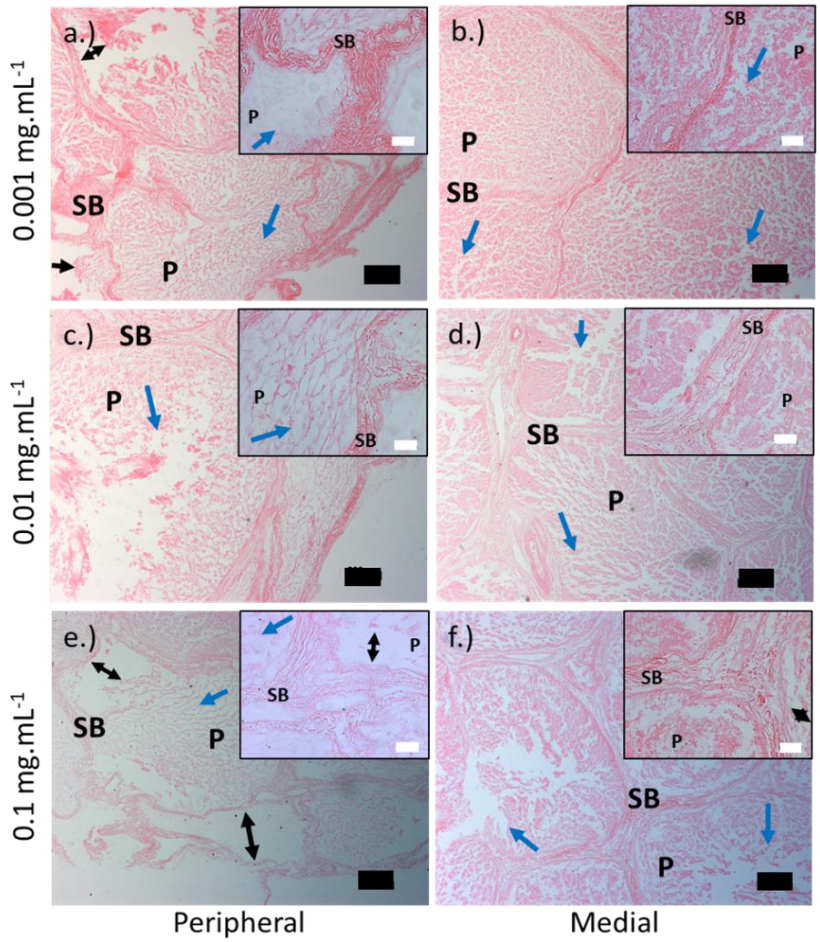

Figure 75. Tissue destruction resulting from collagenase treatment. Greater loss of tissue architecture was seen at peripheral areas (a.), b.) & c.)), compared with medial areas (b.), d.) & f.)) Tissue damage increased with increasing concentrations of collagenase (0.001 mg.mL^{-1} a.) & b.), 0.01 mg.mL^{-1} c.) & d.), 1 mg.mL^{-1} e.) & f.)). Blue arrows = tissue damage, black arrows = detachment of parenchyma from septal bands. Black scale bars = 200 µm, and white scale bars = 50 µm. Each experiment was repeated in triplicate, with representative images shown. n=3

H&E (Section 2.2.8.1). Assessment of tissue degradation was made through comparing the thickness of, and spaces between, parenchymal cords, separation of the collagen within septal

bands and loss of contact between parenchymal cords and septal bands. Greatest tissue loss was seen within peripheral areas, with complete loss of parenchyma seen in peripheral regions of the decellularised porcine liver discs (Figure 75, black arrows). Medial areas were also degraded (Figure 75b.), d.) & f.)), with loss of the connection between sinusoids and parenchymal cords, particularly within the central lobule regions, increased as collagenase concentration increased, and was seen in both peripheral and medial areas (Figure 75, blue arrows). As damage was greatest in discs treated with collagenase for 0.1 mg.mL^{-1}, with loss of peripheral parenchyma seen at this concentration, discs treated with the lowest two concentrations (0.01 mg.mL^{-1} and 0.001 mg.mL^{-1}) were subsequently ~~sterilised~~ immersed in~~with~~ peracetic acid (0.1 % for three hr), rinsed with PBS and seeded with Huh7 as described in Figure 70b.). In brief, decellularised porcine liver discs (n=6) were bisected and seeded in cell suspension for 24 hr. Discs were dynamically cultured in standard media for up to 14 days, with three discs per universal. (as detailed in Figure 70b.). Three discs were removed per condition at day seven, with remaining discs removed at day 14. Media was changed daily. Assessment of cell presence within, and through, septal

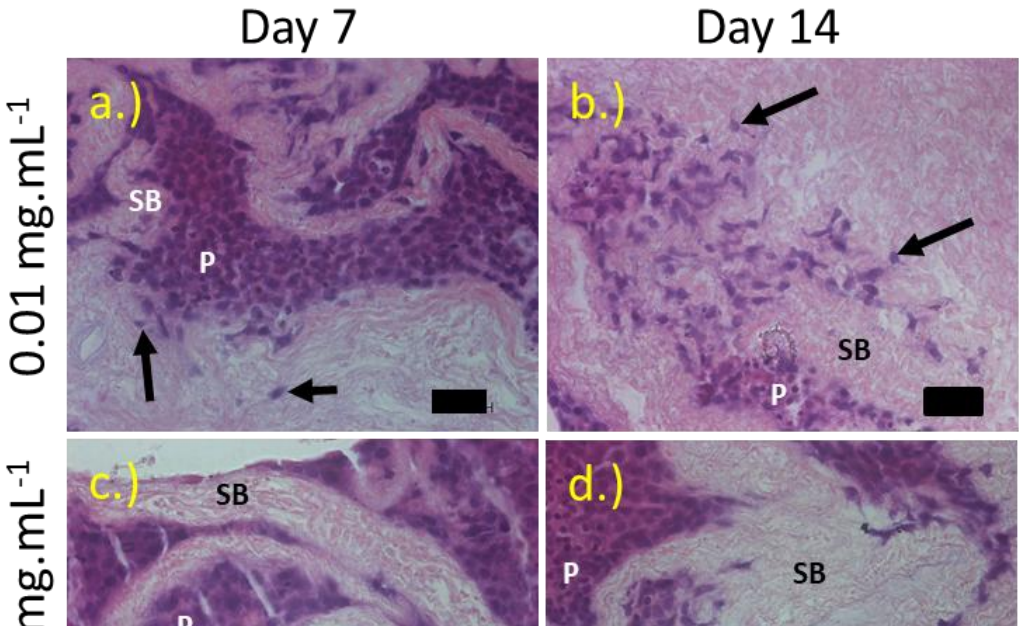

Figure 76. Huh7 distribution after seeding on to decellularised porcine liver discs for up to 14 days. Huh7 were present within the parenchyma, with some penetration within septal bands seen (black arrows). At day seven, more cells were present in septal bands exposed to collagenase at 0.01 mg.mL^{-1} (a.)) than at 0.001 mg.mL^{-1} (c.)), with more cells penetrating further into septal bands after 14 days (b.) and d.)). Black bars = 200 µm, White bars = 50 µm. Purple = cell nuclei, pink = cell cytoplasm / decellularised matrices. SB = septal bands, P = parenchyma. Black arrows = Huh7 cell movement through septal bands. Experiments were repeated in triplicate with representative images shown. n=3

bands as made on H&E stained, formalin-fixed sections of collagenase treated decellularised discs, seeded with Huh7. Greater levels of Huh7 presence within the septal bands and those lobules underlying peripheral lobules were seen on decellularised discs treated with 0.01 mg.mL-1 collagenase (Figure 76a.) & b.)) compared to those treated with 0.001 mg.mL-1 collagenase (Figure 76c.) & d.)). Multiple cells were seen within the septal bands , with those cultured for longer showing greater cell numbers (Figure 76b.) & d.)). No cells were seen within central disc lobules. It was concluded that the use of collagenase or sonication alone did not result in sufficient Huh7 presence within the septal bands initially, to show cell presence in underlying lobules within a sufficient time period of culture. Furthermore, no cells were noted in the centre of the discs with any supplementary method of degradation (data not shown), As a result, combination of both collagenase and sonication was investigated.

5.3.2.7 Experiment Three: Use of sonication and collagenase treatments on decellularised porcine liver tissue to provide better porosity for cell movement.

Decellularised porcine liver discs (n=18) were bisected and treated with 0.01 $mg.mL^{-1}$ collagenase treatment for thirty minutes at room temperature, followed by pulse sonication (cycles of one sec on and one sec off) at 360W for two min. Collagenase and sonicated discs were ~~sterilised~~ immersed in PAA (0.1 %, three hr), aseptically rinsed in sterile PBS and dynamically seeded and cultured in Huh7 suspension as described in Figure 70. Media was changed daily with seeded discs (n=3 per timepoint, per condition) were removed every seven days until 28 days culture. Cell attachment and location was assessed microscopic images of H&E stained sections of seeded discs (Sections 2.2.5.1, 2.2.8.1). Assessment of cell ~~proliferation~~ division was ~~assessed~~ made through immunohistochemically and immunofluorescent staining of tissue sections with the Ki-67 antibody (See Sections 2.2.5.3, 2.2.5.4, 2.2.9.5 and 2.2.9.7) . Assessment of cell function was made using immunohistochemical staining of tissue sections with CYP3A4 antibody~~.~~ H&E staining revealed the presence of cells within peripheral lobules, with fragility of tissues seen at days 7 and 14 in all conditions. Results indicated minimal difference between untreated discs, collagenase treated discs and collagenase and sonicated treated discs. Outer lobules were populated within seven days culture, with all treatment conditions (Figure 77a.) -c.)). Lobules containing cells showed repopulation of entire lobules by day 14 (Figure 77 d.) -f.)), however, marked tissue fragility resulted in lobule detachment from slides during staining. Huh7 repopulated lobules in tissue treated with collagenase and sonicated ~~showed~~ indicated tissue fragility at

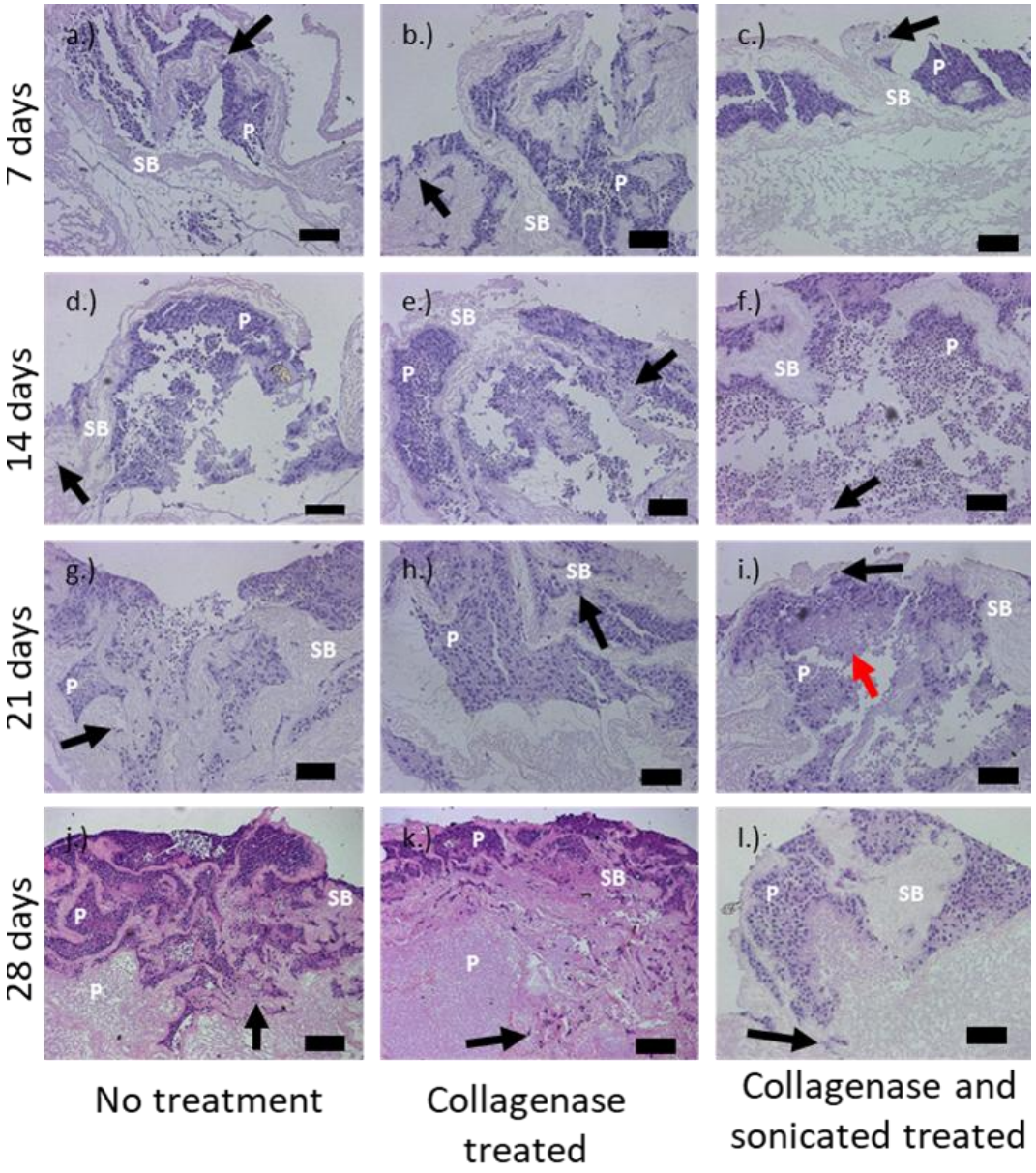

Figure 77. Huh7 cell presence and location after seeding for up to 28 days on untreated, collagenase treated and collagenase and sonicated decellularised porcine liver tissue. At day seven (a.), b.) & c.)) Huh7 were present in outer lobules, with some Huh7 present in septal bands (white arrows). At day 14, lobules containing cells showed recellularisation of entire lobules (c.), d.) & e.)), however cell detachment was present in all conditions indicating tissue fragility. At day 21, collagenase treated & no treatment seeded discs showed the presence of entire lobules reseeded with minimal tissue detachment (g.) & h.)), whereas those treated with collagenase and sonication showed cell detachment during staining. Furthermore, ghost ells were present in collagenase and sonicase treated discs (i.)). At day 28, no detachment was seen (j.), k.) & l.)). No treatment discs (j.)), collagenase treated discs (k.)) & collagenase & sonicated discs (l.)) showed similar amounts of cell penetration through the tissue, however, collagenase treated discs did not show lobular repopulation in deeper areas. .Scale bars = 200 µm on j.) & k.), Scale bars = 50 µm on a.)-i) & l.). Purple = cell nuclei, pink = cell cytoplasm or decellularised matrices. SB = septal bands, P = parenchyma. White arrows = cells in septal bands, blue arrow = ghost cells. n=3

day 21 also (Figure 77i.)). At day 28 all discs ~~showed~~ indicated the presence of Huh7 in peripheral lobules to a lesser or greater amount, with no ~~significant~~ apparent

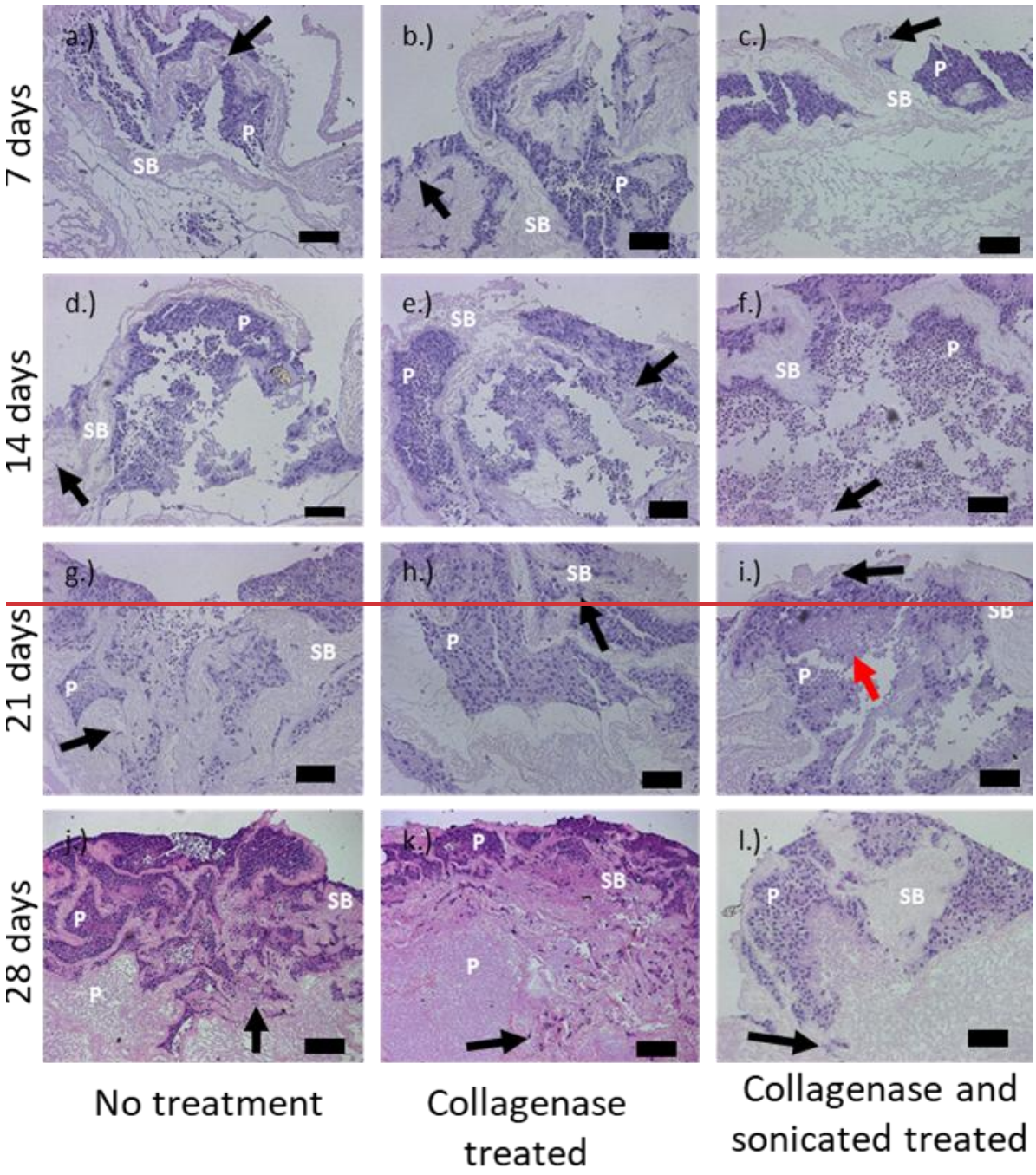

~~significant~~ increase~~enhancement~~ with or without collagenase and/or sonication (Figure 77j.) - l.)). Some Huh7 were present in septal bands at all timepoints (black arrow), with the greatest number seen after 28 days culture in collagenase treated discs (Figure 77k.). Assessment of cell ~~proliferation~~ division through immunohistochemical labelling using the Ki-67 antibody ~~showed~~ indicated Huh7 ~~significant proliferation~~ division~~of Huh7~~ throughout each timepoint (Figure 78, white arrows). ~~.~~ No ~~significant~~ relatable patterns of ~~proliferation~~ division were ~~noted~~ identified

between timepoints or treatments. Not all cells ~~were~~ indicated proliferati on~~ng~~ (Figure 78, red arrows). ~~Significant~~ Marked tissue detachment and insufficient blocking of tissues was noted at all timepoints, with multiple method reiterations applied to staining processes with no ~~significant~~ improvement in either ~~slide~~ tissue attachment, or background staining seen. CYP3A4 functional staining was also performed to assess whether attached cells ~~were~~ indicated being functional after attaching to the tissue, however, background staining was too great to effectively differentiate positive staining (data not shown). As a result of the problems with excessive background staining seen in both Ki-67 and CYP3A4 labelled sections, immunofluorescent staining of tissue sections was performed, as outlined in Section 2.2.9.6, and visualised with a fluorescent microscope (see Section 2.2.5.3) so that background fluorescence could be removed from images using levels obtained ~~using~~ from negative control tissue sections.

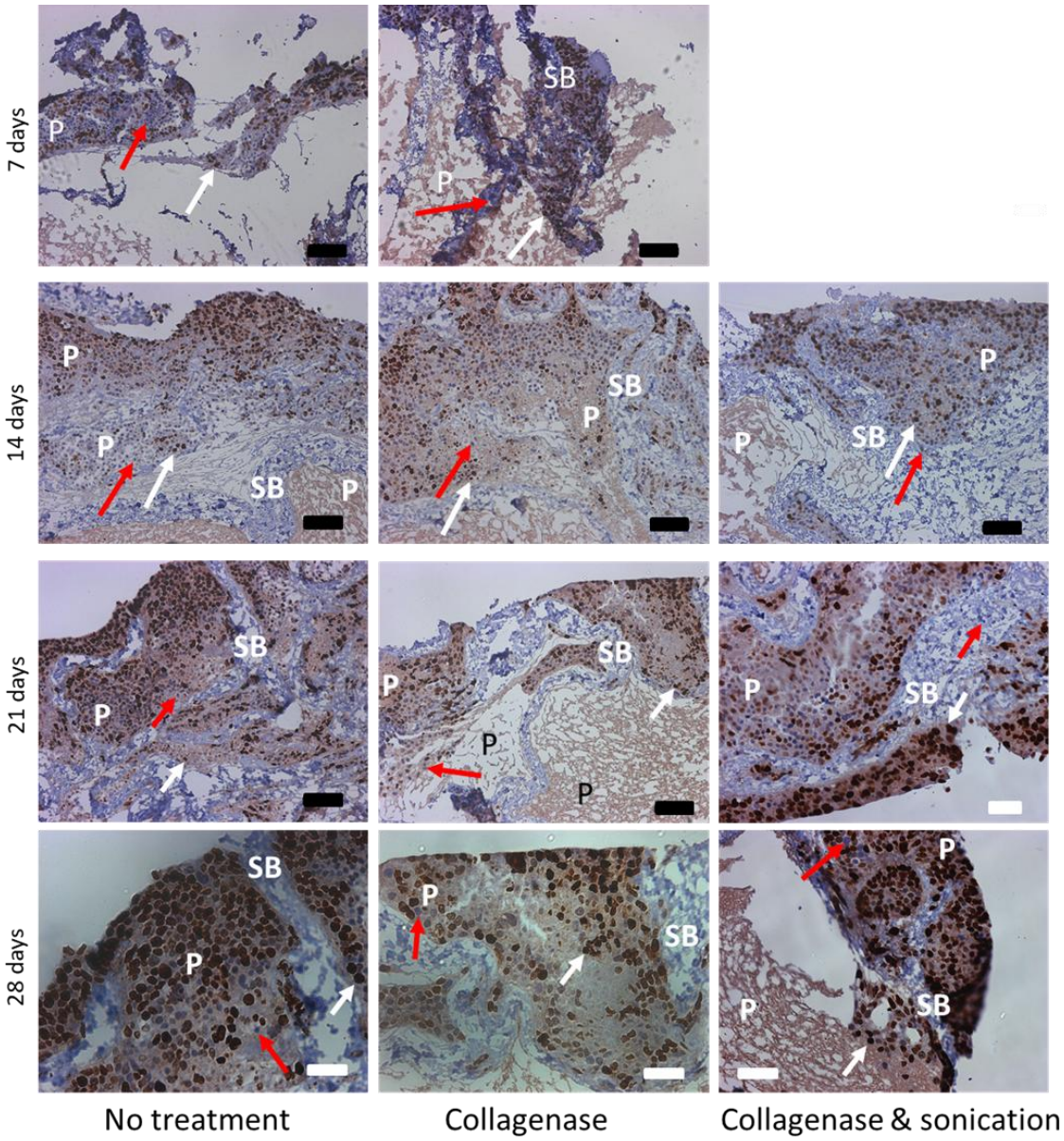

Figure 78. Huh7 proliferation after seeding on decellularised porcine liver discs over 28 days. Proliferating cells were seen at day seven (a.) to b.)) and both proliferating and non-proliferating cells were seen from day 14 onwards (c.)-k.). Loss of overall lobular structure and/or tissue detachment was seen at all timepoints, particularly after seven days culture (a.) & b.). Huh7 were present in septal bands in all timepoints and in discs treated with collagenase, collagenase and sonicated, or not treated. Dark brown – Ki-67 labelled Huh7 cells, light brown = background staining of matrices, blue = retained ECM. P = parenchyma, SB = septal band. Scale bars = 100 µm. n=1

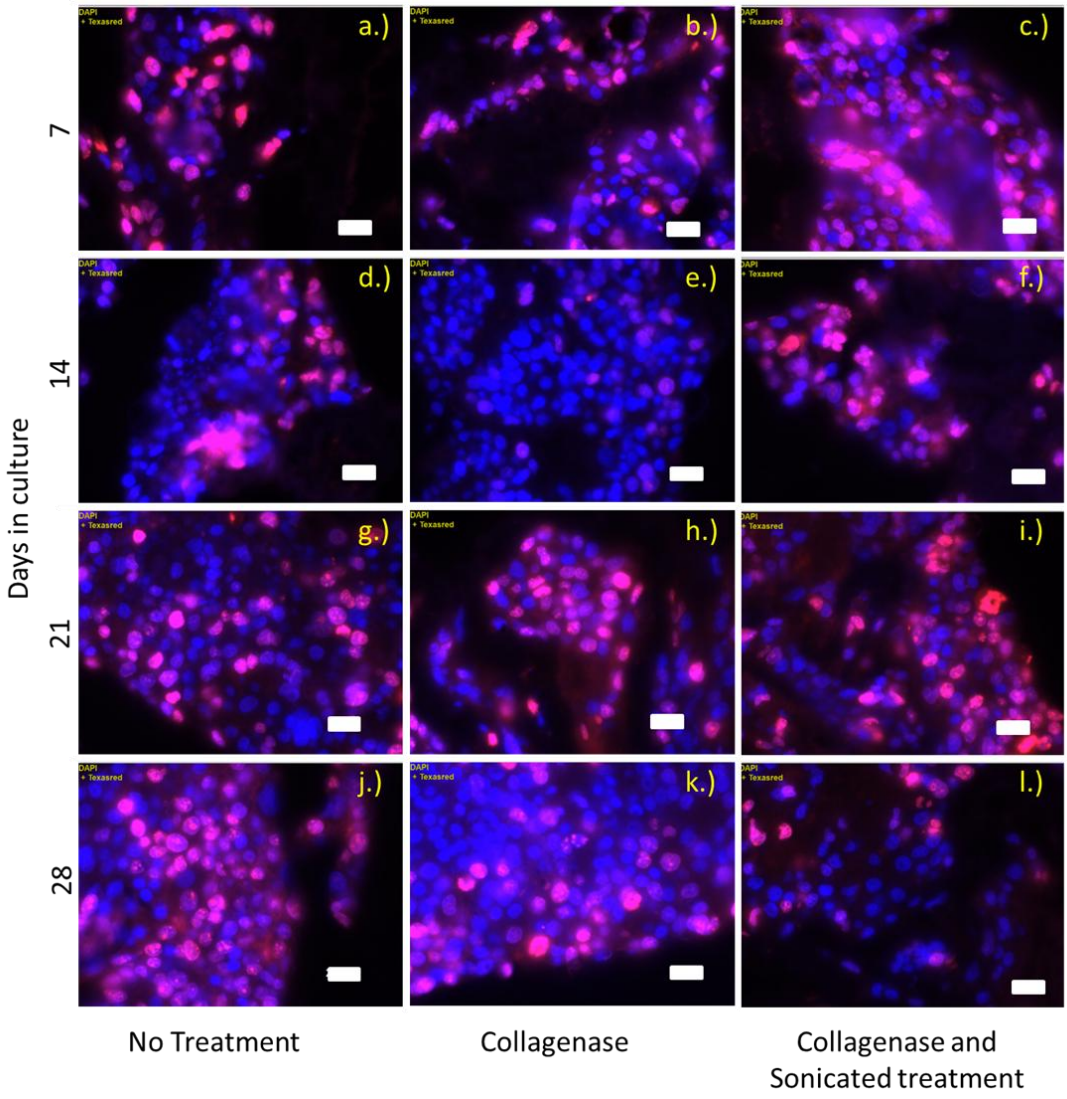

Figure 79. Ki-67 immunofluorescence labelling of Huh7– seeded on decellularised porcine liver discs. Huh7 labelled sections indicated proliferating cells~~proliferated~~ at all timepoints. In decellularised discs not treated with collagenase and/or sonication, proliferation increased across the 28-day culture period. In collagenase treated decellularised discs, reduced proliferation ~~slowed~~ was indicated at day 14 in culture. In collagenase and sonicated discs, slow reductions in proliferation rates ~~reduced at day~~were indicated ~~slowly~~ over the entire 28-day culture period. Blue = nuclei, red = Ki-67 positive regions of the nuclei. Scale bar = 20 µm. n=1

Results indicated that addition of Huh7 cells to decellularised tissue resulted in Huh7 ~~proliferation~~ division across the ~~28-day~~28-day culture period. In non-treated discs, ~~proliferation~~ rates of cell division ~~increased~~ were indicated across the 28-day culture period, with positive nuclear labelling ~~seen~~ across all timepoints. A slight decrea~~crea~~se in ~~proliferation~~ division rates occurred at day 14 in decellularised

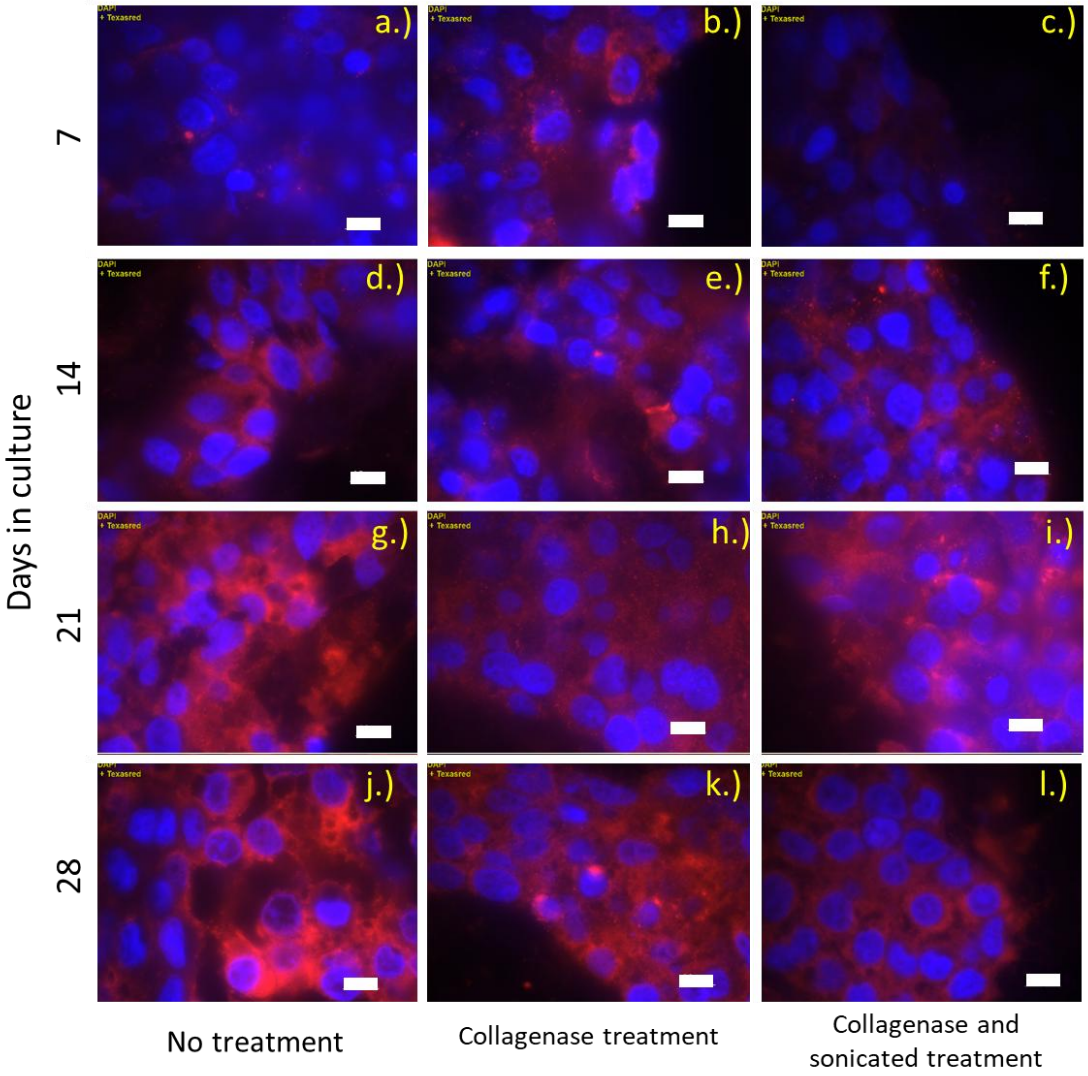

Figure 80. CYP3A4 immunofluorescent labelling of Huh7 seeded on decellularised porcine liver discs. Huh7 expressed the functional protein CYP3A4 at all timepoints in collagenase treated discs, and after 14 days culture in non-treated, and collagenase and sonicated discs after 14 days in culture. CYP3A4 labelled cells indicated increased expression ~~increased~~ across the ~~28 day~~28-day culture period in all disc groups, however, most intense staining was seen at 28-~~-~~days culture in untreated discs. Blue = nuclei, red = CYP3A4 positive regions of the nuclei. Scale bars

discs treated with collagenase. In collagenase and sonicated discs, slow reductions in ~~proliferation~~number of dividing cells ~~rates slowly reduced~~were indicated over the 28-~~-~~day culture period. Positively labelled cells w~~ere~~as~~e~~ greatest at 28-~~-~~day culture in those decellularised discs that had not been treated. When seeded on decellularised porcine liver discs, Huh7 expressed both ~~proliferative~~ divisional and functional cell markers (Ki-67 and CYP3A4 respectively). The use of collagenase

and/or sonication to increase tissue repopulation was not deemed sufficient to indicate repopulation of ~~e~~ the entire decellularised disc.

~~5.~~5.4 Discussion

Results from Chapter 3 (Figure 22) showed that HepaRG grew up to, and in contact with, decellularised porcine liver discs generated in Chapter 3. Subsequent investigations initially determined whether cells would attach to and remain viable on, the discs without DMSO. Results indicated that HepaRG remained viable for up to seven days (Figure 48), ~~proliferated~~ divided up to 14 days (Figure 61) and remained attached to the decellularised porcine liver discs for up to 35 days in culture (Figure 61), although modifications to the initial seeding and culture procedures were required to achieve 35 days. Currently only a few studies have reported successful HepaRG maintenance in 3D structures without the use of DMSO supplemented media, determined through the capability of HepaRG to ~~proliferate~~ divide and/or ~~differentiate~~function. The use of specialised hepatic maturation medium on HepaRG spheroids showed a reduction in time until differentiation occurred (nine to12 days) (Wang et al., 2019b), which is similar to the times for partial differentiation, without DMSO to occur in Chapter 4 (Sections 4.1). Nine-day culture resulted in expression of the majority of genes associated with drug metabolism, albumin and urea secretion. Low concentrations of DMSO were still used (≤0.1 %), albeit at lower levels than those used to induce differentiation of HepaRG in 2D (Cerec et al., 2007). Further investigation of biological and/or chemical media supplementation may identify factors that could enhance cell ~~proliferation~~ division or ~~differentiation~~ function as required. Epidermal growth factor, for example is associated with increased growth rates of foetal liver cells (Koyama et al., 2009) and addition of collagen to decellularised liver ECM increased cell functionality (De et al., 2024). DMSO-free 3D HepaRG culture has also been achieved using alginate encapsulated HepaRG spheroids for up to two weeks (Rebelo et al., 2015). The use of 6 x10^6 cells.mL^{-1} HepaRG embedded in alginate gels generated beads of 500-600 µm in size. Stable cell viability was shown for up to 14 days, with no change in spheroid size, indicating that HepaRG were not ~~proliferating~~ dividing or detaching. Spheroids expressed specific, but not all, functional markers including significantly increased levels of albumin and CPS (carbomyl phosphate synthetase, a protein involved in the urea cycle), comparable levels of the drug metabolism proteins PXR (pregnane X receptor) and CYP1A2, and decreased levels of drug metabolism proteins CYP3A4, CYP2C9 and the HNF-4α transcription factor compared with cells cultured on tissue culture plastic for 28 days total (with 14 days in

DMSO supplemented media) (Rebelo et al., 2015). Retention of HepaRG function implies viability within alginate embedded HepaRG spheroids. Further analysis of hepatic specific genes in HepaRG seeded discs would allow for effective comparison of HepaRG function between these two studies. HepaRG spheroids have also been embedded in collagen I matrices, although with slightly lower cell concentrations (5×10^5 cells.mL^{-1} in collagen Type I (1.5 mg.mL^{-1})). Once again, 3D culture without DMSO showed enhanced expression of functional markers (transcription factors HNF-4α, HNF-1β and functional proteins albumin, and α-fetoprotein). Data from this study shows self-organisation of HepaRG into spheroids that increase in diameter from 15-28 days culture (28 ±7 μm to 50.6 ±11.3 μm respectively) indicating cell ~~proliferation~~ division and were associated with maintenance of cell viability for the first 20 days of culture (ATP production) (Rose et al., 2022). Expression levels peaked at day six, with reductions seen thereafter, alongside the loss of cell viability after day 20, indicates that the increased levels may not be maintained after the culture period (Rose et al., 2022). Quantification of functional levels using an albumin assay, or semi-quantification using Western blots in future studies would indicate whether Huh7 cultured in decellularised porcine liver discs is maintained, increasing or decreasing over the 28-day culture period, and extension of culture times would ascertain how long cells were functional for. The study by Rose *et al.* (2022) indicates that embedding of HepaRG in collagen type I has resulted in increased proliferation, peaking at day 15, and maintenance of cell viability for up to 28 days. As c~~C~~ollagen I was also retained in the decellularised porcine liver discs, alongside retention of collagen III, and partial retention of collagen IV and laminin (Figure 27 and Figure 30), it would be expected that similar functions are retained in seeded discs generated within this Chapter. Further investigation of the variety of HepaRG functions in seeded discs generated in this Chapter would aid in comparison with the study by Rose and colleagues (2022). One further study has successfully reported maintenance of cell viability after 14 days culture, with HepaRG embedded in methacrylate gelatin (GelMa). Bioprinting of HepaRG spheroids in GelMa (100 μL, 2×10^6 cells.mL^{-1}), displayed increased E-cadherin and N-cadherin expression at day 14 (epithelial and mesenchymal cell markers respectively) and reduction in the functional marker MRP2 over the 28-day culture period. HepaRG cultured in 2D with DMSO supplemented media however, showed greater levels overall. ~~Proliferation~~ Cell division was ~~present at~~ low ~~rates~~ throughout the 28-day culture period, increasing slightly from ~10% at day three to

~20% at day 28, which was similar to HepaRG seeded until day 14 within this Chapter (Figure 61) (Cuvellier et al., 2021). This study also noted that cells would not fully differentiate within the

GelMa, unless some cell:cell contact had occurred. This is also seen in Chapter 4, where albumin was produced at day 7, where cells were beginning to contact each other, and CYP3A4 expression was seen after day 11 when multiple cell sides were in contact with neighbouring cells (Sections 4.1). Data shown by Cuvellier *et al.*(2021) and within Chapter 4 indicated the importance of cell:cell contact for differentiation to occur. With cell presence limited within deeper disc regions in this Chapter, it would be expected that seeded HepaRG would only differentiate in peripheral tissue areas where cell:cell contact was the highest. Labelling of tissue sections with a variety of functional proteins would ascertain this. Huh7 have been shown to attach to decellularised porcine liver discs generated in Chapter 3 for up to 28-days also, with positive expression of both proliferative~~on~~ (Ki-67) and functional (CYP3A4) cell markers from day seven, through to 28 (Figure 79 and Figure 80). Sufficient retention of cell viability and proliferation have also been shown in GelMa embedded Huh7 cells for up to 28 days also, with low levels of ~~proliferation~~ division seen at day 5, 10 and 14 (12%, 27% and 20% respectively)(Cuvellier et al., 2021). In comparison, markedly higher ~~proliferation~~ rates of cell division have been noted within this Chapter. Studies involving the seeding of decellularised skin and liver ($1x10^6$ cells.mL^{-1}) have indicated that better proliferation rates are seen with Huh7 encapsulation in decellularised skin, although better function was seen with equal ratio's of decellularised liver and collagen gel (bead size 600-700 µm). Huh7 cells cultured on decellularised skin or decellularised liver with collagen (1:1) were shown to ~~proliferate~~ divide for up to 14 days, with significantly higher levels of albumin expression, as well as CYP1A1 shown with decellularised liver with collagen (1:1) up to 14 days in culture (De et al., 2024). Again, further investigations of cell function in Huh7 seeded decellularised tissues over 28 days culture would isolate the range and timeline of function for effective comparison with the literature.

To achieve HepaRG attachment up to 35 days, modifications to seeding procedures were required, including the use of dynamic culture (Section 5.3.1.2), extension of seeding time (Section 5.3.1.3) and optimisation of seeding density (Section 5.3.1.4). The application of dynamic seeding and culture of both HepaRG and Huh7 resulted in deeper cell ingress than that seen with static seeding and/or culture (Figure 51. and Figure 69.), particularly seen within the parenchyma rather than the septal bands.

Previous comparison of seeding methods has involved the static seeding and dynamic seeding, through pump perfusion or multistep infusion (Soto-Gutierrez et al., 2011) has determined a greater attachment efficiency through the use of multistep infusion (86 ±5%), followed by pump perfusion (69 ±0.5%) and direct injection (12.6 ±9%), with cells initially engrafting around larger vessels and then surrounding parenchyma and resulted in higher albumin secretion and CYP1A1/1A2 activity. Our study did not support HepaRG or Huh7 injection, with limited, if any, cell attachment seen (Sections 5.2.5 and 5.3.1), and supported the low attachment rates reported after injection (Soto-Gutierrez et al., 2011). Results within the literature therefore support that found within this Chapter, indicating that direct parenchymal injection is not a suitable method to recellularise decellularised porcine liver discs. Although multi-step perfusion was not investigated in this study, further increases in cell attachment could be developed ~~through the use of~~with multi-step perfusion. Our work supports the work of others except one, with increased cell distribution also seen in studies using syringe perfusion of HepG2 cells into decellularised rat liver, resulting in significantly higher viability, growth and distribution seen when compared with static culture (Mirmalek-Sani et al., 2013, Sassi et al., 2021). One study (Lang et al., 2011)~~{Lin, 2004 #43}~~ showed a lack of ~~no~~ presence of human hepatocytes ~~primary human hepatocyte~~HepG2 penetration in discs decellularised using a water-based method. Seeding of the discs with ~~1.~~15 x10^5 cells.cm^2 (in 50 µL) ~~, calculated as 10.5 cells.mL^{-1},~~ occurred statically for three hr followed by 24 hr static culture and up to 21 days in dynamic culture on an orbital shaker (10 RPM). Although cell ~~proliferation~~ division only occurred after 14 days in culture, increased layer depth was seen in decellularised discs at day 21 in static culture conditions ~~at day~~. The delayed cell ~~proliferation~~ division and lack of cell penetration seen within this study (Lang et al., 2011)~~{Lin, 2004 #43}~~ may relate to the high cell density or the cell type used when compared to HepaRG and Huh7 cells seeded in this Chapter. Furthermore, the lack of cell penetration into the disc could have resulted from the low speed of rotation applied during culture. Variations of flow plasma rate (0.3, 1.5, 5 & 10 mL.min^{-1}) in HepaRG seeded AMC-BAL have shown that optimal media flow rates differed between function analysed, with ammonia elimination rates best at 5 mL.min^{-1}, urea production best between 1.5-10 mL.min^{-1} and CYP3A4 activity best between 5-10 mL.min^{-1}. No significant difference in APOA1 production was noted between any flow rate. Assessment of

optimal media flow for proliferation were not however investigated (Nibourg et al., 2012). Human foetal stem cells showed different rates of ~~proliferation~~ division than~~t~~ foetal hepatocytes after perfusion seeding in decellularised porcine liver (Barakat et al., 2012). Foetal stem cells also produced ECM components (fibronectin) within three days of seeding, indicating a focus more on ECM remodelling than proliferation. Immunohistochemical labelling of discs with antibodies for native matrix components would ascertain whether this has occurred with HepaRG and/or Huh7 seeded discs generated in this Chapter. The metabolic requirements of tumour cell lines differs to that of primary human hepatocytes, with certain mutations or alterations of signalling pathways such as the PI3K/Akt pathway, components of which are also involved with the Hippo signalling pathway, known to alter the uptake and metabolism of nutrients toward a proliferative state (Vander Heiden et al., 2009, Borreguero-Muñoz et al., 2019). The increased ~~proliferation~~ division and penetration seen by Huh7 cells, as opposed to HepaRG cells may be linked with different rate of glucose uptake and metabolism. Seeding of decellularised porcine liver discs with other cell types alongside more comprehensive functional assessments, would be expected to show further variation in cell penetration, distribution and activity. In this Chapter cell penetration was seen with higher rotational speeds (35 RPM). The high seeding density used by the study (Lin et al., 2004) may also have contributed to the delayed ~~proliferation~~ division seen, as results from this Chapter indicate HepaRG viability reduces when seeded at concentrations higher than 4 x10^6 cells.mL^{-1} (Figure 54), which would result in the release of cell components into the media. Interestingly, in HepG2 cultured states, proliferation marker levels (Ki-67) were highest on static 2D tissue culture plates, whereas functional marker levels (albumin, CYP1A2 and CYP3A4) were highest when dynamically cultured in 3D structures, with gene expression of HNF-4α and CYP1A2, but not albumin, significantly higher in 3D, dynamically cultured primary hepatocytes. Enhancement of cell function and viability was limited to 11 days only (Sassi et al., 2021), however, experiments within this Chapter have shown HepaRG ~~proliferation~~ division at day 14 and Huh7 ~~proliferation~~ division at day 28. Further analysis of cell function would aid in effective comparison of methods, alongside both HepaRG and/or Huh7 cell attachment at day 28. Significantly increased circumferential migration of rat MSCs seeded via pulsatile flow has also been seen in decellularised porcine carotid arteries (Sheridan et al., 2014). Comparison of the methods of flow, or flow rate were not included in this study, although variations in these factors plays an important part in cell attachment and activity. Lower volume

velocities are associated with increased cell attachment (Provin et al., 2008) and oxygen consumption rates vary according to changes in elevation, cell density, media depth and atmospheric oxygen or volume within 3D scaffolds and tissues (Al-Ani et al., 2018, Magliaro et al., 2019, Aleksandrova et al., 2016b). Further investigation of types of flow (bi-directional, oscillating, continuous etc) and flow rates in decellularised porcine liver discs would provide

further guidance to maximise cell attachment and distribution. Comparison of cell attachment between spin and rotational in HepaRG cells indicated that the increased depth of media used in the cell spinner flasks resulted in apoptosis and the formation of ghost cells in deeper disc areas (Figure 69). As a result of the larger cell spinner used, a larger volume of media was required, which in turn increased media depth. The increased depth was thought to limit oxygen diffusion through the media (Al-Ani et al., 2018) and resulted in insufficient oxygen for the seeded cells. Although such a great increase in cell media volume (6 mL to 75 mL) resulted in the formation of apoptotic bodies and ghost Huh7 cells within the decellularised discs (Figure 69), the increase from 4 mL to 6 mL in HepaRG did not. Increased volume of cell suspension (2mL) did not result in the formation of apoptotic bodies or ghost cells, with viability retained in most attached cells and better distribution across peripheral surfaces. The application of Fick's law, which relates to the diffusion of oxygen through a medium, states that oxygen diffusion is reduced by increased medium depth and increased by oxygen concentration gradient (Reviewed in (Place et al., 2017)). Further investigation of flow rates and applications could therefore be made using smaller spinner flasks or increased environmental oxygenation using small roller bottles or bioreactors (Place et al., 2017). What was evident through investigative seeding of HepaRG and Huh7 cells was that both cell types attached to parenchymal tissue to a greater amount than collagenous septal bands. Furthermore, Huh7 showed presence throughout entire lobules when cultured for only 24 hours, with limited Huh7 presence within and/or through septal bands. As limited cell movement has been found through dense tissues, such as decellularised porcine patellar tendon (Ingram et al., 2007), work focused on degradation of the quaternary structure within the septal bands. Results indicated some cell presence in the septal bands and cell presence in deeper tissue areas after 14 days dynamic culture, which increased in number after 28 days dynamic culture. No particular difference was seen between each condition. The original study by Ingram and colleagues (2007) involved investigation of pulse frequency (one to three sec on and

one sec off) as well as frequency of sonication (90W to 456W). A frequency of 360W and above resulted in opening of the spaces in collagen bundles, with higher frequencies also associated with collagen bundle damage. Cell culture on sonicated decellularised tendons showed cell attachment within one day, and penetration within collagenous matric within the centre of the 1 cm^3 scaffold, although matrix disorganisation and the matrix degradation present at day 21 was attributed to lack of mechanical stimulation and/or matrix remodelling.

Cell viability at day 21 showed central matrix disorganisation and reduced cell viability (50%). Although the application of sonication in this study (Section 5.3.2.5) resulted in no advantage in Huh7 cell presence within central disc regions, further investigation of sonication frequency may provide better understanding of septal band degradation, alongside retention of sufficient lobular structure. If this cannot be achieved, the use of other species that do not contain such thick septal bands would be associated with better disc repopulation.

Although the majority of seeding method enhancements, such as the use of dynamic culture and increased seeding time, were successful in both HepaRG and Huh7 cells, HepaRG cells did not show as much distribution within the parenchyma as that seen with Huh7 cells. This may be attributed to the type of cell. Healthy liver hepatocytes are predominantly quiescent, with most cells ~~proliferating~~ dividing only once with ~~and the remaining~~ hepatocytes either ~~proliferating~~ dividing once more, or undergoing apoptosis to reduce the risk of overexpansion (reviewed in (Campana et al., 2021)) ~~within~~. When hepatocyte proliferation is impaired, biliary epithelial cells are also able to contribute to liver regeneration and lead to duct-mediated regeneration in acute liver injury, thought to be controlled through the Hippo signalling cascade mentioned in Chapter 1. Furthermore, both cell types are also thought to be involved in liver regeneration following chronic injury, again through mechanisms involved in the Hippo signalling cascade (Reviewed in (Campana et al., 2021)). Liver damage, is associated with excessive ECM remodelling, with hepatocyte stem cells secreting high levels of ECM. It is therefore proposed that the limited cell movement seen by HepaRG, in comparison with Huh7, result from the increased secretion of ECM from the progenitor like cell type, which is not seen in the well differentiated hepatocyte derived Huh7 cell line. Further antibody labelling of matrix proteins within seeding discs would ascertain whether this is true.

~~2.~~6 General Discussion

The aim of this project was to create a decellularised porcine liver scaffold to develop procedures for the seeding and culture of ECM scaffolds and generation of a functional liver organoid. The first step was the creation of a decellularised porcine liver scaffold, in which the Leeds method, using low concentration sodium dodecyl sulphate (SDS, 0.1% v/v), hypo- and hyper-tonic solutions with nucleases, was employed. Through work summarised in Chapter 3, a decellularised porcine liver scaffold was created using 0.1 % (v/v) SDS, that retained overall ~~histioarchitecture~~histoarchitecture, including parenchymal cords, portal triad and lobular structure. Of note, was the retention of parenchymal reticular fibres (Figure 28. Reticular staining of native and decellularised porcine liver. Variation of reticular staining seen during development of staining technique (a.) to c.)) indicates significant batch variation, with batch comparison of reticular fibre retention between native (d.)) and decellularised (e.)) porcine liver showing retention of reticular fibres within the septal bands (SB) and between parenchymal cords (P). Black = Reticular fibres and nuclei (red arrow), pale pink = matrix components excluding reticular fibres, red blood cells red / dark pink. P = parenchyma, SB = septal band. Scale bars a.) b.) & c.) = 100 µm, d.) = 20 µm and e.) = 50 µm.) known to provide structural support for cellular components, particularly during wound healing (Bancroft and Gamble, 2002). Retention of reticular fibres throughout necrotic tissue repair is thought to be, or the partial reason for, rapid cellular regeneration (Monleón et al., 2022). Furthermore, initiation and/or progression of fibrotic lesion formation are associated with the loss of the reticular network (Wen et al., 2016). Cellular invasion from peripheral areas through the septal bands, is followed by dysregulated matrix production and disorganisation, with excessive collagen deposited, thickening septal bands (Monleón et al., 2022). Binding of cellular integrin β1 to collagen I leads to the activation of PAK/YAP in myofibroblasts, and therefore the Hippo pathway. Myofibroblasts produce collagen in response to environmental stimuli such as hypoxia or DAMPs (damage associated molecular patterns). Retention of the reticular fibres however has the potential to aid in guiding cell movement, and matrix remodelling. Two studies have investigated the retention of reticular fibres (Nari et al., 2013, Naeem et al., 2019), however, none have been reported in decellularised porcine liver. Both authors used~~{, 2013 #49}~~ silver staining impregnation techniques in argyrophilic reactions to

label reticular fibres dark brown / black, however, excessive background staining limited the accuracy in interpretation of the images in both rabbit (Nari et al., 2013) and rat livers (Naeem et al., 2019). ~~{, 2019 #1149}{Naeem, 2019 #1149}~~Reticular fibres were reportedly retained after perfusion decellularisation of rabbit livers using Triton X-100 (3 %), EDTA (0.05 %), EGTA (0.05%) and SDS (0.1%) (Nari et al., 2013). The decellularisation process lost all lobular structure with minimal parenchyma retained, alongside excessive non-specific staining of native tissue made true retention questionable. Retention of reticular fibres was also reported in decellularised rat livers however, images showed retention within the larger structures such as the portal and central veins, as well as the septal bands, and not within the spaces of Disse. Once again, excessive non-specific staining was noted on all reticulin stained sections, making identification of parenchymal reticular fibres difficult (Naeem et al., 2019). It is thought the retention of the fine reticular fibres detailed in Chapter 3 (Figure 28) may have been aided by the thicker septal bands present in porcine tissue, which are not present in other species. This is supported by the retention of some collagen IV and laminin within the portal triad and at the regions where the parenchyma meet the septal bands (Figure 27 and Figure 30). Advantages of the decellularisation methods developed in Chapter 3 show efficient retention of reticular fibres in the parenchyma of porcine tissue, which has not been reported in the literature. Although these fibres have been retained, current knowledge assumes that these will lead to more rapid tissue regeneration. Further study comparing decellularised porcine liver tissue with and without reticular fibres would allow us to determine whether quicker tissue regeneration is seen. Also, labelling the markers of the Hippo signalling pathway would identify the role hepatocyte binding to reticular fibres affects the signalling and remodelling process.

Differences were seen between the attachment patterns of progenitor like HepaRG and the tumour derived cell line Huh7, with HepaRG attaching to peripheral areas and ~~proliferating~~ dividing for 14 days with minimal penetration into the decellularised discs, whereas Huh7 were seen throughout entire lobular areas, in more central regions, and were shown to ~~proliferate~~ divide and/or differentiate for 28 days. What was noted on H&E staining of HepaRG was increased eosin staining intensity within and surrounding the immediate vicinity of the tissue where cells were present, and indicated the deposition of ECM components (Figure 60). As mentioned previously, tissue regeneration involves

dysregulation of the normal balance between matrix degradation and deposition. It is thought that the resulting increased eosin intensity seen may have resulted from the increased deposition of matrix by attached cells. The difference in eosin staining between non-cell containing and cell containing areas were more intense with HepaRG, than with Huh7. The biggest assumption of this theory, however, is that the increased eosin stained tissue results from increased deposition of ECM components. Future work to confirm this would directly compare staining of HepaRG seeded and Huh7 seeded sections, using specific ECM related antibodies such as collagen I or III. The resulting increase in deposition or inhibited reduction of matrix removal, would hinder cell progression and explain the limited penetration seen with HepaRG in comparison to Huh7, as well as the reported delay in ~~proliferation~~ division seen when seeding foetal hepatocyte stem cells compared with foetal hepatocytes reported in the literature (Lin et al., 2004, Barakat et al., 2012). This result highlights the importance of choosing the right cell type for decellularised tissue regeneration. For rapid cell ~~proliferation~~ division in~~of~~ organoids, tumorigenic cell types would be preferred, whereas studies of cellular regeneration and organ development would require cells with a stem or progenitor like phenotype. It is likely that the use of stem or progenitor-like cell lines would require longer timelines for successful regeneration of tissues. Seeding of BAL devices would require the use of non-stem hepatocyte types to minimise the relative deposition of matrix components known to clog membranes (MacDonald et al., 2001). Literature supports liver tissue remodelling, with the formation of fibrotic lesions regressing over time (Caligiuri et al., 2021). Although this has predominantly been investigated in myofibroblasts, increased matrix deposition, indicated within Chapter 5 (Figure 60) shows some hepatic stem cell involvement in the regenerative / wound healing response. Further investigation by seeding of other liver cell types, and co-seeding of more than one liver cell type, would provide further insight into the roles that different liver cells play in tissue regeneration. Further investigation of agents used to enhance MMP degradation or TIMP inhibition may provide a way to enhance HepaRG migration. Once sufficient cell presence has been achieved, reduction and removal of these agents would allow the matrix remodelling to take place in a controlled manner thereby providing a tailored approach to cell movement .

Overall structure was best retained within the inner areas of the tissue, with external areas showing greater loss of overall lobular structure, thinning of parenchymal cords and degradation of septal bands. The resulting difference in structural retention, however, allowed for additional analysis of the effects of tissue degradation on cell attachment. Better retained tissue showed similar attachment rates to areas of greater degradation, however, differences in cell attachment were noted between parenchyma and septal bands. Pore size is important, with polymeric scaffold pore diameters of < 104 ±4 μm being too small for HepG2 invasion and resulting in limited penetration, and those > 200 μm being similar to spaces seen on 2D surfaces (Freyman et al., 2001). Both scaffolds (Scaffold A = 104 ±4μm diameter, Scaffold B =175 ±-6 μm diameter) showed the presence of a homogenous cell layer, predominantly circumferentially surrounding the scaffold pores, with scaffold B showing more cells within pores, than scaffold A. After three days culture, larger pore sizes were associated with greater cell penetration and smaller pore sizes associated with pore coverage by cells, and no change in cell viability (8 days) were seen between HepG2 seeded scaffolds (Asthana et al., 2018). If HepaRG and Huh7 seeded in Chapter 5 were seeded at too high a density, the spatial regions that would have allowed cell ingress may have been covered by the cells initially seeded, thereby preventing any further cell ingress. Assessment of cell viability, although helpful to determine upper cell numbers, does not provide suitable assessment of cellular coverage after seeding. Future work assessing optimal cell seeding density should, therefore, include longer culture times than 48 hr so that evaluation of cell ingress can also be made.

Laminin is largely present in periportal areas of foetal liver, and absent in mature liver, with rapid hepatocyte ~~proliferation~~ division seen on laminin coated plates (Section 1.3). The loss of laminin from parenchymal areas (Figure 30) was therefore expected to result in reduced cell ~~proliferation~~division, however results from Chapter 5 (Section 5.3.1 and 5.3.2), and the literature (Barakat et al., 2012), support increased ~~proliferation~~ cell division in both HepaRG and Huh7 seeded discs. There is also evidence to support enhanced ~~proliferation~~ division of hepatic progenitor cells after chronic liver injury (Ma et al., 2022), and in laminin coated culture plates (Lorenzini et al., 2010, Hsieh et al., 2015). Investigation of the effect of different laminin isoforms on cell ~~proliferation~~ proliferation has shown increased ~~proliferation~~ division of rat hepatic progenitor cells (WB-F344 and rat oval cells) when p53 and laminin (LN-521; subunits α5, β2, γ1) interact (Ma et al., 2022). As integrins are the main receptors for

laminin in the liver (Nishiuchi et al., 2006), specific subunits for cell attachment were also investigated (Ma et al., 2022), with the binding of integrins

α6β1 and/or α3β1 with LN-521 resulting in the greatest rate of HPC ~~proliferation~~division. In addition, activation of p53 resulting from the binding of LN-521 with integrin α6β1 was shown to involve proteins that signal activation of the Hippo signalling pathway (Ma et al., 2022). Binding of integrin α1β3 to collagen and laminin within the spaces of Disse have been shown to provide mechanisms for both hepatocyte attachment, and differentiation through changes in the cellular cytoskeleton and regulation of transcription factor expression, such as HNF 1A and/or HNF4A (Olsavsky Goyak et al., 2010), which are known to be involved with liver development in a differentiation dependent manner (Lv et al., 2021, Wang et al., 2019a). Hippos signalling modulate the switching of the HNF4α transcription factor, altering embryonic gene expression and hepatocyte differentiation (Alder et al., 2014).

The application of flow during cell culture within this study focused on the differences between the use of rotational agitation, using a circular tube (6mL media, white top 30 mL universal) compared with a cell spinner containing 75 mL culture media. The difference between the two methods identified that the use of a cell spinner, rotating solutions at the same speed (35 RPM), resulted in the formation of ghost cells in lower sections of the disc. This was most likely attributed to the volume of media required to effectively use the cell spinner, rather than an investigation of the type of flow applied. Further investigation using smaller cell spinners would ascertain the optimal volume of solution that is need to effectively seed discs and further analysis of other agitative methods may identify more efficacious systems. Investigation into fibroblast seeding on decellularised human dermis indicated that the use of an orbital shaker during seeding, for example, resulted in greater penetration depth (204.8 ±111.8μm) than centrifugal agitation methods (63.5±33.4μm for 300g and 77±48.6μm for 500g) as well as greater number of penetrated cells per idealised compartment (32±11 compared with 16±9 and 27±14 respectively)(Vitacolonna et al., 2015). Centrifugal speeds were shown to have an optimal range, with centrifugal forces <300g being too small to enhance cell penetration, although speeds >300g were seen to induce cell damage (Vitacolonna et al., 2015). Investigations towards the identification of the optimal rotation speed would maximise cell penetration and

minimise cell damage. In skin these were found to be between 300g-500g, however in liver, these may be lower due to the thinner parenchymal structures present. It was further noted that the additional

use of growth factors may enhance penetration further, although the long-term effects of their use if transplanted would provide an increased risk to the patient (Vitacolonna et al., 2015). Their use may also affect results of investigations of liver regeneration or drug compatibility, which must be taken into account. Another study investigating optimal seeding efficiencies of endothelial cells on decellularised porcine urinary bladders has indicated that 6 RPH (revolutions per hr) resulted in the greatest attachment of cells to the decellularised porcine bladder, and higher speeds (30RPH and 60RPH) resulted in no cells attached. Although this study relates to seeding, and not culture of discs, it does highlight that further development of seeding and/or culture procedures is warranted to maximise cell distribution and function.

Application and development of the Leeds method resulted in the creation of decellularised porcine liver discs of up to 10 mm in diameter and 11 mm in depth that retained structural collagens, with some loss of ECM components that are reportedly required for cell adhesion, survival and migration. HepaRG and Huh7 markers for ~~proliferation~~ cell division and cell ~~cell~~ function were identified, based on changes in respective cell morphology. Furthermore, HepaRG and Huh7 cells attached to, and remained viable after seeding onto decellularised porcine liver discs. Cells predominantly attached to parenchymal tissue, with limited penetration into dense collagen septal bands. Greater attachment of cells to the discs were seen with longer time seeding (up to 24 hr vs two hr) in cell suspension.

Dynamic culture resulted in deeper cell ingress than static culture, with limited to no cell attachment seen after cell injection. HepaRG and Huh7 responded differently to the decellularised matrices, with HepaRG cells showing formation of cell layers on peripheral surfaces with minimal cell penetration, and ~~proliferating~~ division for up to two weeks in culture. Huh7, however, showed attachment to and penetration across entire lobules, and expressed both proliferative and functional markers over 28 days in culture, with results indicating differentiation.

Successful creation of a decellularised tissue is a delicate balance between removal of cellular and nuclear components, and retention of the native architecture. The only criteria currently in place is based on the lack of immunological response from DNA strands greater than 200 bp in size, with no criteria for retention of architecture,

spatial arrangement or size, or retention of attachment or growth factors (Crapo et al., 2011). As a result, multiple decellularisation procedures have been reported in the literature, with varying degrees of matrix retention in addition to a variety of seeding

practices. Work detailed throughout this study has reduced the variation in effective cell seeding practice and highlighted further avenues to explore. Additional work related to this study is outlined as follows. Successful generation of decellularised porcine liver were achieved in Chapter 3, Investigation began with assessment of the number of SDS (0.1 %) cycles needed to successfully remove whole cell nuclei. The lowest number (one) was taken forward for further analysis, although, further attempts to reduce SDS exposure were not pursued. Furthermore, other detergents such as Triton X-100 were also not pursued. With effective decellularisation being achieved it would be interesting to ascertain whether degradation could be reduced further whilst also maintaining sufficient removal of nuclear and cellular remnants. If more time was available, the reduction of detergent exposure could have been evaluated through decreasing time in solution and/or SDS concentration to minimise loss of laminin, fibronectin and collagen IV removal. Subsequent assessment of H&E stained tissue sections would be sufficient to identify changes in tissue architecture, with additional DAPI staining to ensure maintenance of whole cell nuclei removal.

Work completed in Chapter 4 supported the different morphological changes seen with proliferative and differentiated cells, with expression of markers of cell division~~proliferative~~ (Ki-67 and PCNA) and cell function~~al~~ ~~markers~~ (albumin and/or CYP3A4) supporting proliferative and differentiated phenotypes appropriately. In HepaRG cells however, literature supports an intermediate phase of partial differentiation, but not defined respective markers of this phenotype. Instead, this intermediate phase is identified ~~thought~~ through marker~~the~~ expression of both ~~proliferative~~ cell division and differentiate ~~ed markers~~ (Parent et al., 2004), as also seen in this study (Figures 42-47). Combined use of multiple markers may therefore identify characteristics of only partial differentiation from full differentiative or proliferative phenotypes. At present there is a small difference in time between albumin and CYP3A4 expression that marks the transition out of a proliferative phenotype, as albumin was found to be expressed before CYP3A4 in HepaRG cells (day seven vs day 11).

It is therefore proposed that future work related to this project would include identification of other markers of cell cycle progression in *in-vitro* cultured HepaRG cells to more effectively monitor the entire differentiative process, including this intermediary phase of partial differentiation. As control of hepatocyte ~~proliferation~~ division and differentiation relies on the Hippo signalling pathway,

recommendations of further work would focus on this pathway as cell:cell contact is associated with phosphorylation of the YAP/TAZ complex and the subsequent translocation into the cytoplasm This could be achieved through either confocal microscopy of immunofluorescently labelled cells, or Western blots. Commercially available urea and/or albumin assays would also provide numerical quantification of functional proteins over time.

Both HepaRG and Huh7 viability were monitored during cell seeding to ensure that cells were not negatively affected by attachment to the decellularised porcine liver discs. Results indicated that HepaRG remained viable for seven days (Figure 45), although subsequent culture over 28 days confirmed the presence of ~~the~~ cell ~~proliferation~~ division up to 14 days and attachment for 28 days (Figure 60 and Figure 61). In Huh7 cells, markers for both ~~proliferative~~ cell division and differentiated ~~cell markers~~ were expressed across the 28-days culture period. Assessment of cell viability using Live / dead labelling was not directly assessed after initial seeding had taken place. As a result, further recommendations to confirm long term assessment of cell viability, activity and presence of apoptosis using Live / dead cell labelling, quantification of media glucose and/or TUNEL assays are advised. Apoptosis may also be assessed through labelling of tissue sections with caspase 3, 7 and 9.

In Chapter 5, eosinophilic staining was seen where HepaRG had attached to the decellularised porcine liver parenchyma and indicated enhanced secretion and deposition of matrix proteins, or inhibition of matrix degradation (Figure 60.). This was not confirmed, as subsequent immunofluorescent staining resulted in excessive non-specific staining and/or tissue detachment. Further development of staining is therefore suggested, for example the use of immunofluorescent staining where non-specific background staining can be removed before image capture, as seen in staining of Huh7 cells (Figure 79 and Figure 80). Imaging could also be further enhanced through the use of z stacks and confocal imaging, which would allow further clarification of cell location and staining pattern within 3D environments so that cell

penetration could be semi-quantified. Variation in cell density is thought to affect cell response either through altering available oxygen and nutrient sources in the immediate cell vicinity, or through altering the level of cell:cell contact inhibition. Further investigation of cell seeding optimisation could be evaluated through repeating cell density evaluations and / or extension of cell seeding times. Results from Chapter 5 (Section 5.3) show increased numbers of attached HepaRG during extension of immersion in cell suspension, only up to 24 hr. Once again, further development to find the threshold level for attachment would involve seeding discs for longer time frames, with assessment of cell viability using Live / dead staining and confocal microscopy recommended, with cell location and/or penetration subsequently confirmed using H&E stained sections of seeded discs if required.

Seeding of Huh7 cells indicated vastly different presentation to that seen with HepaRG cells. At day 7, cells were predominantly located in the parenchyma of the most peripheral lobules, however, by day 28, cells were also present in more medial aspects. This indicated that over time, Huh7 were able to divide~~proliferate~~ and/or move in to more medial tissue parenchyma as confirmed with Ki-67 staining, although further assessment of cell movement could be made through prior call labelling with non-toxic fluorescent protein markers such as cell tracker dyes, which are passed for multiple generations to daughter cells. Longer term options include Q-trackers which are retained through successive cell cycles for longer. Other longer term cell tracking include the use of nanoparticles such as nanodiamonds, super paramagnetic iron oxide although these provide substantially more cell tracking capability than would be required and have higher costs (Ni et al., 2020). ~~.~~ This study has identified two different cell responses to the same decellularised matrices, with progenitor like HepaRG cell line displaying limited ~~proliferation~~ cell division and tissue penetration and the tumorigenic Huh7 cell line expressing markers of both cell ~~proliferation~~ division and differentiation. Understanding whether these would change over more extended time periods would require longer timeframes than 28 days. It is therefore proposed that longer culture periods should be investigated to see whether seeded cells remain viable, ~~proliferate~~ divide and/or ~~differentiate~~ become functional beyond these timeframes. For this to take place, and minimise the risk of contamination, it is proposed that the used of dynamic culture bioreactors or chambers that are able to provide suitable, continuous and

repeatable supplies of media and oxygen to seeded discs whilst minimising risk of contamination. Incorporation of Live / dead labelling of discs every 7 days would allow for contemporaneous assessment of cell viability and through formalin fixation and processing, would provide seeded discs at regular time points to ascertain expressed markers through immunofluorescent or immunohistochemical labelling of phenotype specific antibodies. Furthermore, quantification of glucose could be

made daily to monitor cell activity in a non-destructive manner, although the variation in glucose content may be to small to effectively monitor. Furthermore, labelling of specific nuclear receptor FXR and LXR would aid in the identification of cellular ~~proliferation~~ division or inhibition of the cell cycle in HepaRG respectively (Wigger et al., 2019). FXR and LXR have opposite effects on cell growth and cell cycle progression. Identification and/or quantification of the LXR and FXR nuclear receptors within the HepaRG seeded discs could highlight cell activity and ~~proliferation~~division, with the potential for LXR and FXR agonists to alter the rates of disc repopulation before becoming functional. Application of FXR, or an LXR agonist, during seeding procedures may, therefore, promote cell ~~proliferation~~ division and substantially increase cell number to allow decellularised disc repopulation before differentiation occurs, with removal of the agonist from media allowing HepaRG differentiation to occur at an appropriate moment in time (Wigger et al., 2019). Whether this could be applied to other cell types is yet to be determined. Staining for these receptors in Huh7 may help elucidate whether similar mechanisms are used between the two difference cell types. Application of multi-photon confocal microscopy, alongside fluorophore labelling of proteins of interest (Mayorca-Guiliani et al., 2019) has successfully been employed in 3D structures providing clear and detailed labelling of ECM proteins, and could be used to monitor cell penetration more effectively. Through immunofluorescent staining of over 35 different ECM proteins were successfully achieved, with two main differences noted between this study, and that used in Chapter 5. Time for staining in the study by Mayorca-Guiliani *et al.* (2019) was substantially higher (5 days) compared to immunofluorescent and immunohistochemical labelling (three to four hr) (2.2.9.5 and 2.2.9.6). Secondly the blocking agent used in this study was composed of a solution of 3 % BSA (bovine serum albumin, w/v) to PBS (phosphate buffered saline, 1x) containing 6% serum (goat or donkey depending on source of secondary antibody) that was mixed for up to 30 minutes before use. The blocking agent used within Chapter 3 was a generic pre-made,

commercially available serum-free, protein block that is compatible with primary and secondary antibodies regardless of species. Although Chapter 5 used a variety of serum (1% in PBS), this did not successfully block the background tissue. Furthermore, the immunofluorescent labelled section were viewed using a standard upright microscope (Section 2.2.5.3), and not a confocal microscope, resulting in blurred images. Further development of staining procedures focusing on blocking agents and visualisation methods is required to aid in the analysis of changes in ECM presence and/or location before and after decellularisation, and potentially after seeding has taken place.Cell seeded porcine liver discs have the potential to be used to study the normal processes of tissue growth, regeneration and wound healing. The choice of cell type for seeding is therefore critical to ensure that time is used efficiently to maximise results and truly reflect the method and cell types used to populate, heal and/or regenerate the tissue. Progenitor like cells, such as HepaRG, display remodelling responses to decellularised tissue matrices, identification of the cell signalling pathways undertaken could aid in understanding the complex interplay between activation and inhibition of the Hippo signalling pathway and the requirement for direction of cell movement. Furthermore, use of the entire decellularised disc may result in excessive background fluorescence upon tissue imaging and result in greater media use and greater risk of cell death, as a result of hypoxia. If HepaRG cells were used on thinner slices of decellularised tissue, repopulation of the entire section may be achieved using less reagents, alongside aiding in subsequent tissue imaging. Studies of cell movement may also be made using the Huh7 tumour cell line, where tissue repopulation is more likely. Both cell types could be compared to study the wound healing response in acute and chronic wounds. Currently, there are two proposed methods of cell replacement after injury: ~~proliferation~~ limited division of hepatocytes once or twice, or multiple liver stem cells ~~proliferation~~divisions~~s~~, with the second proposal taking longer to occur. These may be reflective of the use of Huh7 and HepaRG cells respectively. Current work studying wound healing involves measuring cell migration across a scratch induced gap in vitro. Similar approaches may be used with liver discs, where cell seeded tissue may be placed adjacent to, and in contact with, non-seeded tissues, with cell migration monitored over time.

Much liver injury is exacerbated by the formation of fibrotic and cirrhotic lesions. Both fibrosis and cirrhosis are characterised by dysregulation of the matrix remodelling process. The matrix remodelling process is a natural response to injury, involving tissue deposition to cover the wound (scar formation) and reorganisation of the matrix back to a functional tissue. Fibrotic lesions have been shown to regress once the injury has been removed. As HepaRG cells are thought to be involved in increased matrix deposition, or inhibition of matrix metalloproteases, studying this response in HepaRG may highlight further roles of both MMPs and TIMPs during the matrix remodelling process. This could also lead to further development of drugs that are able can minimise the formation of fibrotic and cirrhotic lesions. Excessive deposition of matrix proteins is also seen with the use of bioartificial liver devices, therefore, identification of the regulatory pathways involved in matrix secretion would aid in reducing costs in the use of seeded BAL device membranes and increase in efficacy.

One aspect not currently within scope of this study, was the effect of matrix stiffness on cell phenotype and growth. Hybrid hydrogels of varying elasticities (4%, 6%, 8%) containing HepaRG alone showed variances in cell phenotype, with 4% gels completely degraded, possibly through the lack of matrix secretion. Gels displayed greater levels of antibody relative fluorescence of HNF4α and CYP3A4 with increased hydrogel concentration (6% and 8%) and indicated cellular maturation with greater levels of elastic modulus (Lee et al., 2017). Seeding of two gels of different stiffness ~~gels~~ with Huh7 showed that stiffer gels are associated with lower levels of cell ~~proliferation~~ division and higher levels of cell function~~al levels~~ (albumin and urea secretion) than those cultured in gels of lower stiffness (Calitz et al., 2023). Huh7 and HepaRG cultured in gels of lower elasticity are therefore associated with reduced ~~proliferation~~ division and/or greater cell function. Work investigating the difference in response of the HCC cell line to scaffolds of lower and higher stiffnesses. Interestingly, Huh7 showed different mRNA expression of the transcription factor POU5F1 (POU Class 5 homeobox) also known as OCT4, which is involved in the embryonic development and stem cell pluripotency, which was not shown in HepG2 cells (Calitz et al., 2023). Both Huh7 and HepG2 grown in stiffer matrices showed increased expression of a transcription factor involved in regulation of the epithelial to mesenchymal transition (SNAI1) and is involved in cell survival and differentiation through repression of the adhesion protein E-cadherin (Calitz et al., 2023). Staining / labelling for the

transcription factor SNAI-1 is, therefore, thought to be upregulated in Huh7 cells and maintained, or downregulated in HepaRG. Further analysis of scaffold thickness may identify other proteins involved with hepatocyte, or hepatocyte cell lines differentiation. Stiffness of solid tumours are thought to be higher than surrounding non-cancerous tissues, however, this is not uniform throughout the tumour. Tumour derived cell lines have been shown to adhere to hydrogels with varying stiffnesses (soft = 1.10±0.34, medium = 4.47±1.19 and stiff = 10.61 kPa), although with displaying different cellular and cytoskeletal morphologies. Huh7 attached to soft gels were relatively round, whereas Huh7 cultured on medium and stiff gels had greater surface areas, as well as presenting with stress fibres and actin filament networks. Expression of NANOG, OCT4 and CD133, proteins associated with hepatic tumours, were higher in cells cultured on stiff gels, than those cultured on soft

gels and, the ~~proliferation~~ cell division marker Ki67 was much higher in Huh7 cultured on soft gels, compared with stiff gels (Wei et al., 2022). This is also seen in stiffness studies of non-hepatic cells, with chondroprogenitor cells (ATDC5) displaying significantly higher levels of matrix accumulation in 10% gels than that seen in 5% gels (Carrion et al., 2016). Hepatic stellate cells (HSCs) also show increased activation in decellularised rat liver of high stiffness environments, accompanied by the activation of integrin β1 and YAP, known inducers and components of the Hippo signalling pathway. This activation can be reversed in low stiffness scaffolds, although is associated with apoptosis and the inactivation of integrin β1 and YAP, which are known to be involved with the binding of the actin cytoskeleton to the extracellular matrix ~~-~~and be involved with cellular ~~proliferation~~ division respectively (Chen et al., 2023). Parenchymal areas may therefore show increased cell presence resulting from ~~proliferation~~ cell division due to lower stiffnesses in comparison to the stiffness seen in septal bands where collagen is comparatively denser. Given the studies above, and assuming that all discs decellularised in the same way have the same stiffness, the difference in HepaRG and Huh7 presence may therefore be more reflective of the cell type seeded than the disc. Furthermore, investigations of the differences between tissue types, ie hepatocytes in parenchymal cords vs septal bands of porcine liver, may result from differences in tissue stiffness as well as density. Further investigations to compare adherence and movement of varying cell line maturities within the disc would elucidate whether the difference seen results from cell maturity or cell type. Studies investigating tissue porosity, matrix

stiffness or cell movement could use lyophilised decellularised matrices that are integrated into gels of various densities, as coatings or in supplemented 3D spheroids (Lee et al., 2014) would aid in developing understanding of how cell behaviour can be modified by the environment in which it is cultured.

The progenitor like HepaRG cells showed limited cell ~~proliferation~~ division throughout the 28-day experiment (Figure 60), even though cells were still attached at day 28. Further analysis of the level of cellular differentiation would help identify whether these cells were functional, as opposed to proliferative. As reported in the literature (Chapter 1), after 14 days culture HepaRG cells adopt a semi differentiated state in which DMSO is need to push the cells through to a fully differentiated state. Chapter 4 has shown that nestin and Ki-67 expression reduces, whilst albumin, CYP3A4 and EpCAM expression rises, with day 14 showing expression of all proteins seen. Further antibody staining of the seeded decellularised material from day 14 onwards would help to ascertain whether the seeded, decellularised matrices were able to support the full or partially differentiated state seen without the use of DMSO.

6.1 Conclusions

The present study aimed to develop methodologies to generate porcine liver derived biological scaffolds, upon which liver cells can be seeded and differentiated without the requirement for DMSO supplemented media. Within this study, liver decellularised porcine scaffolds were created using 0.1 % (v/v) SDS, that retained key architectural features such as parenchymal cords and septal bands that delineate liver lobules, as well fine reticular fibres, which have not been identified so definitively before. Furthermore, the decellularised porcine liver retained portal triads within the septal bands, indicating retention of overall tissue vasculature. Although tissue sizes are greater than that seen in some other papers, questions still remain regarding what the nest size would be for each application. The non-cytotoxic decellularised tissue provided a scaffold up which cells can attach, through retention of laminin and collagen IV, and evidenced through attachment of numerous cell types including BHK, L929, as well as HepaRG and Huh7 cells. Results observed in this thesis indicate that some tissue degradation does not always correlate with the loss of cell attachment. Future development is therefore proposed to identify lower exposure times to further limit

tissue degradation and use the variety of tissue degradation states to study the effect of tissue degradation on liver cell function.

Development of seeding methods has identified that cellular injection is not currently advised due to low rates of cell attachment at injection sites, however, the application of flow provides advantages in cell attachment, coverage and location at deeper depths of the tissue. Comparison in the use of either terminally differentiated or progenitor-like cells has also indicated differences in cell behaviour that must be factored in when choosing which type of cell to seed. Progenitor-like HepaRG cells were slower to populate the tissue forming layers on the tissue surface, whereas terminally differentiated Huh7 cells were much faster and were seen throughout liver lobules. Even though the septal bands hindered cell location, evidence suggests that further comparison between the mechanisms of cell replication, attachment and/or location may highlight difference that could pinpoint how cells move, replicate or how cells maintain organ size. Further study of cell signalling related to replication and organ size would develop our understanding of organ development, wound healing and or cell movement. Development and application of the Leeds method to porcine liver has led to decellularised porcine liver scaffolds that could be applied as surface coatings to investigate hepatocyte function and viability when cultured on tissue culture plastic beyond seven days observed on collagen I coated tissue culture plates. Extended culture times on tissue culture plastic, or other membranes, may help provide a mechanism to study the secretion of matrix proteins that limit the applicability and use of liver cells on biological LAD membrane's. Knowledge of the signalling mechanisms that control matrix secretion may identify a way to reduce membrane clogging, thereby extending their functionality during use. Understanding of secretory mechanisms may also help elucidate ways of reducing the formation of cirrhotic lesions that occur in patients affected by chronic liver injury, such as long-term alcohol and/or substance misusers. Analysis of potential treatments that limit matrix secretion could reduce / remove lesion formation and therefore the burden of need for liver transplantation.

Creation of a decellularised porcine liver has therefore opened up the potential to study many avenues of research, not just in tissue formation, wound healing and repair, but also in the control of organ size. It has identified potential ways to develop our understanding of how tissue degradation may affect cell function and

has focused future developments in cell seeding procedures. It is hoped that learnings developed through this thesis can, in addition, be applied across many other tissue types than within the liver.

7 References

AL-ANI, A., TOMS, D., KONDRO, D., THUNDATHIL, J., YU, Y. & UNGRIN, M. 2018. Oxygenation in cell culture: Critical parameters for reproducibility are routinely not reported. *PLoS One,* 13**,** e0204269.

ALDER, O., CULLUM, R., KAN, A., WEI, W., YI, Y., GARSIDE, V., BILENKY, M., GRIFFITH, M., MORRISSY, A., ROBERTSON, GORDON A., THIESSEN, N., ZHAO, Y., CHEN, Q., PAN, D., JONES, STEVEN J. M., MARRA, M. & HOODLESS, P. 2014. Hippo Signaling Influences HNF4A and FOXA2 Enhancer Switching during Hepatocyte Differentiation. *Cell reports,* 9.

ALDRIDGE, A., DESAI, A., OWSTON, H., JENNINGS, L. M., FISHER, J., ROONEY, P., KEARNEY, J. N., INGHAM, E. & WILSHAW, S. P. 2018. Development and characterisation of a large diameter decellularised vascular allograft. *Cell Tissue Bank,* 19**,** 287-300.

ALEKSANDROVA, A. V., BURMISTROVA, O. A., FOMICHEVA, K. A. & SAKHAROV, D. A. 2016a. Maintenance of High Cytochrome P450 Expression in HepaRG Cell Spheroids in DMSO-Free Medium. *Bull Exp Biol Med,* 161**,** 120-4.

ALEKSANDROVA, A. V., PULKOVA, N. P., GERASIMENKO, T. N., ANISIMOV, N. Y., TONEVITSKAYA, S. A. & SAKHAROV, D. A. 2016b. Mathematical and Experimental Model of Oxygen Diffusion for HepaRG Cell Spheroids. *Bull Exp Biol Med,* 160**,** 857-60.

ASH, S. R. 1994. Hemodiabsorption in treatment of acute hepatic failure and chronic cirrhosis with ascites. *Artif Organs,* 18**,** 355-62.

ASTHANA, A., WHITE, C. M., DOUGLASS, M. & KISAALITA, W. S. 2018. Evaluation of cellular adhesion and organization in different microporous polymeric scaffolds. *Biotechnol Prog,* 34**,** 505-514.

BANCROFT, J. D. & GAMBLE, M. 2002. *Theory and practice of histological techniques,* London, Churchill Livingstone.

BAO, J., SHI, Y., SUN, H., YIN, X., YANG, R., LI, L., CHEN, X. & BU, H. 2011. Construction of a portal implantable functional tissue-engineered liver using perfusion-decellularized matrix and hepatocytes in rats. *Cell Transplant,* 20**,** 753-66.

BAPTISTA, P. M., SIDDIQUI, M. M., LOZIER, G., RODRIGUEZ, S. R., ATALA, A. & SOKER, S. 2011. The use of whole organ decellularization for the generation of a vascularized liver organoid. *Hepatology,* 53**,** 604-17.

BARAKAT, O., ABBASI, S., RODRIGUEZ, G., RIOS, J., WOOD, R. P., OZAKI, C., HOLLEY, L. S. & GAUTHIER, P. K. 2012. Use of decellularized porcine liver for engineering humanized liver organ. *J Surg Res,* 173**,** e11-25.

BHOGAL, R. H., HODSON, J., BARTLETT, D. C., WESTON, C. J., CURBISHLEY, S. M., HAUGHTON, E., WILLIAMS, K. T., REYNOLDS, G. M., NEWSOME, P. N., ADAMS, D. H. & AFFORD, S. C. 2011. Isolation of primary human hepatocytes from normal and diseased liver tissue: a one hundred liver experience. *PLoS One,* 6**,** e18222.

BORREGUERO-MUÑOZ, N., FLETCHER, G. C., AGUILAR-ARAGON, M., ELBEDIWY, A., VINCENT-MISTIAEN, Z. I. & THOMPSON, B. J. 2019. The Hippo pathway integrates PI3K-Akt signals with mechanical and polarity cues to control tissue growth. *PLoS Biol,* 17**,** e3000509.

BRAEUNING, A., ITTRICH, C., KÖHLE, C., HAILFINGER, S., BONIN, M., BUCHMANN, A. & SCHWARZ, M. 2006. Differential gene expression in periportal and perivenous mouse hepatocytes. *FEBS Journal,* 273**,** 5051-5061.

BRAITERMAN, L. T. & HUBBARD, A. L. 2009. Hepatocyte Surface Polarity: Its Dynamic Maintenance and Establishment. *The Liver.*

CALABRO, S. R., MACZUREK, A. E., MORGAN, A. J., TU, T., WEN, V. W., YEE, C., MRIDHA, A., LEE, M., D'AVIGDOR, W., LOCARNINI, S. A., MCCAUGHAN, G. W., WARNER, F. J., MCLENNAN, S. V. & SHACKEL, N. A. 2014. Hepatocyte produced matrix metalloproteinases are regulated by CD147 in liver fibrogenesis. *PLoS One,* 9**,** e90571.

CALIGIURI, A., GENTILINI, A., PASTORE, M., GITTO, S. & MARRA, F. 2021. Cellular and Molecular Mechanisms Underlying Liver Fibrosis Regression. *Cells,* 10.

CALITZ, C., ROSENQUIST, J., DEGERSTEDT, O., KHALED, J., KOPSIDA, M., FRYKNÄS, M., LENNERNÄS, H., SAMANTA, A. & HEINDRYCKX, F. 2023. Influence of extracellular matrix composition on tumour cell behaviour in a biomimetic in vitro model for hepatocellular carcinoma. *Sci Rep,* 13**,** 748.

CAMPANA, L., ESSER, H., HUCH, M. & FORBES, S. 2021. Liver regeneration and inflammation: from fundamental science to clinical applications. *Nat Rev Mol Cell Biol,* 22**,** 608-624.

CARRION, B., SOUZANCHI, M. F., WANG, V. T., TIRUCHINAPALLY, G., SHIKANOV, A., PUTNAM, A. J. & COLEMAN, R. M. 2016. The Synergistic Effects of Matrix Stiffness and Composition on the Response of Chondroprogenitor Cells in a 3D Precondensation Microenvironment. *Adv Healthc Mater,* 5**,** 1192-202.

CEREC, V., GLAISE, D., GARNIER, D., MOROSAN, S., TURLIN, B., DRENOU, B., GRIPON, P., KREMSDORF, D., GUGUEN-GUILLOUZO, C. & CORLU, A. 2007. Transdifferentiation of hepatocyte-like cells from the human hepatoma HepaRG cell line through bipotent progenitor. *Hepatology,* 45**,** 957-67.

CHEN, G., DENG, Y., XIA, B. & LV, Y. 2023. In Situ Regulation and Mechanisms of 3D Matrix Stiffness on the Activation and Reversion of Hepatic Stellate Cells. *Adv Healthc Mater,* 12**,** e2202560.

CHEN, Y., LI, J., LIU, X., ZHAO, W., WANG, Y. & WANG, X. 2010. Transplantation of immortalized human fetal hepatocytes prevents acute liver failure in 90% hepatectomized mice. *Transplant Proc,* 42**,** 1907-14.

CHOI, S., SAINZ, B., JR., CORCORAN, P., UPRICHARD, S. & JEONG, H. 2009. Characterization of increased drug metabolism activity in dimethyl sulfoxide (DMSO)-treated Huh7 hepatoma cells. *Xenobiotica,* 39**,** 205-17.

CLEMENT, B., GUGUEN-GUILLOUZO, C., CAMPION, J. P., GLAISE, D., BOUREL, M. & GUILLOUZO, A. 1984. Long-term co-cultures of adult human hepatocytes with rat liver epithelial cells: modulation of albumin secretion and accumulation of extracellular material. *Hepatology,* 4**,** 373-80.

COVIDIEN. 2015. *Permacol(TM) Surgical Implant* [Online]. Available: http://www.covidien.com/surgical/products/hernia-repair/permacol-surgical-implant [Accessed 29 July 2015].

CRAPO, P. M., GILBERT, T. W. & BADYLAK, S. F. 2011. An overview of tissue and whole organ decellularization processes. *Biomaterials,* 32**,** 3233-3243.

CUOMO, R. 2020. Submuscular and Pre-pectoral ADM Assisted Immediate Breast Reconstruction: A Literature Review. *Medicina,* 56**,** 256.

CURCIO, E., SALERNO, S., BARBIERI, G., DE BARTOLO, L., DRIOLI, E. & BADER, A. 2007. Mass transfer and metabolic reactions in hepatocyte spheroids cultured in rotating wall gas-permeable membrane system. *Biomaterials,* 28**,** 5487-97.

CUVELLIER, M., EZAN, F., OLIVEIRA, H., ROSE, S., FRICAIN, J. C., LANGOUËT, S., LEGAGNEUX, V. & BAFFET, G. 2021. 3D culture of HepaRG cells in GelMa and its application to bioprinting of a multicellular hepatic model. *Biomaterials,* 269**,** 120611.

DASH, A., INMAN, W., HOFFMASTER, K., SEVIDAL, S., KELLY, J., OBACH, R. S., GRIFFITH, L. G. & TANNENBAUM, S. R. 2009. Liver tissue engineering in the evaluation of drug safety. *Expert Opin Drug Metab Toxicol,* 5**,** 1159-74.

DE BRUYN, T., CHATTERJEE, S., FATTAH, S., KEEMINK, J., NICOLAÏ, J., AUGUSTIJNS, P. & ANNAERT, P. 2013. Sandwich-cultured hepatocytes: utility for in vitro exploration of hepatobiliary drug disposition and drug-induced hepatotoxicity. *Expert Opin Drug Metab Toxicol,* 9**,** 589-616.

DE KOCK, J., CEELEN, L., DE SPIEGELAERE, W., CASTELEYN, C., CLAES, P., VANHAECKE, T. & ROGIERS, V. 2011. Simple and quick method for whole-liver decellularization: a novel in vitro three-dimensional bioengineering tool? *Arch Toxicol,* 85**,** 607-12.

DE, S., VASUDEVAN, A., TRIPATHI, D. M., KAUR, S. & SINGH, N. 2024. A decellularized matrix enriched collagen microscaffold for a 3D in vitro liver model. *J Mater Chem B,* 12**,** 772-783.

DIFFLEY, M., TANG, A., SAWAR, K., AL-SAGHIR, T., GONTE, M. R., HALL, J., TEPPER, D., DARIAN, V., EVANGELISTA, M. & ATISHA, D. 2025. Comparative Postoperative Complications of Acellular Dermal Matrix and Mesh Use in Prepectoral and Subpectoral One-Stage Direct to Implant Reconstruction: A Retrospective Cohort Study. *Ann Plast Surg,* 94**,** 521-527.

DUNN, J. C., TOMPKINS, R. G. & YARMUSH, M. L. 1991. Long-term in vitro function of adult hepatocytes in a collagen sandwich configuration. *Biotechnol Prog,* 7**,** 237-45.

DUNN, J. C., YARMUSH, M. L., KOEBE, H. G. & TOMPKINS, R. G. 1989. Hepatocyte function and extracellular matrix geometry: long-term culture in a sandwich configuration. *FASEB J,* 3**,** 174-7.

EDWARDS, C. A. & O'BRIEN, W. D., JR. 1980. Modified assay for determination of hydroxyproline in a tissue hydrolyzate. *Clin Chim Acta,* 104**,** 161-7.

ELAUT, G., PAPELEU, P., VINKEN, M., HENKENS, T., SNYKERS, S., VANHAECKE, T. & ROGIERS, V. 2006. Hepatocytes in suspension. *Methods Mol Biol,* 320**,** 255-63.

ELLIS, A. J., HUGHES, R. D., WENDON, J. A., DUNNE, J., LANGLEY, P. G., KELLY, J. H., GISLASON, G. T., SUSSMAN, N. L. & WILLIAMS, R. 1996. Pilot-controlled trial of the extracorporeal liver assist device in acute liver failure. *Hepatology,* 24**,** 1446-1451.

FARNDALE, R. W., BUTTLE, D. J. & BARRETT, A. J. 1986. Improved quantitation and discrimination of sulphated glycosaminoglycans by use of dimethylmethylene blue. *Biochimica et Biophysica Acta (BBA) - General Subjects,* 883**,** 173-177.

FERRINI, J. B., PICHARD, L., DOMERGUE, J. & MAUREL, P. 1997. Long-term primary cultures of adult human hepatocytes. *Chem Biol Interact,* 107**,** 31-45.

FISHER, J. I., E BOOTH, C. 2002. *Decellularisation of tissue implant material*. UK patent application GB0112586.3.

FOX, I. J., CHOWDHURY, J. R., KAUFMAN, S. S., GOERTZEN, T. C., CHOWDHURY, N. R., WARKENTIN, P. I., DORKO, K., SAUTER, B. V. & STROM, S. C. 1998. Treatment of the Crigler-Najjar syndrome type I with hepatocyte transplantation. *N Engl J Med,* 338**,** 1422-6.

FRASER, J. R., LAURENT, T. C. & LAURENT, U. B. 1997. Hyaluronan: its nature, distribution, functions and turnover. *J Intern Med,* 242**,** 27-33.

FREYMAN, T. M., YANNAS, I. V. & GIBSON, L. J. 2001. Cellular materials as porous scaffolds for tissue engineering. *Progress in Materials Science,* 46**,** 273-282.

FUKUMITSU, K., YAGI, H. & SOTO-GUTIERREZ, A. 2011. Bioengineering in Organ Transplantation: Targeting the Liver. *Transplantation Proceedings,* 43**,** 2137-2138.

GEBHARDT, R. 1992. Metabolic zonation of the liver: regulation and implications for liver function. *Pharmacol Ther,* 53**,** 275-354.

GILBERT, T. W., SELLARO, T. L. & BADYLAK, S. F. 2006. Decellularization of tissues and organs. *Biomaterials,* 27**,** 3675-83.

GIORDANO, P., PULLAN, R. D., YSTGAARD, B., GOSSETTI, F., BRADBURN, M., MCKINLEY, A. J., SMART, N. J. & DANIELS, I. R. 2015. The use of an acellular porcine dermal collagen implant in the repair of complex abdominal wall defects: a European multicentre retrospective study. *Tech Coloproctol,* 19**,** 411-7.

GLICKLIS, R., SHAPIRO, L., AGBARIA, R., MERCHUK, J. C. & COHEN, S. 2000. Hepatocyte behavior within three-dimensional porous alginate scaffolds. *Biotechnol Bioeng,* 67**,** 344-53.

GODOY, P., HEWITT, N. J., ALBRECHT, U., ANDERSEN, M. E., ANSARI, N., BHATTACHARYA, S., BODE, J. G., BOLLEYN, J., BORNER, C., BOTTGER, J., BRAEUNING, A., BUDINSKY, R. A., BURKHARDT, B., CAMERON, N. R., CAMUSSI, G., CHO, C. S., CHOI, Y. J., CRAIG ROWLANDS, J., DAHMEN, U., DAMM, G., DIRSCH, O., DONATO, M. T., DONG, J., DOOLEY, S., DRASDO, D., EAKINS, R., FERREIRA, K. S., FONSATO, V., FRACZEK, J., GEBHARDT, R., GIBSON, A., GLANEMANN, M., GOLDRING, C. E., GOMEZ-LECHON, M. J., GROOTHUIS, G. M., GUSTAVSSON, L., GUYOT, C., HALLIFAX, D., HAMMAD, S., HAYWARD, A., HAUSSINGER,

D., HELLERBRAND, C., HEWITT, P., HOEHME, S., HOLZHUTTER, H. G., HOUSTON, J. B., HRACH, J., ITO, K., JAESCHKE, H., KEITEL, V., KELM, J. M., KEVIN PARK, B., KORDES, C., KULLAK-UBLICK, G. A., LECLUYSE, E. L., LU, P., LUEBKE-WHEELER, J., LUTZ, A., MALTMAN, D. J., MATZ-SOJA, M., MCMULLEN, P., MERFORT, I., MESSNER, S., MEYER, C., MWINYI, J., NAISBITT, D. J., NUSSLER, A. K., OLINGA, P., PAMPALONI, F., PI, J., PLUTA, L., PRZYBORSKI, S. A., RAMACHANDRAN, A., ROGIERS, V., ROWE, C., SCHELCHER, C., SCHMICH, K., SCHWARZ, M., SINGH, B., STELZER, E. H., STIEGER, B., STOBER, R., SUGIYAMA, Y., TETTA, C., THASLER, W. E., VANHAECKE, T., VINKEN, M., WEISS, T. S., WIDERA, A., WOODS, C. G., XU, J. J., YARBOROUGH, K. M. & HENGSTLER, J. G. 2013. Recent advances in 2D and 3D in vitro systems using primary hepatocytes, alternative hepatocyte sources and non-parenchymal liver cells and their use in investigating mechanisms of hepatotoxicity, cell signaling and ADME. *Arch Toxicol,* 87**,** 1315-530.

GODOY, P., SCHUG, M., BAUER, A. & HENGSTLER, J. G. 2010. Reversible manipulation of apoptosis sensitivity in cultured hepatocytes by matrix-mediated manipulation of signaling activities. *Methods Mol Biol,* 640**,** 139-55.

GOMEZ-LECHON, M. J., JOVER, R., DONATO, T., PONSODA, X., RODRIGUEZ, C., STENZEL, K. G., KLOCKE, R., PAUL, D., GUILLEN, I., BORT, R. & CASTELL, J. V. 1998. Long-term expression of differentiated functions in hepatocytes cultured in three-dimensional collagen matrix. *J Cell Physiol,* 177**,** 553-62.

GÓMEZ-LECHÓN, M. J., TOLOSA, L., CONDE, I. & DONATO, M. T. 2014. Competency of different cell models to predict human hepatotoxic drugs. *Expert Opin Drug Metab Toxicol,* 10**,** 1553-68.

GRIPON, P., RUMIN, S., URBAN, S., LE SEYEC, J., GLAISE, D., CANNIE, I., GUYOMARD, C., LUCAS, J., TREPO, C. & GUGUEN-GUILLOUZO, C. 2002. Infection of a human hepatoma cell line by hepatitis B virus. *Proc Natl Acad Sci U S A,* 99**,** 15655-60.

GUGUEN-GUILLOUZO, C., CLEMENT, B., BAFFET, G., BEAUMONT, C., MOREL-CHANY, E., GLAISE, D. & GUILLOUZO, A. 1983. Maintenance and reversibility of active albumin secretion by adult rat hepatocytes co-cultured with another liver epithelial cell type. *Exp Cell Res,* 143**,** 47-54.

GUGUEN-GUILLOUZO, C. & GUILLOUZO, A. 2010. General review on in vitro hepatocyte models and their applications. *Methods Mol Biol,* 640**,** 1-40.

GUIDOTTI, L. G. & CHISARI, F. V. 2006. Immunobiology and pathogenesis of viral hepatitis. *Annu Rev Pathol,* 1**,** 23-61.

GUILLOUZO, A., CORLU, A., ANINAT, C., GLAISE, D., MOREL, F. & GUGUEN-GUILLOUZO, C. 2007. The human hepatoma HepaRG cells: a highly differentiated model for studies of liver metabolism and toxicity of xenobiotics. *Chem Biol Interact,* 168**,** 66-73.

GUO, L., DIAL, S., SHI, L., BRANHAM, W., LIU, J., FANG, J. L., GREEN, B., DENG, H., KAPUT, J. & NING, B. 2011. Similarities and differences in the expression of drug-metabolizing enzymes between human hepatic cell lines and primary human hepatocytes. *Drug Metab Dispos,* 39**,** 528-38.

GUTMANN, M., STIMPFL, E., LANGMANN, G., KOUDELKA, H., MIR-KARNER, B. & GRASL-KRAUPP, B. 2023. Differentiated and non-differentiated HepaRG™ cells: A possible in-vitro model system for early hepatocarcinogenesis and non-genotoxic carcinogens. *Toxicol Lett,* 390**,** 15-24.

HAKEEM, A. R. 2018. *Production and Characterisation of Acellular Human Liver Matrix: Potential Auxiliary Liver Graft.* University of Leeds.

HALL, W. D., HURST, J. W. & WALKER, H. K. 1990. *Clinical methods: the history, physical and laboratory examinations,* Boston; London, Butterworths.

HALON, A., PATRZALEK, D. & RABCZYNSKI, J. 2006. Hepatic steatosis in liver transplant donors: rare phenomenon or common feature of donor population? *Transplant Proc,* 38**,** 193-5.

HALPERN, K. B., SHENHAV, R., MATCOVITCH-NATAN, O., TÓTH, B., LEMZE, D., GOLAN, M., MASSASA, E. E., BAYDATCH, S., LANDEN, S., MOOR, A. E., BRANDIS, A., GILADI, A., STOKAR-AVIHAIL, A., DAVID, E., AMIT, I. & ITZKOVITZ, S. 2017. Single-cell spatial

reconstruction reveals global division of labour in the mammalian liver. *Nature,* 542**,** 352-356.

HANSEN, L. K., WILHELM, J. & FASSETT, J. T. 2006. Regulation of hepatocyte cell cycle progression and differentiation by type I collagen structure. *Curr Top Dev Biol,* 72**,** 205-36.

HENKENS, T., PAPELEU, P., ELAUT, G., VINKEN, M., ROGIERS, V. & VANHAECKE, T. 2007. Trichostatin A, a critical factor in maintaining the functional differentiation of primary cultured rat hepatocytes. *Toxicol Appl Pharmacol,* 218**,** 64-71.

HIGGINS, G. M. A., R.M. 1931. Experimental pathology of Liver. I. Restoration of liver of the white rat following partial surgical removal. *Archives of Pathology,* 12**,** 186-202.

HOGG, P., ROONEY, P., LEOW-DYKE, S., BROWN, C., INGHAM, E. & KEARNEY, J. N. 2015. Development of a terminally sterilised decellularised dermis. *Cell Tissue Bank,* 16**,** 351-9.

HSIAO, C. T., CHENG, H. W., HUANG, C. M., LI, H. R., OU, M. H., HUANG, J. R., KHOO, K. H., YU, H. W., CHEN, Y. Q., WANG, Y. K., CHIOU, A. & KUO, J. C. 2017. Fibronectin in cell adhesion and migration via N-glycosylation. *Oncotarget,* 8**,** 70653-70668.

HSIEH, W. C., MACKINNON, A. C., LU, W. Y., JUNG, J., BOULTER, L., HENDERSON, N. C., SIMPSON, K. J., SCHOTANUS, B., WOJTACHA, D., BIRD, T. G., MEDINE, C. N., HAY, D. C., SETHI, T., IREDALE, J. P. & FORBES, S. J. 2015. Galectin-3 regulates hepatic progenitor cell expansion during liver injury. *Gut,* 64**,** 312-21.

HUANG, X., HUANG, Z., GAO, W., GAO, W., HE, R., LI, Y., CRAWFORD, R., ZHOU, Y., XIAO, L. & XIAO, Y. 2022. Current Advances in 3D Dynamic Cell Culture Systems. *Gels,* 8.

HUSSEIN, K. H., PARK, K. M., TEOTIA, P. K., HONG, S. H., YANG, S. R., PARK, S. M., AHN, C. & WOO, H. M. 2013a. Sterilization using electrolyzed water highly retains the biological properties in tissue-engineered porcine liver scaffold. *Int J Artif Organs,* 36**,** 781-92.

HUSSEIN, K. H., PARK, K. M., TEOTIA, P. K., YANG, J. W., KIM, H. M., HONG, S. H., YANG, S. R., PARK, I. C., PARK, S. M. & WOO, H. M. 2013b. Fabrication of a biodegradable xenoantigen-free rat liver scaffold for potential drug screening applications. *Transplant Proc,* 45**,** 3092-6.

INAMORI, M., MIZUMOTO, H. & KAJIWARA, T. 2009. An approach for formation of vascularized liver tissue by endothelial cell-covered hepatocyte spheroid integration. *Tissue Eng Part A,* 15**,** 2029-37.

INGRAM, J. H., KOROSSIS, S., HOWLING, G., FISHER, J. & INGHAM, E. 2007. The use of ultrasonication to aid recellularization of acellular natural tissue scaffolds for use in anterior cruciate ligament reconstruction. *Tissue Eng,* 13**,** 1561-72.

IREDALE, J. P. 1997. Tissue inhibitors of metalloproteinases in liver fibrosis. *Int J Biochem Cell Biol,* 29**,** 43-54.

ISOM, H. C., SECOTT, T., GEORGOFF, I., WOODWORTH, C. & MUMMAW, J. 1985. Maintenance of differentiated rat hepatocytes in primary culture. *Proc Natl Acad Sci U S A,* 82**,** 3252-6.

JALAN, R., SEN, S., STEINER, C., KAPOOR, D., ALISA, A. & WILLIAMS, R. 2003. Extracorporeal liver support with molecular adsorbents recirculating system in patients with severe acute alcoholic hepatitis. *J Hepatol,* 38**,** 24-31.

JIANG, W. C., CHENG, Y. H., YEN, M. H., CHANG, Y., YANG, V. W. & LEE, O. K. 2014. Cryo-chemical decellularization of the whole liver for mesenchymal stem cells-based functional hepatic tissue engineering. *Biomaterials,* 35**,** 3607-17.

JONES, G., HERBERT, A., BERRY, H., EDWARDS, J. H., FISHER, J. & INGHAM, E. 2017. Decellularization and Characterization of Porcine Superflexor Tendon: A Potential Anterior Cruciate Ligament Replacement. *Tissue Eng Part A,* 23**,** 124-134.

JUNGERMANN, K. & KIETZMANN, T. 2000. Oxygen: modulator of metabolic zonation and disease of the liver. *Hepatology,* 31**,** 255-60.

KAJBAFZADEH, A. M., JAVAN-FARAZMAND, N., MONAJEMZADEH, M. & BAGHAYEE, A. 2013. Determining the optimal decellularization and sterilization protocol for preparing a tissue scaffold of a human-sized liver tissue. *Tissue Eng Part C Methods,* 19**,** 642-51.

KANG, L.-I., MARS, W. M. & MICHALOPOULOS, G. K. 2012. Signals and cells involved in regulating liver regeneration. *Cells,* 1**,** 1261-1292.

KELLY, Y. M., ZARINSEFAT, A., TAVAKOL, M., SHUI, A. M., HUANG, C. Y. & ROBERTS, J. P. 2022. Consent to organ offers from public health service "Increased Risk" donors decreases time to transplant and waitlist mortality. *BMC Med Ethics,* 23**,** 20.

KERN, A., BADER, A., PICHLMAYR, R. & SEWING, K. F. 1997. Drug metabolism in hepatocyte sandwich cultures of rats and humans. *Biochem Pharmacol,* 54**,** 761-72.

KIERNAN, F. 1833. The Anatomy and Physiology of the Liver. *Philosophical Transactions of the Royal Society of London,* 123**,** 711-770.

KIM, M., LEE, J. Y., JONES, C. N., REVZIN, A. & TAE, G. 2010. Heparin-based hydrogel as a matrix for encapsulation and cultivation of primary hepatocytes. *Biomaterials,* 31**,** 3596-603.

KOIVUSALO, A. M., VAKKURI, A., HOCKERSTEDT, K. & ISONIEMI, H. 2005. Experience of Mars therapy with and without transplantation in 101 patients with liver insufficiency. *Transplant Proc,* 37**,** 3315-7.

KOYAMA, T., EHASHI, T., OHSHIMA, N. & MIYOSHI, H. 2009. Efficient proliferation and maturation of fetal liver cells in three-dimensional culture by stimulation of oncostatin M, epidermal growth factor, and dimethyl sulfoxide. *Tissue Eng Part A,* 15**,** 1099-107.

KULAKOV, A. *Functions of Cells and Human Body* [Online]. Available: http://fblt.cz/en/skripta/ix-travici-soustava/5-jatra-a-biotransformace-xenobiotik/ [Accessed 28 Jan 2015].

KULAR, J. K., BASU, S. & SHARMA, R. I. 2014. The extracellular matrix: Structure, composition, age-related differences, tools for analysis and applications for tissue engineering. *J Tissue Eng,* 5**,** 2041731414557112.

LANDRY, J., BERNIER, D., OUELLET, C., GOYETTE, R. & MARCEAU, N. 1985. Spheroidal aggregate culture of rat liver cells: histotypic reorganization, biomatrix deposition, and maintenance of functional activities. *J Cell Biol,* 101**,** 914-23.

LANG, R., STERN, M. M., SMITH, L., LIU, Y., BHARADWAJ, S., LIU, G., BAPTISTA, P. M., BERGMAN, C. R., SOKER, S., YOO, J. J., ATALA, A. & ZHANG, Y. 2011. Three-dimensional culture of hepatocytes on porcine liver tissue-derived extracellular matrix. *Biomaterials,* 32**,** 7042-52.

LECLUYSE, E. L., AUDUS, K. L. & HOCHMAN, J. H. 1994. Formation of extensive canalicular networks by rat hepatocytes cultured in collagen-sandwich configuration. *Am J Physiol,* 266**,** C1764-74.

LEE, H. J., SON, M. J., AHN, J., OH, S. J., LEE, M., KIM, A., JEUNG, Y. J., KIM, H. G., WON, M., LIM, J. H., KIM, N. S., JUNG, C. R. & CHUNG, K. S. 2017. Elasticity-based development of functionally enhanced multicellular 3D liver encapsulated in hybrid hydrogel. *Acta Biomater,* 64**,** 67-79.

LEE, J. S., SHIN, J., PARK, H. M., KIM, Y. G., KIM, B. G., OH, J. W. & CHO, S. W. 2014. Liver extracellular matrix providing dual functions of two-dimensional substrate coating and three-dimensional injectable hydrogel platform for liver tissue engineering. *Biomacromolecules,* 15**,** 206-18.

LEE, W., CHO, N. J., XIONG, A., GLENN, J. S. & FRANK, C. W. 2010. Hydrophobic nanoparticles improve permeability of cell-encapsulating poly(ethylene glycol) hydrogels while maintaining patternability. *Proc Natl Acad Sci U S A,* 107**,** 20709-14.

LEGENDRE, A., BAUDOIN, R., ALBERTO, G., PAULLIER, P., NAUDOT, M., BRICKS, T., BROCHETON, J., JACQUES, S., COTTON, J. & LECLERC, E. 2013. Metabolic characterization of primary rat hepatocytes cultivated in parallel microfluidic biochips. *J Pharm Sci,* 102**,** 3264-76.

LI, H. L., LI, Q. Y., JIN, M. J., LU, C. F., MU, Z. Y., XU, W. Y., SONG, J., ZHANG, Y. & ZHANG, S. Y. 2021. A review: hippo signaling pathway promotes tumor invasion and metastasis by regulating target gene expression. *J Cancer Res Clin Oncol,* 147**,** 1569-1585.

LIFECELL 2015. Alloderm(R).

LIN, P., CHAN, W. C., BADYLAK, S. F. & BHATIA, S. N. 2004. Assessing porcine liver-derived biomatrix for hepatic tissue engineering. *Tissue Eng,* 10**,** 1046-53.

LIU, Y. 2022. Study Liver Cytochrome P450 3A4 Inhibition and Hepatotoxicity Using DMSO-Differentiated HuH-7 Cells. *Methods Mol Biol,* 2474**,** 39-46.

LORENZINI, S., BIRD, T. G., BOULTER, L., BELLAMY, C., SAMUEL, K., AUCOTT, R., CLAYTON, E., ANDREONE, P., BERNARDI, M., GOLDING, M., ALISON, M. R., IREDALE, J. P. & FORBES, S. J. 2010. Characterisation of a stereotypical cellular and extracellular adult liver progenitor cell niche in rodents and diseased human liver. *Gut,* 59**,** 645-54.

LU, W. Y., BIRD, T. G., BOULTER, L., TSUCHIYA, A., COLE, A. M., HAY, T., GUEST, R. V., WOJTACHA, D., MAN, T. Y., MACKINNON, A., RIDGWAY, R. A., KENDALL, T., WILLIAMS, M. J., JAMIESON, T., RAVEN, A., HAY, D. C., IREDALE, J. P., CLARKE, A. R., SANSOM, O. J. & FORBES, S. J. 2015. Hepatic progenitor cells of biliary origin with liver repopulation capacity. *Nat Cell Biol,* 17**,** 971-983.

LUO, J., KOROSSIS, S. A., WILSHAW, S.-P., JENNINGS, L. M., FISHER, J. & INGHAM, E. 2014a. Development and Characterization of Acellular Porcine Pulmonary Valve Scaffolds for Tissue Engineering. *Tissue Engineering. Part A,* 20**,** 2963-2974.

LUO, J., KOROSSIS, S. A., WILSHAW, S. P., JENNINGS, L. M., FISHER, J. & INGHAM, E. 2014b. Development and characterization of acellular porcine pulmonary valve scaffolds for tissue engineering. *Tissue Eng Part A,* 20**,** 2963-74.

LV, D.-D., ZHOU, L.-Y. & TANG, H. 2021. Hepatocyte nuclear factor 4α and cancer-related cell signaling pathways: a promising insight into cancer treatment. *Experimental & Molecular Medicine,* 53**,** 8-18.

MA, M., HUA, S., MIN, X., WANG, L., LI, J., WU, P., LIANG, H., ZHANG, B., CHEN, X. & XIANG, S. 2022. p53 positively regulates the proliferation of hepatic progenitor cells promoted by laminin-521. *Signal Transduct Target Ther,* 7**,** 290.

MACDONALD, J. M., WOLFE, S. P., ROY-CHOWDHURY, I., KUBOTA, H. & REID, L. M. 2001. Effect of flow configuration and membrane characteristics on membrane fouling in a novel multicoaxial hollow-fiber bioartificial liver. *Ann N Y Acad Sci,* 944**,** 334-43.

MACSWEEN, R. N. M. 1994. *Pathology of the liver,* Edinburgh, Churchill Livingstone.

MAGGI, U., DE CARLIS, L., YIU, D., COLLEDAN, M., REGALIA, E., ROSSI, G., ANGRISANI, M., CONSONNI, D., FORNONI, G., PICCOLO, G. & DEFEO, T. M. 2020. The impact of the COVID-19 outbreak on liver transplantation programs in Northern Italy. *Am J Transplant,* 20**,** 1840-1848.

MAGLIARO, C., MATTEI, G., IACOANGELI, F., CORTI, A., PIEMONTE, V. & AHLUWALIA, A. 2019. Oxygen Consumption Characteristics in 3D Constructs Depend on Cell Density. *Frontiers in Bioengineering and Biotechnology,* 7.

MALARKEY, D. E., JOHNSON, K., RYAN, L., BOORMAN, G. & MARONPOT, R. R. 2005. New insights into functional aspects of liver morphology. *Toxicol Pathol,* 33**,** 27-34.

MANSILLA, E., DRAGO, H., STURLA, F., BOSSI, S., SALAS, E., MARIN, G. H., IBAR, R. & SORATTI, C. 2007. Matrix superhighways configurations: new concepts for complex organ regeneration. *Transplant Proc,* 39**,** 2431-3.

MARION, M. J., HANTZ, O. & DURANTEL, D. 2010. The HepaRG cell line: biological properties and relevance as a tool for cell biology, drug metabolism, and virology studies. *Methods Mol Biol,* 640**,** 261-72.

MARTINEZ-HERNANDEZ, A. & AMENTA, P. S. 1993. The hepatic extracellular matrix. I. Components and distribution in normal liver. *Virchows Arch A Pathol Anat Histopathol,* 423**,** 1-11.

MARTINEZ-HERNANDEZ, A. & AMENTA, P. S. 1995. The extracellular matrix in hepatic regeneration. *FASEB J,* 9**,** 1401-10.

MARTINI, F. 2006. *Fundamentals of Anatomy and Physiology: International Edition*, Pearson Education, Limited.

MATSUMURA, K. N., GUEVARA, G. R., HUSTON, H., HAMILTON, W. L., RIKIMARU, M., YAMASAKI, G. & MATSUMURA, M. S. 1987. Hybrid bioartificial liver in hepatic failure: preliminary clinical report. *Surgery,* 101**,** 99-103.

MATTEI, G., DI PATRIA, V., TIRELLA, A., ALAIMO, A., ELIA, G., CORTI, A., PAOLICCHI, A. & AHLUWALIA, A. 2014. Mechanostructure and composition of highly reproducible decellularized liver matrices. *Acta Biomater,* 10**,** 875-82.

MAYORCA-GUILIANI, A. E., WILLACY, O., MADSEN, C. D., RAFAEVA, M., ELISABETH HEUMÜLLER, S., BOCK, F., SENGLE, G., KOCH, M., IMHOF, T., ZAUCKE, F., WAGENER, R., SASAKI, T., ERLER, J. T. & REUTEN, R. 2019. Decellularization and antibody staining of mouse tissues to map native extracellular matrix structures in 3D. *Nat Protoc,* 14**,** 3395-3425.

MCCLELLAND, R., WAUTHIER, E., URONIS, J. & REID, L. 2008. Gradients in the liver's extracellular matrix chemistry from periportal to pericentral zones: influence on human hepatic progenitors. *Tissue Eng Part A,* 14**,** 59-70.

MEHTA, V., KARNAM, G. & MADGULA, V. 2024. Liver-on-chips for drug discovery and development. *Mater Today Bio,* 27**,** 101143.

MENG, Z., MOROISHI, T. & GUAN, K. L. 2016. Mechanisms of Hippo pathway regulation. *Genes Dev,* 30**,** 1-17.

MICHALOPOULOS, G. K. 2007. Liver regeneration. *J Cell Physiol,* 213**,** 286-300.

MICHALOPOULOS, G. K. 2014. Advances in liver regeneration. *Expert Rev Gastroenterol Hepatol***,** 1-11.

MICHALOPOULOS, G. K. & DEFRANCES, M. C. 1997. Liver regeneration. *Science,* 276**,** 60-6.

MILLIS, J. M., CRONIN, D. C., JOHNSON, R., CONJEEVARAM, H., CONLIN, C., TREVINO, S. & MAGUIRE, P. 2002. Initial experience with the modified extracorporeal liver-assist device for patients with fulminant hepatic failure: system modifications and clinical impact. *Transplantation,* 74**,** 1735-46.

MIRMALEK-SANI, S. H., SULLIVAN, D. C., ZIMMERMAN, C., SHUPE, T. D. & PETERSEN, B. E. 2013. Immunogenicity of decellularized porcine liver for bioengineered hepatic tissue. *Am J Pathol,* 183**,** 558-65.

MOGHE, P. V., BERTHIAUME, F., EZZELL, R. M., TONER, M., TOMPKINS, R. G. & YARMUSH, M. L. 1996. Culture matrix configuration and composition in the maintenance of hepatocyte polarity and function. *Biomaterials,* 17**,** 373-85.

MOGHE, P. V., COGER, R. N., TONER, M. & YARMUSH, M. L. 1997. Cell-cell interactions are essential for maintenance of hepatocyte function in collagen gel but not on matrigel. *Biotechnol Bioeng,* 56**,** 706-11.

MONLEÓN, E., LUCÍA, Ó., GÜEMES, A., LÓPEZ-ALONSO, B., ARRIBAS, D., SARNAGO, H., HERNAEZ, A., BURDÍO, J. M. & JUNQUERA, C. 2022. Liver tissue remodeling following ablation with irreversible electroporation in a porcine model. *Front Vet Sci,* 9**,** 1014648.

MUELLER, D., TASCHER, G., MÜLLER-VIEIRA, U., KNOBELOCH, D., NUESSLER, A. K., ZEILINGER, K., HEINZLE, E. & NOOR, F. 2011. In-depth physiological characterization of primary human hepatocytes in a 3D hollow-fiber bioreactor. *J Tissue Eng Regen Med,* 5**,** e207-18.

NAEEM, E. M., SAJAD, D., TALAEI-KHOZANI, T., KHAJEH, S., AZARPIRA, N., ALAEI, S., TANIDEH, N., REZA, T. M. & RAZBAN, V. 2019. Decellularized liver transplant could be recellularized in rat partial hepatectomy model. *J Biomed Mater Res A,* 107**,** 2576-2588.

NAKABAYASHI, H., TAKETA, K., MIYANO, K., YAMANE, T. & SATO, J. 1982. Growth of Human Hepatoma Cell Lines with Differentiated Functions in Chemically Defined Medium. 42**,** 3858-3863.

NARI, G. A., CID, M., COMIN, R., REYNA, L., JURI, G., TABORDA, R. & SALVATIERRA, N. A. 2013. Preparation of a three-dimensional extracellular matrix by decellularization of rabbit livers. *Rev Esp Enferm Dig,* 105**,** 138-143.

NHSBT. 2024. *Annual Report on Liver Transplantation 2023/2024. NHS Blood and Transplant* [Online]. Available: https://nhsbtdbe.blob.core.windows.net/umbraco-assets-corp/34641/nhsbt-liver-transplantation-report-2324.pdf [Accessed 12th December 2024].

NI, J. S., LI, Y., YUE, W., LIU, B. & LI, K. 2020. Nanoparticle-based Cell Trackers for Biomedical Applications. *Theranostics,* 10**,** 1923-1947.

NIBOURG, G. A., BOER, J. D., VAN DER HOEVEN, T. V., ACKERMANS, M. T., VAN GULIK, T. M., CHAMULEAU, R. A. & HOEKSTRA, R. 2012. Perfusion flow rate substantially contributes to the performance of the HepaRG-AMC-bioartificial liver. *Biotechnol Bioeng,* 109**,** 3182-8.

NISHIUCHI, R., TAKAGI, J., HAYASHI, M., IDO, H., YAGI, Y., SANZEN, N., TSUJI, T., YAMADA, M. & SEKIGUCHI, K. 2006. Ligand-binding specificities of laminin-binding integrins: A comprehensive survey of laminin–integrin interactions using recombinant α3β1, α6β1, α7β1 and α6β4 integrins. *Matrix Biology,* 25**,** 189-197.

NORBERTCZAK, H. T., FERMOR, H. L., EDWARDS, J. H., ROONEY, P., INGHAM, E. & HERBERT, A. 2022. Decellularised human bone allograft from different anatomical sites as a basis for functionally stratified repair material for bone defects. *J Mech Behav Biomed Mater,* 125**,** 104965.

NYBERG, S. L., HARDIN, J., AMIOT, B., ARGIKAR, U. A., REMMEL, R. P. & RINALDO, P. 2005. Rapid, large-scale formation of porcine hepatocyte spheroids in a novel spheroid reservoir bioartificial liver. *Liver Transpl,* 11**,** 901-10.

OLSAVSKY GOYAK, K. M., LAURENZANA, E. M. & OMIECINSKI, C. J. 2010. Hepatocyte differentiation. *Methods Mol Biol,* 640**,** 115-38.

ONG, L. J. Y., CHONG, L. H., JIN, L., SINGH, P. K., LEE, P. S., YU, H., ANANTHANARAYANAN, A., LEO, H. L. & TOH, Y. C. 2017. A pump-free microfluidic 3D perfusion platform for the efficient differentiation of human hepatocyte-like cells. *Biotechnol Bioeng,* 114**,** 2360-2370.

PALAKKAN, A. A., HAY, D. C., PR, A. K., TV, K. & ROSS, J. A. 2013. Liver tissue engineering and cell sources: issues and challenges. *Liver International,* 33**,** 666-676.

PARENT, R., MARION, M. J., FURIO, L., TREPO, C. & PETIT, M. A. 2004. Origin and characterization of a human bipotent liver progenitor cell line. *Gastroenterology,* 126**,** 1147-56.

PARK, K. M. & WOO, H. M. 2012. Systemic decellularization for multi-organ scaffolds in rats. *Transplant Proc,* 44**,** 1151-4.

PASCHOS, N. K., BROWN, W. E., ESWARAMOORTHY, R., HU, J. C. & ATHANASIOU, K. A. 2014. Advances in tissue engineering through stem cell-based co-culture. *J Tissue Eng Regen Med*.

PEPE-MOONEY, B. J., DILL, M. T., ALEMANY, A., ORDOVAS-MONTANES, J., MATSUSHITA, Y., RAO, A., SEN, A., MIYAZAKI, M., ANAKK, S., DAWSON, P. A., ONO, N., SHALEK, A. K., VAN OUDENAARDEN, A. & CAMARGO, F. D. 2019. Single-Cell Analysis of the Liver Epithelium Reveals Dynamic Heterogeneity and an Essential Role for YAP in Homeostasis and Regeneration. *Cell Stem Cell,* 25**,** 23-38.e8.

PLACE, T. L., DOMANN, F. E. & CASE, A. J. 2017. Limitations of oxygen delivery to cells in culture: An underappreciated problem in basic and translational research. *Free Radic Biol Med,* 113**,** 311-322.

PRESTWICH, G. D., LIU, Y., YU, B., SHU, X. Z. & SCOTT, A. 2007. 3-D culture in synthetic extracellular matrices: new tissue models for drug toxicology and cancer drug discovery. *Adv Enzyme Regul,* 47**,** 196-207.

PROVIN, C., TAKANO, K., SAKAI, Y., FUJII, T. & SHIRAKASHI, R. 2008. A method for the design of 3D scaffolds for high-density cell attachment and determination of optimum perfusion culture conditions. *J Biomech,* 41**,** 1436-49.

RAPPAPORT, A. M., BOROWY, Z. J., LOUGHEED, W. M. & LOTTO, W. N. 1954. Subdivision of hexagonal liver lobules into a structural and functional unit; role in hepatic physiology and pathology. *The Anatomical Record,* 119**,** 11-33.

RAZA, A., COLLEY, H. E., BAGGALEY, E., SAZANOVICH, I. V., GREEN, N. H., WEINSTEIN, J. A., BOTCHWAY, S. W., MACNEIL, S. & HAYCOCK, J. W. 2017. Oxygen Mapping of Melanoma Spheroids using Small Molecule Platinum Probe and Phosphorescence Lifetime Imaging Microscopy. *Scientific Reports,* 7.

REBELO, S. P., COSTA, R., ESTRADA, M., SHEVCHENKO, V., BRITO, C. & ALVES, P. M. 2015. HepaRG microencapsulated spheroids in DMSO-free culture: novel culturing approaches for enhanced xenobiotic and biosynthetic metabolism. *Arch Toxicol,* 89**,** 1347-58.

REID, L. M., FIORINO, A. S., SIGAL, S. H., BRILL, S. & HOLST, P. A. 1992. Extracellular matrix gradients in the space of Disse: relevance to liver biology. *Hepatology,* 15**,** 1198-203.

REN, H., SHI, X., TAO, L., XIAO, J., HAN, B., ZHANG, Y., YUAN, X. & DING, Y. 2013. Evaluation of two decellularization methods in the development of a whole-organ decellularized rat liver scaffold. *Liver Int,* 33**,** 448-58.

RIPPIN, S. J., HAGENBUCH, B., MEIER, P. J. & STIEGER, B. 2001. Cholestatic expression pattern of sinusoidal and canalicular organic anion transport systems in primary cultured rat hepatocytes. *Hepatology,* 33**,** 776-82.

ROELOFSEN, H., VOS, T. A., SCHIPPERS, I. J., KUIPERS, F., KONING, H., MOSHAGE, H., JANSEN, P. L. & MÜLLER, M. 1997. Increased levels of the multidrug resistance protein in lateral membranes of proliferating hepatocyte-derived cells. *Gastroenterology,* 112**,** 511-21.

ROSE, S., CUVELLIER, M., EZAN, F., CARTERET, J., BRUYÈRE, A., LEGAGNEUX, V., NESSLANY, F., BAFFET, G. & LANGOUËT, S. 2022. DMSO-free highly differentiated HepaRG spheroids for chronic toxicity, liver functions and genotoxicity studies. *Arch Toxicol,* 96**,** 243-258.

SAINZ, B., JR. & CHISARI, F. V. 2006. Production of infectious hepatitis C virus by well-differentiated, growth-arrested human hepatoma-derived cells. *J Virol,* 80**,** 10253-7.

SAINZ, B., JR., TENCATE, V. & UPRICHARD, S. L. 2009. Three-dimensional Huh7 cell culture system for the study of Hepatitis C virus infection. *Virol J,* 6**,** 103.

SAKAI, Y., NARUSE, K., NAGASHIMA, I., MUTO, T. & SUZUKI, M. 1996. Large-scale preparation and function of porcine hepatocyte spheroids. *Int J Artif Organs,* 19**,** 294-301.

SASSI, L., AJAYI, O., CAMPINOTI, S., NATARAJAN, D., MCQUITTY, C., SIENA, R. R., MANTERO, S., DE COPPI, P., PELLEGATA, A. F., CHOKSHI, S. & URBANI, L. 2021. A Perfusion Bioreactor for Longitudinal Monitoring of Bioengineered Liver Constructs. *Nanomaterials (Basel),* 11.

SAVIANO, A., HENDERSON, N. C. & BAUMERT, T. F. 2020. Single-cell genomics and spatial transcriptomics: Discovery of novel cell states and cellular interactions in liver physiology and disease biology. *J Hepatol,* 73**,** 1219-1230.

SCHAEFER, O., OHTSUKI, S., KAWAKAMI, H., INOUE, T., LIEHNER, S., SAITO, A., SAKAMOTO, A., ISHIGURO, N., MATSUMARU, T., TERASAKI, T. & EBNER, T. 2012. Absolute quantification and differential expression of drug transporters, cytochrome P450 enzymes, and UDP-glucuronosyltransferases in cultured primary human hepatocytes. *Drug Metab Dispos,* 40**,** 93-103.

SCHÉELE, S., NYSTRÖM, A., DURBEEJ, M., TALTS, J. F., EKBLOM, M. & EKBLOM, P. 2007. Laminin isoforms in development and disease. *J Mol Med (Berl),* 85**,** 825-36.

SCHMELZER, E., TRIOLO, F., TURNER, M. E., THOMPSON, R. L., ZEILINGER, K., REID, L. M., GRIDELLI, B. & GERLACH, J. C. 2010. Three-dimensional perfusion bioreactor culture supports differentiation of human fetal liver cells. *Tissue Eng Part A,* 16**,** 2007-16.

SCHMUCKER, D. L., MOONEY, J. S. & JONES, A. L. 1978. Stereological analysis of hepatic fine structure in the Fischer 344 rat. Influence of sublobular location and animal age. *J Cell Biol,* 78**,** 319-37.

SCHRAMM, C., BUBENHEIM, M., ADAM, R., KARAM, V., BUCKELS, J., O'GRADY, J. G., JAMIESON, N., POLLARD, S., NEUHAUS, P., MANNS, M. M., PORTE, R., CASTAING, D., PAUL, A., TRAYNOR, O., GARDEN, J., FRIMAN, S., ERICZON, B. G., FISCHER, L., VITKO, S., KRAWCZYK, M., METSELAAR, H. J., FOSS, A., KILIC, M., ROLLES, K., BURRA, P., ROGIERS, X. & LOHSE, A. W. 2010. Primary liver transplantation for autoimmune hepatitis: a comparative analysis of the European Liver Transplant Registry. *Liver Transpl,* 16**,** 461-9.

SCHUPPAN, D., RUEHL, M., SOMASUNDARAM, R. & HAHN, E. G. 2001. Matrix as a modulator of hepatic fibrogenesis. *Semin Liver Dis,* 21**,** 351-72.

SEMINO, C. E., MEROK, J. R., CRANE, G. G., PANAGIOTAKOS, G. & ZHANG, S. 2003. Functional differentiation of hepatocyte-like spheroid structures from putative liver progenitor cells in three-dimensional peptide scaffolds. *Differentiation,* 71**,** 262-70.

SEMLER, E. J., LANCIN, P. A., DASGUPTA, A. & MOGHE, P. V. 2005. Engineering hepatocellular morphogenesis and function via ligand-presenting hydrogels with graded mechanical compliance. *Biotechnol Bioeng,* 89**,** 296-307.

SEMLER, E. J., RANUCCI, C. S. & MOGHE, P. V. 2000. Mechanochemical manipulation of hepatocyte aggregation can selectively induce or repress liver-specific function. *Biotechnology and Bioengineering,* 69**,** 359-369.

SHERIDAN, W. S., RYAN, A. J., DUFFY, G. P., O'BRIEN, F. J. & MURPHY, B. P. 2014. An experimental investigation of the effect of mechanical and biochemical stimuli on cell migration within a decellularized vascular construct. *Ann Biomed Eng,* 42**,** 2029-38.

SHIRAKIGAWA, N., IJIMA, H. & TAKEI, T. 2012. Decellularized liver as a practical scaffold with a vascular network template for liver tissue engineering. *J Biosci Bioeng,* 114**,** 546-51.

SIVERTSSON, L., EK, M., DARNELL, M., EDEBERT, I., INGELMAN-SUNDBERG, M. & NEVE, E. P. 2010. CYP3A4 catalytic activity is induced in confluent Huh7 hepatoma cells. *Drug Metab Dispos,* 38**,** 995-1002.

SKARDAL, A., SMITH, L., BHARADWAJ, S., ATALA, A., SOKER, S. & ZHANG, Y. 2012. Tissue specific synthetic ECM hydrogels for 3-D in vitro maintenance of hepatocyte function. *Biomaterials,* 33**,** 4565-75.

SOLDATOW, V. Y., LECLUYSE, E. L., GRIFFITH, L. G. & RUSYN, I. 2013. In vitro models for liver toxicity testing. *Toxicol Res (Camb),* 2**,** 23-39.

SOLTYS, K. A., SOTO-GUTIÉRREZ, A., NAGAYA, M., BASKIN, K. M., DEUTSCH, M., ITO, R., SHNEIDER, B. L., SQUIRES, R., VOCKLEY, J., GUHA, C., ROY-CHOWDHURY, J., STROM, S. C., PLATT, J. L. & FOX, I. J. 2010. Barriers to the successful treatment of liver disease by hepatocyte transplantation. *Journal of Hepatology,* 53**,** 769-774.

SOTO-GUTIERREZ, A., ZHANG, L., MEDBERRY, C., FUKUMITSU, K., FAULK, D., JIANG, H., REING, J., GRAMIGNOLI, R., KOMORI, J., ROSS, M., NAGAYA, M., LAGASSE, E., STOLZ, D., STROM, S. C., FOX, I. J. & BADYLAK, S. F. 2011. A whole-organ regenerative medicine approach for liver replacement. *Tissue Eng Part C Methods,* 17**,** 677-86.

STATZER, C. & EWALD, C. Y. 2020. The extracellular matrix phenome across species. *Matrix Biol Plus,* 8**,** 100039.

STÖCKER, E. & HEINE, W. D. 1971. Regeneration of liver parenchyma under normal and pathological conditions. *Beitrage zur Pathologie,* 144**,** 400-408.

STOCKER, E., WULLSTEIN, H. K. & BRAU, G. 1973. Capacity of regeneration in liver epithelia of juvenile, repeatedly partially hepatectomized rats. Autoradiographic studies after continuous infusion of 3H thymidine. *VIRCHOWS ARCH.ABT.B ZELLPATH.,* 14**,** 93-103.

TAGUCHI, K., MATSUSHITA, M., TAKAHASHI, M. & UCHINO, J. 1996. Development of a bioartificial liver with sandwiched-cultured hepatocytes between two collagen gel layers. *Artif Organs,* 20**,** 178-85.

TAN, H. K. 2004. Molecular adsorbent recirculating system (MARS). *Ann Acad Med Singapore,* 33**,** 329-35.

UDENFRIEND, S. 1966. Formation of hydroxyproline in collagen. *Science,* 152**,** 1335-40.

UYGUN, B. E., PRICE, G., SAEDI, N., IZAMIS, M. L., BERENDSEN, T., YARMUSH, M. & UYGUN, K. 2011. Decellularization and recellularization of whole livers. *J Vis Exp*.

UYGUN, B. E., SOTO-GUTIERREZ, A., YAGI, H., IZAMIS, M. L., GUZZARDI, M. A., SHULMAN, C., MILWID, J., KOBAYASHI, N., TILLES, A., BERTHIAUME, F., HERTL, M., NAHMIAS, Y., YARMUSH, M. L. & UYGUN, K. 2010. Organ reengineering through development of a transplantable recellularized liver graft using decellularized liver matrix. *Nat Med,* 16**,** 814-20.

VACANTI, J. P. & KULIG, K. M. 2014. Liver cell therapy and tissue engineering for transplantation. *Seminars in Pediatric Surgery,* 23**,** 150-155.

VAFAEE, T., THOMAS, D., DESAI, A., JENNINGS, L. M., BERRY, H., ROONEY, P., KEARNEY, J., FISHER, J. & INGHAM, E. 2018. Decellularization of human donor aortic and pulmonary valved conduits using low concentration sodium dodecyl sulfate. *J Tissue Eng Regen Med,* 12**,** e841-e853.

VANDER HEIDEN, M. G., CANTLEY, L. C. & THOMPSON, C. B. 2009. Understanding the Warburg effect: the metabolic requirements of cell proliferation. *Science,* 324**,** 1029-33.

VITACOLONNA, M., BELHARAZEM, D., HOHENBERGER, P. & ROESSNER, E. D. 2015. Effect of dynamic seeding methods on the distribution of fibroblasts within human acellular dermis. *Cell Tissue Bank,* 16**,** 605-14.

WANG, X., CUI, J., ZHANG, B. Q., ZHANG, H., BI, Y., KANG, Q., WANG, N., BIE, P., YANG, Z., WANG, H., LIU, X., HAYDON, R. C., LUU, H. H., TANG, N., DONG, J. & HE, T. C. 2014. Decellularized liver scaffolds effectively support the proliferation and differentiation of mouse fetal hepatic progenitors. *J Biomed Mater Res A,* 102**,** 1017-25.

WANG, X., HASSAN, W., ZHAO, J., BAKHT, S., NIE, Y., WANG, Y., PANG, Q. & HUANG, Z. 2019a. The impact of hepatocyte nuclear factor-1α on liver malignancies and cell stemness with metabolic consequences. *Stem Cell Res Ther,* 10**,** 315.

WANG, Z. Y., LI, W. J., LI, Q. G., JING, H. S., YUAN, T. J., FU, G. B., TANG, D., ZHANG, H. D., YAN, H. X. & ZHAI, B. 2019b. A DMSO-free hepatocyte maturation medium accelerates hepatic differentiation of HepaRG cells in vitro. *Biomed Pharmacother,* 116**,** 109010.

WARING, J. F., CIURLIONIS, R., JOLLY, R. A., HEINDEL, M., GAGNE, G., FAGERLAND, J. A. & ULRICH, R. G. 2003. Isolated human hepatocytes in culture display markedly different gene expression patterns depending on attachment status. *Toxicol In Vitro,* 17**,** 693-701.

WEBER, A., TOUBOUL, T., MAINOT, S., BRANGER, J. & MAHIEU-CAPUTO, D. 2010. Human foetal hepatocytes: isolation, characterization, and transplantation. *Methods Mol Biol,* 640**,** 41-55.

WEI, J., YAO, J., YANG, C., MAO, Y., ZHU, D., XIE, Y., LIU, P., YAN, M., REN, L., LIN, Y., ZHENG, Q. & LI, X. 2022. Heterogeneous matrix stiffness regulates the cancer stem-like cell phenotype in hepatocellular carcinoma. *J Transl Med,* 20**,** 555.

WELLS, R. G. 2008. The role of matrix stiffness in regulating cell behavior. *Hepatology,* 47**,** 1394-1400.

WEN, S. L., FENG, S., TANG, S. H., GAO, J. H., ZHANG, L. H., TONG, H., YAN, Z. P. & FANG, D. Z. 2016. Collapsed Reticular Network and its Possible Mechanism during the Initiation and/or Progression of Hepatic Fibrosis. *Sci Rep,* 6**,** 35426.

WIGGER, L., CASALS-CASAS, C., BARUCHET, M., TRANG, K. B., PRADERVAND, S., NALDI, A. & DESVERGNE, B. 2019. System analysis of cross-talk between nuclear receptors reveals an opposite regulation of the cell cycle by LXR and FXR in human HepaRG liver cells. *PLoS One,* 14**,** e0220894.

WILCOX, H. E., KOROSSIS, S. A., BOOTH, C., WATTERSON, K. G., KEARNEY, J. N., FISHER, J. & INGHAM, E. 2005. Biocompatibility and recellularization potential of an acellular porcine heart valve matrix. *J Heart Valve Dis,* 14**,** 228-36; discussion 236-7.

WILSHAW, S. P., ROONEY, P., BERRY, H., KEARNEY, J. N., HOMER-VANNIASINKAM, S., FISHER, J. & INGHAM, E. 2012. Development and characterization of acellular allogeneic arterial matrices. *Tissue Eng Part A,* 18**,** 471-83.

YAGI, H., FUKUMITSU, K., FUKUDA, K., KITAGO, M., SHINODA, M., OBARA, H., ITANO, O., KAWACHI, S., TANABE, M., COUDRIET, G. M., PIGANELLI, J. D., GILBERT, T. W., SOTO-GUTIERREZ, A. & KITAGAWA, Y. 2013. Human-scale whole-organ bioengineering for liver transplantation: a regenerative medicine approach. *Cell Transplant,* 22**,** 231-42.

YOUNG, B., O'DOWD, G. & WOODFORD, P. 2014. *Wheater's functional histology: a text and colour atlas,* Philadelphia, PA, Churchill Livingston/Elsevier.

ZERN, M. A. & REID, L. M. 1994. Extracellular Matrix: Chemistry, Biology, and Pathobiology with Emphasis on the Liver. *Perspectives in Biology and Medicine,* 38**,** 139.

ZHANG, F., LU, Y. & ZHENG, S. 2012. Peroxisome proliferator-activated receptor-γ cross-regulation of signaling events implicated in liver fibrogenesis. *Cell Signal,* 24**,** 596-605.

ZHANG, J., DUAN, Z. P., HE, J. Q., ZHANG, L. L., CHEN, S. B., ZOU, C. Y., XIN, S. J., WU, W. F., MA, B. R., CHEN, Y., KONG, M., LIU, M. & HAN, D. K. 2006. [Survival analysis on liver failure patients treated with an artificial liver support system]. *Zhonghua Gan Zang Bing Za Zhi,* 14**,** 647-51.

ZHANG, Y., HE, Y., BHARADWAJ, S., HAMMAM, N., CARNAGEY, K., MYERS, R., ATALA, A. & VAN DYKE, M. 2009. Tissue-specific extracellular matrix coatings for the promotion of cell proliferation and maintenance of cell phenotype. *Biomaterials,* 30**,** 4021-8.

ZHOU, X. M., MIAO, J. Y., YANG, Y., ZHAO, L., WANG, X., XU, L., DING, J., WU, K. C., FAN, D. M. & WANG, M. M. 2004. Clinical experience with molecular adsorbent recirculating system (MARS) in patients with drug-induced liver failure. *Artif Organs,* 28**,** 483-6.